ADVANCING THE EUROCODE NORMATIVE CRITERIA FOR HIGH-SPEED RAILWAY BRIDGES

GONÇALO CABRAL FERREIRA

U.PORTO

FEUP FACULDADE DE ENGENHARIA
UNIVERSIDADE DO PORTO

Thesis submitted for the degree of Doctor in Civil Engineering.

Supervisor: Doctor Pedro Aires Moreira Montenegro e Almeida

Co-supervisor: Professor Doctor Rui Artur Bártolo Calçada

Co-Supervisor: Professor Doctor António Abel Ribeiro Henriques

Faculty of Engineering
University of Porto

2025

Cofinanciado por:

Advancing the Eurocode Normative Criteria for High-Speed Railway Bridges

Au milieu de l'hiver, j'apprenais enfin
qu'il y avait en moi un été invincible.

— Albert Camus

Mesmo no silêncio
sabemos cantar.

— José Mário Branco

Ao Mário
e ao meu padrinho, Luís Cabral.

THESIS EXAMINATION COMMITTEE

This thesis was presented for examination on July 25th 2025, at the Faculty of Engineering of the University of Porto, by the following committee:

President of the committee
Doctor Álvaro Alberto de Matos Ferreira da Cunha, Full Professor, Faculty of Engineering of the University of Porto

Examiners
Univ.-Prof. Dipl.-Ing. Dr.techn. Christoph Adam, University of Innsbruck
Doctor José Maria Goicolea Ruigomez, Full Professor, Technical University of Madrid
Doctor Xavier das Neves Romão, Associate Professor, Faculty of Engineering of the University of Porto
Doctor Diogo Rodrigo Ferreira Ribeiro, Coordinator Professor, School of Engineering, Polytechnic of Porto

Supervisor
Doctor Pedro Aires Moreira Montenegro e Almeida, Assistant Researcher, Faculty of Engineering of the University of Porto

ABSTRACT

Railways are essential to build a more sustainable future. In a time of rising concerns regarding climate, rail transport is highlighted as the greener alternative. The European Union is focused on developing high-capacity and environmentally-friendly rail networks, as demonstrated by the efforts in establishing the Europe's Rail Joint Undertaking, through which research projects have worked towards improving the life cycle of infrastructures. High-speed railway bridges are vital parts of rail networks whose design is conditioned by norms such as the Eurocodes. This thesis builds upon concerns expressed not only by the scientific community but also by regulatory bodies regarding gaps identified in the Eurocodes.

A three-part literature review is presented as a basis for research. The first includes the design dispositions in European, Chinese, and Japanese norms; the second focuses on methodologies to assess the dynamic behaviour of the train-bridge system; the third goes over probabilistic methods to evaluate structural safety. The gaps identified in this review motivate the three main objectives of the thesis.

The first is to evaluate the limitations of the EN 1991-2 High-Speed Load Model (HSLM), considering that it may not cover new trains and that its limits of validity may be inconsistent. Randomly generated articulated, conventional, and regular train load models are generated and compared with the HSLM's envelope on a case study bridge. In addition to train signatures, dynamic analyses are presented, for which a novel tool to decrease computational cost in moving loads analysis is introduced. It is found that a load model can abide by the norm's limits but still not be covered by the HSLM. At the same time, the current HSLM envelope is partially suited to cover new trains.

The second objective addresses deck acceleration in ballasted bridges, limited to 3.5 m/s^2 by the EN 1990. This value is based on the application of a seemingly arbitrary safety factor of 2.0. To test its suitability, the physical limit for ballast stability of 7.0 m/s^2 is compared with design accelerations calculated at critical speeds corresponding to probabilities of failure of 10^{-4}. This target pertains to the fact that, while deck acceleration does not compromise structural safety, ballast instability may lead to derailment, and therefore, it is considered an Ultimate Limit State. To determine design accelerations, new definitions are put forward, clarifying the EN 1991-2's dispositions. The assessment of critical speeds conditioned by low probabilities of failure is done with a newly proposed algorithm based on subset simulation. Results from four case study bridges show that a bridge can be designed with a deck acceleration greater than the norm's current limit while staying within the target probability of failure, thereby without jeopardizing the traffic safety.

The third goal is to understand the existence of a limit for deck acceleration in ballastless bridges. In these structures, the EN 1990's limit of 5 m/s^2, in addition to being based on the same safety factor, likely reflects an assumption

that a deck acceleration of 10 m/s^2 (i.e. circa 1 g) is indicative of wheel-rail detachment. Using both lateral and vertical dynamics, derailment criteria are calculated on five case study bridges containing different rail irregularities. A new three-dimensional model based on the HSLM is developed for this parametric study. The simulations' results do not suggest that there is a strong correlation between deck acceleration and derailment criteria.

The normative recommendations from this work constitute suggestions towards advancing the Eurocodes in further revisions. By allowing new, faster trains to operate on existing lines, the lifecycle of high-speed railway bridges can be extended.

KEYWORDS High-speed; Railway bridges; Eurocode; Running safety; Probabilistic analysis.

RESUMO

A ferrovia é essencial para a construção de um futuro mais sustentável. Numa fase de crescente preocupação com as questões ambientais, o transporte ferroviário destaca-se como a alternativa mais verde. A União Europeia está determinada em desenvolver redes ferroviárias de elevada capacidade e respeitadoras do ambiente, tal como demonstrado pelos esforços em estabelecer a Empresa Comum do Setor Ferroviário Europeu (Europe's Rail), através da qual os projetos de investigação desenvolvidos têm contribuído para aumentar o ciclo de vida das infraestruturas. As pontes ferroviárias de alta velocidade são parte vital das redes ferroviárias, cujo dimensionamento é condicionado por normas como os Eurocódigos. Esta tese sustenta-se nas preocupações expressas não só pela comunidade científica, mas também pelas entidades reguladoras quanto às lacunas identificadas nos Eurocódigos.

Como base para a investigação, é apresentada uma revisão de literatura em três partes. A primeira inclui as disposições de dimensionamento das normas Europeias, Chinesas e Japonesas; a segunda enquadra as metodologias de avaliação do comportamento dinâmico do sistema ponte-comboio; a terceira diz respeito aos métodos probabilísticos de avaliação da segurança estrutural. As lacunas identificadas motivam os três principais objetivos da tese.

O primeiro é avaliar as limitações do High-Speed Load Model (Modelo de Carga HSLM) da EN 1991-2, considerando que poderá não abranger novos comboios e que os seus limites de validade poderão ser inconsistentes. Através do caso de estudo de uma ponte, são gerados aleatoriamente modelos de cargas de comboios articulados, convencionais e regulares, sendo comparados com a envolvente do HSLM. Para além das assinaturas dos comboios, são apresentadas análises dinâmicas, obtidas através de uma nova ferramenta para redução do custo computacional em análise de cargas móveis. Verifica-se que um modelo de carga pode respeitar os limites da norma, mas ainda assim não estar abrangido pelo HSLM. Ao mesmo tempo, a atual envolvente do HSLM é parcialmente adequada a incluir novos comboios.

O segundo objetivo diz respeito à aceleração do tabuleiro em pontes balastradas, limitada pela EN 1990 a 3.5 m/s^2. Este valor é baseado na aplicação de um fator de segurança aparentemente arbitrário de 2.0. De modo a testar a sua adequação, o limite físico de estabilidade do balastro de 7.0 m/s^2 é comparado com acelerações de dimensionamento calculadas com velocidades críticas correspondentes a probabilidades de falha de 10^{-4}. Este alvo diz respeito ao facto de que, embora a aceleração do tabuleiro não comprometa a segurança estrutural, a instabilidade do balastro pode levar ao descarrilamento, sendo por isso considerado um Estado Limite Último. Para determinar acelerações de dimensionamento, são propostas novas definições, clarificando as disposições da EN 1991-2. A avaliação de velocidades críticas condicionadas por probabilidades de falha baixas é feita com um algoritmo inovador baseado em simulação de subconjuntos. Os resultados do caso de estudo de quatro pontes demonstram

que uma ponte pode ser dimensionada com uma aceleração do tabuleiro maior do que o limite da norma, permanecendo dentro da probabilidade de falha alvo, sem comprometer a segurança de circulação.

O terceiro objetivo é compreender a existência do limite de aceleração do tabuleiro em pontes não-balastradas. Nestas estruturas, o limite de 5 m/s^2 da EN 1991-2, para além de ser baseado no mesmo fator de segurança, aparenta refletir o pressuposto de que uma aceleração do tabuleiro de 10 m/s^2 (ou seja, cerca de 1 g) indica a perda do contacto roda-carril. Utilizando tanto dinâmica vertical como lateral, são calculados critérios de descarrilamento num caso de estudo com cinco pontes, com diferentes níveis de irregularidade dos carris. É desenvolvido um novo modelo tridimensional baseado no HSLM. Os resultados das simulações não sugerem que exista uma forte correlação entre aceleração do tabuleiro e critérios de descarrilamento.

As recomendações normativas deste trabalho constituem sugestões para atualizar os Eurocódigos em futuras revisões. Ao permitir que novos comboios mais rápidos possam circular nas linhas existentes, o ciclo de vida das pontes ferroviárias de alta velocidade pode ser alargado.

PALAVRAS-CHAVE Alta velocidade; Pontes ferroviárias; Eurocódigo; Segurança de circulação; Análise probabilística.

PUBLICATIONS

The development of this thesis resulted in the following publications:

ARTICLES IN INTERNATIONAL JOURNALS

Silva, A., D. Ribeiro, P. Montenegro, G. Ferreira, A. Andersson, A. Zangeneh, R. Karoumi, and R. Calçada (2023). "New Contributions for Damping Assessment on Filler-Beam Railway Bridges Framed on In2Track EU Projects." *Applied Sciences (Switzerland)* 13.4. ISSN: 2076-3417. DOI: 10.3390/app13042636.

Ferreira, G., P. Montenegro, A. Andersson, A. A. Henriques, R. Karoumi, and R. Calçada (2024a). "Critical analysis of the current Eurocode deck acceleration limit for evaluating running safety in ballastless railway bridges." *Engineering Structures* 312, p. 118127. ISSN: 0141-0296. DOI: 10.1016/j.engstruct.2024.118127.

Ferreira, G., P. Montenegro, J. R. Pinto, A. A. Henriques, and R. Calçada (2024c). "A discussion about the limitations of the Eurocode's high-speed load model for railway bridges." *Railway Engineering Science* 32.2, pp. 211–228. ISSN: 2662-4745. DOI: 10.1007/s40534-023-00321-5.

Ferreira, G., Montenegro P., C. Adam, A. A. Henriques, and R. Calçada (2025). "Evaluation of the Eurocode's Safety Factor for Deck Acceleration Limit on Ballasted Track Railway Bridges." Submitted for publication.

Granato, E., G. Ferreira, P. Montenegro, A. A. Henriques, R. Calçada, and T. Bittencourt (2025). "Probabilistic Analysis of Train Running Safety on Bridges: A State-of-the-Art Review." *International Journal of Rail Transportation* 0.0, pp. 1–39. ISSN: 2324-8378. DOI: 10.1080/23248378.2024.2447033. URL: https://doi.org/10.1080/23248378.2024.2447033.

INTERNATIONAL CONFERENCE PROCEEDINGS

Ferreira, G., P. Montenegro, A. A. Henriques, and R. Calçada (2022a). "Probabilistic Approach for Assessment of Track Stability Safety Factor on Ballasted Railway Bridges." *The Fifth International Conference on Railway Technology: Research, Development and Maintenance*. Montpellier, France. DOI: 10.4203/ccc.1.6.12.

– (2022b). "Uncertainty and Track Stability: Analysis of Partial Safety Factors for High-Speed Railway Bridges." *Lecture Notes in Civil Engineering*. Vol. 200 LNCE, pp. 1216–1225. ISBN: 978-3-030-91876-7. DOI: 10.1007/978-3-030-91877-4_138.

– (2024b). "New Perspectives on Running Safety in Ballastless Railway Bridges." *The Sixth International Conference on Railway Technology: Research, Development and Maintenance*. Prague, Czech Republic. DOI: 10.4203/ccc.7.15.8.

Ferreira, G., A. Silva, A. A. Henriques, P. Montenegro, D. Ribeiro, and R. Calçada (2021). "Análise Probabilística Da Aceleração Vertical Em Tabuleiros de Pontes Ferroviárias de Alta Velocidade." *Congresso Reabilitar & Betão Estrutural 2020*. Lisboa. ISBN: 978-989-53078-1-4. URL: https://repositorio-aberto.up.pt/handle/10216/140849.

Ferreira, G., P. Montenegro, A. A. Henriques, and R. Calçada (2022). "Critérios de Segurança Ao Descarrilamento Em Pontes Ferroviárias de Alta Velocidade Com via Não-Balastrada." *6as Jornadas Portuguesas de Engenharia de Estruturas*. Lisboa. URL: https://repositorio-aberto.up.pt/handle/10216/147473.

– (2024). "Avaliação Eficiente Da Segurança Estrutural de Pontes Ferroviárias de Betão Com Base Na Simulação de Subconjuntos." *Encontro Nacional Do Betão Estrutural 2024 - BE2024*. Porto. ISBN: 978-972-752-327-6. URL: https://repositorio-aberto.up.pt/handle/10216/165346.

AGRADECIMENTOS

O trabalho de investigação que resultou na presente tese começou já há vários anos. Ainda que consciente da dimensão do desafio a que me propunha, seria impossível antever todas as curvas e percalços possíveis, aos quais se acrescentou sem aviso uma pandemia de proporções históricas. Contudo, a ideia de que fazer um doutoramento é uma tarefa solitária foi sempre contestada pela realidade, e nela se encontram a solidariedade, companheirismo e ajuda de muitos. Por isso, ainda que o trabalho tenha uma só assinatura, tenho a sorte de afirmar que as páginas que se seguem são o reflexo do esforço coletivo de um grande número de pessoas – e felizmente nem todos são engenheiros! Assim, aproveito estas linhas para inscrever para a posteridade (pelo menos no repositório da Universidade do Porto) o meu profundo e sincero agradecimento:

- Ao meu orientador, o Doutor Pedro Aires Moreira Montenegro e Almeida pelo apoio, confiança e acima de tudo pela amizade. Foi um privilégio ter a dedicação e o apoio incansável de um investigador que é referência na sua área. Tenho a sorte de presenciar, para além da competência científica, os valores e boa disposição que fazem do meu orientador um exemplo profissional e pessoal.

- Ao meu co-orientador, o Professor Doutor Rui Artur Bártolo Calçada pelas ideias fundamentais para esta tese e pelo entusiasmo que transmite. Foi há quase uma década que o Prof. Calçada ajudou a incutir o gosto pelas áreas da ferrovia e dinâmica estrutural. Agradeço-lhe pela motivação para acreditar que vale a pena ser cientista.

- Ao meu co-orientador, o Professor Doutor António Abel Ribeiro Henriques, pelos conhecimentos transmitidos e pela presença constante. Sob a sua orientação, Estatística passou de ser uma cadeira distante para passar a ser a minha área preferida da Matemática. Agradeço-lhe pela persistência e pelo rigor com que se dedicou a esta tese.

- À Fundação para a Ciência e a Tecnologia, pelo financiamento através da bolsa de doutoramento PD/BD/143007/2018 (Programa Doutoral iRail - Innovation in Railway Systems and Technologies). Este trabalho foi ainda financiado por: Financiamento Base - UIDB/04708/2020 e Financiamento programático - UIDP/04708/2020 da Unidade de Investigação CONSTRUCT - Instituto de I&D em Estruturas e Construções - financiada por fundos nacionais através da FCT/MCTES (PIDDAC).

- To the Shift2Rail Joint Undertaking, for the financial support through the IN2TRACK2 and IN2TRACK3 projects, funded under the European Union's Horizon 2020 research and innovation programme under grant agreements No. 826255 and No. 101012456, respectively.

- To the Europe's Rail Joint Undertaking, for the financial support through the InBridge4EU project, funded under the Horizon Europe research and innovation programme under grant agreement No. 101121765 (HORIZON-ER-JU-2022-ExplR-02). Views and opinions expressed are however those of the author(s) only and do not necessarily reflect those of the European Union or Europe's Rail Joint Undertaking. Neither the European Union nor the granting authority can be held responsible for them.

- Ao Departamento de Engenharia Civil da FEUP, na pessoa de Marta Poinhas, pelo apoio aos trabalhos de investigação e de divulgação da atividade científica. Agradeço-lhe por zelar pelos estudantes de doutoramento do DEC, mesmo quando estes deixam a entrega de um papel para o último dia.

- Ao Doutor João Miguel Rocha pela amabilidade de ter disponibilizado as ferramentas e dados do seu doutoramento e pelo contributo que deu na definição da metodologia probabilística.

- Ao José Rui Pinto, pelo apoio no estudo dos modelos de carga, trabalho que resultou na publicação do primeiro artigo desta tese.

- To Andreas Andersson, for his contribution to the study of ballastless bridges, for co-authoring the second paper of this thesis, and for his continuous support since the days of In2Track2 and through many conferences and meetings since.

- To Professor Christoph Adam, who kindly supervised my research visit to the Unit of Applied Mechanics at the University of Innsbruck, providing a pivotal moment in this research work, and for co-authoring the third paper of this thesis; to Doctor Patrick Salcher for his help in applying subset simulation to railway bridges; to Paul König and Konstantinos Tsalouchidis for their friendship and for introducing me to the world of indoor bouldering.

- Ao Eduardo Granato, pela ajuda na revisão de métodos probabilísticos e pela amabilidade de me ter convidado a escrever um artigo de revisão fundamental nesta área.

- Aos amigos de percurso Artur Silva e Marco António, por toda a ajuda ao longo destes anos, pela paciência e pelos momentos de convívio sem os quais esta viagem teria sido impossível.

- To Reza Allahvirdizadeh, Ian Bucknall, Matthias Baeßler, José M. Goicolea, Günther Grunert, Raid Karoumi, Pedro Museros, Xavier Romão, Diogo Ribeiro, and Patrick Simon, for the many fruitful discussions and valuable input in various stages of this work. I thank this group of experts for their advice, and I would be honoured to be considered among their fellow academics.

- Aos entusiastas da ferrovia Diogo Metelo, Hugo Guia, João Fernandes, José Pedro Ferreira, Luís Monteiro, Sara Santos e Sérgio Pinho, por to-

das as conversas que motivaram continuamente este trabalho e pelo enriquecimento cultural constante que me proporcionam.

- Aos engenheiros de sempre, António, David, João Carvalho, João Fonseca, João Gomes, João Nuno, José Diogo, Jorge Wolfs, Manuel Aranha, Manuel Fernandes, Mário, Pedro e Tiago, pela amizade de tantos anos e por todos os momentos de boa disposição. Agradeço-lhes a motivação para o trabalho científico, já que o futebolístico não passou na *peer review*.

- À Carolina, ao Francisco e aos meus compadres, por serem os raios de sol que desanuviam qualquer dia nublado.

- Aos meus pais e padrinhos, por serem desde sempre os pilares do meu percurso.

- À minha irmã Madalena, por zelar sempre pelo meu bem-estar, e ao Pedro e à Inês, por zelarem por ela.

- Ao Mário, cujo sorriso desafia todas as Leis da Física.

- À Catarina, por tudo.

CONTENTS

LIST OF FIGURES

LIST OF TABLES

ACRONYMS

BAM	Bundesanstalt für Materialforschung und -prüfung
CA	Concrete-asphalt
CC	Consequence class
CS	Coordinate system
CDF	Cumulative Distribution Function
CEN	Commité European de Normalisation
CENELEC	Comité Européen de Normalisation Électrotechnique
CV	Coefficient of variance
DER	Decomposition of Excitation at Resonance
EGD	European Green Deal
ERA	European Union Agency for Railways
ERRAC	European Railway Research Advisory Council
ERRI	European Rail Research Institute
EYR	European Year of Rail
FEM	Finite Elements Method
FORM	First-order reliability method
GPD	Generalized Pareto Distribution
HSLM	High-Speed Load Model
HSR	High-Speed Railway(s)
JCSS	Joint Committee for Structural Safety
LM71	Load Model 71
MCMC	Markov Chain Monte Carlo
MMA	Modified Metropolis Algorithm
PDEM	Probability Density Estimation Method
PDF	Probability Density Function
PSD	Power Spectral Density
RIL	Residual Influence Line
SI	Spectral Index
SLLS	Single Load Linear Superposition
SNCF	Société Nationale des Chemin de Fer

SORM	Second-order reliability method
SVM	Support Vector Machine
TSI	Technical Specifications for Interoperability
TBI	Train-Bridge Interaction
TTBI	Train-Track-Bridge Interaction
VSI	Vehicle Structure Interaction

1 INTRODUCTION

1.1 SCOPE

"Why Rail?"

This was the question that the European Commission's Directorate-General for Mobility and Transport (European Commission) (2021) used to promote the European Year of Rail (EYR) in 2021 (Figure 1.1). The EYR was an initiative of the European Parliament and Council of the European Union (2020) that solidified rail transport at the centre of conversations and policymaking in Europe. This question aptly puts forward three of the main advantages of rail transportation:

TERRITORIAL COHESION The EYR document calls attention to the role that the rail sector has in assuring "social, economic and territorial cohesion on continental, national, regional and local level", making clear that rail transportation is a key aspect of the European Union's characteristic free movement of people and goods.

SUSTAINABILITY The EYR stemmed from the implementation of the European Green Deal (EGD) (Comission to the European Parliament et al., 2019) as a plan for sustainable action within the European Union regarding environmental and climate concerns. In a recent report, the European Union Agency for Railways (2024a) (ERA) states that railways account for only 0.5% of all transport emissions.

SAFETY Statistically, railway transport accounts for a comparably low number of fatalities (less than 0.1 per billion passenger-km from 2012 to 2021 (European Union Agency for Railways, 2024b)). The EYR grouped this aspect with comfort and affordability to underscore Rail's popularity.

The transportation sector, as a whole, is responsible for slightly less than a quarter of greenhouse gas emissions in the European Union (European Union Agency for Railways, 2024a). The EGD sets a goal of reducing that share by 90% by the year 2050 by giving priority to multimodal transportation, setting the goal of shifting a "substantial part" of inland freight from roads (which currently account for 75% of all freight transportation) to railways and inland waterways. In fact, the European Union Agency for Railways (2020) underscores that "rail will become the backbone that supports an environmentally sustainable multimodal transport system and will be favoured as a transport mode by the new generation", foreseeing development in high-speed lines. This trend is verified in the statistics found in the Directorate-General for Mobility and Transport (European Commission) (2024) regularly published pocketbook, stating that there are currently 12,015 km of high-speed railway lines in the European Union, with 1,601 km under construction (Figure 1.2).

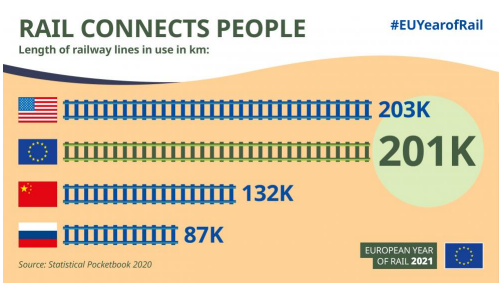

(a)

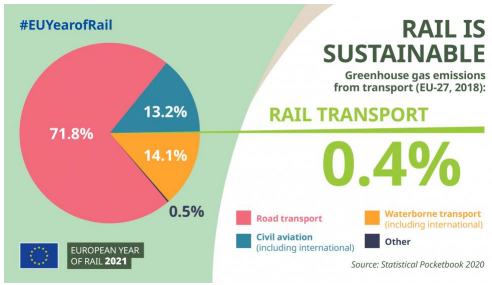

(b)

(c)

Figure 1.1: EYR facts and figures. (a) length of rail networks; (b) sustainability; (c) safety. (adapted from Directorate-General for Mobility and Transport (European Commission) (2021))

This vision of the future, placing Rail in the centre of mobility in Europe, is aligned with the ERRAC's research agenda (European Railway Research Advisory Council, 2024) and vision for 2050 (Mazzino et al., 2017). These guidelines plan a future focused on social cohesion and decarbonization, with the rail sector serving these purposes anchored on technological innovation, such as automation, digitalization, and intelligent asset lifecycle management. Railways are the core of safe and environmentally conscious travel, as evidenced by the European Union's recent investment of €7 billion in sustainable transport projects (80% of which in railways) (Directorate-General for Mobility and Transport (European Commission), 2025).

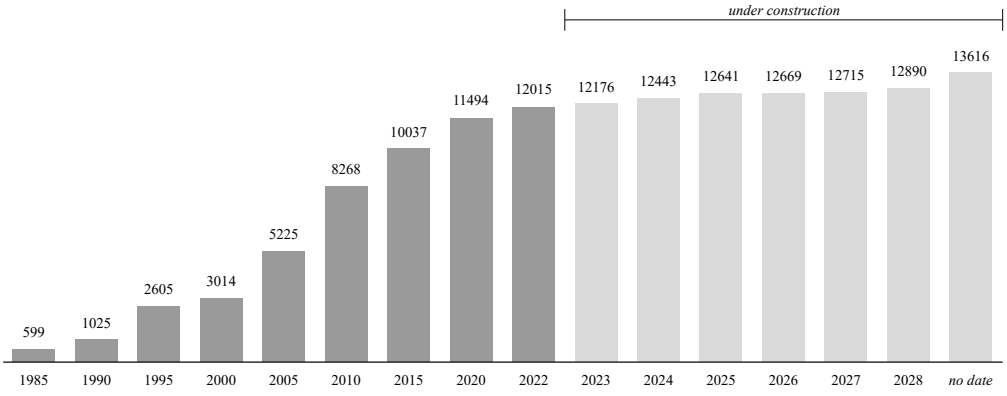

Figure 1.2: Length of high-speed lines in the European Union (data from Directorate-General for Mobility and Transport (European Commission) (2024)).

1.2 BACKGROUND

To achieve significant transformations in the rail sector's operations and to foster scientific breakthroughs in various disciplines related to railways, strict cooperation is needed between regulators, corporations, academia and the general public. To that end, the Council of the European Union (2021) established the Europe's Rail Joint Undertaking (taking the place of the Shift2Rail Joint Undertaking (Council of the European Union, 2014)), a public-private partnership aimed at innovating the rail sector.

Europe's Rail regularly funds research projects through calls for proposals. The work presented in this thesis contributed to the fulfilment of two past projects (IN2TRACK2, 2018; IN2TRACK3, 2021), with the results being integrated into the projects' deliverables at various stages of progress.

More recently, some of the present thesis' contents have also been aligned with the InBridge4EU (2023) project, which was successfully funded by Europe's Rail through a Horizon Europe call for proposal (EU Funding & Tenders Portal, 2025). This project addresses a technical note published by the European Union Agency for Railways (2022) regarding the work necessary for closing the Technical Specifications for Interoperability's open points on bridge dynamics. One of the topics of that document focuses on the deck acceleration limit of the Eurocode EN 1990 (CEN, 2023a), for both ballasted and ballastless track bridges. The traffic stability criteria are a priority of the European railway regulatory body, as well as of the infrastructure managers.

These research projects highlight the importance of bridges in rail networks. In fact, there are an estimated 300,000 bridges across European rail lines, with a study of 220,000 of them by Paulsson et al. (2010) characterizing the set as being composed of arches (41%), concrete bridges (23%), steel beam bridges (22%) and steel concrete composite bridges (14%). The topic of running safety on railway bridges has been widely studied in recent years (Allahvirdizadeh et al., 2024b; Gong et al., 2020; Montenegro et al., 2021; Zhang et al., 2022), making clear that the safe and efficient operation of railway networks is dependent on the design and assessment of railway bridges, which are susceptible to dynamic effects.

1.3 OBJECTIVES

This thesis aims to provide new perspectives and develop techniques that can assist in advancing the Eurocode's normative dispositions for the design and assessment of high-speed railway bridges. The objectives listed below stem from the gaps identified in the literature review and the necessities that academia and regulatory bodies have identified. The following objectives focus on potential knowledge transfer from academic to industry practices:

a) **Evaluating the High-Speed Load Model's limits of validity** The HSLM is a necessary tool, according to the TSI (European Comission, 2002). However, its limits of validity, as defined in the EN 1991-2 (CEN, 2023b), may be inexact. The same norm is also lacking in defining some of its parameters, which can make it difficult to address this question. It is

also pertinent to check the model's readiness to encompass trains whose dimensions are already outside the predicted range, such as the ICE-4 (Glatz and Fink, 2021).

b) **Developing an expedited methodology to test load models** Using moving loads analysis, testing different load models on the same bridge model can be simplified using a linear superposition method.

c) **Developing an optimized methodology for probabilistic assessment** Foreseeing the need to work with strict reliability targets, a subset simulation application for railway bridges can be tested.

d) **Improving the safety factor for deck acceleration in ballasted bridges** The EN 1990 limiting value (CEN, 2023a) is based on a seemingly arbitrary safety factor, applied to a physical limit for ballast instability. The hypothesis that this factor is overestimated is tested, which can lead to higher permissible accelerations. To that end, it is crucial to clarify what constitutes upper and lower bound estimates of mass and stiffness, called for by the EN 1991-2.

e) **Testing the relation between acceleration and derailment in ballastless bridges** Without the physical phenomenon of ballast instability, the EN 1990 limit for ballastless bridges is seemingly based on the assumption that deck acceleration is an indicator of running safety. The hypothesis that this relation is inexistent is tested, which can lead to the removing this limit.

It is evidenced that the present thesis proposes to focus on issues found in the EN 1990 and the EN 1991-2, which constitute the three problems addressed in the core chapters of this document:

PROBLEM 1: "Identification of the HSLM limitations"

PROBLEM 2: "Enhanced safety factor for the deck acceleration limit on ballasted bridges"

PROBLEM 3: "Analysis of the deck acceleration criterion on ballastless track bridges"

1.4 OUTLINE OF THE DOCUMENT

This thesis comprises six chapters. The present introduction is followed by a literature review (Chapter 2) that goes over a multitude of normative criteria (Section 2.2). The same chapter includes reviews of high-speed railway bridge dynamics (Section 2.3) and of the probabilistic assessment of running safety on bridges (Section 2.4). A critical overview of existing studies in application to railway bridges allows the identification of the research gaps currently addressed.

The first problem, related to the limitations of the HSLM, is addressed in Chapter 3, with research questions being listed in Section 3.1. A methodology

to assess the limits of validity of the HSLM is proposed in Section 3.2 and a novel contribution to dynamic assessment methodologies (Single Load Linear Superposition) is given in Section 3.3. The thesis' first case study bridge (and general 2D modelling approach) is presented in Section 3.4, as well as variable sets to generate random train load models. The simulation results are shown in Section 3.5, both in terms of train signatures and dynamic analysis. The initial research questions are answered in Section 3.6.

The second problem, focusing on the safety factor for deck acceleration in ballasted bridges, constitutes Chapter 4. After listing research questions in Section 4.1, a methodology is presented in Section 4.2, in which a novel definition for a safety factor is proposed, based on critical speeds and design scenarios. Section 4.3 describes a subset simulation application, including the proposal of an efficient algorithm to determine critical speeds. Three more case study bridges are presented in Section 4.4. The algorithm is optimized in Section 4.5 and applied in Section 4.6.1. Deterministic scenarios for bridge design are proposed in Section 4.6.2, and the safety factors are given in Section 4.6.3. Finally, normative recommendations are given in Section 4.7, before answering the research questions in Section 4.8.

The third problem, concerning running safety on ballastless bridges, is the topic of Chapter 5, with its initial considerations (Section 5.1) listing research questions. The methodology in Section 5.2 analyses the deck acceleration levels in comparison to derailment criteria. 3D bridge models, as well as an adaptation of the HSLM, are presented in Section 5.3. The dynamic analyses results in Section 5.4 are complemented with a study of increased rail irregularities, differences in bridge rigidity, and the effect on riding comfort. Recommendations for the norm's revision are given in Section 5.5, after which the research questions are answered (Section 5.6).

Lastly, Chapter 6 summarizes the main findings (Section 6.1) and lists recommendations for further research (Section 6.2).

2 LITERATURE REVIEW

2.1 INITIAL CONSIDERATION

The design of civil engineering structures is governed by norms that ensure safe practices and standard construction. In many ways, these norms condition railway infrastructures, and railway bridges are no exception. In the case of high-speed railway bridges, their design must fulfil, among others, various safety and serviceability normative criteria related to the dynamic behaviour of the structure under railway traffic. Therefore, in addition to studying norms, a thorough evaluation of normative criteria must be built upon foundational knowledge of bridge dynamics and reliability analysis.

The present chapter is divided into three main parts. Firstly, in Section 2.2, European, Chinese, and Japanese normative criteria are presented, emphasising bridge deformation and vibration verifications. Several related studies are discussed, providing a critical overview. Fundamental aspects of railway bridge dynamics are detailed in the second part (Section 2.3), from design considerations to the modelling and analysis of the train-bridge dynamic system. Lastly, the third part (Section 2.4) describes different levels of probabilistic analysis and its applications to design norms and railway bridges. The concluding remarks in Section 2.5 point to the research opportunities that can be derived from the knowledge gaps.

2.2 NORMATIVE CRITERIA

Wherever railway networks are present, there are sets of rules that govern how the infrastructures are built and maintained and how the rolling stock can and cannot operate. These regulations, often with normative value, provide the foundation for assessing railway structures, not only in terms of their limit states but also concerning running safety and other matters such as passenger comfort.

There are distinct norms in different parts of the world, reflecting the specific regional needs of various networks and geographical constraints. Thus, the present section goes over the norms currently in use in Europe (Section 2.2.1), China (Section 2.2.2) and Japan (Section 2.2.3). Different derailment criteria are presented in Section 2.2.4, and a critical overview is provided in Section 2.2.5.

2.2.1 *European criteria*

The necessary verifications in European norms regarding railway bridges are presented in the EN 1990 (CEN, 2023a) (Annex A, Section A.2) and in the EN 1991-2 (CEN, 2023b). In this section, the criteria controlling track stability

are listed regarding deformation limits (Section 2.2.1.1) and vibration limits (Section 2.2.1.2).

2.2.1.1 *Bridge deformation*

In the vertical direction, the maximum deck displacement due to rail traffic is limited to ensure that any given track radius does not compromise running safety. For any span of length L, the EN 1990 limits this value to $L/600$. This value must be greater than the maximum displacement caused by the Load Model 71 (LM71) (from the EN 1991-2, representing the vertical action of normal traffic) and, if necessary, the maximum displacement due to Load Models SW/0 (in the case of continuous bridges) and SW/2 (representing heavy rail traffic). The LM71 and SW/0 models are presented in Section 2.3.1.

Regarding transversal deflection, the EN 1990 limits both the maximum horizontal rotation ($r_{\max}$) and maximum change of radius of curvature ($\theta_{h,\max}$) (listed on Table 2.1 for different speeds V). This rotation refers either to the angle at the end of the deck, θ_h, or the variation of rotation between adjacent spans, $\theta_{h1} + \theta_{h2}$ (illustrated in Figure 2.1). For a span of length L, with a transverse deflection of δ_h, the radius of curvature r is given by:

$$r = \frac{L^2}{8\delta_h} \tag{2.1}$$

To perform this verification, the structure must be considered with the characteristic loading of the LM71 or SW/0, as appropriate, multiplied by the dynamic factor (the same applies if designing with a real train) and classifying factor α. Additionally, nosing and centrifugal force, wind effects, and transverse temperature differential must also be taken into account.

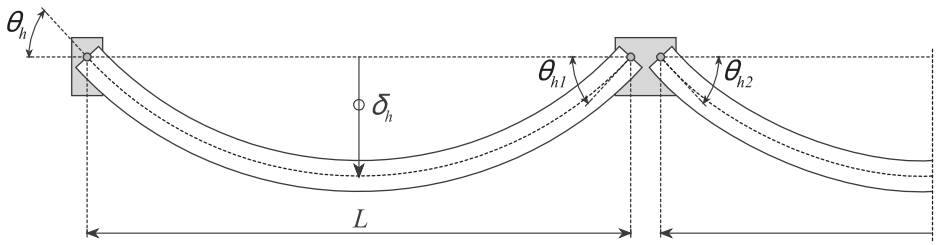

Figure 2.1: Transverse deflection (adapted from Montenegro et al. (2021)).

Furthermore, the EN 1990 limits the vertical and longitudinal displacements at the end of the deck on the upper surface, referring to the EN 1991-2. Even though these norms do not state additional limitations in the case of dynamic analysis being required, the French norm (SNCF, 1998) limits the deck's rotation θ (with a distance h (m) between the rail and the support) over an abutment:

$$\theta \leq \frac{2 \times 10^{-3}}{h} \tag{2.2}$$

and the relative rotation $\theta_1 + \theta_2$ between adjacent decks:

$$\theta_1 + \theta_2 \leq \frac{4 \times 10^{-3}}{h} \tag{2.3}$$

V (km/h)	$\theta_{h,\max}$ (radian)	$r_{\max}$	
		SINGLE DECK	MULTI-DECK BRIDGE
$V \leq 120$	0.0035	1700	3500
$120 < V \leq 200$	0.0020	6000	9500
$V > 200$	0.0015	14000	17500

Table 2.1: Maximum horizontal rotation and change of radius of curvature.

These displacement checks intend to limit rail and fastening system stress and avoid track instability. In the longitudinal direction, the relative displacement δ_h (Figure 2.2a and Figure 2.2b) due to traction and braking between decks or between a deck and an abutment is limited to 5 mm for continuously welded rails without expansion devices or 30 mm if rail expansion devices are present on both the deck's ends. An exception is made if the ballast layer presents a movement gap in addition to the rail expansion devices. In the same direction, but due to the LM71 (or SW/0, if applicable), the limiting value is 8 mm if considering the combined behaviour of both structure and track or 10 mm otherwise. In the vertical direction, the displacement δ_v (Figure 2.2c) caused by actions such as the LM71 (or SW/0) or unfavourable temperature variation is limited to 3 mm in lines with speeds up to 160 km/h or 2 mm otherwise.

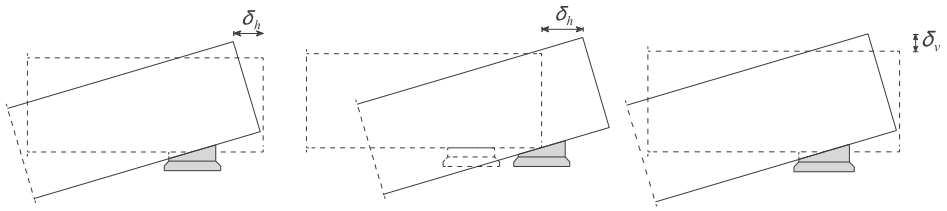

(a) (b) (c)

Figure 2.2: Displacement at the end of the deck. (a) Longitudinal (fixed support); (b) Longitudinal (guided support); (c) Vertical. (adapted from Montenegro et al. (2021))

The EN 1990 also limits the maximum twist for any given deck loaded with the LM71 (or SW/0 or SW/2), affected by the dynamic and classifying factors and the HSLM with centrifugal effects. Considering a track with gauge s of 1.435 m, the maximum twist t over a development of 3 m (depicted in Figure 2.3) is limited to the values presented in Table 2.2. The French norm (SNCF, 1998) has an additional limitation for speeds greater than 220 km/h of 1.2 mm/3 m. Given that this check relates only to twist due to traffic actions, the norm also states that the total twist (adding also twist that may already be present, like in the case of a transition curve) must not exceed 7.5 mm/3 m.

Deformation control is also used to assess passenger comfort indirectly. Even though the governing factor is the vertical acceleration measured inside the coach b_v (considered very good if lower than 1.0 m/s^2, good if lower than

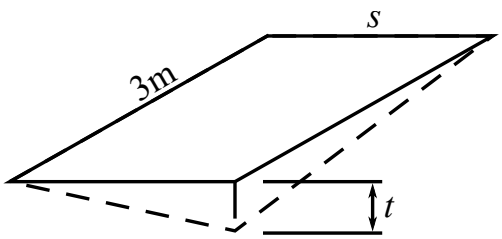

Figure 2.3: Deck twist (adapted from CEN (2023a)).

V (km/h)	t (mm/3 m)
$V \leq 120$	4.5
$120 < V \leq 200$	3.0
$V > 200$	1.5

Table 2.2: Maximum deck twist.

1.3 m/s^2 and acceptable if lower than 2.0 m/s^2), the EN 1990 offers a check of the maximum vertical deflection δ of the deck, along a track's axis, depending on the span L, running speed V, number of spans and their respective configuration. δ is calculated with the LM71 (multiplied by the appropriate dynamic factor and a classifying factor of 1) on a single track, even if multiple tracks are present. Figure 2.4 shows the maximum values for L/δ , considering 3 or more simply supported spans and a target b_v of 1 m/s^2. These values can be divided by b_v if the target is different and should be multiplied by 0.7 if the number of spans is inferior to 3 or by 0.9 if there are three or more continuous spans.

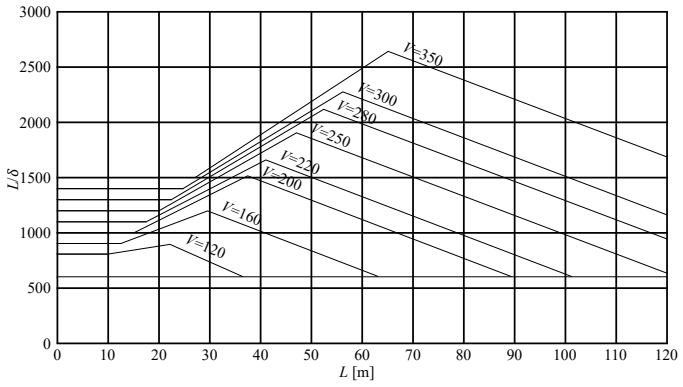

Figure 2.4: Maximum deflection for passenger comfort (adapted from CEN (2023a)).

2.2.1.2 *Bridge vibration*

The EN 1990 provides limits to the maximum vertical deck acceleration for ballasted and ballastless tracks (such as slab tracks). The former has to do with

preventing the loss of stability of the ballast layer, and the latter with avoiding the loss of wheel-rail contact. The limit values are, respectively, 3.5 m/s^2 (with the exception of a zone not exceeding 2 sleeper spacings that can go up to 5 m/s^2) and 5 m/s^2. To obtain the design acceleration, a dynamic analysis is needed (with real trains and, if applicable, the HSLM), and it should encompass modes with frequencies up to the maximum of 30 Hz, 1.5 times the first frequency of the considered element, or the third mode's frequency.

In ballasted tracks, the SNCF originally observed issues with the ballast layer in special test runs using the TGV train running at resonant speeds in bridges equipped with accelerometers. The problems that the SNCF identified (such as the formation of voids under the sleepers, loss of ballast compaction and particles, track alignment issues, and excessive concrete cracking) coincided with acceleration levels between 0.7 g and 0.8 g (ERRI D 214/RP 9, 1999). The limit value's definition was then conducted by the ERRI's technical committee D214 (ERRI D 214/RP 8, 1999). The experimental campaign, held at the German Federal Institute for Materials Research and Training (BAM), concerned a ballasted track (simulated by a 3 m steel box (Box A) filled with ballast and four embedded sleepers connected by rails) subjected to varying vertical acceleration amounts, whose frequencies ranged from 2 Hz to 20 Hz. These tests confirmed a previous investigation by the SNCF demonstrating that the ballast layer loses its interlocking capabilities when it experiences accelerations upwards of 0.7 g (Zacher and Baeßler, 2008). The fact that EN 1991-2 then provides a limit of ∼0,35 g for ballasted tracks is indicative of a safety factor of 2 (in ballastless tracks, the implied safety factor is also 2 since the limit is half the 1 g acceleration that could cause loss of wheel-rail contact). In fact, in ERRI D 214/RP 9 (1999), it is clearly stated:

> "From the results of the various tests and observed measurements of the behaviour of track and ballast on bridges subject to resonant loading it can be seen that adverse behaviour commences with deck accelerations of the order of 0.7 to 0.8 g. Applying a Factor of Safety of 2 results in a permitted maximum deck acceleration of 3.5 m/s^2 for ballasted track."

Zacher and Baeßler (2008) replicated these tests by devising an experiment in which a 1.05 m by 1.05 m steel box (Box B) was filled with ballast and an embedded sleeper and then subjected to vertical vibrations (with an extended frequency range up to 20 Hz), while measuring the acceleration in the box a_b and in the sleeper a_s. Figure 2.5 shows the transfer function between the ballast and the sleeper for both boxes. The tests measured simultaneously the sleeper settlement and its lateral displacement while being sensitive to the number of acceleration cycles. The measured transfer function is also compared to a numerical model, confirming that its maximum corresponds to 60 Hz. Additionally, the authors assessed the lateral resistance of the sleeper by measuring its lateral displacement when the test setup was subject to 500 vertical acceleration cycles. Figure 2.6 displays the tests' results, where each line represents a test with frequencies from 10 Hz to 60 Hz. The authors highlight the low displacements registered for acceleration values below 0.7 g and the

fact that the results are independent of the frequency. In another experiment, Baeßler (2008) measured the vertical and horizontal displacements in a test setup consisting of a sleeper, supported by ballast, subjected to a cyclical load between 10 kN and 50 kN, with a frequency of 1.5 Hz. Figure 2.7 shows the long-term effects of such loads, with a considerable increase after 250,000 cycles. In that scenario, the maximum measured acceleration was 4.9 g.

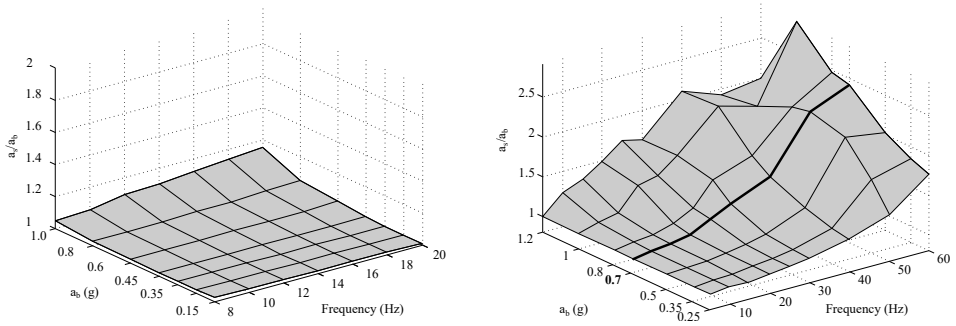

(a) (b)

Figure 2.5: Ballast transfer function. (a) Box A; (b) Box B. (adapted from Zacher and Baeßler (2008)).

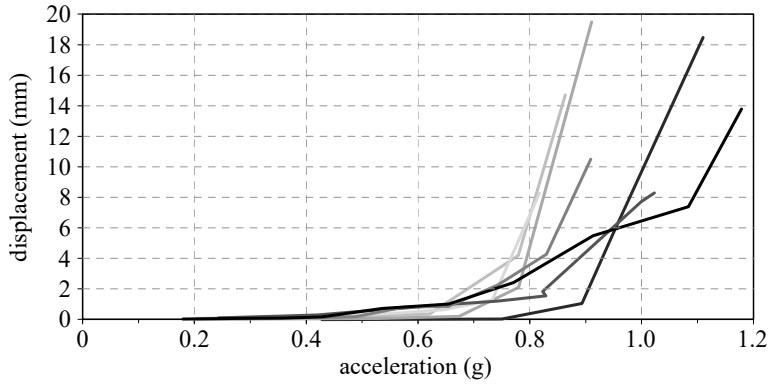

Figure 2.6: Sleeper lateral displacement (adapted from Zacher and Baeßler (2008)).

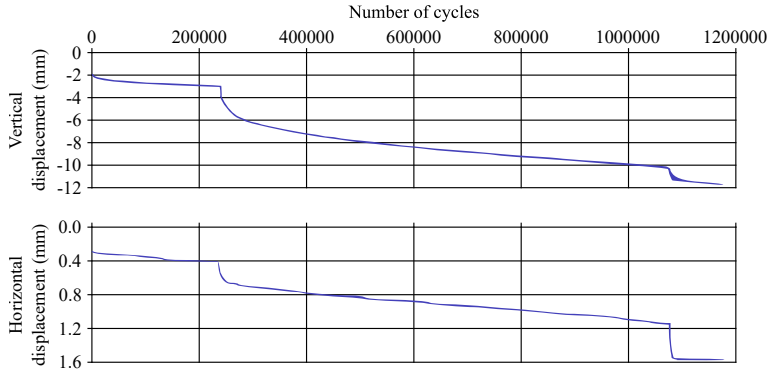

Figure 2.7: Long term sleeper displacement (adapted from Baeßler (2008)).

Zacher and Baeßler (2008) recommend that exceptionally, acceleration values above the current limits could be allowed for 10 vibration cycles, up to a maximum of 0.55 g for ballasted tracks and 0.75 g for ballastless tracks (it is also recommended that the dynamic analysis should be conducted with frequencies up to the minimum of 60 Hz or the third natural frequency of the considered member). These values originate from a safety factor of 1.3, the same as that used in Germany for soil loading capacity. Using a surrogate models methodology, Allahvirdizadeh et al. (2024a) find a safety factor of 1.38.

In the lateral direction, the only limit presented in the EN 1990 is that the first natural frequency of vibration in that direction should not be lower than 1.2 Hz. This restriction originated in the studies by ERRI D 181/RP 6 (1995) with the purpose of avoiding amplified dynamic responses in the trains due to the bridge's lateral frequency. However, it should be mentioned that in long, continuous structures, regardless of the lateral frequency being lower than 1.2 Hz, the associated wavelengths are much longer than the vehicles', circumventing the issue. For this reason, the current norm (CEN, 2023a) improves upon its previous version (CEN, 2005) by specifying that the limit applies to an evaluation for each span, disregarding lateral flexibility. Moreover, Montenegro et al. (2021) note that since this verification is due to the prevention of resonance between bridge and train, it is worthy of special attention in the case of structures with high-rise piers.

2.2.1.3 *High-Speed Load Model*

The European Commission's regulation on the Technical Specifications for Interoperability (TSI) for infrastructure (European Comission, 2002) states that railway bridges designed for speeds greater than 200 km/h, where a dynamic analysis is required, must consider the High-Speed Load Model (HSLM). This load model is presented in the EN 1991-2 as a means to "represent the loading from passenger trains at speeds exceeding 200 km/h".

The definition of an all-encompassing load model began with the ERRI's UNIV-A train. This load model took the properties of the Eurostar articulated train (with an individual axle load of 170 kN and a 3.5 m bogie wheelbase) and applied a coach length varying between 18 m and 27 m. The objective was to guarantee that the signature envelope of this model could cover the effects

caused by both articulated (Eurostar and Thalys 2) and conventional (ICE2 and ETR) trains. However, this model proved to be insufficient to cover the effects of the Virgin and Talgo trains (Marvillet and Tartary, 2003), namely for the excitation wavelengths λ of 24 m for the former and between 12.5 m and 14.0 m for the latter. This drawback led to the definition of a new set of 10 reference trains. These trains' signatures S_0 and their envelope can be seen in Figure 2.8, for wavelengths λ up to 30 m.

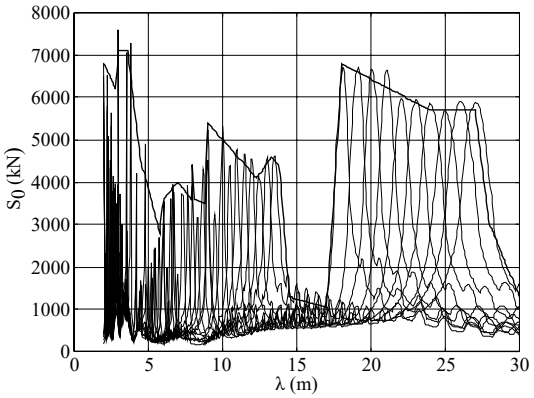

Figure 2.8: HSLM signatures and envelope (adapted from Marvillet and Tartary (2003)).

In the EN 1991-2, this set of load models is referred to as the HSLM-A (configured as illustrated in Figure 2.9). They are defined by the number of intermediate coaches N, coach length D, bogie axle spacing d and individual axle load P (listed in Table 2.3). Additionally, the EN 1991-2 presents the HSLM-B model for spans with less than 7 m (except for continuous or complex structures; regardless, the HSLM-B is also applicable if a complex structure has significant floor vibration modes), consisting of N point forces of 170 kN, with a regular spacing d.

UNIVERSAL TRAIN	N	D (m)	d (m)	P (kN)
A1	18	18	2.0	170
A2	17	19	3.5	200
A3	16	20	2.0	180
A4	15	21	3.0	190
A5	14	22	2.0	170
A6	13	23	2.0	180
A7	13	24	2.0	190
A8	12	25	2.5	190
A9	11	26	2.0	210
A10	11	27	2.0	210

Table 2.3: Properties of the HSLM-A Universal Trains.

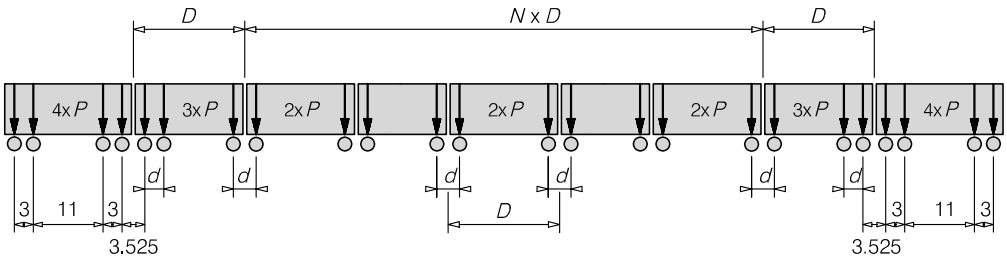

Figure 2.9: HSLM-A configuration (adapted from CEN (2023b)).

The limits of validity of the HSLM-A are listed in Annex E of the EN 1991-2 concerning articulated, conventional, and regular trains. The three types of trains are illustrated in Figure 2.10, where:

- P is the individual axle load;
- D is the coach length or distance between regularly repeating axles;
- d_{BA} is the distance between axles of the same bogie;
- d_{BS} is the distance between the centres of adjacent vehicle bogies;
- D_{IC} is the intermediate coach length (for regular trains);
- e_C is the distance between consecutive axles on the coupling of two train-sets (regular trains).

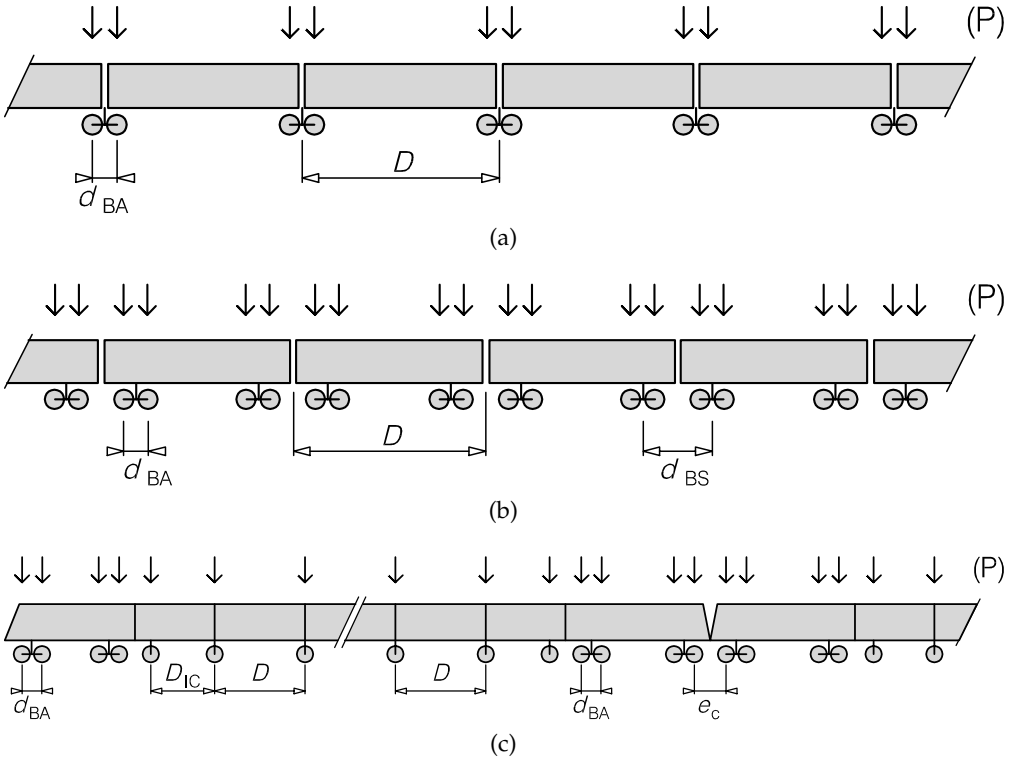

Figure 2.10: Train type configurations (adapted from CEN (2023b)). (a) articulated train; (b) conventional train; (c) regular train.

P is limited to 170 kN or, in the case of conventional trains, the lesser of 170 kN and the value that meets Equation 2.4, where P_{HSLMA}, d_{HSLMA} and D_{HSLMA} are the corresponding properties of the Universal Trains. This can be a single Universal Train if D matches an existing D_{HSLMA} or two Universal trains; otherwise, selecting the two whose D_{HSLMA} values are just greater and just lesser than D.

$$4P\cos\left(\frac{\pi d_{BS}}{D}\right)\cos\left(\frac{\pi d_{BA}}{D}\right) \leq 2P_{HSLMA}cos\left(\frac{\pi d_{HSLMA}}{D_{HSLMA}}\right) \tag{2.4}$$

D should be between 18 m and 27 m for articulated and conventional trains, or between 10 m and 14 m for regular trains, and d_{BA} should take a value between 2.5 m and 3.5 m. While the norm lacks in providing limits for d_{BS}, it states that D/d_{BA} and $(d_{BS} - d_{BA})/d_{BA}$ should not approach integer values and that d_{BS} must be in accordance with Equation 2.4. D_{IC} must be between 8 m and 11 m and e_C between 7 m and 10 m. In addition, there are also limits for total train weight (10000 kN), length (400 m) and unsprung axle mass (2 tonnes).

2.2.2 *Chinese criteria*

The normative criteria regarding high-speed railway bridges in China can be found in the Code for Design of High-Speed Railway, TB 10621-2014 (National Railway Administration of the People's Republic of China, 2014) and in the Code for Design on Railway Bridge and Culvert, TB 100022017 (National Railway Administration of the People's Republic of China, 2017)). The necessary checks are presented in terms of deformation control (Section 2.2.2.1) and dynamic response (Section 2.2.2.2).

2.2.2.1 *Bridge deformation control*

The numerical calculations necessary to perform deformation control checks are static analyses with dead and live loads, with the latter being the ZK model for high-speed railways. In the vertical direction, the Chinese norms limit the maximum deflection to a fraction of the span L, with variations according to design speed and span length. These values result from a series of dynamic analyses that accounted for the interaction between train and bridge in several scenarios with varying structural solutions and spans and, therefore, reflect safety criteria such as the derailment factor and wheel unloading. Table 2.4 lists the limiting values, considering a double-track, simply supported structure consisting of at least three spans, with up to 168 m (steel bridges) or 128 m spans (concrete bridges) and piers of no more than 50 m. For other configurations, the values must be multiplied by 1.1 (for three or more continuous spans), 1.4 (for two continuous spans or less than three simply supported spans), or 0.6 (for single tracks). In addition, Table 2.5 presents the maximum allowed displacement due to residual creep. As for lateral displacement of the deck, it is limited to $L/4000$ due to the combined effects of swaying, centrifugal force, wind and thermal loads.

	SPAN (m)		
SPEED (km/h)	$L \leq 40$	$40 < L \leq 80$	$L > 80$
250	L/1400	L/1400	L/1000
300	L/1500	L/1600	L/1100
350	L/1600	L/1900	L/1500

Table 2.4: Maximum vertical displacement.

	SPAN (m)	
TRACK TYPE	$L < 50$	$L > 50$
Ballasted	10 mm	10 mm
Ballastless	10 mm	min $\{20$ mm; $L/5000\}$

Table 2.5: Maximum vertical displacement due to residual creep.

In both vertical and lateral directions, checks are also made to ensure that a level of rotation is not exceeded at the beam ends. The maximum allowed values for vertical rotation are presented in Table 2.6, regarding rotation at the abutments θ, rotation between consecutive spans $\theta_1 + \theta_2$ and unsupported length L_h (m), as can be seen in Figure 2.11, for a structure subjected to live loads. Considering lateral rotation, the limit values are presented in Table 2.7 (the lateral displacement of the piers must be added to all effects listed for calculating lateral displacement). Since the piers and abutments are prone to experience settlements that can worsen the beam end rotation, these displacements are also limited according to the values in Table 2.8, and should be calculated using dead loads. It is worth noting that the limit values for deformation of ballastless tracks are more rigidly defined, and therefore, to assure smoothness in the track, the entirety of China's long-span high-speed bridges are ballasted (Hu et al., 2014). Lastly, the maximum allowed deck twist in the Chinese norms for high-speed traffic is 1.5 mm over a 3 m track development.

		MAX. ROTATION (rad)	
TRACK TYPE		θ	$\theta_1 + \theta_2$
Ballasted		2.0‰	4.0‰
Ballastless	if $L_h \leq 0.55$	1.5‰	3.0‰
Ballastless	if $0.55 < L_h \leq 0.75$	1.0‰	2.0‰

Table 2.6: Maximum vertical rotation.

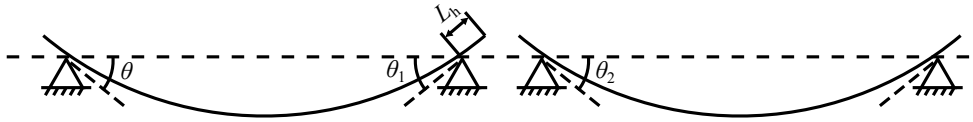

Figure 2.11: Vertical rotation reference (adapted from Montenegro et al. (2021)).

	SPAN (m)	
SPEED (km/h)	$L < 40$	$L > 40$
< 200	1.5‰ rad	1‰ rad
> 200	1‰ rad	1‰ rad

Table 2.7: Maximum lateral rotation.

	SETTLEMENT	
TRACK TYPE	Uniform	Differential between adjacent elements
Ballasted	30 mm	15 mm
Ballastless	20 mm	5 mm

Table 2.8: Maximum allowed settlement.

2.2.2.2 *Dynamic response*

The aforementioned Chinese norms call for specific dynamic analyses that consider train-bridge interaction (TBI). This analysis is only optional if considering a simply supported double-track box girder up to 32 m, a train measuring between 24 m and 26 m and a natural structural frequency limited by the values in Table 2.9. Otherwise, a full TBI analysis must be conducted, considering the real train that will operate on the bridge. Through these calculations, the following safety indices should be obtained (explained according to Lu and C. Cai (2020)):

- Derailment coefficient Y/Q: overall assessment of derailment safety;
- Wheel unloading rate $\Delta Q/Q$: derailment due to one-sided wheel load reduction;
- Wheelset lateral force ΣY: train's impact on railways;
- Lateral framework acceleration: train's lateral stability.

In this description, Y represents the wheel-rail lateral contact force, Q is the vertical contact force, and ΔQ is the wheel load reduction. Y/Q is limited to 0.8 and $\Delta Q/Q$ must be less than 0.6. The maximum value for ΣY is $10 + Q_0/3$, where Q_0 represents the static wheel load. The lateral framework acceleration must not exceed the threshold of 8 m/s^2 six consecutive times, considering a 0.5 Hz to 10 Hz band-pass filter.

	SPAN (m)		
SPEED (km/h)	20	24	32
250	$100/L$	$100/L$	$120/L$
300	$100/L$	$120/L$	$130/L$
350	$120/L$	$140/L$	$150/L$

Table 2.9: Natural frequency limit.

Considering the dynamic response of the deck, its acceleration is limited to 3.5 m/s^2 in ballasted tracks and 5.0 m/s^2 in ballastless tracks, with a 20 Hz low-pass filter.

2.2.3 *Japanese criteria*

The Japanese norms for high-speed railway bridges are stated in the Design Standard for Railway Structures (Railway Technical Research Institute, 2006). This section presents the considerations therein, in terms of ordinary (Section 2.2.3.1) and seismic conditions (Section 2.2.3.2). The Design Standard for Railway Structures uses deck displacement and rotation measurements as a metric for the various safety evaluations that it calls for, namely:

- δ, girder deflection caused by the passing vehicle;
- δ_r, alignment irregularities (vertical and lateral);
- θ_r, relative rotation to adjacent elements (vertical and lateral).

Even though this surpasses the need for dynamic analysis, the limit values the norm presents result from several such analyses and thereby provide indices that reflect safety concerns such as derailment factors and unloading rates. It is worth noting that the Japanese norms provide guidance towards the verification of track restorability, in addition to safety checks.

2.2.3.1 *Ordinary conditions*

Under ordinary conditions, δ, δ_r (in the vertical direction), and θ_r are respectively limited by the values in Table 2.10 (where L is the span length), Table 2.11, and Table 2.12, when considering high-speed traffic (in this case, the Shinkansen train). Concerning the verification of track restorability, both vertical and lateral δ_r and θ_r are conditioned according to Table 2.13. A track can, therefore, remain operable without repairs if these conditions are met.

	NUMBER OF SPANS		
SPEED (km/h)	Single span	Multi-span ($L < 70$ m)	Multi-span ($L > 70$ m)
260	$L/700$	$L/1200$	$L/1400$
260	$L/900$	$L/1500$	$L/1700$
260	$L/1100$	$L/1900$	$L/2000$

Table 2.10: δ limit values.

	SPAN (m)	
SPEED (km/h)	Single span	Multi-span
260	2.0 mm	3.0 mm
300	1.5 mm	2.5 mm
360	1.0 mm	2.0 mm

Table 2.11: Vertical δ_r limit values.

	SPAN (m)	
SPEED (km/h)	Vertical	Lateral
210	4.0	2.0
260	3.0	1.5 (parallel shift) 1.5 (folding)
300	2.5	1.0
360	2.0	1.0

Table 2.12: θ_r limit values ($\times 1/1000$).

		$\theta_r(\times 1/1000)$		δ_r (mm)	
DIRECTION	TRACK TYPE	50 N Rail	50 kg Rail	50 N Rail	60 kg Rail
Vertical	Slab track	3.5	3.0	3.0	2.0
	Ballast track	6.0	7.0	3.0	2.0
Horizontal	Slab track	4.0	4.0	2.0	2.0
	Ballast track	5.5	5.5	2.0	2.0

Table 2.13: Restorability limit values (ordinary conditions).

2.2.3.2 *Seismic conditions*

As for the verification of safety under seismic conditions, the norm provides guidance to limit the differential displacement of track surfaces and the lateral vibration displacement of the structure when subjected to Level-1 earthquake motion. The displacement limit values, regarding lateral θ_r and δ_r, are shown in Table 2.14. To evaluate the vibration limit, it is necessary to compute the Spectral Index (SI) to be compared to the norm's limits, which can be done by following the procedure presented by Luo (2005):

1. Calculate the equivalent natural period of the structure T_{eq} (s) and acceleration response by using an equivalent stiffness from a pushover analysis;
2. Obtain the response spectrum of velocity S_v, by applying the action from the first step;
3. Compute $SI = \int_{0.1}^{0.25} S_v(h,t)dT$ where S_v is a function of the damping ratio h and time.

4. Verify whether the obtained SI is lower than the norm's limiting values (Figure 2.12, where G^* is the ground classification):

$$\text{Limit } SI \text{ (mm)} = \begin{cases} 3 - 8500T_{eq} + 6650 & \text{if } T_{eq} < 0.3 \text{ s} \\ 4100 & \text{if } 0.3 \leq T_{eq} \leq 1.2 \text{ s} \\ 1375T_{eq} + 2450 & \text{if } T_{eq} > 1.2 \text{ s} \end{cases} \tag{2.5}$$

Track restorability under seismic conditions is assessed similarly to the ordinary conditions by evaluating vertical and lateral δ_r and θ_r. The limit values are presented in Table 2.15.

	Lateral θ_r ($\times 1/1000$)			
	Parallel Shift			
MAX. SPEED (km/h)	$L = 10$ m	$L = 10$ m	Folding	Lateral δ_r (mm)
130	7.0	7.0	8.0	14.0
160	6.0	6.0	6.0	12.0
210	5.5	3.5	4.0	10.0
260	5.0	3.0	3.5	8.0
300	4.5	2.5	3.0	7.0
360	4.0	2.0	2.0	6.0

Table 2.14: Displacement limit values (seismic conditions).

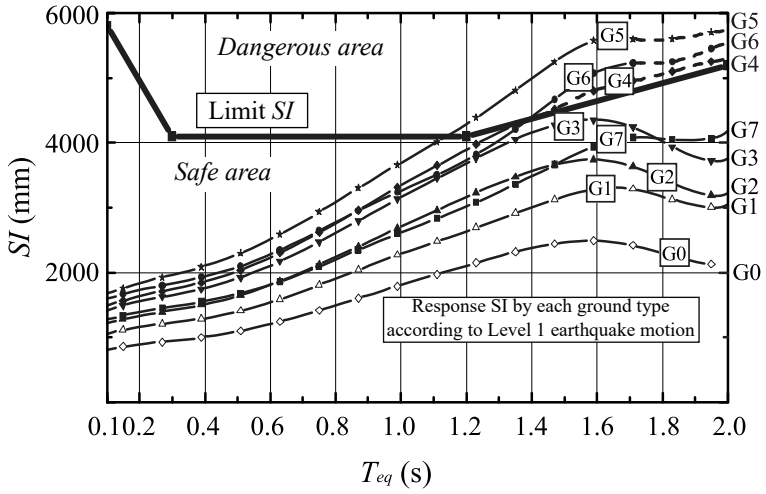

Figure 2.12: SI limit values (adapted from Railway Technical Research Institute (2006)).

		$\theta_r(\times 1/1000)$		δ_r (mm)	
DIRECTION	TRACK TYPE	50 N Rail	50 kg Rail	50 N Rail	60 kg Rail
Vertical	Slab track	5.0	3.5	4.5	3.5
	Ballast track	7.5	6.5	3.5	4.0
Horizontal	Slab track	6.0	6.0	2.0	2.0
	Ballast track	8.0	8.0	2.0	2.0

Table 2.15: Restorability limit values (seismic conditions).

2.2.4 *Derailment criteria based on wheel-rail contact forces*

The occurrence of derailment is a common concern in railway operations. In the design of railway bridges, the prevention of this phenomenon is mostly accounted for by employing indirect measures. In the previous sections, the presented deflection and vibration limits that are used to control running safety and passenger comfort are useful tools that conservatively contain the likelihood of derailment. In regular engineering practice, it is unreasonable to expect that more complex TTBI models are regularly used, which would allow for the explicit evaluation of derailment. These direct measures are based on the calculation of wheel-rail contact forces and the knowledge of derailment mechanisms, which can typically be divided into wheel flange climbing (Section 2.2.4.1), track panel shift (Section 2.2.4.2), gauge widening (Section 2.2.4.3), and wheel unloading (Section 2.2.4.4).

2.2.4.1 *Wheel flange climbing*

Wheel flange climbing is the mechanism by which the innermost part of a train's wheel describes a climbing movement over the rail's head. Since this can happen in the presence of significant lateral forces, the criteria that evaluate this mechanism are based on the ratio between lateral Y and vertical Q contact forces. The Nadal (1908) criterion evaluates the equilibrium of forces on the contact point between the flange of the wheel and the rail and can be expressed as a function of the normal contact F_n and lateral creep F_η forces, or of the angle γ and friction coefficient μ (Equation 2.6). In Europe, this criterion is limited to 0.8 by the TSI (European Comission, 2002). The same limit is present in the Chinese norm (National Railway Administration of the People's Republic of China, 2017) and in the Japanese norm (Railway Technical Research Institute, 2006) with the duration of 15 ms. In North America (AAR, 2015), it is limited to 1.0 for more than 50 ms or a distance of 3 feet.

$$\xi_N = \frac{Y}{Q} = \frac{\tan\gamma - \dfrac{F_\eta}{F_n}}{1 + \dfrac{F_\eta}{F_n}\tan\gamma} = \frac{\tan\gamma - \mu}{1 + \mu\tan\gamma} \tag{2.6}$$

The Weinstock (1984) criterion also compares lateral and vertical contact forces at the contact point, with the addition of considering both wheels (A and B) of the wheelset WS. The ratio in the flanging wheel is, therefore, given by the Nadal equation, while in the other wheel, it is equivalent to the friction coefficient since the contact point is usually at a low contact angle (Equation 2.7). This criterion is limited in North America to 1.5. Figure 2.13 illustrates the wheel flange climbing mechanism.

$$\xi_W = \sum_{WS} \frac{Y}{Q} = \frac{\tan \gamma_A - \mu_A}{1 + \mu_A \tan \gamma_A} + \mu_B \tag{2.7}$$

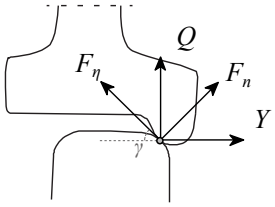

Figure 2.13: Wheel flange climbing.

2.2.4.2 *Track panel shift*

Track panel shift occurs when repeated lateral loads cause a displacement of the sleepers and rails in ballasted tracks, as represented in Figure 2.14. To prevent it, the Prud'homme (1967) criterion limits the lateral forces applied by the vehicle to the track. Since residual deformation is due to accumulated incremental deformation after each load application, limiting the loads above a given value is essential to maintain operating conditions. The limit of the sum of the lateral forces over both wheels of each wheelset is given as a function of the static load per wheel Q_0:

$$\xi_P = \sum_{WS} Y = 10 + \frac{2Q_0}{3} \tag{2.8}$$

This criterion is limited to 1.0 in Europe (European Comission, 2002), and it is comparable to the Chinese lateral force criterion presented in Section 2.2.2.2.

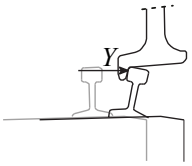

Figure 2.14: Track panel shift.

2.2.4.3 *Gauge widening*

Gauge widening can occur in the presence of large lateral deformations and can cause rail rollover, determined by the overturning moment calculated about

the pivot point on the external side of the base of the rail. Since, for this phenomenon, the torsional stiffness of the length of rail between wheels is significant, the criterion is calculated accounting for all wheels on a bogie by comparing the ratio between the sum of the lateral and vertical forces at each side of the bogie to the ratio between the rail's width d and height h:

$$\xi_R = \frac{\sum Y}{\sum Q} = \frac{d}{h} \tag{2.9}$$

The rail rollover criterion, represented in Figure 2.15, is limited in North America to 0.6 (AAR, 2015).

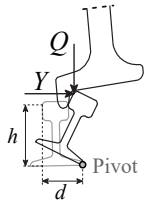

Figure 2.15: Rail rollover due to gauge widening.

2.2.4.4 *Wheel unloading*

The wheel unloading derailment mechanism concerns the loss of contact between wheel and rail and is evaluated via the ratio between the reduction of the vertical loads ΔQ and the static load in a wheelset as:

$$\xi_U = \frac{\Delta Q}{Q_0} = \frac{Q_0 - Q}{Q_0} = 1 - \frac{Q}{Q_0} \tag{2.10}$$

It can also be assessed for an entire bogie (comprising wheelsets i and j) as:

$$\xi_U = 1 - \frac{Q_i + Q_j}{2Q_0} \tag{2.11}$$

The wheel unloading index, illustrated in Figure 2.16, is generally limited in Europe to 0.9 (CEN, 2010), with a stricter limited 0.6 for twisted track conditions (CEN, 2016). The same value is presented in the Chinese norm (National Railway Administration of the People's Republic of China, 2017). A limit of 0.8 is given in Japan (Railway Technical Research Institute, 2006), and 0.9 in North America (AAR, 2015).

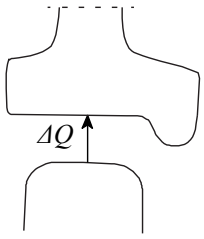

Figure 2.16: Wheel unloading.

Similarly, for situations with significant lateral loading, the overturning coefficient (limited to 0.8 by the Chinese norm (State Administration for Market

Regulation and Standardization Administration of PRC, 2019)) considers the ratio between the difference of the dynamic forces in the leeward Q_L and windward Q_W wheels and the static load:

$$\xi_{OT} = \frac{Q_L - Q_W}{Q_0} \tag{2.12}$$

2.2.5 *Critical overview and existing studies*

Based on the study of existing literature, the overview presented in this subsection is divided into three parts, corresponding to the problems identified in Section 1.3.

2.2.5.1 *Studies concerning the High-Speed Load Model*

The research needed to develop the HSLM began with the idea of separating the train's dynamic response from the bridge's response to facilitate the comparison of the dynamic loading effects caused by different trains. Such separation led to the definition of a train spectrum, in the form of a train signature, successfully obtained through the DER method (detailed in Section 2.3.3). Since the original ERRI report (ERRI D 214/RP 6, 1999), other authors continued to contribute to the development of this type of train spectra for analysing the structural response under railway traffic. Vestroni and Vidoli (2007) developed an approach based on a non-dimensional representation of the bridge response and Fourier transform of the train loads. Matsuoka et al. (2019) defined the train spectrum of the Italian ETR-1000 train to study the influence of local deck vibrations on assessing the maximum accelerations in a steel-composite high-speed railway bridge. Auersch (2021) studied resonant effects in railway bridges using modal force excitation techniques and train axle sequence spectra.

Although the HSLM continues to be the most complete load model currently available, some authors have recently discussed its limits of validity. One aspect is related to the fact that the current limits of validity of the HSLM defined in Annex E of EN 1991-2 are not broad enough to cover new and future trains. An example of such limitation is the recent introduction into service of the German high-speed train ICE4 with a coach length D of 28.75 m (Glatz and Fink, 2021), which has been reported to cause acceleration responses on railway bridges that are not covered by the HSLM envelope. In fact, Reiterer et al. (2021) observed that the ICE4 can produce vertical deck acceleration more than double that of the HSLM-A. In the 2023 version of the EN 1991-2 (CEN, 2023b), it is already noted that the HSLM may not cover some existing high-speed trains.

This problem is currently leading to new proposals for load models for railway dynamic analysis, in which two international consortia, one from the European project In2Track3 (Andersson et al., 2021; IN2TRACK3, 2021) and another from the German Federal Railway Authority (Reiterer et al., 2022, 2023; Vorwagner et al., 2021), stand out. Both works are focused on the definition of alternative load models (as exemplified in Figure 2.17 and Figure 2.18) that may cover the effects of recent and future trains characterized by design parameters outside the ranges of variations of the current HSLM, but that were

adopted by vehicle manufactures due to competition and economic reasons. In both approaches, the authors assess the train signature envelopes, as well as bridge responses obtained with dynamic numerical FEM analysis. Regarding the latter, Vorwagner et al. (2021) reported that their study covers a wide range of train configurations and bridge characteristics, totalling more than 17 million dynamic analyses. Such scale brings with it concerns about the computational cost associated with performing dynamic analysis on FE models.

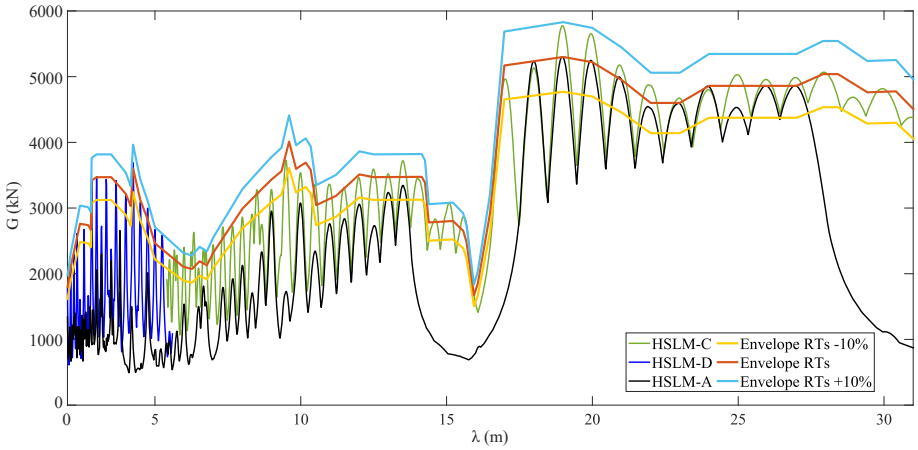

Figure 2.17: Train spectra G of the load models proposed by the In2Track3 project compared to real trains (RT), for $\xi = 0.5$ (adapted from IN2TRACK3 (2021)).

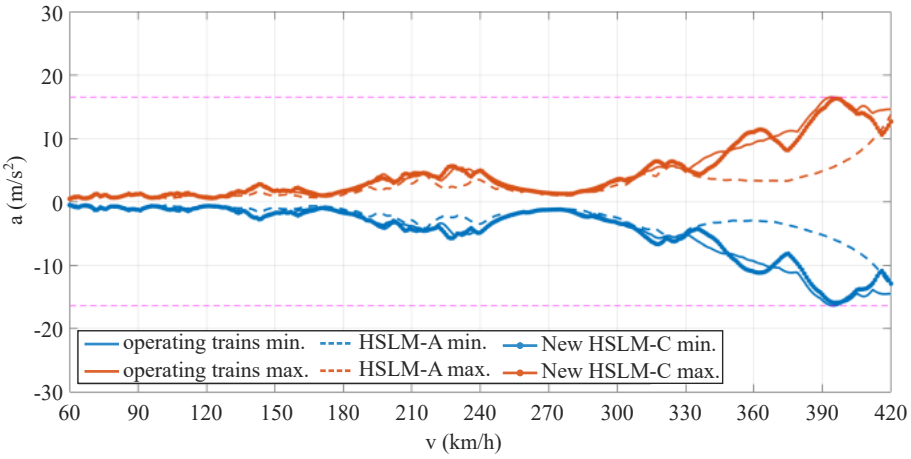

Figure 2.18: Acceleration results of a new load model proposed by the German Federal Railway Authority project on an existing concrete railway bridge (adapted from Reiterer et al. (2023)).

Envisaging the possibility of train manufacturers designing new high-speed trains that do not fully meet the geometric limits stipulated by Annex E due to economic reasons (avoiding short-length coaches, for example), Unterweger et al. (2017) investigated the most critical parameters that need to be fulfilled to ensure that the new vehicle is in line with the HSLM. The authors performed a study with eight fictitious trains characterized by limit values specified in Annex E, or slightly outside those limits ($D = 16$ m, $D = 28.5$ m, the spacing of

axles within a bogie $d_{BA} = 1.5$ m, and $d_{BA} = 5.4$ m), to assess which properties most contribute to larger responses in a set of single-span railway bridges. They proposed a methodology to identify the most critical bridges, in terms of length and first natural frequency, to reduce the number of bridges that must be investigated with the introduction in the network of new and more aggressive trains, and concluded that from all train parameters ranges stipulated by Annex E, only a few are critical for the bridge response, mainly the distance d_{BA}, for which a slight variation in its value may strongly affect the resonance phenomena.

Although the scientific community is already studying the lack of coverage of the HSLM regarding new trains, studies related to the HSLM's coverage of its current limits of validity (as well as addressing the lack of definition of some HSLM limiting parameters in the Eurocode) are still scarce in the literature. Museros et al. (2021) assessed the effects caused by articulated trains that fulfil the validity limits of the HSLM stipulated by Annex E of EN 1991-2. They concluded that the limitation that defines the ratio between the coach length D over the axle spacing within a bogie d_{BA} should be close to an integer value is not essential. In contrast, only very few cases of articulated trains defined within the premises of Annex E would lead to an exceedance in the vertical acceleration limits. However, the limits of validity regarding conventional or regular trains were outside this work's scope. Since only articulated trains were studied, no conclusions were drawn regarding the lack of information about the d_{BS} distance.

2.2.5.2 *Studies concerning the acceleration limit for ballasted tracks*

The presented European, Chinese, and Japanese norms share some common characteristics, mainly the reliance on indirect measurements as indicators for running safety. The displacement and acceleration levels that are calculated using load models are widely used for such assessments. However, it should be noted that the safety indices and limits in the norms themselves are the product of more complex analyses conducted during the base research for the regulations. Nevertheless, the Chinese norms specifically call for train-bridge interaction analysis in some cases while providing direct safety indices, for which the consideration of both vertical and lateral contact forces is required.

One common aspect in European and Chinese norms is the limit for deck acceleration (both use a 3.5 m/s^2 limit for ballasted tracks and a 5.0 m/s^2 limit for ballastless tracks, with the only difference being the considered frequency range). In the Eurocode, the limit for ballasted tracks is based on tests performed at BAM, commissioned by the ERRI (ERRI D 214/RP 8, 1999) to validate the then European pre-standard ENV. Though originally the reports were motivated by concerns expressed by the SNCF regarding ballast instability in test runs, around the same time, in the UK, Network Rail also commissioned tests to address permissible acceleration. Regarding those tests, Norris et al. (2003) suggest that instead of focusing on the unlikely loss of stability of an entire bridge deck, it is vital to understand how much of the ballast area becomes unstable. Still in the early 2000s, W. M. Zhai et al. (2004) proposed a new manner of numerically modelling the ballast layer, considering load distribution and shear effects.

This model was validated with full-scale field experiments, finding similar acceleration peaks greater than 4 g. Also, on full-scale tests, Rebelo et al. (2008) note that the vertical component of deck acceleration is a sensitive parameter, linking it with the potential instability of the ballast layer. The authors state that the ballast contributes intricately to the dynamic response, given its relation to the structure's stiffness and, consequently, to the resonance assessment. After calibrating FE models, the study concludes that there are relevant non-linear effects of structural stiffness, as well as of the ballast.

The importance of the ballast layer towards the overall bridge stiffness is addressed by Heiland et al. (2022) after noticing differences between experimental and numerical assessment of natural frequencies. Using models based on soil dynamics and a small-scale test rig (Figure 2.19), the researchers found no significant changes in bending frequencies related to varying ballast stiffness. Given the intrinsic uncertainty in modelling characteristics, Stollwitzer et al. (2024) developed a large-scale, 1:1 rig (Figure 2.20) to investigate ballast stiffness. The findings concerning track stability state that momentary excessive vibration levels have close to no effect on ballast instability. Even though isolated events can be innocuous, their cumulative effect can be relevant. This topic is addressed by Menezes (2024), considering the accumulated damage in a way analogue to fatigue analysis, allowing for an assessment of lifespan status concerning lateral track stability. The mitigation of the overall effects of acceleration is also a topic of study. A practical solution to control the amount of ballast bed vibration is the usage of ballast mats, which have also been tested on bridges (Hou et al., 2022).

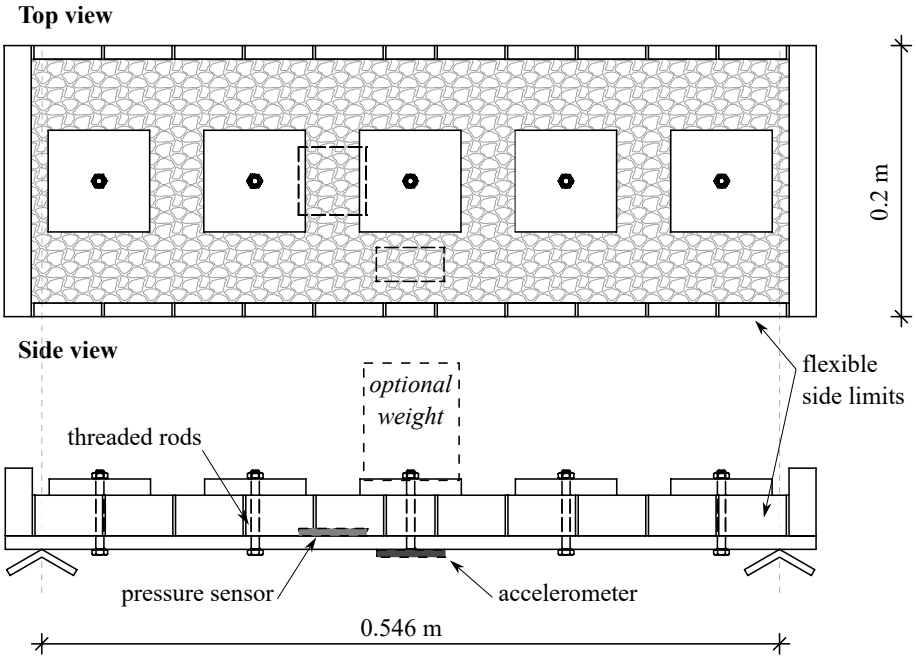

Figure 2.19: Small-scale test rig with ballast layer (adapted from Heiland et al. (2022)).

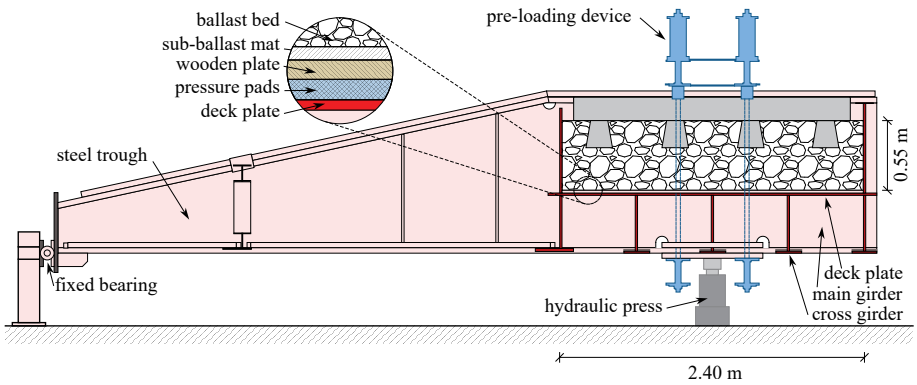

Figure 2.20: Large-scale test rig with ballast layer and sleepers (adapted from Stollwitzer et al. (2024)).

2.2.5.3 *Studies concerning the acceleration limit for ballastless tracks*

The acceleration limit for ballastless tracks is likely based on the assumption that a train wheel may detach from the rail when the deck experiences accelerations upwards of 1 g. Comparing this value to the limit inscribed in the norm suggests that a safety factor 2.0 was adopted to guarantee a safety margin (similar to what happened with ballasted tracks). However, as Zacher and Baeßler (2008) note, the ballastless track's limit had not been proofed either numerically or experimentally. In fact, the validity of such a margin was not originally based upon a probabilistic method, which has led to the proposal of alternatives (such as the study by Allahvirdizadeh et al. (2022), whose computational model is shown in Figure 2.21) and studies that give a certain percentage allowance over the limit (Moliner et al., 2017).

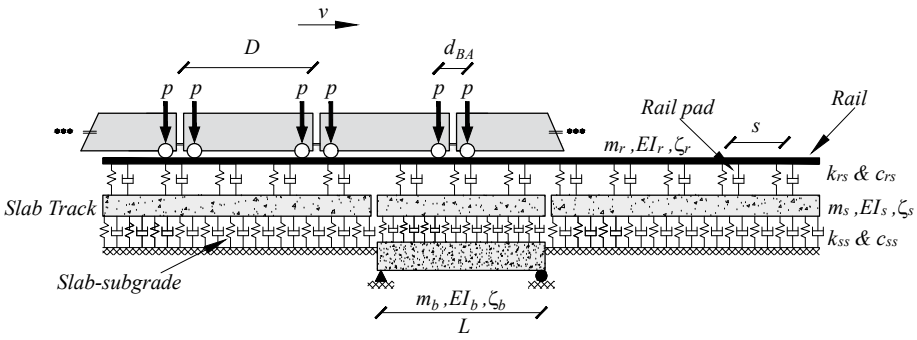

Figure 2.21: Train-bridge model, with reference to span L, spacing s, running speed v, linear mass, rigidity, and damping of the beam (m_b, EI_b, ζ_b), slab (m_s, EI_s, ζ_s), and rails (m_r, EI_r, ζ_r), stiffness and damping of the subgrade (k_{ss}, c_{ss}) and pads (k_{rs}, c_{rs}), coach length D, axle distance d_{BA} and axle load p (adapted from Allahvirdizadeh et al. (2022)).

While the limit for ballasted tracks is connected with a physically assessed phenomenon, the limit for ballastless (or slab) tracks is seemingly based on the assumption that a train running on a bridge experiencing accelerations upwards of 1 g is at risk. Yet, preliminary studies by Arvidsson et al. (2018) showed that, for the particular case of non-ballasted bridges, when the deck acceleration reaches 1 g, it does not necessarily lead to wheel detachments, i.e.

the fact that a point is subjected to 1 g acceleration does not imply the lifting of the entire train's mass. Therefore, it is essential to define recommendations to define a more accurate design criterion based on advanced Train-Track-Bridge Interaction TTBI simulations that can explicitly assess the risk of derailment and ensure traffic safety. On the influence exerted by the track itself, it is noted by Yang and Yau (2017) (whose train-bridge model can be seen in Figure 2.22) that neglecting the rails can lead to an underestimation of results at high speeds, while X. Cai et al. (2016) point out the connection between the level of track irregularities and derailment coefficient.

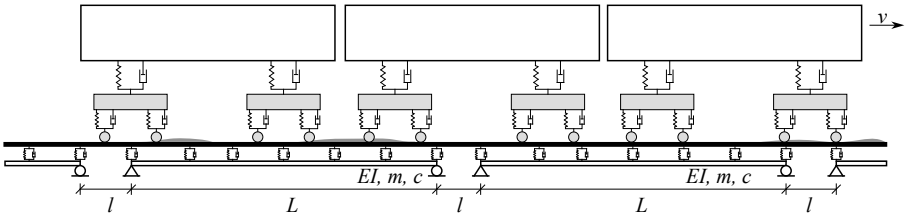

Figure 2.22: Train-bridge model, with reference to span L, gap l, running speed v and rigidity, linear mass, and damping of the beam (EI, m, c) (adapted from Yang and Yau (2017)).

Other studies on the performance of high-speed ballastless track bridges have focused on dynamic assessment, such as Yang and Yau (2017), finding deck accelerations above the normative limit on shorter spans. Contributions have also been made to the evaluation of deck acceleration, with Matsuoka et al. (2019) and Yotsui et al. (2024) focusing on the effects of local deck vibrations, or García-Macías and Martínez-Castro (2020) and Museros et al. (2013) proposing faster computational methods. Different authors have also approached the safety of ballastless bridges under seismic actions (Cao et al., 2021; L. Chen and Jiang, 2013; Y. Chen et al., 2023; Liu et al., 2021), while the previously mentioned research by Arvidsson et al. (2018) did not consider the lateral dynamics in the train-bridge interaction analysis, focusing solely on vertical dynamics. Other studies on ballastless bridges addressed the issues caused by settlement in subgrade-bridge transition zones (H. Chen et al., 2014; He et al., 2018) and running comfort (Lai et al., 2022).

2.3 HIGH-SPEED RAILWAY BRIDGE DYNAMICS

High-speed railway bridges are civil engineering structures that present particular dynamic characteristics, starting with the nature of their loading. Trains are themselves structures with their own dynamic properties, running over and at the same time interacting with a bridge. Railway bridges and viaducts are also especially prone to the occurrence of resonance phenomena due to the impact of the axle loads and their regular, repetitive cadence. As such, special considerations are made regarding this possibility. The present section goes over normative requirements regarding the dynamic analysis of railway bridges (Section 2.3.1), before going over the steps needed to conduct them

(Section 2.3.2). In Section 2.3.3, an overview of simplified spectral methods, moving loads analysis, and interaction analysis is shown.

2.3.1 *Design considerations regarding dynamic effects on high-speed railway bridges*

There are regulatory demands that consider dynamic effects at different levels when designing or assessing an HSR bridge. At the simplest level, European norms provide dynamic factors affecting static analyses. Nonetheless, there are situations where the norm calls for dynamic analyses.

2.3.1.1 *Static analysis and dynamic factors*

To perform static analyses, the EN 1991-2 (CEN, 2023b) defines several load models to represent different traffic actions, from unloaded trains to heavy traffic. For high-speed lines, it is worth mentioning the Load Model 71 (LM71), the Load Model SW/0 and the High-Speed Load Model (HSLM).

The LM71 exists to represent the static vertical effects of normal traffic. Regarding characteristic values, it consists of four point loads of 250 kN and a distributed load of 80 kN/m, arranged as shown in Figure 2.23a. These values are to be affected by a classifying factor $\alpha \in \{0.75, 0.83, 0.91, 1.00, 1.21, 1.33, 1.46\}$, whose value may differ in different countries. Similarly, the EN 1991-2 defines the Load Model SW/0 to represent the vertical static effects on continuous structures, illustrated in Figure 2.23b. Additionally, the norm presents the HSLM, which is a set of train configurations intended to represent the actions of high-speed passenger trains (with speeds greater than 200 km/h). A detailed explanation of this load model can be found in Section 2.2.1.3.

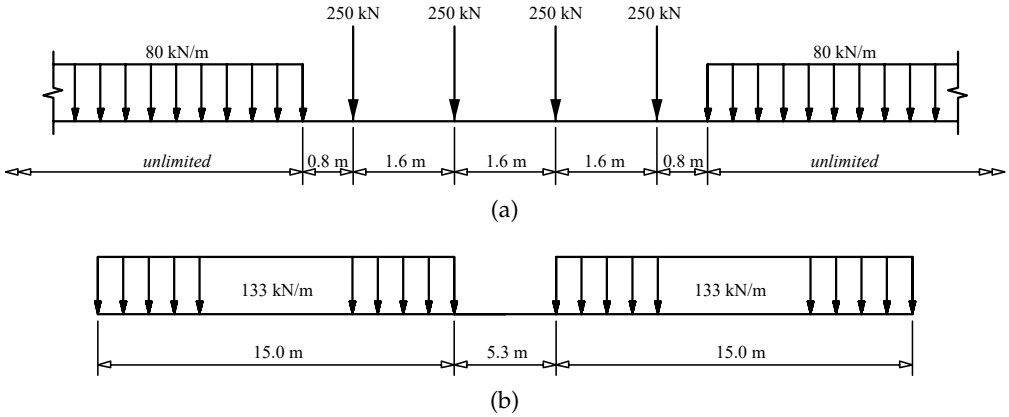

Figure 2.23: EN 1991-2 Load models (adapted from CEN (2023b)). (a) LM71; (b) SW/0.

Furthermore, the EN 1991-2 is sensitive to the dynamic repercussions caused by moving traffic on bridges, naming inertial response, resonance, and varying wheel loads as influential effects. It also lists the governing factors for dynamic effects: traffic speed, span length, track irregularities, vehicle mass and imperfections, support regularity, track components and structural mass, frequencies, and damping. To account for some of the added effects due to dynamic action, the EN 1991-2 defines the dynamic factor Φ, although it should be noted that

it does not cover resonance effects. This factor, to be applied to the LM71 and SW/0, can either take the value of Φ_2 (Equation 2.13) or Φ_3 (Equation 2.14), whether the track has careful or standard maintenance, respectively. In Equation 2.13 and Equation 2.14, L_Φ (m) is the determinant length, and its definition is dependent on the physical properties of the structural element in the analysis.

$$\Phi_2 = \frac{1.44}{\sqrt{L_\Phi} - 0.2} + 0.82 \qquad (1.00 \leq \Phi_2 \leq 1.67) \tag{2.13}$$

$$\Phi_3 = \frac{2.16}{\sqrt{L_\Phi} - 0.2} + 0.73 \qquad (1.00 \leq \Phi_2 \leq 2.00) \tag{2.14}$$

If real trains (or the HSLM) are being considered for calculation, Annex C of the EN 1991-2 indicates the dynamic factor $1 + \varphi$. This factor can either take the value of $1 + \varphi' + 0.5\varphi''$ or $1 + \varphi' + 0.5\varphi''$ for tracks of careful or standard maintenance, respectively. As with the previously discussed factor, the validity is limited to non-resonant phenomena. Equation 2.15 gives the part of the dynamic actor that represents the dynamic amplification due to traffic, and Equation 2.17 stands for the part that accounts for the effect of track and wheel irregularities. In these equations, v is the maximum speed (m/s), and n_0 corresponds to the bridge's first natural bending frequency (Hz).

$$\varphi' = \begin{cases} \dfrac{K}{1 - K + K^4} & \text{if } K < 0.76 \\ 1.325 & \text{if } K \geq 0.76 \end{cases} \tag{2.15}$$

where

$$K = \frac{v}{2L_\Phi \times n_0} \tag{2.16}$$

$$\varphi'' = \frac{\alpha}{100}\left[56e^{-\left(\frac{L_\Phi}{10}\right)^2} + 50\left(\frac{L_\Phi n_0}{20} - 1\right)e^{-\left(\frac{L_\Phi}{20}\right)^2}\right] \geq 0 \tag{2.17}$$

with

$$\alpha = \begin{cases} \dfrac{v}{22} & \text{if } v \leq 0.76\text{m/s} \\ 1 & \text{if } v > 0.76\text{m/s} \end{cases} \tag{2.18}$$

The factors' applicability is conditioned by the lower (Equation 2.19) and upper (Equation 2.20) limits of n_0.

$$n_0 \geq \begin{cases} \dfrac{80}{L_\Phi} & \text{if } 4\text{ m} \leq L_\Phi \leq 20\text{ m} \\ 23.58L_\Phi^{-0.592} & \text{if } 20\text{ m} \leq L_\Phi \leq 100\text{ m} \end{cases} \tag{2.19}$$

$$n_0 \leq 94.76L_\Phi^{-0.748} \tag{2.20}$$

2.3.1.2 *Dynamic analysis requirements*

To determine whether a dynamic analysis is required, the EN 1991-2 presents a flowchart, reproduced in Figure 2.24. The decision process depends on the maximum line speed V (km/h), span L (m), first natural frequencies for bending n_0 (Hz) and torsion n_T (Hz), and maximum nominal speed v (m/s). The notes on the flowchart refer to the following considerations:

a) The EN 1991-2 considers as a "simple structure" a simply supported bridge whose performance is similar to that of a beam or simple plate;

b) Mandatory dynamic analysis if a real train operates at a resonant speed;

c) φ'_{dyn} represents the dynamic enhancement for real trains;

d) Only if complying with EN 1990 (CEN, 2023a) limits;

e) Only if $V \leq 200$ km/h;

f) If n_0 exceeds Equation 2.20, dynamic analysis follows the norm's Annex C;

g) Ig n_0 is below Equation 2.19, dynamic analysis follows the norm's Section 8.4.6.

If a dynamic analysis must be conducted, the load models to adopt are the HSLM (Section 2.2.1.3) (in order to comply with the interoperability requirements) and the load configurations of any real trains planned to be employed on the line the bridge is located in. The European Rail Research Institute's (ERRI) technical committee D214 lists the properties of 7 real trains in Annex E of its report RP9 (ERRI D 214/RP 9, 1999). An overview of this data can be consulted in Table 2.16, where N is the number of axles, L_t (m) is the total length of the train, P (kN) is the most frequent axle load and d (m) is the distance between regularly spaced axle groups. The train types can either be articulated (double axle bogies shared by adjacent cars), conventional (two independent double axle bogies per car) or regular (single axle bogies shared by adjacent cars) (see Figure 2.10).

TRAIN	TYPE	N	L_t	P	d
ETR Y500	Conventional	48	295.7	120	26.1
Eurostar 373	Articulated	48	386.67	170	18.7
ICE2	Conventional	56	350.52	112	26.4
Talgo AV2	Regular	40	356.05	170	13.14
TGV Atlantique	Articulated	60	468.14	170	18.7
Thalys 2	Articulated	52	393.34	170	18.7
Virgin	Conventional	44	258.7	170	23.9

Table 2.16: Properties of the real trains for moving loads analysis (adapted from ERRI D 214/RP 9 (1999))

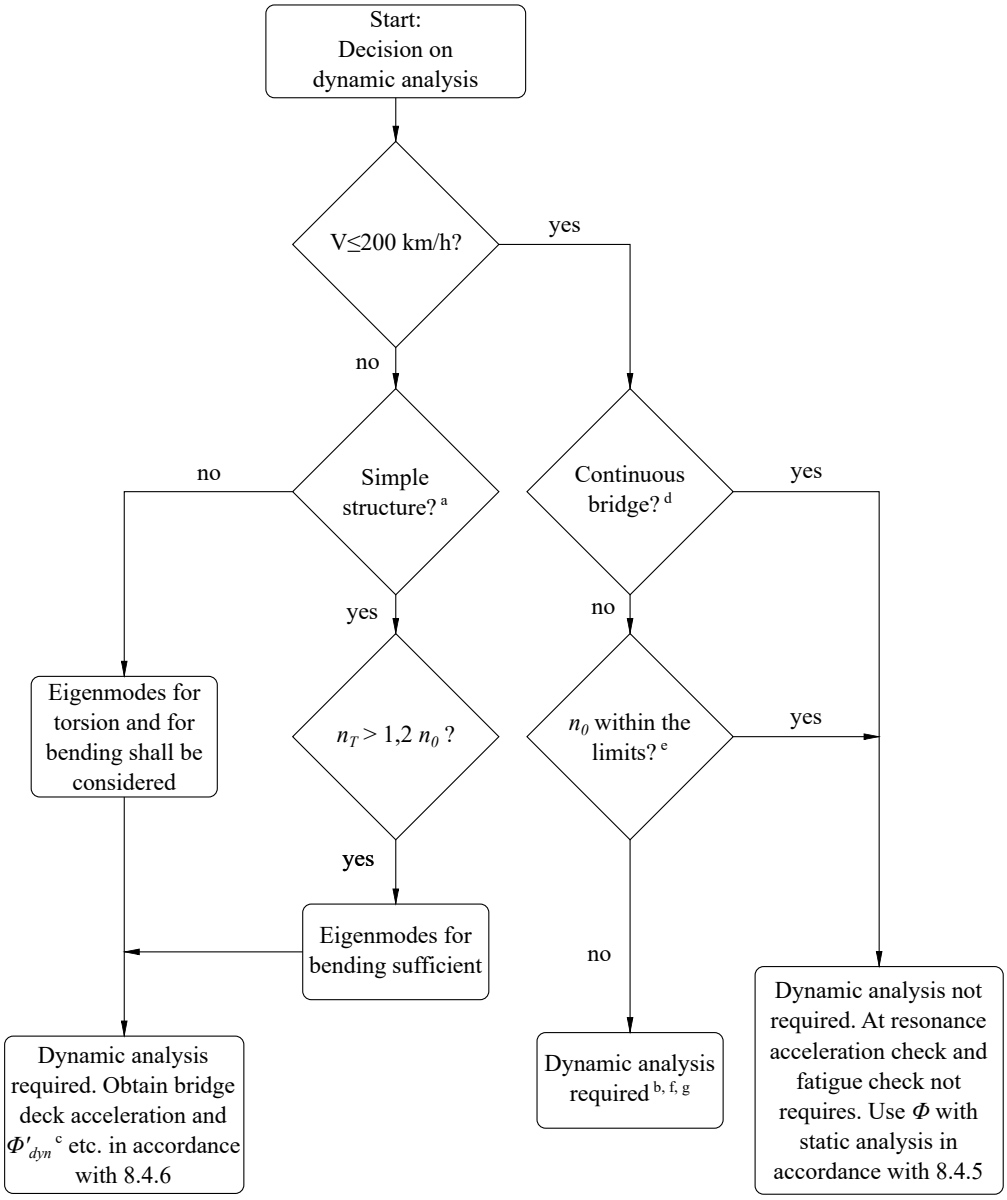

Figure 2.24: Flowchart to determine the need for dynamic analysis (adapted from CEN (2023b)).

2.3.2 *The bridge-train dynamic system*

In its most complex form, a railway bridge subjected to a moving train can be thought of as a system comprising two structures that interact dynamically with each other. Below, the steps necessary to perform dynamic analyses on such structures are presented, from the modelling requirements that are needed to account for the formulation and methods to solve the dynamic equations that derive from it.

2.3.2.1 *Modelling the dynamic system*

To conduct a dynamic analysis, the dynamic system must be modelled in a way that accurately reproduces its behaviour while at the same time aiming at being computationally efficient. Both parts (train and bridge) are themselves dynamic systems. Therefore, the complexity and level of detail associated with these models can vary substantially depending on the needed analysis type, ranging from the simpler moving loads to the more complex vehicle-structure interaction. Notwithstanding, the EN 1991-2 enumerates a few requirements to take into consideration.

Regarding loading, it is stated that the running speed range must be considered in a range from 40 m/s up to 1.2 times the maximum line speed at the site. The norm also warns that the speed steps should be closer together around resonant speeds v_i, which for simple structures can be estimated by:

$$v_i = n_0 \lambda_i \tag{2.21}$$

where n_0 is the first bending frequency and λ_i (m) is the excitation wavelength, given as the ratio between the regular spacing of axle groups d (m) and an integer $i \in \{1, 2, 3, 4\}$.

As for the bridge, the norm defines a lower bound estimate of critical damping ξ (%), which can be seen in Table 2.17 (where L (m) is the span), given that this parameter greatly conditions the dynamic response at resonant speeds. These values encompass the results of several experimental assessment campaigns performed in situ on service phase bridges (ERRI D 214/RP 9, 1999).

BRIDGE TYPE	$L < 20$ m	$L \geq 20$ m
Steel and composite	$0.5 + 0.125(20 - L)$	0.5
Prestressed concrete	$1.0 + 0.07(20 - L)$	1.0
Filler beam and reinforced concrete	$1.5 + 0.07(20 - L)$	1.5

Table 2.17: Lower limit of critical damping ξ (%).

Furthermore, it is stated that the bridge's mass must be considered in two distinct ways. In one scenario, the mass must be set to a lower bound estimate, which produces the maximum acceleration values. In the other scenario, the mass is set to its upper bound estimate to correspond to the lowest resonant speeds.

Regarding the estimation of stiffness, the norm determines that it must be lower-bounded in order to avoid overestimating the bridge's natural frequency and, consequently, the resonant speeds. The aforementioned considerations can be promptly incorporated into numerical analyses, such as those recurring to the Finite Element Method (FEM).

Moreover, a separate model must be made to represent the train accurately. According to ERRI D 214/RP 9 (1999), each car of a conventional train can be represented as consisting of a car body (with mass M_c and rotational inertia I_c), two double axle bogies (with mass M_b and rotational inertia I_b) and four wheel-sets (with mass M_ws). The connection between the car and the bogies (secondary suspension) is represented by two spring-dashpot sets (with stiffness K_s and damping coefficient c_s). Similarly, the connection between the bogies and the wheel-sets (primary suspension) comprises four spring-dashpot sets (with stiffness K_p and damping coefficient c_p). As stated by Calçada (1995), the stiffness of the wheel-rail connection K_h can be represented by:

$$K_h = \frac{3}{2} c_h^{2/3} F^{1/3} \tag{2.22}$$

where F is the static axle load and c_h is a constant that depends on the wheel's radius and usage. A representation of these variables can be seen in Figure 2.25, where D, d_{BA} and d_{BS} are the lengths presented in Section 2.2.1.3.

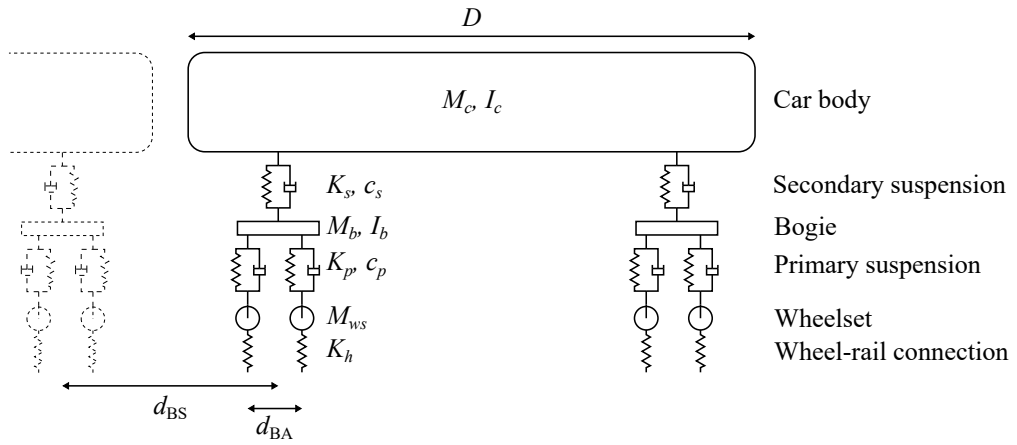

Figure 2.25: Single vehicle model representation (adapted from ERRI D 214/RP 9 (1999)).

2.3.2.2 *Formulating the dynamic problem*

Considering the train loads as a set of moving loads $\mathcal{F}(t)$ applied externally to the bridge, the dynamic problem can be seen as an equilibrium between these and the inertial, damping, and elastic forces, respectively $\mathcal{F}_i(t)$, $\mathcal{F}_d(t)$ and $\mathcal{F}_e(t)$, in any given moment of time t:

$$\mathcal{F}_i(t) + \mathcal{F}_d(t) + \mathcal{F}_e(t) = \mathcal{F}(t) \tag{2.23}$$

Given the structure's displacement vector $u(t)$ and its mass, damping, and stiffness matrices (respectively $\mathcal{M}$, $\mathcal{C}$, and $\mathcal{K}$), the dynamic equation can be rewritten as:

$$\mathcal{M}\ddot{u}(t) + \mathcal{C}\dot{u}(t) + \mathcal{K}u(t) = \mathcal{F}(t) \tag{2.24}$$

Clough and Penzien (1975) define a Rayleigh damping matrix as a linear combination of the mass and stiffness matrices, with the constants c_1 and c_2:

$$\mathcal{C} = c_1\mathcal{M} + c_2\mathcal{K} \tag{2.25}$$

For a structure whose i-th and j-th vibration mode's angular frequencies are ω_i and ω_j, with damping coefficients ξ_i and ξ_j, c_1 and c_2 can be given by:

$$\begin{Bmatrix} c_1 \\ c_2 \end{Bmatrix} = 2\frac{\omega_i\omega_j}{\omega_j^2 - \omega_i^2} \begin{bmatrix} \omega_j & -\omega_i \\ -\frac{1}{\omega_j} & \frac{1}{\omega_i} \end{bmatrix} \begin{Bmatrix} \xi_i \\ \xi_j \end{Bmatrix} \tag{2.26}$$

2.3.2.3 *Solving the dynamic problem*

Regardless of the complexity employed in modelling the train and bridge system (whether 2D or 3D, moving loads or vehicle-structure interaction), the differential dynamic equations that govern the problem need to be solved for each instant of time.

One available approach is the Newmark method (Newmark, 1959), which uses direct integration to solve the differential dynamic equations, depending on two parameters, γ and β. While the former weighs how the initial and final acceleration values influence the velocity, the latter does it in relation to displacement (Rocha, 2015). Given the displacement, velocity, and acceleration at an instant t, and assuming that the acceleration varies linearly, the equations at instant $t + \Delta t$ can be written as:

$$\dot{u}_{t+\Delta t} = \dot{u} + (1-\gamma)\ddot{u}_t\Delta t + \gamma\ddot{u}_{t+\Delta t}\Delta t \tag{2.27}$$

$$u_{t+\Delta t} = u_t + \dot{u}_t\Delta t + \left(\frac{1}{2} - \beta\right)\ddot{u}\Delta t^2 + \beta\ddot{u}_{t+\Delta t}\Delta t^2 \tag{2.28}$$

giving

$$\mathcal{M}\ddot{u}(t+\Delta t) + \mathcal{C}\dot{u}(t+\Delta t) + \mathcal{K}u(t+\Delta t) = F(t+\Delta t) \tag{2.29}$$

This method is unconditionally stable for:

$$\gamma > \frac{1}{2} \tag{2.30}$$

and its maximum stability occurs if:

$$\beta = \frac{\gamma + 1/2}{4} \tag{2.31}$$

If $\gamma = 1/2$ and $\beta = 1/4$, the method is second-order accurate and is known as the constant average acceleration method.

The method's sensitivity to the chosen time-step value is an important aspect to consider. For a maximum considered frequency of f_{max} (Hz), maximum number of modes n, maximum train speed v_{max} (m/s) and bridge span L (m), ERRI D 214/RP 9 (1999) states that the time increment Δt (s) should be taken as:

$$\Delta t = \min \left\{ \frac{1}{8 f_{\max}}; \frac{L}{4 n v_{\max}} \right\} \tag{2.32}$$

Another popular approach is the modal superposition method (Chopra, 1995), which translates the dynamic problem into a representation of itself using modal coordinates, standing for the contribution of each vibration mode to the total response. This idea works by using a set of uncoupled dynamic equations with a single unknown each, which is the modal coordinate y. Considering the N mode shapes φ, a structure's free vibration can be described as:

$$\sum_{i=1}^{N} \varphi_n y_i \tag{2.33}$$

Given that a mode's vibration, whose natural frequency is ω can be described by:

$$y_n(t) = A_n \cos \omega_n + B_n \sin \omega_n \tag{2.34}$$

the time variation of the structure's displacement can be obtained through:

$$u(t) = \varphi_n(y_n(t)) \tag{2.35}$$

which gives:

$$\left[\mathcal{K} - \omega_n^2 \mathcal{M}\right] \varphi_n = 0 \tag{2.36}$$

Aside from the null solution, this equation translates a problem of eigenvalues, existing N real solutions for ω_n^2. To each mode corresponds a natural frequency ω_n and a mode shape φ_n.

It is worth noting that there is orthogonality between any two modes, which allows for constructing a vectorial (rather than geometrical) modal space. Knowing this characteristic, it is possible to verify that any matrix being multiplied on the left by a transposed modal vector and to the right by a different modal vector results in a scalar 0. Taking the mass matrix $\mathcal{M}$ as an example, and two distinct modes n and m:

$$\varphi_n^T \mathcal{M} \varphi_m = 0 \tag{2.37}$$

As such, it is possible to obtain the scalars M_n, C_n and K_n, known respectively as the generalized mass, damping, and stiffness for mode n by using (again taking $\mathcal{M}$ as an example):

$$M_n = \varphi_n^T \mathcal{M} \varphi_n \tag{2.38}$$

Consequently, the uncoupled equation takes the form of:

$$M_n \ddot{y}_n + C_n \dot{y}_n + K_n \, y_n = F_n(t) \tag{2.39}$$

which produces N equations each with the single unknown y_n:

$$\ddot{y}_n + 2\xi_i \omega_n \dot{y} + \omega_n^2 y_n = \frac{F_n(t)}{M_n} \tag{2.40}$$

This method has the computational advantage of allowing a structure's dynamic response to be characterized with a finite number of modes, which can be selected through a preliminary analysis. Depending on the model's complexity, the first few vibration modes may be sufficient to calculate the response accurately, given a train's dynamic load.

2.3.3 *Dynamic analysis methodologies*

Knowing the aforementioned methodologies, an accurate depiction of the dynamic effects of a train running on a bridge is attainable. Considering the train's model as a moving set of point loads often suffices for normative verification of limit states, such as the maximum allowed deck acceleration. Nevertheless, obtaining other quantities like the car body acceleration (for the assessment of passenger comfort) or the variations in the wheel-rail contact forces (to evaluate derailment risk) depends on a more complex analysis that takes into consideration the interaction between the two dynamic systems (train and structure). As such, the numerical models needed for such analyses must represent all relevant dynamic properties, including the track's components: rails, rail pads, sleepers, ballast, or slab. On the other direction of complexity, there are methodologies that rapidly, even if crudely, assess the dynamic response of railway bridges and that are useful for quick comparisons.

2.3.3.1 *Spectral methods*

The present section addresses two common simplified methodologies described in ERRI D 214/RP 9 (1999): Decomposition of Excitation at Resonance (DER) and Residual Influence Line (RIL).

The DER method, introduced in ERRI D 214/RP 6 (1999) is applicable to single span bridges under the cumulative conditions that:

- inertial interaction is ignored;
- only the first vibration mode is considered;
- the response is decomposed into a Fourier series, retaining only the resonance term;
- the results are independent of time.

Using this method, the maximum mid-span acceleration $\ddot{y}$ can be estimated as a product of a constant factor C_t, a function for the influence line $A(\cdot)$, and the train spectrum $G(\cdot)$:

$$\ddot{y} \leq C_t A \left(\frac{L}{\lambda} \right) G(\lambda) \tag{2.41}$$

where λ is the wavelength of the excitation. For a bridge with a first modal frequency of f_0, generalized stiffness K, span L, and linear mass m, the constant factor C_t is given by:

$$C_t = \frac{8\pi f_0^2}{K} = \frac{8}{mL\pi} \tag{2.42}$$

and the influence line function $A(\cdot)$ by:

$$A\left(\frac{L}{\lambda}\right) = \left| \frac{\cos\left(\frac{\pi L}{\lambda}\right)}{\left(\frac{2L}{\lambda}\right)^2 - 1} \right| \tag{2.43}$$

Considering a train load model consisting of n loads, where each load number k at a coordinate x_k has a value P_k, on a bridge with a damping ratio ξ, its spectrum $G(\cdot)$ is given by:

$$G(\lambda) \cong \max_{i=1,n-1} \frac{1}{\xi x_i} \left[\sqrt{\left(\sum_{k=0}^{i} P_k \cos\left(\frac{2\pi x_k}{\lambda}\right)\right)^2 + \left(\sum_{k=0}^{i} P_k \sin\left(\frac{2\pi x_k}{\lambda}\right)\right)^2} \left(1 - e^{-2\pi\xi \frac{x_i}{\lambda}}\right) \right] \tag{2.44}$$

There are known limitations of the DER method, namely due to:

- the influence of high wavelengths and short trains on the resonance criteria;
- values of zero of the influence line;
- overestimation of the response for high damping coefficients.

Nonetheless, the method can also be used to approximate the maximum mid-span displacement y, given the first angular frequency ω_0 and the static displacement given by the train loads y_{stat}, as:

$$y \cong y_{stat} + \frac{\ddot{y}_{max}}{\omega_0^2} \tag{2.45}$$

One major aspect of the application of this method is that it introduces the concept of train signature. Since the train spectrum does not allow for an assessment of the train effect separate from the bridge response due to its dependence on the damping coefficient, the train signature $S_0(\lambda)$ is the result of:

$$S_0(\lambda) = \lim_{\xi \to 0} G(\lambda) \tag{2.46}$$

which is given by:

$$S_0(\lambda) \cong \max_{i=1,n-1} \frac{1}{\xi x_i} \left[\sqrt{\left(\sum_{k=0}^{i} P_k \cos\left(\frac{2\pi x_k}{\lambda} \right) \right)^2 + \left(\sum_{k=0}^{i} P_k \sin\left(\frac{2\pi x_k}{\lambda} \right) \right)^2} \right] \tag{2.47}$$

The signatures allow for fast comparisons between the effects of different trains. Knowing the signatures of trains in operation on a given line, a new train can be deemed either apt or inapt for running on that line simply by comparing the signature of the new vehicle to the existing trains' signatures.

The RIL method is applicable to simply supported spans with bridge-like behaviour and is better suited for non-resonant speeds. It is based on the assumption that trains are substantially lengthier than bridges and that the dynamic response is greater as the train's final load leaves the bridge.

Similarly to the DER method, the RIL method estimates the maximum deck acceleration as:

$$\ddot{y}_{max} = C_a A(r) G(\lambda) \tag{2.48}$$

and the maximum displacement as:

$$y_{max} = C_d A(r) G(\lambda) \tag{2.49}$$

where the constant term for acceleration is:

$$C_a = \frac{1}{M} \tag{2.50}$$

and for displacement:

$$C_d = \frac{1}{M\omega_0^2} \tag{2.51}$$

A parameter r can be defined depending on the train's speed v and a bridge's span L and first natural frequency n_0:

$$r = \frac{v}{L n_0} \tag{2.52}$$

A dynamic response factor, independent of the train, can be defined as:

$$A(r) = \frac{1}{1-r^2} \sqrt{e^{-2\xi\frac{\pi}{r}} + 1 + 2\cos\left(\frac{\pi}{r}\right) e^{-2\xi\frac{\pi}{r}}} \tag{2.53}$$

The factor that incorporates the accumulation of the loads' effects $G(\lambda)$ is given as:

$$G(\lambda) = \max_{i=1,n-1} \left[\left(\sum_{k=0}^{i} P_k \cos\left(2\pi \frac{x_1 - x_k}{\lambda} \right) e^{-2\pi\xi\frac{x_1 - x_k}{\lambda}} \right)^2 + \left(\sum_{k=0}^{i} P_k \sin\left(2\pi \frac{x_1 - x_k}{\lambda} \right) e^{-2\pi\xi\frac{x_1 - x_k}{\lambda}} \right)^2 \right]^{1/2} \tag{2.54}$$

This method's limitations include an underestimation of acceleration for $\lambda < (2L/3)$, an underestimation of mid-span displacement (since it does not account for the active vibration phase) and an overall overestimation of results for certain λ values if a trains' power car axles are considerably heavier than the remainder.

2.3.3.2 *Moving loads*

In a finite elements model, more than knowing the position of each point load at any given moment, it is necessary to obtain the equivalent nodal loads on the path intended for a load to travel in. To do so, Albuquerque (2008) formulates a methodology to condense all equivalent nodal forces in a matrix $\mathcal{P}$. This begins by determining the total time t_t (s) needed for a train's load model with length L_t (m) to completely move across a bridge with a span L (m), starting in a position Y_t (m) before the bridge, at speed v (m/s):

$$t_t = \frac{L + L_t + |Y_t|}{v} \tag{2.55}$$

The number of steps m needed for an analysis with a time-step Δt (s) is given by:

$$m = \frac{t_t}{\Delta t} + 1 \tag{2.56}$$

and the first column of $\mathcal{P}$ can be filled with the values corresponding to each time increment:

$$\mathcal{P}_{i,1} = t_i = (i-1)\Delta T \qquad , \qquad i \in \{1, 2, \ldots, m\} \tag{2.57}$$

A vector $\mathcal{Y}_j$ can then be filled with the longitudinal coordinate of each node j that comprises the rail, i.e. the load path. A k number of vectors $\mathcal{Y}_k$ must also be employed, containing the position of each load at a time t. Then, a form function is applied to determine the nodal force N in a node j at instant t if the nodes have a regular spacing a:

$$\mathcal{N}_{j,k}(t) = \begin{cases} \dfrac{1}{2} \times \dfrac{Y_k(t) - Y_{j-2}}{2 \times a} & \text{if } Y_{j-2} \leq Y_k(t) \leq Y_j \\ \dfrac{1}{2} - \dfrac{1}{2} \times \dfrac{Y_k(t) - Y_j}{2 \times a} & \text{if } Y_j \leq Y_k(t) \leq Y_{j+2} \\ 0 & \text{if } Y_k \notin \left[Y_{j-2}; Y_{j+2}\right] \end{cases} \tag{2.58}$$

As such, the total load over each node j at a given time t_i can be calculated by:

$$F_j(T_i) = \sum_k N_{j,k}(t_i) \times F_k \tag{2.59}$$

and matrix $\mathcal{P}$ can be filled with every nodal load, giving:

$$\mathcal{P} = \begin{bmatrix} 0 & F_1(0) & \cdots & F_n(0) \\ \vdots & \vdots & \ddots & \vdots \\ t_i & F_1(t_i) & \cdots & F_n(t_i) \\ \vdots & \vdots & \ddots & \vdots \\ t_n & F_1(t_m) & \cdots & F_n(t_m) \end{bmatrix} \tag{2.60}$$

2.3.3.3 *Train-Bridge Interaction*

ITERATIVE METHOD To implement a methodology where the vehicle interacts with the structure, both the train and bridge dynamic subsystems can be considered as independent structures. The dynamic equations can be written as in the following equation, where the indices b and t denote the bridge and train, respectively:

$$\begin{bmatrix} \mathcal{M}_b & 0 \\ 0 & \mathcal{M}_t \end{bmatrix} \begin{bmatrix} \ddot{u}_b(t) \\ \ddot{u}_t(t) \end{bmatrix} + \begin{bmatrix} \mathcal{C}_b & 0 \\ 0 & \mathcal{C}_t \end{bmatrix} \begin{bmatrix} \dot{u}_b(t) \\ \dot{u}_t(t) \end{bmatrix} + \begin{bmatrix} \mathcal{K}_b & 0 \\ 0 & \mathcal{K}_t \end{bmatrix} \begin{bmatrix} u_b(t) \\ u_t(t) \end{bmatrix} = \begin{bmatrix} \mathcal{F}_b(t) \\ \mathcal{F}_t(t) \end{bmatrix} \tag{2.61}$$

During the analysis period, the systems are made compatible and are calculated through time by direct integration. In this iterative process, it is necessary to ensure that there is contact between the two structures, i.e. that the displacements and forces are at equilibrium. To do so, the following steps can be applied (Calçada, 1995) on each iteration i:

1. The load $P^i(t)$ is applied to the bridge, consisting of the static load from the vehicle weight and the dynamic load resulting from the previous iteration, such that $P^i(t) = P_{stat} + P^{i-1}_{dyn}(t)$. On the first iteration, the dynamic component of the load can take the value of $P_{dyn}(t - \Delta t)$. These loads are converted into equivalent loads, and the structure can be solved, obtaining the displacements $u^i_b(t)$;

2. Simultaneously, the train's model is subjected to support settlements $u^i_t(t) = u^{i-1}_b(t)$. The resulting support reactions $P^i_t(t)$ are the dynamic forces $P^i_{dyn}(t)$ for the next iteration;

3. Finally, the results are checked for convergence using the ratio:

$$\frac{P^i_{dyn}(t) - P^{i-1}_{dyn}(t)}{P^{i-1}_{dyn}(t)} \tag{2.62}$$

If the resulting value is greater than a preset tolerance, at least one more iteration is needed, and i is incremented. Otherwise, convergence has been achieved, and t is incremented by Δt. Even though this example is limited to vertical interaction scenarios, it allows for the modelling of track irregularities in that direction by altering a residual part of the rail nodes' coordinates.

DIRECT METHOD The direct method (Neves et al., 2012) introduces additional compatibility equations relating the displacement of the train's contact nodes to the bridge's nodal displacements. Thus, track irregularities can be accounted for, and FEM can be employed to model both bridge and train. In the direct method, the governing equations constitute a single system, where the unknowns are the displacements and contact forces. The following system can be solved via a factorization algorithm rather than iteratively:

$$\begin{bmatrix} \mathcal{K}_{FF} & \mathcal{D}_{FX} \\ \mathcal{H}_{XF} & 0 \end{bmatrix} \begin{bmatrix} \mathcal{A}^{t+\Delta t}_f \\ \mathcal{X}^{t+\Delta t} \end{bmatrix} = \begin{bmatrix} \mathcal{F}_f \\ \mathcal{R} \end{bmatrix} \tag{2.63}$$

where $\mathcal{K}_{FF}$ is the effective stiffness matrix of the train-bridge system, $\mathcal{D}_{FX}$ and $\mathcal{H}_{XF}$ are transformation matrices relating the local CS of the contact forces with the global CS, $\mathcal{A}_f^{t+\Delta t}$ and $\mathcal{X}^{t+\Delta t}$ are, respectively, the nodal displacements and contact forces, $\mathcal{F}_f$ is the loads vector and $\mathcal{R}$ is the rail irregularities vector.

LATERAL WHEEL-RAIL CONTACT METHOD The approaches hitherto described do not account for lateral contact forces between wheel and rail, nor for the possibility of loss of contact. To overcome these limitations, more complex methodologies divide the contact problem into its geometrical, normal, and tangential parts.

The geometrical problem consists of knowing which contact points exist between the wheel and the rail. In an "offline contact search" approach (Antolín et al., 2012; Bozzone et al., 2011; Olmos and Astiz, 2018), the contact surface's geometry and possible contact points are calculated in advance and stored in a lookup table. This approach is based on the assumption that the wheels are rigid bodies that contact the rail in a single point and that contact occurs at all times. The outputs are the relative displacements and rotation, which are used for the dynamic analysis and for further calculation of the normal and tangential parts. This procedure is cost-effective, albeit neglecting the possible penetration between wheel and rail. Contrarily, in "online contact search", the contact points are determined iteratively at every instant of the dynamic analysis. The wheels' flexibility can be considered, as well as wheel-rail penetration effects, which allows multiple contact points to exist. Contact points can be predicted and calculated by searching pairs of nodes (G. Chen and W.M., 2004; Shabana et al., 2005) or by describing the surfaces with functions (Falomi et al., 2011; Marques et al., 2020; Pombo et al., 2007; Sugiyama and Suda, 2009).

The normal contact problem consists of determining the surface contact area and the existing stress. Hertz (1882) contact theory assumes an elliptical contact area and a semi-elliptical stress distribution, assuming frictionless surfaces, constant curvature, and no plastic deformations. For more detailed analyses, Multi-Hertzian contact assumes an area constituted of multiple ellipses (Pascal, 1993), and Non-Hertzian contact assumes a semi-elliptical stress distribution in the direction of movement (Ayasse and Chollet, 2005; Meymand et al., 2016; Quost et al., 2006).

The tangential contact consists of evaluating tangential forces due to rolling friction, i.e. from the fact that between two contacting bodies, there may exist, simultaneously, areas adhering and others slipping. This problem was extensively addressed by Kalker (1967, 1979, 1982), who developed the CONTACT and FASTSIM programmes, and, ultimately, the USETAB lookup tables (Kalker, 1996). This method of storing precalculated tangential creep forces, for the purpose of being interpolated during the dynamic analysis, is also used by Montenegro et al. (2015).

2.4 PROBABILISTIC ASSESSMENT OF RUNNING SAFETY ON BRIDGES

The assessment of safety of civil engineering structures, whether regarding ultimate or serviceability limit states, is seldom a matter of plainly calculating

actions to be compared to documented resistance values. Instead, a level or threshold of risk is involved, which is a consequence of the uncertainties associated with the problem. These relate to material's physical and geometrical properties, modelling approximations and simplifications, statistical estimations and even human factors (Henriques, 1998). The inclusion of uncertainty into structural safety assessment can be categorized into the following levels:

- Level 0: Purely deterministic
- Level I: Semi-probabilistic
- Level II: Reliability techniques
- Level III: Simulation methods

2.4.1 *Purely deterministic and semi-probabilistic methodologies*

Historically, structural safety assessment frameworks reflect the accumulated generational knowledge of past building endeavours. This empirical way of work was the accepted way of work until the 19th century, when a scientific method came into existence, combining the novel understanding of elasticity theory with some added safety. Designating the action's stress component by σ_E and the material's limit of resistance by σ_R, and considering a safety factor γ_S this deterministic relation can be given as:

$$\sigma_E \leq \frac{\sigma_R}{\gamma_S} \tag{2.64}$$

This method depended on practical experience to dictate its safety factors. It relied on assumptions on the elastic behaviour of structures that do not necessarily translate into an accurate analysis of failure. The need to mitigate the shortcomings on both the action and resistance sides lead to the development of a semi-probabilistic approach.

The semi-probabilistic approach includes using characteristic values and partial safety factors, which translate the uncertainty of the assessment problem. Considering that the load effects follow a normal distribution $E \sim N\left(\mu_E, \sigma_E^2\right)$, the characteristic load E_k corresponds generally to the 95th percentile, so that:

$$\begin{aligned} \Phi\left(\frac{E_k - \mu_E}{\sigma_E}\right) = 0.95 \quad &\Leftrightarrow \\ \Leftrightarrow \quad \frac{E_k - \mu_E}{\sigma_E} \approx 1.645 \quad &\Leftrightarrow \\ \Leftrightarrow \quad E_k \approx \mu_E + 1.645\sigma_E \end{aligned} \tag{2.65}$$

where Φ is the standard normal distribution (zero mean and unit variance). Similarly, the characteristic value of resistance is usually given as the 5th percentile of its normal distribution $R \sim N\left(\mu_R, \sigma_R^2\right)$ as:

$$\begin{aligned} & \Phi\left(-\frac{\mu_k - R_k}{\sigma_R}\right) = 0.05 && \Leftrightarrow \\ \Leftrightarrow \quad & \frac{\mu_R - R_k}{\sigma_R} \approx 1.645 && \Leftrightarrow \\ \Leftrightarrow \quad & R_k \approx \mu_E - 1.645\sigma_E \end{aligned} \tag{2.66}$$

A schematic representation of these distributions and values can be seen in Figure 2.26. The aforementioned partial safety factors are the product of higher-detailed probabilistic analysis and can differ according to the considered limit state. For load effects and resistance, they are designated, respectively, as γ_E and γ_R. The verification of safety is a comparison between the design values of the actions' effects, E_d, and resistance, R_d:

$$\begin{aligned} & E_d \leq R_d && \Leftrightarrow \\ \Leftrightarrow \quad & \gamma_E E_k \leq \frac{R_k}{\gamma_R} \end{aligned} \tag{2.67}$$

Although incorporating the statistical variability of parameters as an indicator of safety, this methodology does not accurately describe structural behaviour near failure. Probabilistic methodologies are presented in the following sections to include the risk assessment of actual failure.

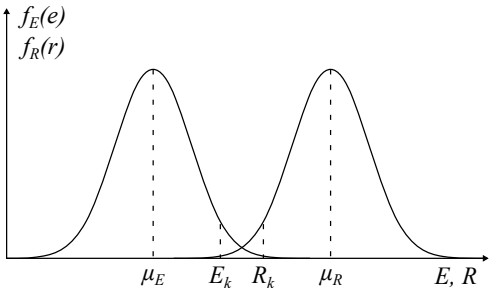

Figure 2.26: Characteristic and mean values of actions and resistance.

2.4.2 *Probabilistic methodologies*

2.4.2.1 *Analytical approach*

In a probabilistic assessment framework, both actions, E, and resistance, R, are seen as random variables, and the probability of failure P_f is defined as:

$$P_f = P(R \leq E) \tag{2.68}$$

which can be understood as the probability of not complying with a certain limit state condition. Considering the probability density functions (PDF) of the

actions, f_E, and of the resistance, f_R, their joint PDF, f_{RE}, and a failure domain D (assuming E and R are independent, allowing the joint PDF to be taken as the multiplication of the independent PDFs), P_f can be given as:

$$P_f = \int_D f_{RE}(r,e)\, dr\, de = \int_{-\infty}^{+\infty} \int_{-\infty}^{e>r} f_R(r) \cdot f_E(e)\, dr\, de \tag{2.69}$$

Taking the cumulative distribution function (CDF) of R as:

$$F_R(r) = \int_{-\infty}^{r} f_R(y)\, dy \tag{2.70}$$

this gives the probability of failure:

$$P_f = \int_{-\infty}^{+\infty} F_r(e) \cdot f_E(e)\, de \tag{2.71}$$

This convolution integral, of which Figure 2.27 illustrates a graphical interpretation, can only be solved analytically if both E and R follow, for instance, a normal distribution. In this case, a new random variable $M = R - E$ (known as the safety margin) can be obtained by combining E and R so that $M \sim N(\mu_M, \sigma_M^2)$, where $\mu_M = \mu_R - \mu_E$ and $\sigma_M^2 = \sigma_R^2 + \sigma_E^2$. Therefore, the probability of failure can be written as:

$$P_f = P(R \leq E) = P(M \leq 0) = \Phi\left(\frac{0 - \mu_M}{\sigma_M}\right) \tag{2.72}$$

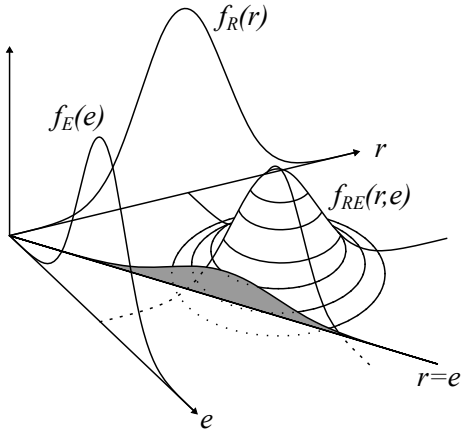

Figure 2.27: Convolution integral of the probability of failure (adapted from Melchers, Robert (1999))

2.4.2.2 *Reliability approach*

THE RELIABILITY INDEX Substituting μ_M and σ_M by their definitions on the right side of Equation 2.72, gives:

$$P_f = \Phi\left(\frac{\mu_R - \mu_E}{\sqrt{\sigma_E^2 + \sigma_E^2}}\right) = \Phi(-\beta) \tag{2.73}$$

This parameter β, known as the reliability index (Cornell, 1969), is represented alongside the safety margin distribution in Figure 2.28, and can be expressed as:

$$\beta = \frac{\mu_M}{\sigma_M} \tag{2.74}$$

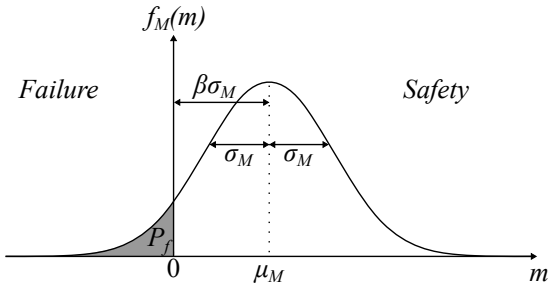

Figure 2.28: Reliability index on the safety margin distribution (adapted from Melchers, Robert (1999)).

Considering the replacement that can transform a random normally distributed variable X into a standardized normal variable Y_X:

$$Y_X = \frac{X - \mu_X}{\sigma_X} \tag{2.75}$$

the safety margin can be expressed according to the standardized actions Y_E and resistance Y_R as:

$$M = \mu_R + Y_R\sigma_R - \mu_E - Y_E\sigma_E \tag{2.76}$$

Observing Figure 2.29, the point closest to the origin is P_0*, and it is known as the design point, which is the most likely to occur in the limit state. Since this point is at a distance β from the origin, the reliability index can be thought of as a vector with direction cosines α_R and α_E. These serve as indicators of the index's sensitivity towards each variable and are given as:

$$\alpha_R = \frac{\partial M/\partial Y_R}{\sqrt{(\partial M/\partial Y_R)^2 + (\partial M/\partial Y_E)^2}} = \frac{\sigma_R}{\sqrt{\sigma_R^2 + \sigma_E^2}} \tag{2.77}$$

$$\alpha_E = \frac{\partial M/\partial Y_E}{\sqrt{(\partial M/\partial Y_R)^2 + (\partial M/\partial Y_E)^2}} = -\frac{\sigma_E}{\sqrt{\sigma_R^2 + \sigma_E^2}} \tag{2.78}$$

Furthermore, considering a safety margin function that is a linear combination of n normally independent distributed random variables with weight a so that:

$$M = a_0 + \sum_{i=1}^{n} a_i X_i \tag{2.79}$$

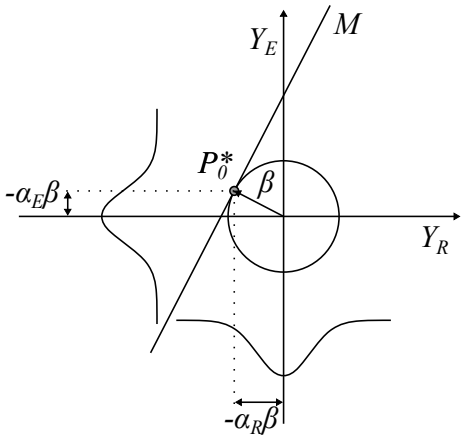

Figure 2.29: Design point and reliability index direction cosines (adapted from Cremona (2013)).

and its mean E and variance V:

$$E(M) = a_0 + \sum_{i=1}^{n} a_i E(X_i) \tag{2.80}$$

$$V(M) = \sum_{i=1}^{n} a_i^2 V(X_i) \tag{2.81}$$

the reliability index in this situation is given by:

$$\beta = \frac{E(M)}{\sqrt{V(M)}} \tag{2.82}$$

Substituting the X variables with their respective standardized forms Y, the direction cosines can be obtained with:

$$\alpha_i = \frac{\partial M/\partial Y_i}{\sqrt{\sum_{j=1}^{n} \left(\partial M/\partial Y_j\right)^2}} = \frac{a_i \sigma_{X_i}}{\sqrt{\sum_{j=1}^{n} \left(a_j \sigma_{X_j}\right)^2}} \tag{2.83}$$

SECOND-MOMENT RELIABILITY The previously described methodology applies to particular cases when the limit state can be described as a linear combination of independent normally distributed random variables. However, this does not describe most situations where the limit state is non-linear. Nonetheless, a linear approximation is possible. A limit state function $g(\mathcal{X})$ can be evaluated by a first-order Taylor expansion in a design point X^* as:

$$g(\mathcal{X}) \cong g(\mathcal{X}^*) + \sum_{i=1}^{n} \left.\frac{\partial g(\mathcal{X})}{\partial X_i}\right|_{\mathcal{X}^*} \cdot (X_i - X_i^*) \tag{2.84}$$

Considering hypothetical correlation coefficients ρ, the Basler-Cornell reliability index β_C is defined by:

$$\beta_C = \frac{E(g)}{\sqrt{V(g)}} = \frac{g(\mathcal{X}^*) + \sum_{i=1}^{n} \left.\frac{\partial g(\mathcal{X})}{\partial X_i}\right|_{\mathcal{X}^*} \cdot (E(X_i) - X_i^*)}{\sqrt{\sum_{i=1}^{n}\sum_{j=1}^{n} \left.\frac{\partial g(\mathcal{X})}{\partial X_i}\right|_{\mathcal{X}^*} \cdot \left.\frac{\partial g(\mathcal{X})}{\partial X_j}\right|_{E(\mathcal{X}^*)} \cdot \rho_{ij} \cdot \sigma_{X_i} \cdot \sigma_{X_j}}} \tag{2.85}$$

Since this method's results are heavily dependent on the chosen design point, the Hasofer-Lind reliability index β_{H-L} (Hasofer and Lind, 1974) employs a transformation of the X variables into their standardized form Y, and as such can be understood as the distance between the origin of the transformed variable space and a new design point Y^*, as:

$$\beta_{H-L} = -\sum_{i=1}^{n} Y_i^* \alpha_i \tag{2.86}$$

where the direction cosines are:

$$\alpha_i = \frac{\frac{\partial g}{\partial Y_i}}{\sqrt{\sum_{i=1}^{n} \left(\frac{\partial g}{\partial Y_i}\right)^2}} \tag{2.87}$$

This linearization is known as the first-order reliability method (FORM). Figure 2.30 illustrates β_{H-L} in the case of two standardized variables, Y_1 and Y_2. Given the non-linear nature of g, finding Y^* is an iterative process, in order to comply with:

$$\beta = \min_{y \in \{g(Y)=0\}} \sqrt{\sum_{i=0}^{n} y_i^2} \tag{2.88}$$

for which methods such as the Rackwitz-Fiessler algorithm (Rackwitz and Fiessler, 1978) can be employed.

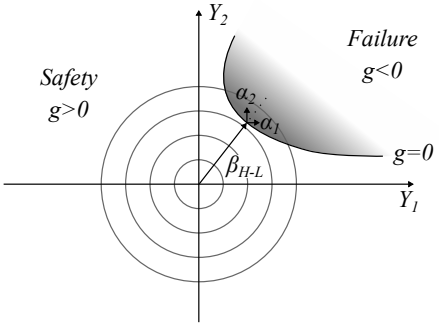

Figure 2.30: Hasofer-Lind reliability index (adapted from Cremona (2013)).

The discussed procedures apply only to normally distributed and independent variables, and therefore, some modifications must be employed if the variables are otherwise presented:

- In the case of the variables being non-normal, they can be equated into normal distributions, e.g. by applying the Paloheimo transformation (using a normal distribution that keeps the same mean value and a carefully selected percentile close to P_f) or the normal-tail transformation (that matches the original and transformed normal functions' PDF and CDF);

- If the variables are normally distributed but present some degree of correlation between them, it is necessary to transform them into uncorrelated variables. To do so, a transformation matrix can be applied, comprising the eigenvectors of the original variables' covariance matrix or a Cholesky decomposition.
- Should the variables be correlated but present non-normal distributions, they can be transformed using methods such as the Rosenblatt transformation (using a series of conditional PDFs to materialize the joint PDF) or the Nataf transformation (employing only the marginal distribution functions and correlation matrix).

The FORM lacks in translating the curved nature of a limit state's function. Since it linearizes the limit state on the design point, this method does not take into account the different probabilities of failure associated with a curved limit. Conversely, the second-order reliability method (SORM) is sensitive to curvatures by incorporating a second-order Taylor expansion at the design point:

$$\begin{aligned} g(\mathcal{X}) \cong g(\mathcal{X}^*) + \sum_{i=1}^{n} \left.\frac{\partial g(\mathcal{X})}{\partial X_i}\right|_{\mathcal{X}^*} \cdot (X_i - X_i^*) \\ + \frac{1}{2} \sum_{i=1}^{n} \sum_{j=1}^{n} \left.\frac{\partial^2 g(\mathcal{X})}{\partial X_i \partial X_j}\right|_{\mathcal{X}^*} \cdot (X_i - X_i^*) \cdot (X_j - X_j^*) \end{aligned} \tag{2.89}$$

Breitung (1984) proposes an approximated second-order probability of failure P_{f_2} using the principal curvatures at the design point κ_i:

$$P_{f_2} \cong \Phi(-\beta) \cdot \prod_{i=1}^{n} (1 + \beta \cdot \kappa_i)^{-1/2} \tag{2.90}$$

Figure 2.31 illustrates the FORM and SORM approximations to a non-linear limit state.

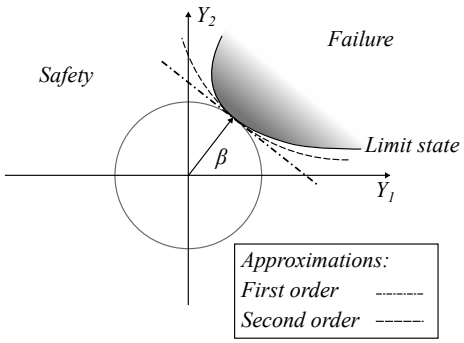

Figure 2.31: First and second order approximations (adapted from Cremona (2013)).

2.4.3 *Simulation approach*

The reliability-based approaches presented so far rely on the ability to describe the limit state function explicitly, enabling derivatives to be taken. Nevertheless, in applications related to structural analysis, namely high-speed railway

bridges, the response surface is usually highly non-linear and reflects the uncertainties arising from the variability of the structural systems' mechanical and geometrical properties. The implicit nature of the limit state as a function of the problem's variables calls for the employment of simulation techniques, in which a discrete number of deterministic problems are calculated, given a sample of the random variables.

2.4.3.1 *Monte Carlo Simulation*

CRUDE MONTE CARLO In its simplest form, a Monte Carlo simulation is conducted by sampling each of the problem's variables N times and checking if the desired limit condition g is met for each set of randomly selected values. If n sets of values produce systems that fall on the unsafe side of the limit state ($g \leq 0$), the probability of failure is approximated by:

$$P_f \cong \hat{P}_f = \frac{n}{N} \tag{2.91}$$

To conduct these trials, the problem's random variables $\mathcal{X}$ must be well described according to their probabilistic characteristics, as their PDF $f_{\mathcal{X}}(\mathcal{X})$, so that the generation of random values $\hat{\S}_i$ is possible. These can be obtained from random numbers u_i occurring in a uniform distribution $U \in \,]\,0,1\,[$ as follows:

- For a uniform discrete random variable $R = \{k, k+1, \ldots, n\}$, the random integers r_i are given by

$$r_i = \text{Int}\,(n \cdot u_i) + k \tag{2.92}$$

  where Int is a function that returns the integer part of a number.

- For continuous distributions with known analytical CDFs F_X, the random values x_i are obtained with

$$x_i = F_X^{-1}(u_i) \tag{2.93}$$

- For standardized normally distributed random variables, using the Box-Muller transformation, a pair of random values z_1 and z_2 is given by:

$$z_1 = (-2 \ln u_1)^{1/2} \cos(2\pi u_2) \tag{2.94}$$
$$z_1 = (-2 \ln u_1)^{1/2} \sin(2\pi u_2) \tag{2.95}$$

Considering the obtained random values and an evaluation function I with a value 1 if $g(\mathcal{X}) \leq 0$ and value 0 otherwise, P_f is approximated by:

$$P_f = \int_{g(\mathcal{X}) \leq 0} I\left[g(\mathcal{X}) \leq 0\right] f_{\mathcal{X}}(\mathcal{X}) d\mathcal{X} \cong \hat{P}_f = \frac{\sum_{i=1}^{n} I\left[g\left(\hat{\mathcal{X}}^i\right) \leq 0\right]}{N} \tag{2.96}$$

This form of the Monte Carlo simulation is known as Crude Monte Carlo, given that it only depends on the number of simulations N to obtain good enough results. Therefore, an important step is to evaluate the accuracy and

efficiency of the simulations. Considering each simulation as a Bernoulli trial, the coefficient of variance (CV) of P_f is given by:

$$\mathrm{CV}_{P_f} = \frac{\sqrt{\frac{(1-P_f)P_f}{N}}}{P_f} \tag{2.97}$$

Consequently, it can be concluded that the higher the number N is, the lower CV is, therefore giving a more accurate simulation. Conversely, as the number of realizations rises, so does the computational cost of running those calculations. As such, an adequate number of simulations must balance both accuracy and efficiency.

For a confidence interval C, Broding et al. (1964) suggest a number N given by:

$$N > \frac{-\ln 1 - C}{P_f} \tag{2.98}$$

Another approach, by Bjerager (1991), gives:

$$\frac{1}{Pf} \leq N \leq \frac{10}{P_f} \tag{2.99}$$

ENHANCED SAMPLING Generally, a crude Monte Carlo simulation yields a noteworthy variance of the approximate probability of failure. Since, in most cases, the target probabilities of failure are considerably low, the simulated results of the sampled variables fall in a region far from the limit state, contributing to the dispersion of results. Considering the variance of $\hat{P}_f$ given by:

$$\mathrm{Var}\left[\hat{P}_f\right] = \frac{\mathrm{Var}\left[I(g(\mathcal{X}) \leq 0)\right]}{N} \tag{2.100}$$

one way of reducing it would be to increase the sample size N. Since this escalates the computational cost, another approach is to employ variance reduction techniques by improving the manner by which the samples are obtained.

If there is some knowledge or sufficient estimation regarding the limit state's region that contributes the most for the evaluation function to give non-positive values, an importance sampling density function $h(\mathcal{X})$ can be applied, giving a probability of failure and the corresponding estimate of:

$$P_f = \int_{g(\mathcal{X})\leq 0} I\left[g(\mathcal{X}) \leq 0\right] \frac{f_{\mathcal{X}}(\mathcal{X})}{h(\mathcal{X})} h(\mathcal{X}) d\mathcal{X} \cong \hat{P}_f = \frac{\sum_{i=1}^{n} I\left[g\left(\hat{x}^{(i)}\right) \leq 0\right]}{N} \frac{f_{\mathcal{X}}(\hat{\mathcal{X}}_i)}{h(\hat{\mathcal{X}})} \tag{2.101}$$

In turn, using importance sampling, the estimate's variance is given by:

$$\mathrm{Var}\left[\hat{P}_f\right] = \frac{1}{N} \int_{g(\mathcal{X})\leq 0} \frac{f^2_{\mathcal{X}}(\mathcal{X})}{h(\mathcal{X})} d\mathcal{X} - \hat{P}_f^2 \tag{2.102}$$

and therefore the variance can be fairly reduced if an accurate sampling function is selected.

Alternatively, variance can be reduced by using stratified sampling. This concept partitions the sample domain Ω into m number of strata, so that:

$$\Omega = \cup_{i=1}^{m} \Omega_i \tag{2.103}$$

and each interval has an associated probability of failure given by:

$$P_{f_i} = \int_{\Omega_i} f_{\mathcal{X}}(\mathcal{X}) h(\mathcal{X}) d(\mathcal{X}) \tag{2.104}$$

In each region, Ω_i, with N_j simulations, the probability of occurrence is P_j, and the approximation of the probability of failure is, therefore:

$$\hat{P}_f = \sum_{j=1}^{m} \left[P_j \frac{1}{N_j} \sum_{i=1}^{n} I[g(\mathcal{X}_i) \leq 0] \right] \tag{2.105}$$

Using this form of stratified sampling, the variance becomes:

$$\text{Var}\left[\hat{P}_f\right] = \sum_{i=1}^{m} \frac{P_i^2 \sigma_i^2}{N_i} \tag{2.106}$$

where

$$\sigma_i^2 = \frac{1}{P_i} \int_{\Omega_i} f_{\mathcal{X}}^2(\mathcal{X}) h(\mathcal{X}) d(\mathcal{X}) - \frac{\hat{P}_{f_i}^2}{P_i^2} \tag{2.107}$$

Thus, the overall variance can be reduced if the stratification process adequately foresees the failure region.

A specific form of stratified sampling, developed by McKay et al. (1979), is known as the Latin Hypercube. In this method, the stratification process must ensure that the probability of occurrence of each of the strata is equal. Then, a random value for each interval in each variable is taken as a representative. The combination of sample points is made so that no representative value is taken twice (each stratum contributes a single time to the simulation). Figure 2.32 presents a graphical interpretation of this approach, where each dot represents a sample.

2.4.4 *Enhanced methodologies*

Given the computational costs that scale according to the quantity of Monte Carlo simulations required for a given problem, considering structural reliability assessment purposes, where the considered probabilities of failure are residual, efforts have been made in order to reduce the number of needed simulations. Thus, the methods presented in this section focus on the edge regions of the limit state's distribution functions, for which regular Monte Carlo simulations may not provide sufficient information.

2.4.4.1 *Tail modelling*

To extract the same information from a lower number of sample points, it is conceivable to fit a CDF to the obtained data points. This must be done carefully

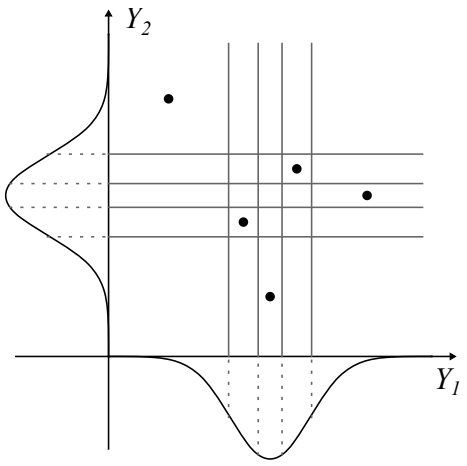

Figure 2.32: Latin Hypercube Sampling.

since, in structural reliability problems, the interest is on the lower probabilities side of the cumulative distribution, i.e. the left-hand tail. With insufficient data points, a fitted distribution that satisfactorily represents the middle part of the results does not necessarily do the same for extreme values. Therefore, while a normal distribution can be a good fit for approximating the central values of sampled results, for the purposes of tail modelling, the Generalized Pareto Distribution (GPD) is applicable. This right-skewed distribution is a function of shape and scale parameters, ξ and Ψ, and for a designated exceedance z, its CDF is given by (Ramu et al., 2010):

$$F_{\xi,\psi}(z) = \begin{cases} 1 - \left(1 + \frac{\xi}{\psi} z\right)^{-\frac{1}{\xi}} & \text{if } \xi \neq 0 \\ 1 - e^{\left(-\frac{z}{\psi}\right)} & \text{if } \xi = 0 \end{cases} \tag{2.108}$$

Other functions can also be employed to model a distribution's tails. Rocha (2015) presents a formulation of a sigmoid function with fitting parameters b, c, d, x_0 and y_0 that gives a probability P of:

$$P_f(x) = y_0 + \frac{d}{\left[a + e^{-\left(\frac{x - x_0}{b}\right)}\right]^c} \tag{2.109}$$

The author calls attention to the importance of choosing an appropriate threshold to fit a tail modelling distribution, for it can accentuate the central values if it is too low or, conversely, be too dependent on the few data points on the extreme ends if it is too high. To overcome that matter, the same author uses a set number of data points of the tail for estimating a regression.

2.4.4.2 *Extrapolation of the probability of failure and confidence interval*

An enhanced Monte Carlo simulation methodology was presented by Naess et al. (2009), in which the number of simulations needed to estimate small

probabilities of failure is reduced. From the safety margin M, an extended class is defined by a scale parameter $0 \leq \lambda \leq 1$ as:

$$M(\delta) = M - \mu_M(1-\lambda) \tag{2.110}$$

For a given value of λ, there are $N_f(\lambda)$ sampled experiments that fail the design condition, and therefore the estimated probability of failure and respective CV are given by:

$$\hat{P}_f(\lambda) = \frac{N_f(\lambda)}{N} \tag{2.111}$$

$$\mathrm{CV}_{\hat{P}_f(\lambda)} = \sqrt{\frac{1-P_f(\lambda)}{P_f(\lambda)N}} \tag{2.112}$$

Consequently, the 95% confidence interval is given by:

$$C^{\pm} = \hat{P}_f(\lambda)\left(1 \pm 1.96 \cdot \mathrm{CV}_{\hat{P}_f(\lambda)}\right) \tag{2.113}$$

Considering an approximation function $q(\lambda)$, P_f is approximated by:

$$P_f(\lambda) \underset{\lambda \to 1}{\approx} q(\lambda) e^{-a(\lambda-b)^c} \tag{2.114}$$

and afterwards, $q(\lambda)$ is taken as a value q, for $\lambda_0 \leq \lambda \leq 1$. Thus, the fitting function depends on four parameters (a, b, c and q). Determining them is a matter of minimizing a mean square error function, with weights w_j for a series of values in the appropriate interval:

$$F(a,b,c,q) = \sum_{j=1}^{M} w_j \left(\log \hat{P}_f(\lambda_j) - \log q + a(\lambda_j - b)^c\right)^2 \tag{2.115}$$

$$w_j = \left(\log C^+(\lambda_j) - \log C^-(\lambda_j)\right)^{-2} \tag{2.116}$$

Furthermore, fixing b and c transforms the problem into a linear regression. So, considering x_j and y_j as:

$$x_j = (\lambda_j - b)^c \tag{2.117}$$

$$y_j = \log \hat{P}_f(\lambda_j) \tag{2.118}$$

the optimal values of a and $\log q$ are given by:

$$a^*(b,c) = -\frac{\sum_{j=1}^{M} w_j (x_j - \bar{x})(y_j - \bar{y})}{\sum_{j=1}^{M} w_j (x_j - \bar{x})^2} \tag{2.119}$$

$$\log q^*(b,c) = \bar{y} + a^*(b,c)\bar{x} \tag{2.120}$$

To find the optimal b^* and c^*, and the corresponding a^* and q^*, the Levenberg-Marquardt algorithm can be applied to the function:

$$\tilde{F}(b,c) = F(q^*(b,c), a^*(b,c), b, c) \tag{2.121}$$

2.4.4.3 *Subset simulation*

Subset simulation is a technique developed by Au and Beck (2001) to assess small probabilities of failure by breaking the failure event F into conditional intermediate events F_i. The goal is to effectively compute the probabilities of these situations and consequently reduce the number of samples needed as an alternative to importance sampling, which the authors point out is not feasible to higher dimension variable spaces. Considering a division into m intermediate fail events, the probability of F becomes:

$$P_F = P(F_i) \prod_{i=1}^{m-1} P(F_{i+1}|F_i) \tag{2.122}$$

While with simple Monte Carlo simulations a small probability of failure implies using numerous sample points, with this partitioning, a small probability can be seen as the product of more considerable intermediate probabilities, for which the calculations are not as costly. Nonetheless, for the determination of the intermediate's events probabilities, the authors detail a Markov Chain Monte Carlo (MCMC) simulation, using a Modified Metropolis Algorithm (MMA) to account for a large number of independent components.

This methodology can be applied by reproducing the following steps:

1. Estimate the probability for the first event $P(F_1)$ with $\tilde{P}_1$ by using a direct Monte Carlo simulation (similar to Equation 2.96);
2. With the samples from the first step, which are distributed with a PDF $q(\cdot|F_1)$, other Markov chain samples can be simulated with the MMA, guaranteeing that they keep the same PDF;
3. With these samples, estimate $P(F_2|F_1)$ with the estimator $\tilde{P}_2$;
4. In F_2, use the samples (that have PDF $q(\cdot|F_2)$) to get more samples, in order to estimate $P(F_3|F_2)$;
5. Repeat until the final event.
6. The probability of failure is estimated by:

$$\tilde{P}_F = \prod_{i=1}^{m} \tilde{P}i \tag{2.123}$$

A visualization of subset simulation, based on Zuev (2013), is given in Figure 2.33. The same authors offer a useful description of the MMA to generate the following level's samples $\tilde{x}$ from the current's x:

1. Generate a candidate state ξ, for each of the k number of variables:
   a) Use a proposal PDF q_k (such as a Gaussian distribution centred at the variable's current value x_k) to obtain new values $\eta \sim q_k(\cdot|x_k)$;
   b) Using a typical Gaussian PDF ϕ, calculate the acceptance ratio

$$r_k = \frac{\phi(\eta_k)}{\phi(x_k)} \tag{2.124}$$

c) Generate a random number between 0 and 1. If this number is less than min $\{1, r_k\}$, the candidate state is accepted for the current variable $(\xi_k = \eta_k)$. Otherwise, the variable's value is kept $(\xi_k = x_k)$

2. If the candidate state is inside the current failure domain $(\xi \in F_1)$, accept the candidate $(\tilde{x} = \eta)$. Otherwise, keep the original state $(\tilde{x} = x)$.

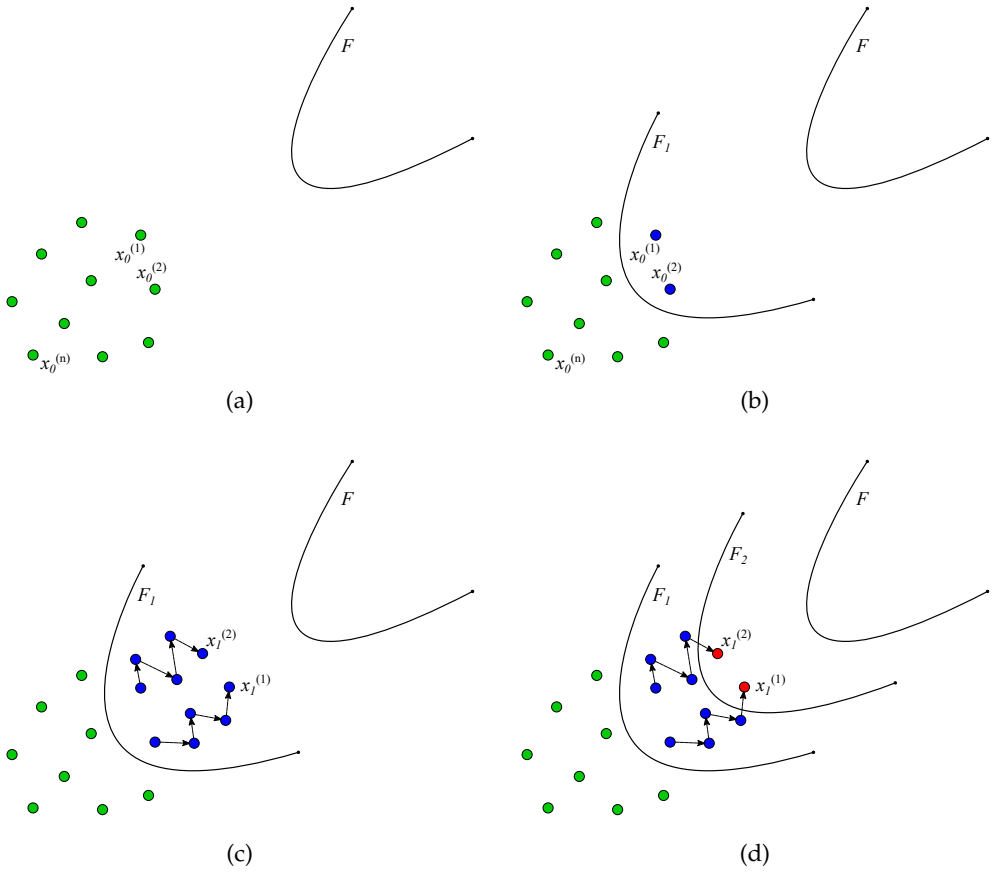

Figure 2.33: Subset simulation illustration. (a) initial crude Monte Carlo; (b) the two states closest to F determine F_1; (c) new samples are generated with the MMA; (d) F_2 is determined. (adapted from Zuev (2013))

In subset simulation applications, it is noted that special attention must be given to the choice of the PDFs and of the intermediate failure events. To complement subset simulation, Bourinet et al. (2011) propose a methodology entitled ^{2}*SMART* (Subset simulation by Support-vector Margin Algorithm for Reliability esTimation) which employs Support Vector Machine (SVM) classification. The authors significantly reduce the number of necessary samples, especially in high dimensional spaces, by using SVM classification (instead of crude Monte Carlo) to assess each step's probability of failure. This allows the new samples to be obtained from an active learning scheme rather than from a passive one. By carefully selecting informative points, the SVM classifier is iterated without the addition of a large number of samples.

2.4.5 *Application to design norms*

Some methods discussed in this chapter have normative importance in current design codes. These standards serve the purpose of setting limit states, whether ultimate or serviceability limit states and issuing the design rules to provide solutions on their safe side. The amount of safety associated with each limit state and method of calculation is the result of a careful balance between design, cost and the desired reliability. Currently, norms such as the Eurocodes use mainly semi-probabilistic approaches (as described in Section 2.4.1), and therein reliability is integrated into partial safety factors.

2.4.5.1 *Target probabilities of failure*

The subject of determining the target probabilities of failure (or reliability indices) of rare calamitous events is a task left to the decision-makers in charge of the various codes and norms. However, the accepted amounts of risk reflect society's sensitiveness towards the occurrence of said events, especially when dealing with ultimate limit states that put human lives at risk. Accounting for the cost associated with lowering the probabilities of failure arises a matter of optimizing this balance. To distinguish risks, the EN 1990 (CEN, 2023a) establishes five consequence classes (CC) as follows (adapted from CEN (2023a)):

- CC4: Extreme consequence for loss of human life or personal injury and huge economic, social or environmental consequences.
  - Examples: nuclear power plants or dams.
- CC3: High consequence for loss of human life or personal injury and very great economic, social or environmental consequences.
  - Examples: buildings or parts of buildings where a very large number of people could be affected by failure, like grandstands, concert halls, or high-rise buildings.
- CC2: Medium consequence for loss of human life or personal injury and considerable economic, social or environmental consequences.
  - Examples: buildings or parts of buildings not covered by CC1 or CC3.
- CC1: Low consequence for loss of human life or personal injury and small economic, social or environmental consequences.
  - Examples: buildings or part of buildings where very few people could be affected by failure, such as agricultural or storage buildings.
- CC0: Very low consequence for loss of human life or personal injury and insignificant economic, social or environmental consequences.
  - Examples: elements other than structural.

These CC refer to structural members, with the requirement that individual members may be associated with different CC than the rest of the structure. In Annex A of the EN 1990, railway bridges on main lines are classified in CC3a (lower CC3).

Associated with CC1, CC2 and CC3, the EN 1990 norm presents minimum values of the reliability index β (and approximated P_f) in Annex C, as listed in Table 2.18, (for an ultimate limit state), for two different reference periods.

	REFERENCE PERIOD	
CONSEQUENCE CLASS	1 year	50 years
CC3	5.2 $(P_f \approx 10^{-7})$	4.3 $(P_f \approx 10^{-5})$
CC2	4.7 $(P_f \approx 10^{-6})$	3.8 $(P_f \approx 10^{-4})$
CC1	4.2 $(P_f \approx 10^{-5})$	3.3 $(P_f \approx 5 \times 10^{-4})$

Table 2.18: Minimum values of β (adapted from CEN (2023a)).

Furthermore, the norm sets a factor k_F to differentiate actions by reliability. This can be applied to safety factors γ_F used on fundamental combinations. For consequence classes CC1, CC2 and CC3, k_F it is, respectively, 0.9, 1.0 and 1.1 (it is noted that for bridges, CC3a corresponds to a k_F of 1.0).

Although the discussed target reliability indices (and associated probabilities of failure) apply only to the design phase of new structures, other codes provide guidance for the assessment of existing structures. The Probabilistic Model Code from the Joint Committee for Structural Safety (JCSS) (JCSS, 2001) presents three consequence classes depending on a ratio ρ between total costs (including the cost of failure) and construction costs (adapted from JCSS (2001)):

- Class 3 Large Consequences (ρ between 5 and 10): Risk to life, given a failure, is high, or economic consequences are significant.
  - Examples: main bridges, theatres, hospitals, high rise buildings.
- Class 2 Moderate Consequences (ρ between 2 and 5): Risk to life, given a failure, is medium or economic consequences are considerable.
  - Examples: office buildings, industrial buildings, apartment buildings.
- Class 1 Minor Consequences (ρ less than approximately 2): Risk to life, given a failure, is small to negligible and economic consequences are small or negligible
  - Examples: agricultural structures, silos, masts.

Table 2.19 presents the target reliability indices (as well as corresponding probabilities of failure) for these consequence classes (considering an ultimate limit state and 1-year reference period), depending on the relative cost of safety measure. For serviceability, this code gives a target reliability of 1.3 if the relative cost of safety measure is high, 1.7 if it is medium, and 2.3 if it is low.

	CONSEQUENCE CLASS		
RELATIVE COST OF SAFETY MEASURE	Class 1	Class 2	Class 3
Large	3.1 $(P_f \approx 10^{-3})$	3.3 $(P_f \approx 5 \times 10^{-4})$	3.7 $(P_f \approx 10^{-4})$
Normal	3.7 $(P_f \approx 10^{-4})$	4.2 $(P_f \approx 10^{-5})$	4.4 $(P_f \approx 5 \times 10^{-6})$
Small	4.2 $(P_f \approx 10^{-5})$	4.4 $(P_f \approx 5 \times 10^{-6})$	4 .7 $(P_f \approx 10^{-6})$

Table 2.19: Minimum values of β (adapted from JCSS (2001)).

2.4.5.2 *Partial safety factors*

Since the Eurocodes incorporate reliability through the use of partial safety factors, the EN 1990 provides guidance for their calibration. Considering the verification of safety in Equation 2.67 and the direction cosines of Equation 2.77 and Equation 2.78, the safety check regarding a target reliability index β_0 can be rewritten as:

$$\mu_R - \beta_0 \alpha_R \sigma_R \geq \mu_E + \beta_0 \alpha_E \sigma_E \tag{2.125}$$

This formulation is applicable to the linear combination of two normally independent distributed variables. Annex C of the EN 1990 states the design values for this and other distributions (adapted from CEN (2023a)):

- Normal distribution:

$$\mu - \alpha\beta\sigma \tag{2.126}$$

- Lognormal distribution with $\text{CV} = \sigma/\mu < 0.2$:

$$\mu e^{-\alpha\beta \cdot \text{CV}} \tag{2.127}$$

- Gumbel distribution with $u = \mu - \dfrac{0.577}{a}$ and $a = \dfrac{\pi}{\sigma\sqrt{6}}$

$$u - \frac{1}{a} \ln\{-\ln \Phi(-\alpha\beta)\} \tag{2.128}$$

For the direction cosines, if $0.16 < \sigma_E/\sigma_R < 7.6$ the norm indicates a value of -0.7 for α_E and 0.8 for α_R. If the actions are the result of several variables, for the non-leading variables, α is given as $0.4 \times 0.7 = 0.28$.

2.4.6 *Application to railway bridges*

Railway bridges are crucial parts of rail lines, and the possibility of their failure not only causes economic losses due to the suspension of operation but

also poses a risk to human life if derailment happens. Therefore, the socially acceptable probabilities of failure are low. However, the study of a reliability problem with low target probabilities and complex models can come at a significant computational cost.

In recent years, researchers have worked on techniques to solve these problems in computationally efficient ways. Mao et al. (2016) have employed the Probability Density Estimation Method (PDEM) as an alternative to the Monte Carlo Method to determine vibrations in a train-bridge interaction model, including irregularities and assuming always maintained contact between the wheels and the rails. From initial representative values of random variables, the authors obtain time-history probability density functions of the response, improving efficiency without compromising accuracy. The authors found the random nature of the train's load and of the concrete's elasticity modulus to be the most influential, as opposed to damping and structural mass, which can, therefore, be regarded as deterministic. The same method is used by Bittner et al. (2024) with a simplified 2D bridge model, by Xu et al. (2023) for assessing wind effects, and by Xin et al. (2020), who demonstrate with 3D interaction analysis that results with a sample size of 195 for the PDEM are similar to Monte Carlo sample sizes of 3,000 to 5,000 (as can be seen in Figure 2.34). In the same study, an approach to sensitivity analysis of input parameters is presented, with the authors concluding that the combination of different parameters controls sensitivity more than the individual effect of each of them. Another method, the Response Surface Model (RSM), is utilized by Park and Towashiraporn (2014) for risk assessment of railway bridges subjected to seismic actions.

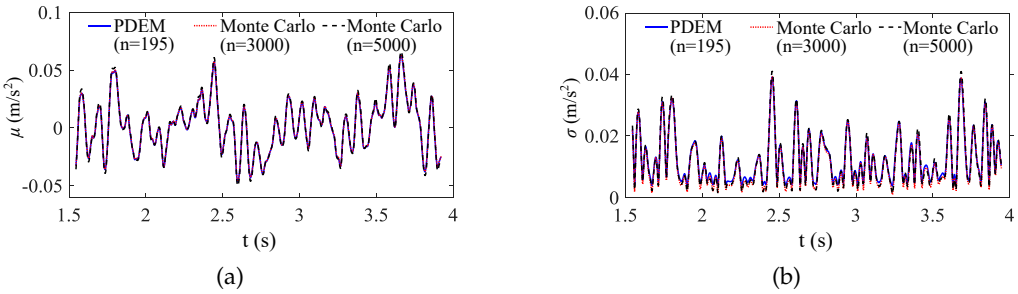

Figure 2.34: Comparison of PDEM and Monte Carlo for lateral car body acceleration. (a) mean μ; (b) standard deviation σ. (adapted from Xin et al. (2020))

Concerning train-bridge simulations, Rocha et al. (2016) evaluated the wheel unloading coefficient as a safety indicator, using GPD (exemplified in Figure 2.35) in conjunction with the Monte Carlo method. For target probabilities in the order of 10^{-4} (a target from the JCSS), the authors were able to estimate probabilities with sample sizes of 20,000. Allahvirdizadeh et al. (2020) present another approach for calculating the probability of exceedance of a limit state, employing the FORM, which is suitable for problems that can be described analytically. In that study, it is found that the deterministic approach doesn't provide a constant safety level and that reliability is sensitive to the deck's moment of inertia and to the vehicle's car-body length. A semi-probabilistic

method comparable to FORM is devised by Grigoriou and Brühwiler (2016), using data from a monitoring campaign.

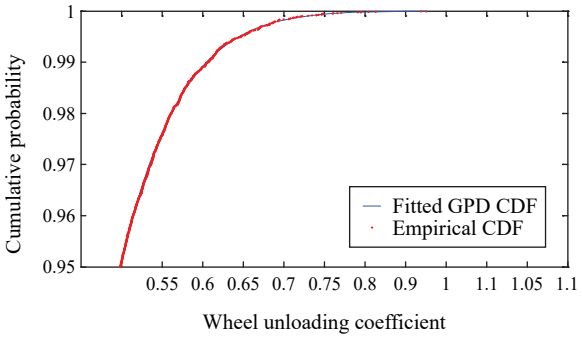

Figure 2.35: Fitted GPD of wheel unloading coefficient at 405 km/h (adapted from Rocha et al. (2016)).

Salcher et al. (2014) address the uncertainty of damping, temperature and of the material and geometrical properties through line sampling and Latin hypercube sampling. Later, Hirzinger et al. (2019) add subset simulation and asymptotic sampling as alternative methods. To assess probabilities of failure in the order of 10^{-3} (considering a serviceability limit state), the authors find an equivalence between a Monte Carlo simulation and line sampling with a sample size of two orders of magnitude smaller. To account for the effects of random rail irregularities, Salcher and Adam (2020) compare subset simulation results (illustrated in Figure 2.36) with a fitted analytical response on a small number of Monte Carlo trials. Another study on the probabilities of exceedance of bridge acceleration, by Hirzinger et al. (2020), considers the speed range as another source of variability. The authors measure probabilities of failure using different metrics, including a weighted probability of failure.

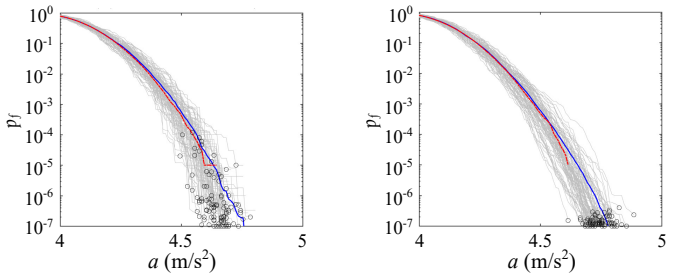

Figure 2.36: Probabilities of failure p_f and exceeded acceleration a at 85 m/s with random rail irregularities. (a) random phase angles; (b) random amplitudes. (adapted from Salcher and Adam (2020))

2.5 CONCLUDING REMARKS

The documents presented in this chapter, regarding norms, dynamic analysis methods, and probabilistic analysis, establish the basis to study the problems listed in Section 1.3. The review of literature conducted in the present chapter

allows the identification of research gaps in the topics that motivate the next chapters in this thesis. In the case of Eurocodes, which are essential tools used daily across Europe, it is worth noting that they are not immutable, as they are frequently discussed and are currently under revision (CEN/TC 250, 2023).

Concerning the EN 1991-2, it is noted that it lacks in defining some HSLM parameters. The accuracy of its limits of validity can also be questioned, as well as the load model's readiness for new and future trains. This can be achieved via a stochastic study of the dynamic effects of different load models in comparison to the current HSLM-A envelope. In the same norm, the dispositions that call for higher and lower bounds estimates for a bridge model's mass and stiffness can also be clarified with parametric studies of the influence of geometric, material, and mechanical random variables.

In the EN 1990, the limits for vertical deck acceleration in both ballasted and ballastless bridges appear to be based on an arbitrary safety factor of 2.0. On ballasted tracks, considering that there is an experimentally assessed physical limit for the acceleration above which track instability can occur, it is worth investigating what the permissible acceleration could be and, by extension, the safety factor associated with it. This evaluation must be made in terms of an acceptable probability of failure (considering the possible consequences of malfunction and maintenance costs), constituting a reliability assessment problem. The employment of enhanced simulation techniques is key to performing such a study, avoiding computational and time constraints.

Also in the EN 1990, for ballastless tracks, the possible assumption that vertical accelerations of about 1 g may cause loss of wheel-rail contact is subject to questioning. This can be addressed by comparing deck acceleration with explicit derailment criteria. The calculation of such indicators is made with the knowledge of wheel-rail contact forces, for which the utilization of complex TTBI models is necessary.

3

PROBLEM 1: IDENTIFICATION OF THE HSLM LIMITATIONS

3.1 INITIAL CONSIDERATION

To generalize the design of railway bridges subjected to significant dynamic effects caused by the train passages, usually those designed for speeds greater than 200 km/h, the European Commission's regulation on the TSI for infrastructure (European Comission, 2002) states that these structures must be checked through the High-Speed Load Model (HSLM), from the EN 1991-2 (CEN, 2023b). Despite the model's popularity and regular usage (Museros et al. (2013) state that it is "probably, the most popular articulated train prescribed by regulations"), there has been discussion surrounding its limitations and applicability, as mentioned in Section 2.2.5. Based on such discussion, the following research questions arise:

1. Is the current HSLM suited to represent future (and existing) trains that do not necessarily respect its limits?
2. How well do the 10 HSLM-A train configurations cover the dynamic effects of all possible articulated, conventional, and regular trains that they are meant to do?
3. Does the lack of definition of some HSLM limiting parameters, such as the distance between the centres of bogies between adjacent vehicles d_{BS} in conventional trains, affect the evaluation of these same limits?

In this chapter, attention is given to the first question by systematically checking how the HSLM covers, or not, the effects caused by trains defined within a wider parameter interval than that defined in the norm. Regarding the second one, the effects caused by a vast set of randomly generated train load models with properties within the limits specified in Annex E of the EN 1991-2, both articulated, conventional and regular, are compared with those caused by the HSLM. Such comparison is performed both in terms of analytical signature envelopes of both sets, as well as with a complete numerical dynamic analysis carried out in a specific case study bridge to explicitly compute its maximum acceleration response and compare it with the HSLM acceleration envelopes.

An optimised method to perform dynamic moving load analyses is also proposed to increase computational efficiency. Moreover, the lack of definition regarding some geometrical parameters in Annex E of the EN 1991-2 raised in the third question, especially the distance d_{BS} in conventional trains, is also addressed in this chapter to analyse how this issue may affect the validity of the HSLM.

The work presented in the current chapter was initially developed in the context of the IN2TRACK2 (2018) project to raise awareness for this issue.

Alternative dynamic load models were later proposed in the IN2TRACK3 (2021) project and in a project from the German Federal Railway Authority (Reiterer et al., 2022; Vorwagner et al., 2021). This chapter also reflects the work developed in Ferreira et al. (2024b) (Appendix A) and is structured in five sections. The methodology to compare the HSLM effects with those caused by the theoretical trains randomly generated through the procedure stipulated in Annex E of the EN 1991-2 is presented in Section 3.2, with the dynamic assessment methods being described in Section 3.3. The numerical models used are described in Section 3.4, while Section 3.5 is dedicated to the results obtained in the preliminary analysis performed with the train signature technique and in the complete dynamic analysis carried out with the case study bridge. The main conclusions are summarized in Section 3.6, and recommendations for future work are proposed.

3.2 METHODOLOGY

The methodology presented in this section addresses the questions listed in Section 3.1, with the goal of evaluating how well the HSLM-A covers train load models made possible by Annex E of the EN 1991-2 (CEN, 2023b) and also other trains whose properties fall outside those limits, to account for potential future vehicles.

The proposed methodology consists firstly of creating two sets of randomly generated load model configurations:

SET A : load models that abide by the EN 1991-2's limits;

SET B : load models obtained by considering wider limits than the norm's to account for already existing non-abiding trains (such as the ICE4 with its coach length D of 28.75 m (Glatz and Fink, 2021)) and for future trains.

The sets are created for each of the three train types, as detailed in Section 3.4.2 (sets A_a and B_a for articulated trains, A_c and B_c for conventional trains, and A_r and B_r for regular trains). Afterwards, the dynamic signatures of all randomly generated trains and HSLM-A universal trains can be calculated using Equation 2.44. Then, to validate the conclusions and provide further discussion, the dynamic response of all random trains is obtained for an example bridge, presented in Section 3.4.1.

Since the SLLS approach (detailed in Section 3.3.2) is being used, only one dynamic analysis needs to be carried out since all different moving loads results can be derived from the single load response. The same procedure is done for the 10 HSLM-A trains, thus allowing for a comparison to be established using the maximum vertical deck acceleration as a metric.

In this chapter, the selected example is the Canelas bridge. The sample size for the randomly generated sets is 100,000, the variable's distribution is uniform, and the speed range is from 140 km/h to 420 km/h, with 10 km/h intervals (assuming a maximum line speed of 350 km/h, the EN 1991-2 defines the maximum design speed as 1.2 times that value, which gives $1.2 \times 350 = 420$). The samples for the random variables (D, d_{BA}, d_{BS}, e_C, D_{IC}

and D_L) are generated using a random number suited for uniform distributions, scaled to the limits detailed in Section 2.2.1.3.

A representative diagram of this methodology is presented in Figure 3.1. The single load dynamic response is computed with a custom-built moving loads analysis application using MATLAB® (2018).

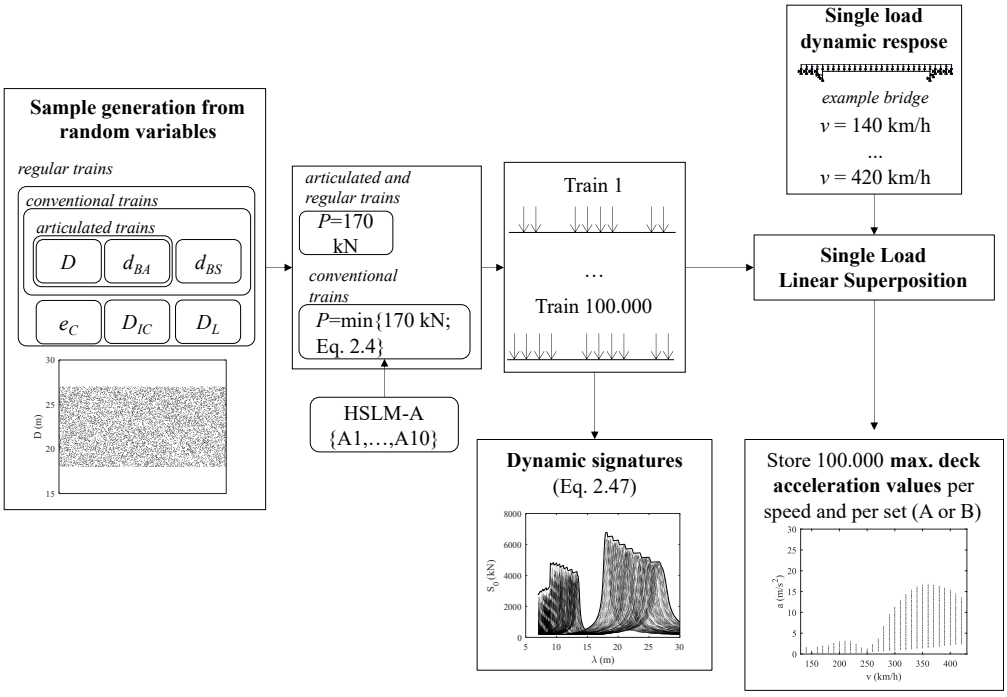

Figure 3.1: Overview of the methodology used for the assessment of the HSLM's limits of validity.

3.3 DYNAMIC ASSESSMENT

3.3.1 *Train signatures*

The concept of a train signature is part of the DER method, introduced by ERRI D 214/RP 6 (1999). A detailed explanation of the technique can be found in Section 2.3.3. This expedited approach is used for a preliminary assessment of the randomly generated trains and of the HSLM-A trains. The signature curves are obtained with Equation 2.47.

3.3.2 *Single load linear superposition*

The fulfilment of this chapter's objectives depends on the ability to perform several thousand dynamic analyses in varying scenarios. Whether considering the random variation of a train's geometrical configuration or the randomness of bridge characteristics, there are advantages in simplifying the dynamic analysis process. In the scope of this work, the metric being evaluated in ballasted bridges is the vertical deck acceleration; therefore, dynamic analysis with moving loads is sufficient. For this approach, different train models are

described as a series of individual axle loads and the distances between them, similarly to how the HSLM is usually represented.

Generally, the first step in such an analysis is to determine the individual nodal loads for each axle load and rail node. Instead, the proposed procedure (SLLS) considers the dynamic effects caused by a single moving load of an arbitrary positive value P, travelling at the desired speed v. The resulting response (such as an acceleration or displacement time history) is then scaled to the corresponding axle load and added to the total response, with a time offset related to the speed and the distance between axles.

An example is presented, considering a simple load model comprising four axle loads of 147.15 kN each, with a regular spacing of 3 m, running at a speed of 200 km/h. The overall effect is evaluated on the mid-span displacement of an 11.5 m simply supported bridge. Figure 3.2a depicts the displacement d caused by a single load, while Figure 3.2b illustrates the multiplication and offset of that same response. The dashed line in Figure 3.2c represents the sum of these effects, and the bold line is the response of a separate calculation on which the entire load model was set to run over the bridge model. The maximum absolute difference between the results of the two approaches is 3.6312×10^{-6}.

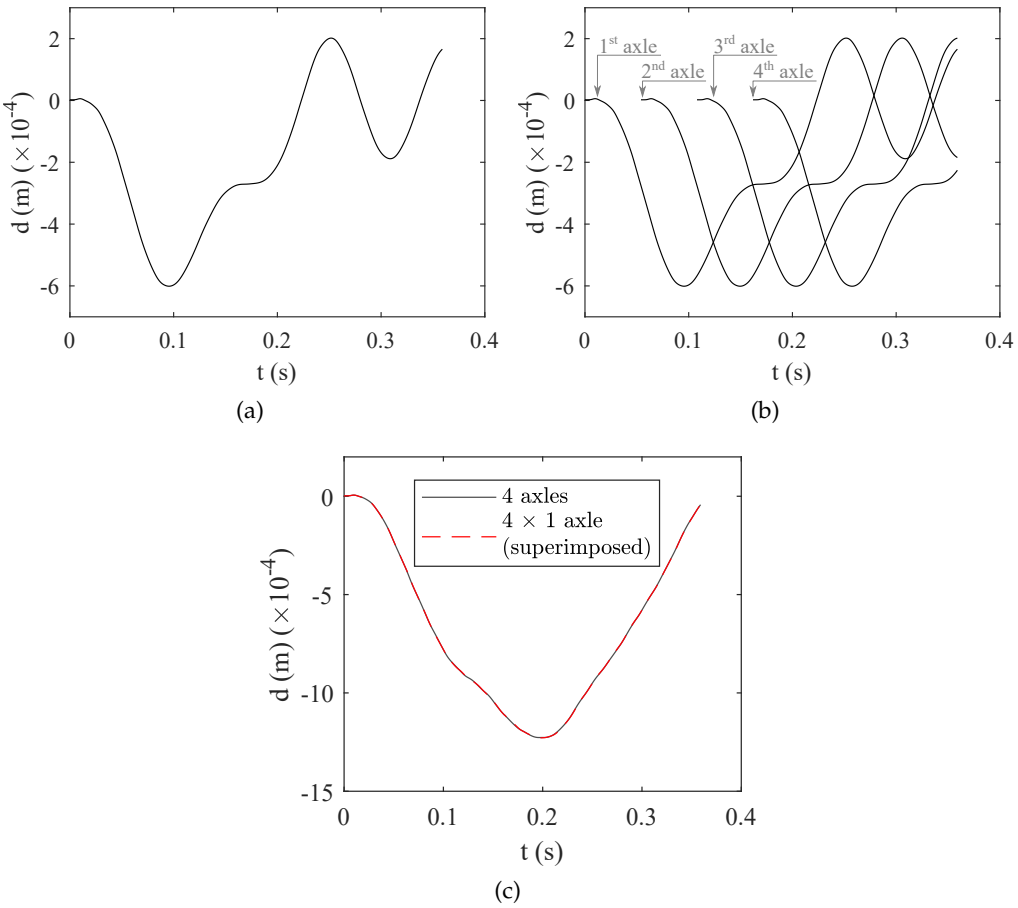

Figure 3.2: Mid-span displacement caused by a single load and combined effect. (a) single load; (b) four axles; (c) combined response

The main advantage of implementing this approach is reducing computation time since the number of necessary time steps can be significantly reduced (the total running length corresponds only to the bridge model length instead of the sum of the bridge and train lengths). Also, by calculating the isolated response of an axle load, any load model response can be replicated by scaling and superimposing the known effects. The offset in the combination of actions can reproduce different axle spacings, and the scaling can even be adjusted to different values in the same load model, e.g. in cases where the loads of the power car are superior. Furthermore, if after the calculation of the effects for several load models on a bridge, a new load model is required to be taken into consideration, there is no need for additional dynamic analysis since the dynamic equations only have to be accessed once per speed value in order to save the single axle response.

The limitations of this methodology have to do with the moving load analysis, limiting its applicability to scenarios with no nonlinear aspects, such as wheel-rail contact. This leaves out train-bridge interaction analysis and the evaluation of criteria related to contact forces or car body acceleration. For the scope of the present work, this means that the discussed superposition method is applicable to the assessment of deck acceleration on ballasted tracks.

An example application is presented in Figure 3.3 for the HSLM-A1 train. A single load $P = 170\ kN$ moves at a speed $v = 200\ km/h$, causing the mid-span displacement seen in Figure 3.3a. On a commercially available 4-core computer, this operation took 149.751 s to complete, and the SLLS response, presented in Figure 3.3b, was computed in 0.121 s. In comparison, the entire load model of the HSLM-A1 that produces the response seen in the same figure took 34 min to be calculated.

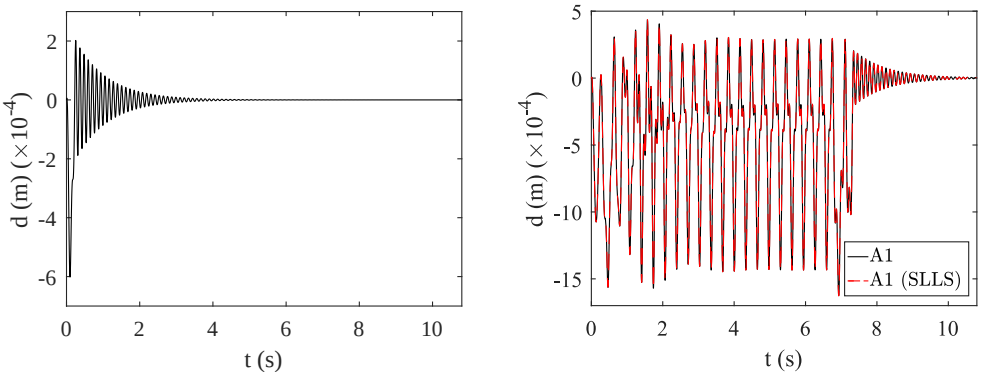

Figure 3.3: Mid-span displacement caused by a single load and combined effect of the HSLM-A1. (a) single load; (b) HSLM-A1.

3.4 NUMERICAL MODELLING

3.4.1 *Case study bridge*

The case study selected for the methodology to be applied to was the Canelas bridge (a view of its first span and the typical cross-section can be seen in Figure 3.4). This structure was built in 1996, integrating the Northern Line of the Portuguese Railway Network. The bridge was selected due to the existence of previous research work, focusing on both numerical and experimental studies (Bonifácio et al., 2014; Pimentel et al., 2007; Rocha et al., 2016), including fieldwork performed during the In2Track2 and In2Track3 projects (Silva et al., 2023).

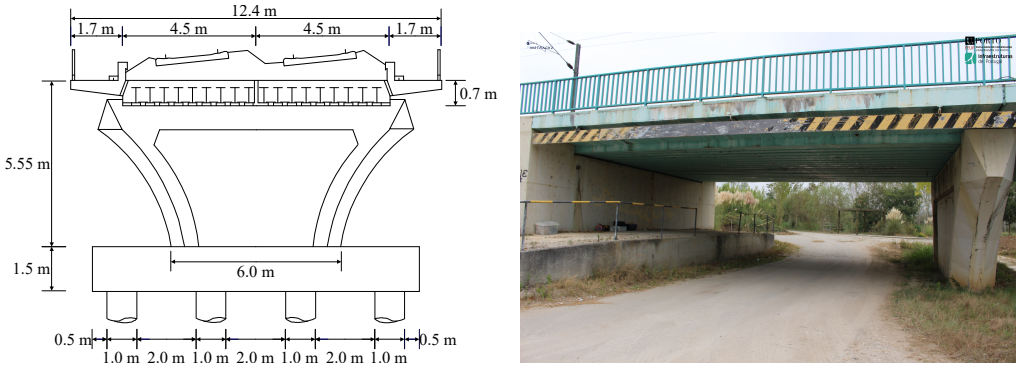

(a) (b)

Figure 3.4: Canelas bridge. (a) cross-section (unit: m) (adapted from Pimentel et al. (2007)); (b) view of the first span.

The Canelas bridge is a filler beam structure made up of 6 simply supported, 11.5 m spans. Each span comprises two independent decks (one for each track), built with directly cast concrete slabs on nine embedded HEB500 rolled steel profiles. The track consists of UIC60 rails, wooden sleepers, and a ballast bed. The decks are supported by sets of neoprene bearings located directly under the steel profiles on each support.

Since vertical deck acceleration is the only metric to be extracted, a 2D Finite Elements model of a single deck suffices. The model employed adapts the approach proposed by Rocha (2015), who developed a model using FEMIX (2009) applying appropriate technical workarounds regarding the software's availability of finite element types (namely by employing specially calculated artificial material properties to model springs as linear elastic beams). For this work, ANSYS® (2018) Parametric Design Language was used, utilizing the following available element types:

- COMBIN14: spring-dashpot elements, used in the track (for the stiffness of the ballast layer and of the rail pads, and also as shear stiffness) and in the support bearings (accounting for the neoprene layer's flexibility in the vertical and horizontal directions);
- MASS21: mass point elements, representing the localized sleepers' mass;

- BEAM3: beam elements used for the rails and the deck (reduced to a single beam).

The material and geometrical properties used for the model are listed in Table 3.1. Structural damping is considered in the model through the setting of Rayleigh damping factors, using the frequencies of the first and second vertical vibration modes. On this topic, it is noted that the original EN 1991-2 (CEN, 2003) contained provisions for the adoption of additional damping in bridges with spans less than 30 m to account for an expected response reduction due to train-bridge interaction. Even though this statement is currently absent from the norm (CEN, 2023b), a comparative assessment of this effect is made in a selected set of analyses (Section 3.5.2.2). The vertical stiffness of the ballast layer K_b is given by Equation 3.1 so that the load distribution effects proposed by W. M. Zhai et al. (2004) are incorporated.

$$K_b = \begin{cases} K_b = \dfrac{2(l_e l - _b)\tan\alpha}{ln\left[\left(\dfrac{l_e}{l_b}\right)(l_b + 2h_b\tan\alpha)/(l_e + 2h_b\tan\alpha)\right]} & \text{if } h_b\tan\alpha \leq \dfrac{l_s}{2} \\ K_b = \dfrac{K_{b1}K_{b2}}{K_{b1}+K_{b2}} & \text{if } h_b\tan\alpha > \dfrac{l_s}{2} \end{cases} \tag{3.1}$$

where

$$K_{b1} = \frac{2(l_e - l_b)\tan\alpha}{\ln\left[(l_e l_s)/(l_b(l_e + l_s - l_b))\right]}E_b \tag{3.2}$$

and

$$K_{b2} = \frac{l_s(l_s - l_b + 2l_e + 2h_b\tan\alpha)\tan\alpha}{l_b - l_s + 2h_b\tan\alpha}E_b \tag{3.3}$$

Furthermore, load degradation underneath the sleepers was found to have a negligible effect on the deck's global response. The stiffness of the spring elements that represent the support bearings is given by Equation 3.4 for the vertical direction $K_{s,v}$ and by Equation 3.5 for the horizontal direction $K_{s,h}$. The equations, given by Manterola (2006) and Rocha (2015), account for all nine bearings (each comprised of two neoprene layers measuring 0.25 m × 0.15 m × 0.004 m and four layers of 0.25 m × 0.15 m × 0.008 m). In the equations, n_b is the number of bearings, n_l is the number of neoprene layers in each bearing, t_i is the thickness of each layer, a and b the dimensions 0.15 m and 0.25 m respectively, f_1 a form factor depending on a and b, and f_2 a factor for dynamic loading that depends on G_n.

$$K_{s,v} = \frac{n_b}{\sum_{i=1}^{n_l}\dfrac{t_i^3}{3G_n a^3 b f_1 f_2}} \tag{3.4}$$

$$K_{s,h} = \frac{n_b abG_n}{\sum_{i=1}^{n_l} t_i} \tag{3.5}$$

PROPERTY NAME	SYMBOL	VALUE	UNITS
Reinforced concrete density	ρ_C	2.5	t/m^3
Concrete elasticity modulus	E_C	36.1	GPa
Slab thickness	t_{slab}	0.7	m
Slab width	b_{slab}	4.475	m
Area of the steel profiles	A_S	0.01975	m^2
Structural damping	ξ	2%	–
Ballast density	ρ_b	1.8	t/m^3
Ballast elasticity modulus	E_b	120	MPa
Ballast layer height	h_b	450	mm
Load distribution angle	α	25	°
Sleeper mass	m_s	272.5	kg
Rail pad stiffness	k_p	350	kN/mm
Track shear stiffness	k_t	2×10^4	kN/m/m
Neoprene shear modulus	G_n	0.975	MPa
Steel elasticity modulus	E_S	210	GPa
Permanent loads	m_p	1.4	ton/m
Width of the sleeper underside	l_b	0.3	m
Half sleeper effective support	l_e	0.95	m
Sleeper spacing	l_s	0.6	m

Table 3.1: Properties of the FE model.

A schematic view of the FEM model of the Canelas bridge is given in Figure 3.5. The respective ANSYS® (2018) model is shown in Figure 3.6, simultaneously with the shape of the first vertical bending mode. Its frequency is 8.60 Hz, which is in proximity to the 8.70 Hz frequency experimentally assessed by Bonifácio et al. (2014). The figure also clarifies how two additional 2.3 m track segments were added on both sides of the deck. These extensions serve the purpose of providing space for the transition of the moving loads so that they can begin crossing the deck without being subjected to an abrupt change in track stiffness.

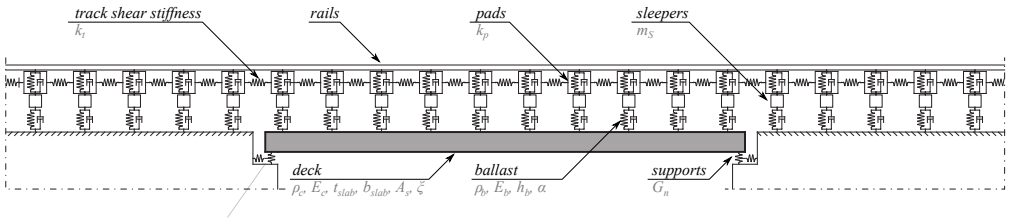

Figure 3.5: Schematic representation of the Canelas bridge model and its variables.

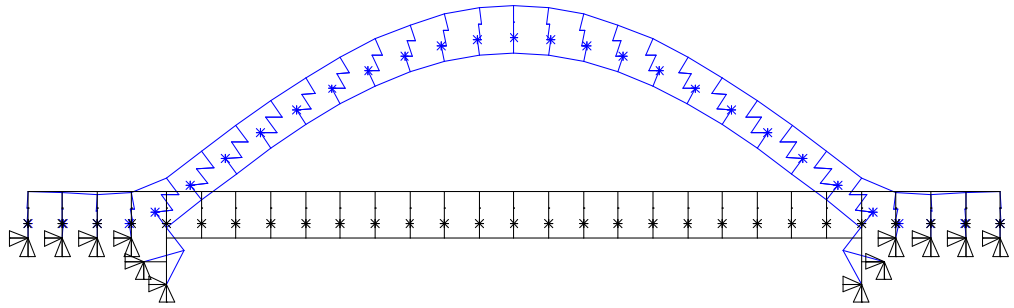

Figure 3.6: Finite elements model of the Canelas bridge (in blue, the deformed shape of the first vertical bending mode).

3.4.2 *Load model configurations*

The load model configurations presented in this section are devised with the objective of studying the difference between train configurations that abide by the HSLM-A's limits (presented in Section 2.2.1.3) and load models outside those limits. For articulated trains, the sets of random variables are listed in Table 3.2, where set A_a contains the variables as defined in the norm and set B_a has the wider limits, intended to represent the influence of future (and existing) trains that do not necessarily respect the norm's limits. The point load value P is set to its maximum allowed value of 170 kN since the highest value corresponds to the maximum acceleration registered.

	SET A_a		SET B_a	
VARIABLE	MIN. (M)	MAX. (M)	MIN. (M)	MAX. (M)
D	18	27	15	30
d_{BA}	2.5	3.5	2	4

Table 3.2: Random variables for articulated trains.

The variables for conventional trains are presented in Table 3.3. As previously discussed, there are no set limits for variable d_{BS}, and for that reason, its values on set A_c (which stem from the real trains of types A, D and F from ERRI D 214/RP 9 (1999)) remain unaltered on set B_c. Since the maximum allowed value of P for conventional trains is the lesser of 170 kN and the value resulting from Equation 2.4, all randomly generated samples undergo that check.

As for regular trains, the random variables are itemized in Table 3.4. An additional variable D_L is here defined to represent the length of each train set's first and last coaches. Its limits are the same both in set A_r and set B_r due to the same reason considered for variable d_{BS} (which for regular trains represents the distance between the centremost bogies of the first and last coaches and the closest axle of the intermediate coach). In both sets, P has a value of 170 kN.

	SET A_c		SET B_c	
VARIABLE	MIN. (M)	MAX. (M)	MIN. (M)	MAX. (M)
D	18	27	15	30
d_{BA}	2.5	3.5	2	4
d_{BS}	5.5	8.5	5.5	8.5

Table 3.3: Random variables for conventional trains.

	SET A_r		SET B_r	
VARIABLE	MIN. (M)	MAX. (M)	MIN. (M)	MAX. (M)
D	10	14	8	16
d_{BA}	2.5	3.5	2	4
D_{IC}	8	11	6	13
e_C	7	10	5	12
d_{BS}	5.5	8.5	5.5	8.5
D_L	15.5	18.5	15.5	18.5

Table 3.4: Random variables for regular trains.

3.5 SIMULATION RESULTS

The simulation results are presented in the current section, following the methodology described in Section 3.2. Firstly, the results concerning the dynamic signatures are given, which are calculated directly from the sampled distances. Afterwards, the dynamic responses on the case study bridge are provided. Additionally, for each type of train, the influence of the individual variables is evaluated by assessing selected samples from sets B_a,B_a, B_c and B_r.

3.5.1 *Analysis based on train signatures*

Given that the case study bridge is a simply supported span, in order to study the HSLM-A, the following dynamic signatures are presented for wavelengths starting at 7 m, as per the EN 1991-2. Figure 3.7 represents the envelope of articulated trains' signatures for both sets, as the line in red. Each of the 10 light grey lines represents one of the HSLM-A universal trains. It can be seen that the load model provides good coverage of the complying articulated trains, particularly above wavelengths of 6 m, while the sampled set B_a produces higher spectra.

For conventional trains, the dynamic signatures represented in Figure 3.8 also show a better coverage for set A_c than for set B_c. It appears to exist, however, a lack of coverage in wavelengths up to 12 m, even for the complying set A_c. This

finding motivates looking into the dynamic analyses to understand whether this is due to the influence of any variable.

As for regular trains, in Figure 3.9, the shown dynamic signatures lead to a similar conclusion regarding the difference between sets A_r and B_r, particularly in the fact that even in set A_r lower wavelengths (up to 17 m) can lead to results above the HSLM-A's. On the other hand, the more significant difference to the HSLM-A dynamic signatures in the 17 m to 30 m range is noted compared to the previously discussed articulated and conventional train types.

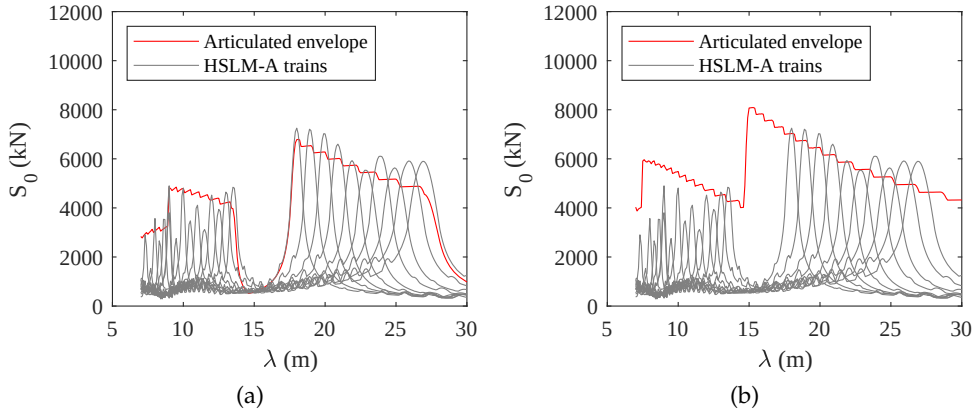

Figure 3.7: Dynamic signatures of the articulated trains. (a) set A_a; (b) Set B_a.

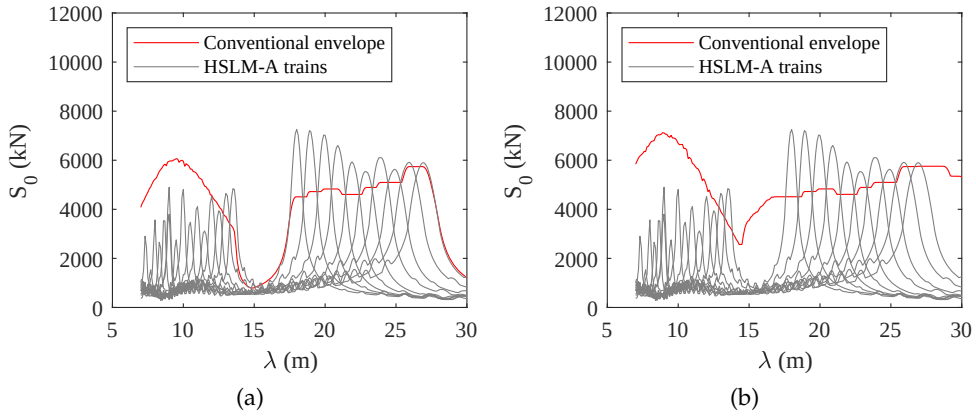

Figure 3.8: Dynamic signatures of the conventional trains. (a) set A_c; (b) Set B_c.

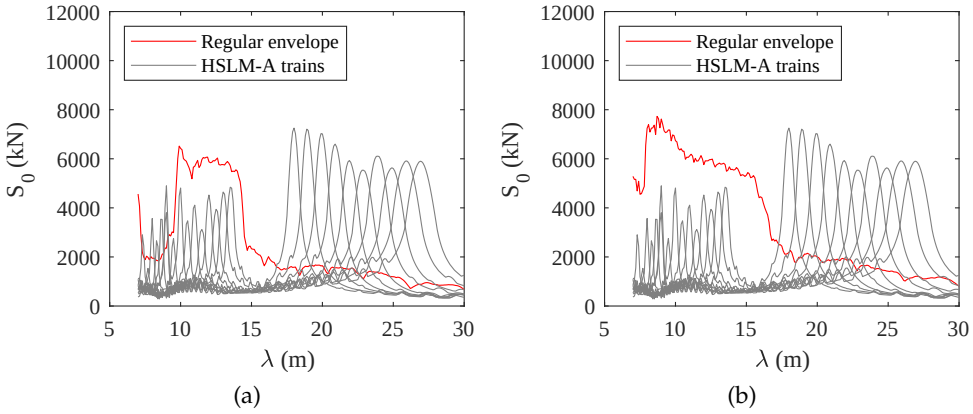

Figure 3.9: Dynamic signatures of the articulated trains. (a) set A_r; (b) Set B_r.

3.5.2 *Dynamic analysis*

The following results represent the entire stochastic dynamic analyses performed on the case study bridge, with the same randomly generated train configurations that constitute sets A and B for the three types of trains. The goal is to validate the conclusions obtained from the signature analysis regarding the HSLM coverage and to better understand which variables contribute the most to the presence of extreme values. The current section reflects a total of 17.4 million dynamic analyses, i.e. the product of the sample size (100,000), number of speed values (29) and number of sets of random variables (6 sets: A_a, B_a, A_c, B_c, A_r, B_r).

3.5.2.1 *Articulated trains*

The results from the dynamic analyses regarding articulated trains are represented in Figure 3.10, for both sets, where each dot represents the maximum vertical deck acceleration calculated for each sampled train. The line in full, which remains unaltered in both sets, is the envelope of the 10 HSLM-A universal train responses, as per the graph in Figure 3.1. Observing the results, it can be seen that the sample set generated within the norm's limits is adequately covered by the HSLM, apart from a few outliers (which is in accordance with the findings by Museros et al. (2021)). As expected, the load model does not cover the resulting values from set B_a, especially in higher velocities. This finding is unfavourable towards the first question listed in Section 3.1, even though this matter is not the main focus of the study.

To better understand the independent influence of each variable, Figure 3.11 and Figure 3.12 present selections of results from set B_a, alternately highlighting a variable's influence when it is taken above or below the stated limits of validity while selecting the complying values for the other variables. From Figure 3.11, it can be seen that there is a similar contribution from simulated trains whose coach length is inferior to the limit and due to those that are above it.

As for the distance between axles (Figure 3.12), while its lower values lead to higher results, its consequences are not as notorious. In fact, as D decreases,

resonant effects become more noticeable in the bridge, taken as the example in this chapter.

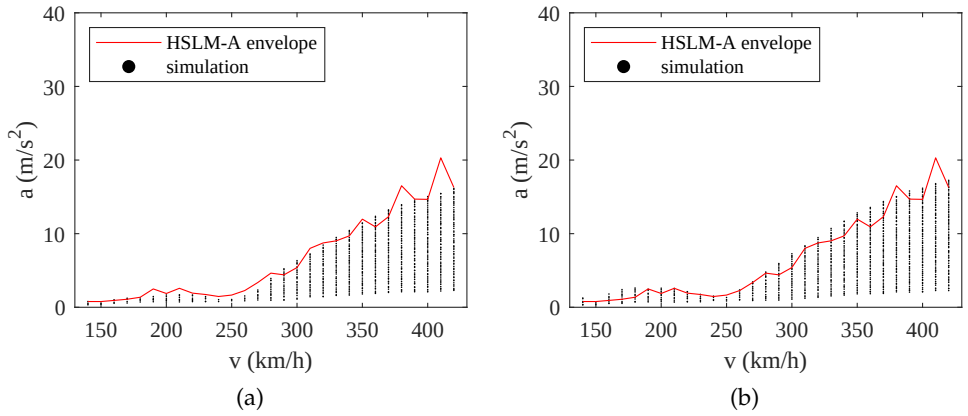

Figure 3.10: Dynamic response of the articulated trains. (a) set A_a; (b) Set B_a.

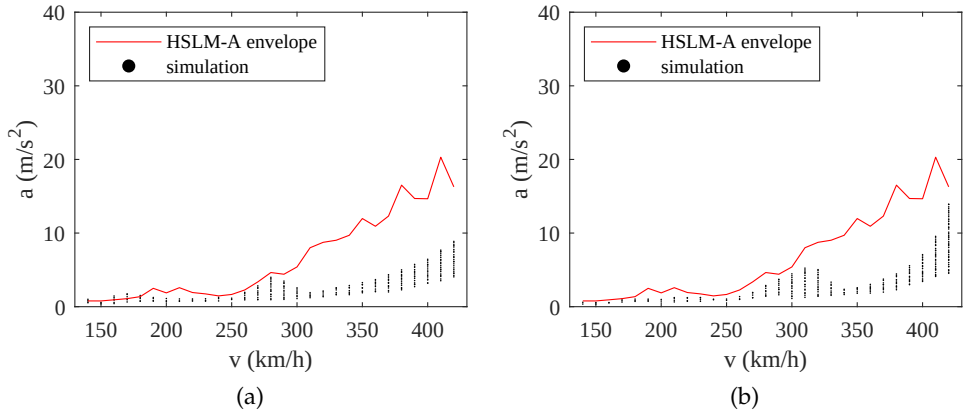

Figure 3.11: Selected results from set B_a highlighting variable D: (a) 15 m $\leq D \leq$ 18 m, 2.5 m $\leq d_{BA} \leq$ 3.5 m; (b) 27 m $\leq D \leq$ 30 m, 2.5 m $\leq d_{BA} \leq$ 3.5 m.

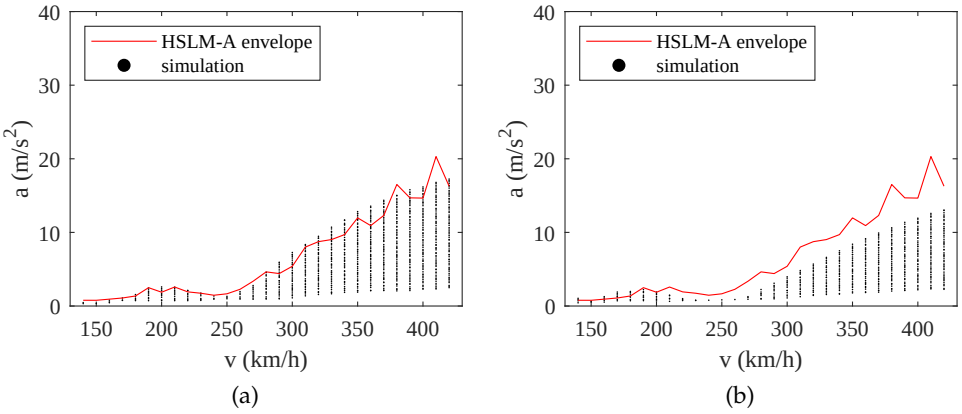

Figure 3.12: Selected results from set B_a highlighting variable d_{BA}: (a) 18 m $\leq D \leq$ 27 m, 2 m $\leq d_{BA} \leq$ 2.5 m; (b) 18 m $\leq D \leq$ 27 m, 3.5 m $\leq d_{BA} \leq$ 4 m.

3.5.2.2 *Conventional trains*

The results of the dynamic analyses with conventional trains are shown in Figure 3.13. In it, it is noted that even set A_c, which is in accordance with the normative limits, includes load model configurations that cause dynamic effects greater than those produced by the HSLM-A universal trains. The lack of coverage discussed with the dynamic signatures is once more present in a corresponding range of wavelengths. In fact, considering that the frequency of the first vertical bending mode for the bridge is 8.60 Hz, the wavelength range corresponding to the 280 km/h to 370 km/h speed range is 9.04 m to 11.95 m.

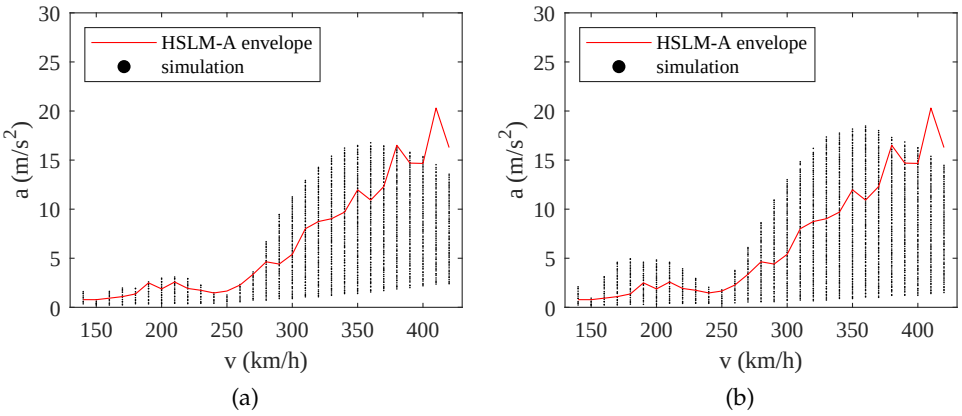

Figure 3.13: Dynamic response of the conventional trains. (a) set A_c; (b) Set B_c.

As stated in Section 3.4.1, Sets A_c and B_c were selected to infer the effects of including additional damping in the dynamic analyses. For that, a new single load was generated from the FE model of the Canelas bridge, considering a total

structural damping ξ_{total} given by the formula found in the original EN 1991-2 (CEN, 2003) of:

$$\xi_{total} = \xi + \Delta\xi = 2\% + \frac{0.0187L - 0.00064L^2}{1 - 0.0441L - 0.0044L^2 - 0.000255L^3}\% \\ = 2\% + 0.476\% = 2.476\% \quad (3.6)$$

The results of the dynamic analyses, as well as the HSLM envelopes generated with additional damping, are given in Figure 3.14. Both the simulations' distributions and the envelopes have the appearance of scaled-down versions of the responses without additional damping of Figure 3.13. The relation between the randomly generated train load models and the HSLM is maintained, and the issue raised before, i.e. noticing that there are load configurations in set A_c that surpass the HSLM-A envelope, is still observable. The lack of a substantial effect is, therefore, consistent with the removal of the additional damping provision in the current EN 1991-2 (CEN, 2023b).

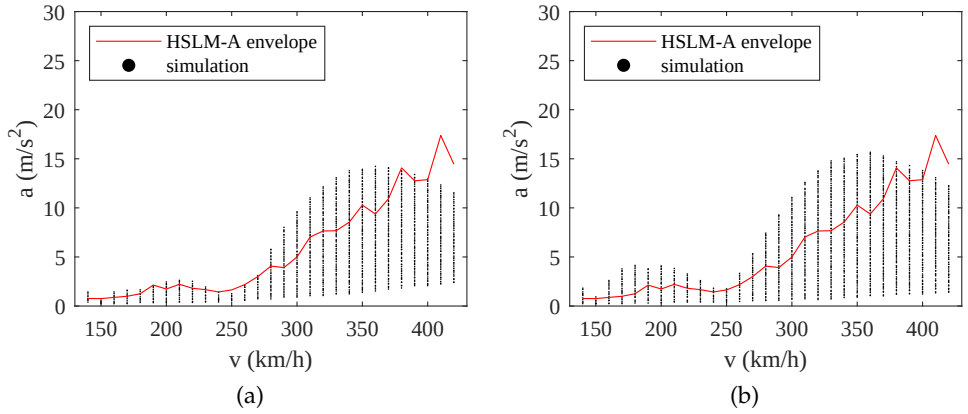

Figure 3.14: Dynamic response of the conventional trains, considering additional structural damping. (a) set A_c; (b) Set B_c.

Regarding the individual variables' influence, it can be seen once more that the exceedingly higher values on the highest speeds correspond to the lowest values of D (Figure 3.15). On the other hand, it is the higher values of d_{BA} that result in lower acceleration peaks (Figure 3.16). In fact, the only scenario where the outlying values between 280 km/h and 370 km/h tend to disappear is the scenario that considers d_{BA} values above the allowed limit. To better understand this phenomenon, Figure 3.17 shows the distribution of variable d_{BS} from simulations whose dynamic response is superior to that of the HSLM, for two example speed values within the 280 km/h to 370 km/h range. It is visible that the outlying simulated trains correspond to increasingly higher values of this variable. This observation underlines the pertinence of the third question listed in Section 3.1 since the Eurocode could be clearer in defining limits for this distance. When looking at the distribution of variable d_{BA} from the same samples (illustrated in Figure 3.18), a concentration on lower values appears. Therefore, it can be concluded that the most aggressive scenarios correspond to higher d_{BS} and lower d_{BA}. Indeed, as d_{BS} increases (approaching

D in its values), the regularity of the moving loads grows, contributing to dynamic effects. As for d_{BA}, as it decreases, the effect of the pair of moving loads approaches that of a single double-load.

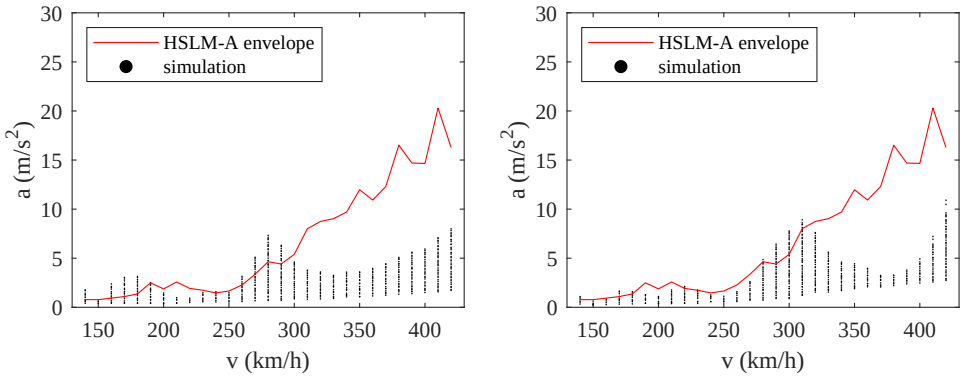

Figure 3.15: Selected results from set B_c highlighting variable D: (a) 15 m $\leq D \leq$ 18 m, 2.5 m $\leq d_{BA} \leq$ 3.5 m; (b) 27 m $\leq D \leq$ 30 m, 2.5 m $\leq d_{BA} \leq$ 3.5 m.

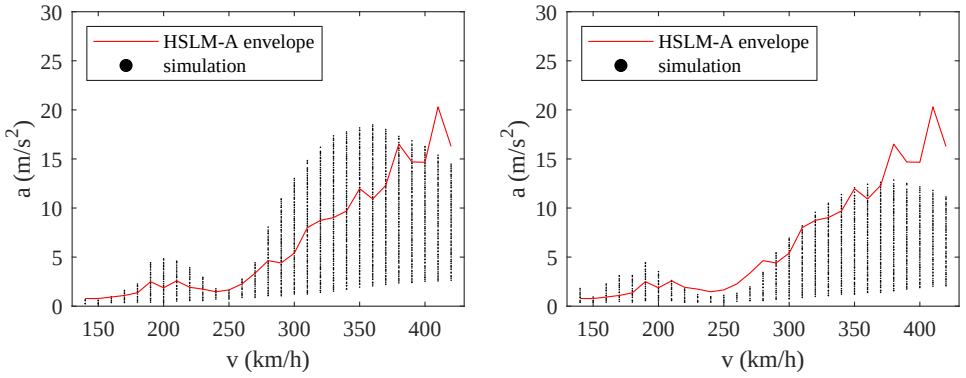

Figure 3.16: Selected results from set B_c highlighting variable d_{BA}: (a) 18 m $\leq D \leq$ 27 m, 2 m $\leq d_{BA} \leq$ 2.5 m; (b) 28 m $\leq D \leq$ 27 m, 3.5 m $\leq d_{BA} \leq$ 4 m.

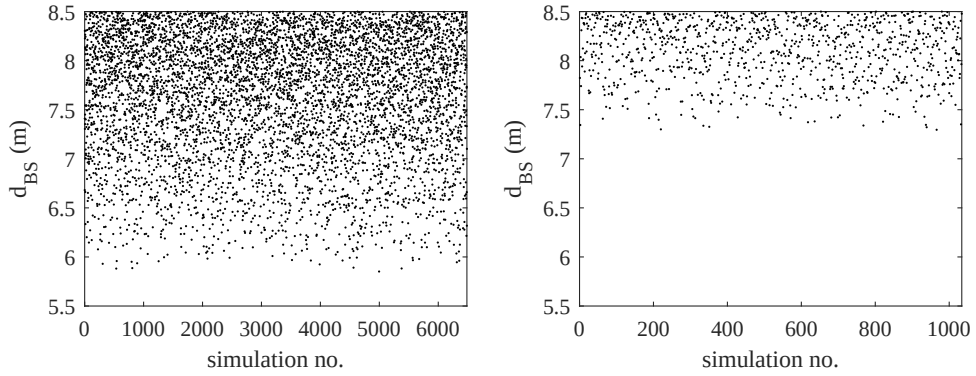

Figure 3.17: Distribution of variable d_{BS} from simulations of the dynamic response of conventional trains above the HSLM envelope, from set B_c: (a) 300 km/h;(b) 350 km/h.

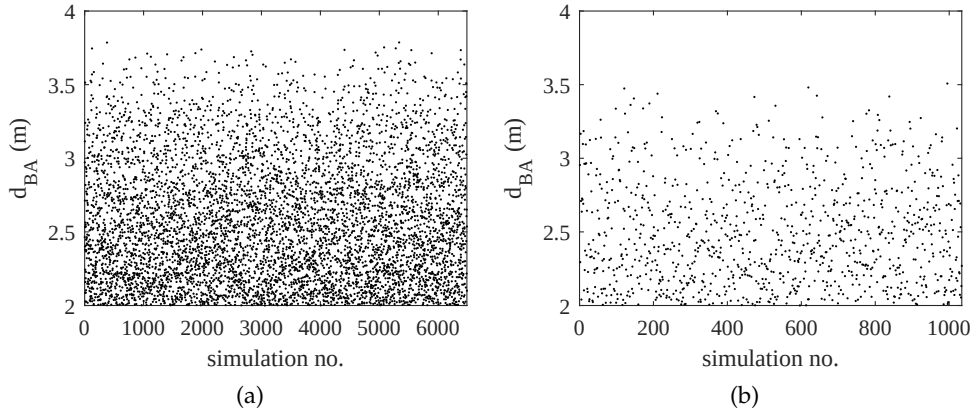

Figure 3.18: Distribution of variable d_{BA} from simulations of the dynamic response of conventional trains above the HSLM envelope, from set B_c: (a) 300 km/h;(b) 350 km/h.

3.5.2.3 *Regular trains*

The dynamic responses of sets A_r and B_r, corresponding to the regular trains, are presented in Figure 3.19. While both sets contain train load configurations that result in acceleration values above the HSLM-A's, distributions on set A_r tend to follow the trend of the envelope more closely throughout the entire speed range. From the individual variable influence, in this case, there is some variability caused by D (Figure 3.20), while variable d_{BA} (Figure 3.21) is the less influential. The same can be observed for the D_{IC} (Figure 3.22) and e_C (Figure 3.23) variables, although it should be highlighted that the former only controls four load distances and the latter a single one.

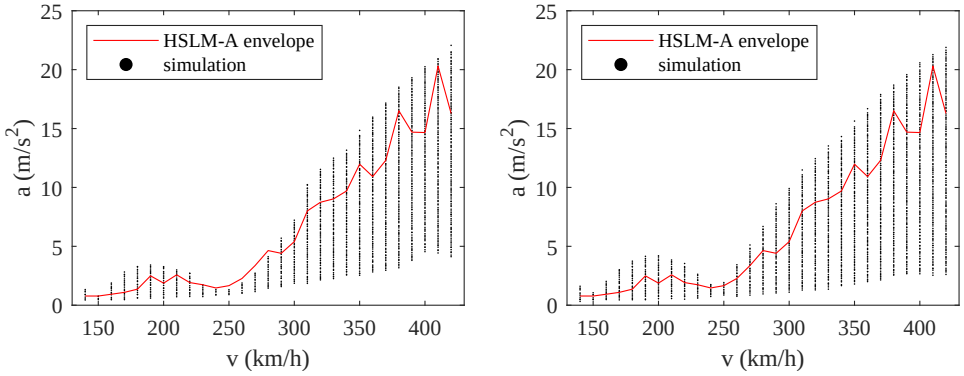

Figure 3.19: Dynamic response of the regular trains. (a) set A_r; (b) Set B_r.

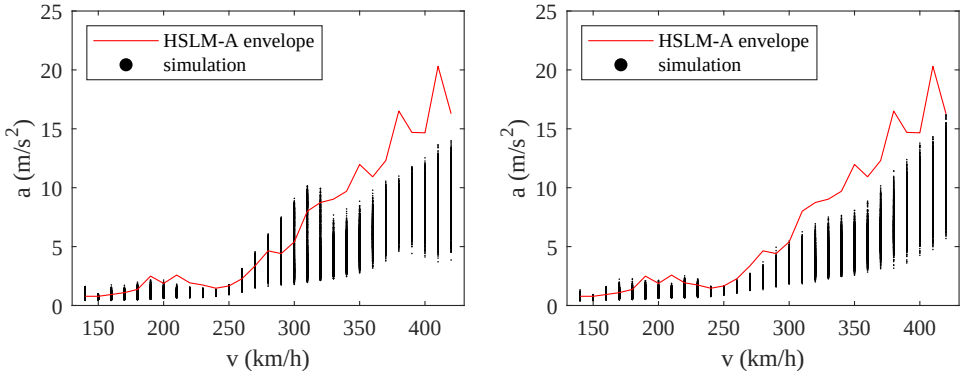

Figure 3.20: Selected results from set B_r highlighting variable D: (a) 8 m $\leq D \leq$ 10 m, 2.5 m $\leq d_{BA} \leq$ 3.5 m, 8 m $\leq D_{IC} \leq$ 11 m, 7 m $\leq e_C \leq$ 10 m; (b) 14 m $\leq D \leq$ 16 m, 2.5 m $\leq d_{BA} \leq$ 3.5 m, 8 m $\leq D_{IC} \leq$ 11 m, 7 m $\leq e_C \leq$ 10 m.

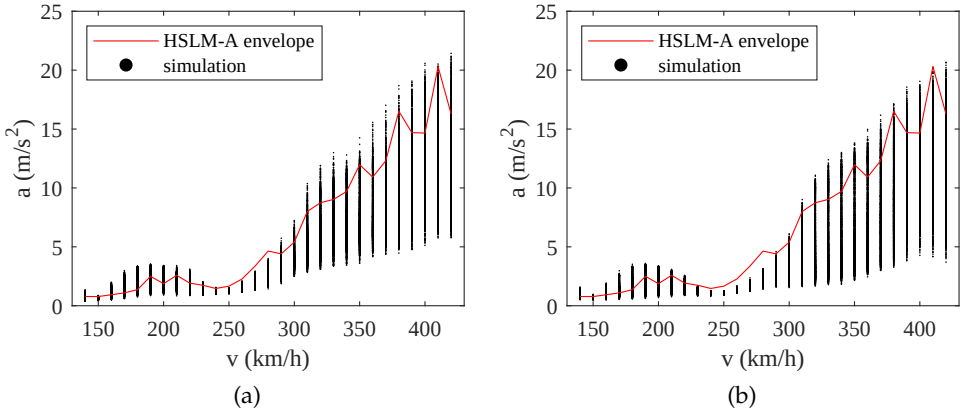

Figure 3.21: Selected results from set B_r highlighting variable d_{BA}: (a) 10 m $\leq D \leq$ 14 m, 2 m $\leq d_{BA} \leq$ 2.5 m, 8 m $\leq D_{IC} \leq$ 11 m, 7 m $\leq e_C \leq$ 10 m; (b) 10 m $\leq D \leq$ 14 m, 3.5 m $\leq d_{BA} \leq$ 4 m, 8 m $\leq D_{IC} \leq$ 11 m, 7 m $\leq e_C \leq$ 10 m.

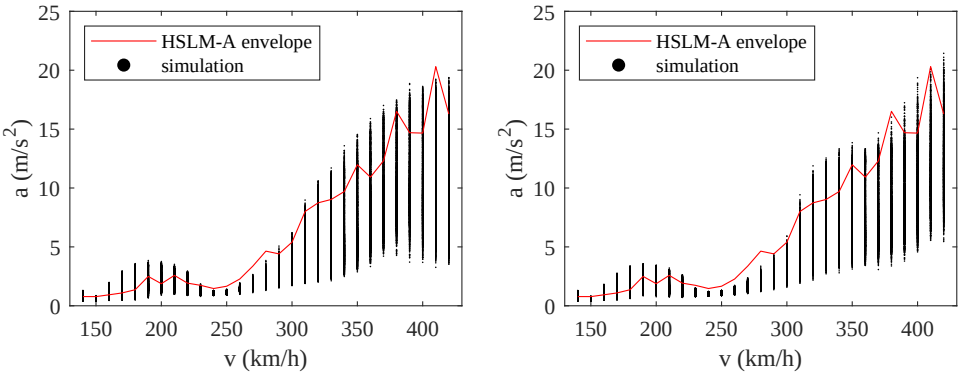

Figure 3.22: Selected results from set B_r highlighting variable D_{IC}: (a) 10 m $\leq D \leq$ 14 m, 2.5 m $\leq d_{BA} \leq$ 5.5 m, 6 m $\leq D_{IC} \leq$ 8 m, 7 m $\leq e_C \leq$ 10 m; (b) 10 m $\leq D \leq$ 14 m, 2.5 m $\leq d_{BA} \leq$ 3.5 m, 11 m $\leq D_{IC} \leq$ 13 m, 7 m $\leq e_C \leq$ 10 m.

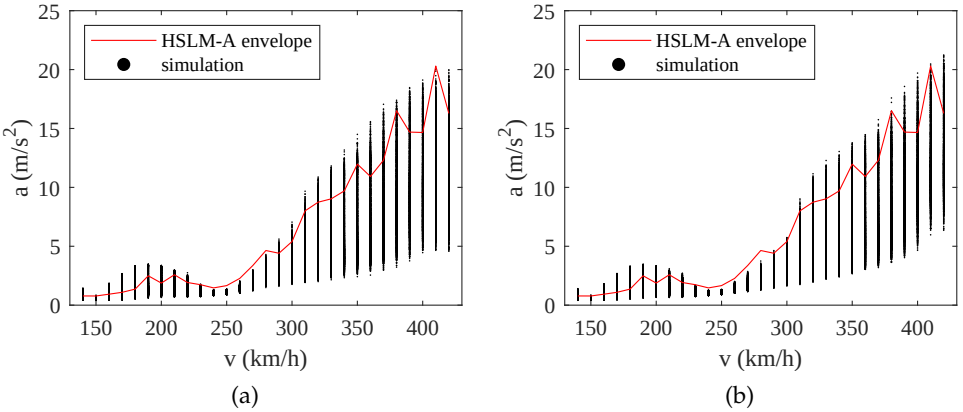

Figure 3.23: Selected results from set B_r highlighting variable e_C: (a) 10 m $\leq D \leq$ 14 m, 2.5 m $\leq d_{BA} \leq$ 5.5 m, 8 m $\leq D_{IC} \leq$ 11 m, 5 m $\leq e_C \leq$ 7 m; (b) 10 m $\leq D \leq$ 14 m, 2.5 m $\leq d_{BA} \leq$ 3.5 m, 8 m $\leq D_{IC} \leq$ 1m̃, 10 m $\leq e_C \leq$ 12 m.

3.6 CONCLUDING REMARKS

Concerning the research questions proposed in Section 3.1, the observed conclusions can be listed as follow:

1. With the extended limits considered in this chapter, it can be said that the HSLM-A is partially suited to represent some future trains, given the similarity in the results for both sets A and B on speeds up to 400 km/h (on the selected example bridge), or wavelengths excluding the 15 m to 17 m range. Nevertheless, this should not be thought of as a lack of readiness of the load model but more as an indicator of the need for future-proofing;

2. The 10 HSLM-A universal trains do not cover the dynamic effects of some theoretical train load models that can be constructed abiding by the EN 1991-2 limits of validity. This happens in some limit cases of articulated trains, but it is most prevalent in conventional and regular trains. It should be noted that the last two train types lack in the definition of some variables. In conventional trains, there is a relation between the non-complying trains and the increasing distance between centres of adjacent vehicle's bogies. In fact, as this variable increases, the effect of consecutive bogies acts progressively more as individual loads and less as pairs, which in turn leads to higher vertical acceleration levels due to the contribution that the loads' repetition has to the existence of resonant effects;

3. The detail in defining variable d_{BS} in the norm is insufficient, and this constitutes an obstacle to the evaluation of the HSLM's limits of validity, which is made more apparent when this variable's importance is noted. There is also a challenge in defining the two distances, which are not mentioned in the norm, necessary to characterize regular trains.

It is understood that there are issues with the current load model, and therefore, there is some margin for improvement in Annex E of the EN 1991-2, not only by providing better definitions of some distances but also by adjusting the HSLM-A's universal trains. In this regard, future work should focus on parametric studies for the definition of the proposed load models, including equivalent train-track-bridge interaction models with replication of the HSLM's effects. The methodology applied in this work to assess the case study bridge's dynamic response and the HSLM's adequacy in covering the effects of different trains can be utilized and replicated for a number of different high-speed railway bridges.

4

PROBLEM 2: ENHANCED SAFETY FACTOR FOR THE DECK ACCELERATION LIMIT ON BALLASTED BRIDGES

4.1 INITIAL CONSIDERATION

In the Eurocode EN 1990 (CEN, 2023a), track stability in ballasted bridges is conditioned by a vertical deck acceleration limit of 3.5 m/s^2. Since experimental studies show that ballast instability occurs at around 7.0 m/s^2, as mentioned in Section 2.2.1.2, the normative limit seems to be arbitrarily based on a safety factor of 2.0. The study of the suitability of a lower safety factor, which is the topic of this chapter, constitutes a probabilistic assessment problem.

Considering the discrepancy between the normative limit and the experimentally assessed acceleration limit, the following research questions are posed:

1. How can critical train speeds associated with low probabilities of failure be evaluated in a timely manner?
2. How to set up scenarios to calculate the acceleration in the design phase?
3. Can the safety factor (i.e., the ratio of the physical acceleration limit to the permissible value) be less than 2.0?

To address these issues, the present chapter, which follows the work detailed in Ferreira et al. (2025) (Appendix B), proposes definitions for critical speed, design scenarios, and safety factor in Section 4.2, followed by the introduction of an algorithm for the efficient assessment of the critical speeds in Section 4.3. Four case study bridges are presented in Section 4.4. A parametric study to optimize the critical speed algorithm is given in Section 4.5, allowing the calculation of critical speeds in Section 4.6. In the same Section, after a sensitivity analysis of the random variables, two design scenarios are proposed, and the final safety factors are calculated. Normative recommendations are discussed in Section 4.7, and the main conclusions are listed in Section 4.8.

4.2 METHODOLOGY

The present section describes the procedure to calculate safety factors on existing bridges and provides the necessary definitions. It is divided into three steps, which are outlined in Fig. Figure 4.1 and developed in the following subsections. The first step (Section 4.2.1) is determining at what speed a load model causes an excessively high deck acceleration. Using bridge models constructed with random variables, this first step involves probabilistic analysis. Having found this critical speed (v_{crit}), the second step (Section 4.2.2) is to determine the acceleration value that can be calculated with fixed values for the variables (instead of probabilistic analysis). The instructions on how to set the variables to do a deterministic analysis are hereinafter referred to as the design

scenarios. Employing such scenarios is beneficial to ensure that trustworthy results are attainable in the engineering practice of bridge design with simple analyses. The third step (Section 4.2.3) is to locate, in the design scenarios, the acceleration value at the critical speed, here named "design acceleration" (a_{Ed}). The margin between this value and the physical limit of 7.0 m/s^2 (a_{Rl}) indicates the distance to safety. Therefore, the safety factor (γ_{bt}) can finally be estimated by dividing 7 by the design acceleration.

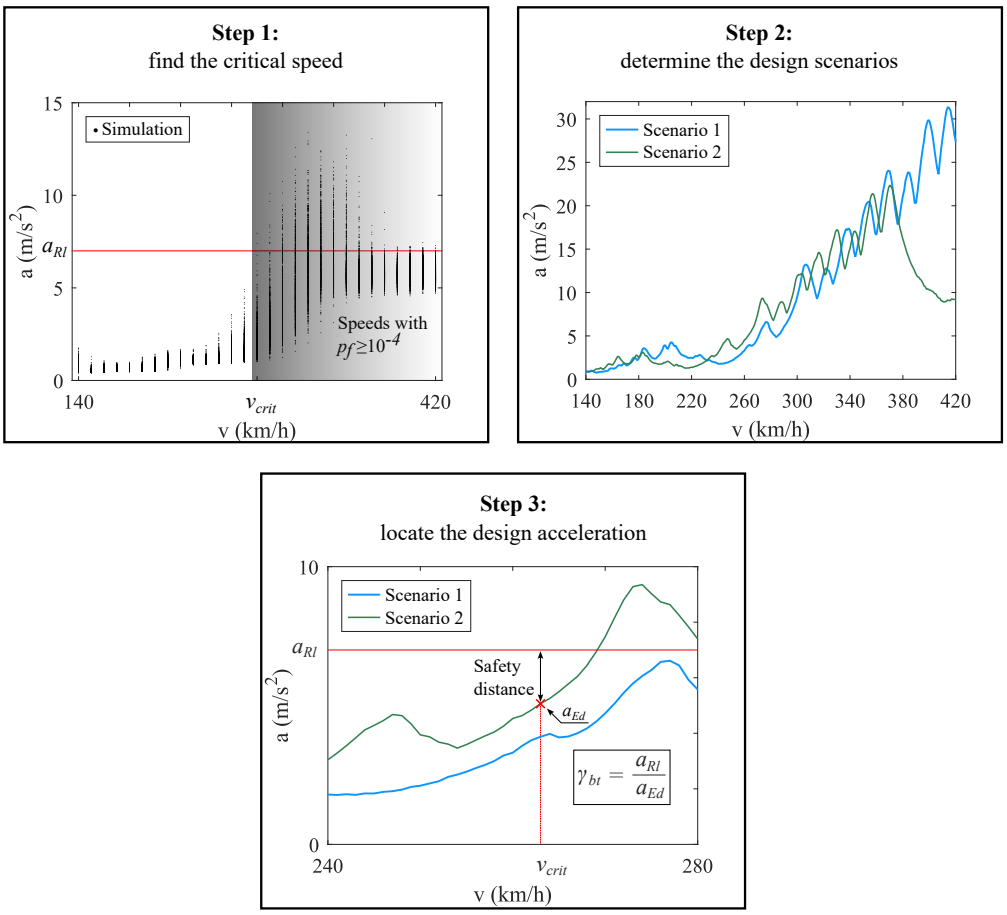

Figure 4.1: Overview of the methodology for estimation of safety factors for the deck acceleration criterion.

4.2.1 *Step 1: Find the critical speed*

This study of ballasted track bridges assesses failure due to track instability (loss of stability of the ballast layer), assuming that the 7.0 m/s^2 value for vertical deck acceleration is a physical value that acts as the safety threshold (considering the experimental studies discussed in Section 2.2.1.2). Therefore, a failure event is considered to have occurred if a bridge deck experiences a vertical acceleration a greater than this limit (a_{Rl}) when subjected to any load model at any given train speed. It is also assumed that the loss of stability can ultimately lead to derailment and that this risk corresponds to Class 3 consequences, as defined in the Probabilistic Model Code of the Joint Committee for

Structural Safety (JCSS, 2001) (discussed in Section 2.4.5.1 and Table 2.19). In this thesis, it is considered that the relative cost of safety measure (extensive measurements through safety inspections over significant periods of time) is large. This combination of consequence and cost corresponds, in the Probabilistic Model Code, to a target reliability index β of 3.7, which is equivalent to probabilities of failure in the order of magnitude of 10^{-4} (the same target from Rocha et al. (2016) and Allahvirdizadeh et al. (2024a)). The probability of failure p_f is therefore defined as:

$$p_f = P\left(a \geq a_{Rl}\right) \tag{4.1}$$

When testing a load model, different train speeds result in different maximum values of vertical deck acceleration. For this study, a critical speed is defined, for a given load model, as the lowest speed that causes the following condition:

$$p_f \geq 10^{-4} \tag{4.2}$$

The High-Speed Load Model (HSLM-A, presented in Section 2.2.1.3) (CEN, 2023b), whose purpose is to represent the envelope of actions of real high-speed rolling stock traffic, is employed in this work. This load model, which is used for the design of high-speed railway bridges, is given as a set of 10 configurations of axle loads and spacings and is intended for moving loads analysis. For a given bridge, critical speeds can be calculated for each of the 10 HSLM-A. These individual critical speeds $v_{crit,i}$ form a set. The minimum value of the set gives the critical speed v_{crit} of the bridge:

$$v_{crit} = \min\left(\{v_{crit,i}\}_{i=1}^{10}\right) \tag{4.3}$$

4.2.2 *Step 2: Determine the design scenarios*

The scenarios for bridge design are defined in this thesis as sets of deterministic values attributed to structural and track variables utilized to calculate the dynamic response of railway bridges. Two sets are defined in accordance with the provisions of the EN 1991-2 (CEN, 2023b), which requires a lower bound estimate of stiffness and structural damping and both upper and lower bound estimates of mass. This procedure is meant to maximize the acceleration response and to avoid overestimating the resonant speed. In spite of this statement being present in the Eurocode, the norm does not specify which variables are to be considered in the estimates, nor what constitutes upper or lower bounds. Since in this chapter either normal or uniform distributions are utilized, the bounds are proposed as follows:

NORMAL DISTRIBUTIONS: For variables with distribution $N\left(\mu, \sigma^2\right)$, adopt as bounds $\mu \pm 1.64\sigma$, corresponding to the 5% and 95% percentiles.

UNIFORM DISTRIBUTIONS: For uniformly distributed random variables $U\left(a, b\right)$, adopt the respective minima and maxima.

Regarding the selection of random variables to be included in the definition of scenarios, it should be noted that depending on the complexity of the models employed, stiffness, damping, and mass can be related to more than one variable and even share variables. Therefore, it is necessary to perform a parametric study of the relative influence of each variable. The proposed methodology for such a study starts with setting all variables to their mean value and calculating the resulting deck acceleration envelope considering the 10 HSLM-A. The response vector is $\mathcal{X}$ for a given speed range with k speed values. Then, each variable is independently set to its upper or lower bound, resulting in a new response vector $\mathcal{Y}$, with the same length k. To evaluate the influence of each variable, the variance of the absolute difference between the vectors is calculated as:

$$\mathrm{Var}\left(|\mathcal{X}-\mathcal{Y}|\right)=\frac{\sum_{i=1}^{k}\left(|\mathcal{X}_i-\mathcal{Y}_i|-\mathrm{E}\left(|\mathcal{X}_i-\mathcal{Y}_i|\right)\right)}{n-1} \tag{4.4}$$

Consequently, the most influential variables are included in the definition of the two design scenarios. Both scenarios use a lower bound on the variables that control stiffness and damping. The first scenario (S1) uses a lower bound estimate of mass, while the second (S2) uses an upper bound. The variables that are not considered influential enough after the parametric study are taken at their mean values. This step of the methodology concludes with the calculation of the response envelope of both scenarios under the effect of the 10 HSLM-A configurations.

4.2.3 *Step 3: Locate the design acceleration*

At this point, the maximum speed that can be considered safe is already known. The remaining question is how far away the design scenarios are from the actual failure events. The value on the envelope of the design scenarios at v_{crit} is here given the name of design acceleration a_{Ed}. The safety factor, henceforth referred to as γ_{bt}, is defined in this thesis as the ratio between the physical value a_{Rl} and the acceleration calculated in the design phase a_{Ed}, and is given by:

$$\gamma_{bt}=\frac{a_{Rl}}{a_{Ed}}=\frac{7}{a_{Ed}} \tag{4.5}$$

4.3 SUBSET SIMULATION APPLICATION FOR THE ESTIMATION OF CRITICAL SPEED

4.3.1 *Application basics*

Monte Carlo simulation, while a highly reliable approach, implies an escalation in computational cost as the intended target probabilities of failure get lower. In fact, as discussed in Section 2.4.3.1, the appropriate sample size N to assess a 10^{-4} probability, according to Equation 2.99 (Bjerager, 1991), would be from 10,000 to 100,000. Such a number would be feasible for moving loads analysis and lower complexity 2D finite elements models. However, any change in the

train's running speed or load requires a new analysis. Therefore, the search for critical speed can quickly grow to hundreds of thousands (or millions) of dynamic analyses.

Subset simulation (presented in detail in Section 2.4.4.3) is hence chosen to estimate the probabilities of failure. With this method, p_f is estimated as the conditional probability of reaching the unsafe region in a reliability problem through successive increments of intermediate failure events. Au and Beck (2001) calculate p_f as:

$$p_f = P(F_i) \prod_{i=1}^{m-1} P(F_{i+1}|F_i) \tag{4.6}$$

where F_i are m number of intermediate events (or levels) such that $F_1 \supset F_2 \supset \ldots F_m$. For the first level, $P(F_1)$ is estimated with a crude Monte Carlo simulation, provided a reasonable N. The resulting acceleration values are ordered from highest (belonging to F_1) to lowest (farthest from F_1), as illustrated in Figure 4.2a. Given a selected arbitrary intermediate probability p_0, the $(p_0 \times N)$-th value is classified as the cut-off y^*. The states of the random variables corresponding to values greater than or equal to y^* are used as generators (x) to generate the sample of the next level $(\tilde{x})$, using the Modified Metropolis Algorithm (Section 2.4.4.3). This ensures that the states of the variables of the resulting sample are inside F_1. It is visible, in the example in Figure 4.2b, how every result in $i = 2$ is greater or equal to the cut-off that defines F_1. The process is repeated (Figure 4.2c and Figure 4.2d) until y^* is found inside F_m (i.e., $P(F_i) > p_0$). With $p_0 = 0.1$, probabilities of the order of magnitude of $10^{-4} = 0.1 \times 0.1 \times 0.1 \times 0.1$ are attainable with four levels ($F_m = F_4$). Note that in Figure 4.2d, with $p_0 = 10$ and $N = 100$, $y*$ is in the 10th ordered position. Since in that example there are 13 results equal or greater than $y*$, $P(F_4) = 13/100 = 0.13 > p_0$, and as such, $p_f = 0.13 \prod_{i=1}^{4-1} 0.1 = 1.3 \times 10^{-4}$.

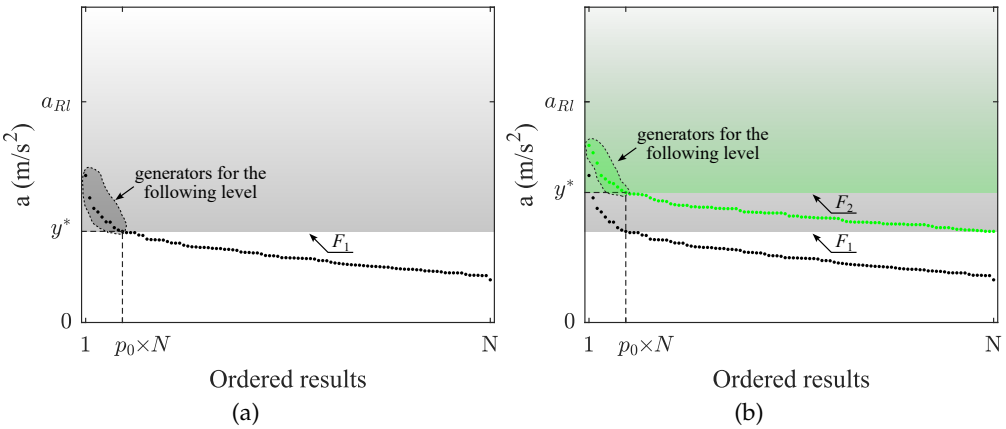

Figure 4.2: Visualization of subset simulation. (a) $i = 1$; (b) $i = 2$; (c) $i = 3$; (d) $i = 4$.

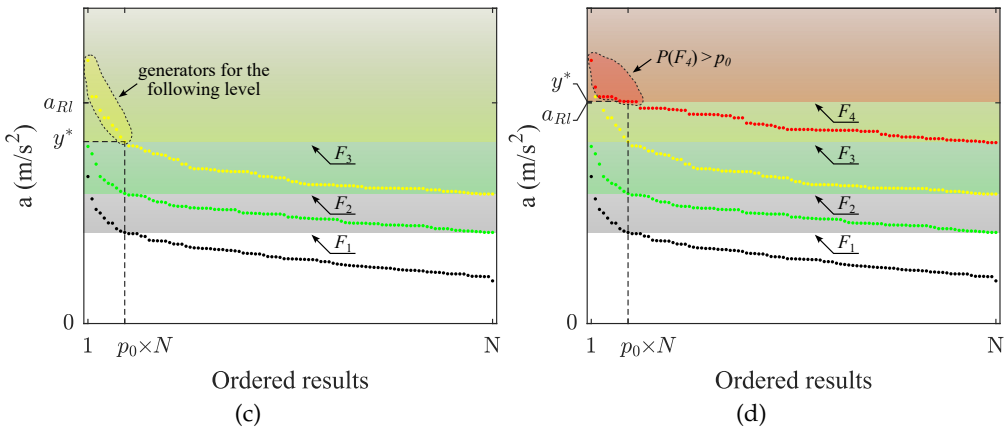

Figure 4.2: (continued) Visualization of subset simulation. (a) $i = 1$; (b) $i = 2$; (c) $i = 3$; (d) $i = 4$.

The diagram in Figure 4.3 illustrates how subset simulation is applied in practice for this study. Initially, the random variables are sampled (using MATLAB® (2018)) and combined with existing constant quantities to create the input for the FE model, which is created in ANSYS® (2018). The dynamic response is calculated for the desired load model (i.e. one of the 10 HSLM-A configurations) using the Single Load Linear Superposition method (introduced in Section 3.3.2) because of its efficacy and ease of application. It is then filtered with a low-pass Type II Chebyshev filter, cut off at 60 Hz (although the EN 1990 only requires the consideration of frequencies up to 30 Hz, studies have highlighted the importance of extending the frequency range (Horas, 2011)) and the maximum absolute acceleration is stored for each randomly generated bridge. After this crude Monte Carlo phase, if no stopping criterion is met, the level counter is increased, and the ordered results greater or equal to y^* are used as the seeds for the Markov Chain Monte Carlo (MCMC). The MMA implementation is based on Uribe (2016). In this work, the adopted proposal PDFs to obtain candidates η from the current state of a variable x_k are:

- for Gaussian distributed variables $N\left(\mu, \sigma^2\right)$: $\eta \sim N\left(x_k, \sigma^2\right)$;
- for uniformly distributed variables $U\left(a, b\right)$: $\eta \sim N\left(x_k, \dfrac{(b-a)^2}{12}\right)$;

With the samples of the next level, new FE models are obtained, and the dynamic responses for the new set are calculated. The process stops after the $P(F_i) > 0.1$ condition occurs (after which p_f can be estimated) or if $i = 4$ (i.e., if the subset simulation is already in the fourth level, any possible p_f would be lower than 10^{-4}, and therefore not worthy of further exploration for the purposes of this thesis). If $i \leq 4$, p_f is given by:

$$p_f = (p_0)^{i-1} \times P(F_i) \tag{4.7}$$

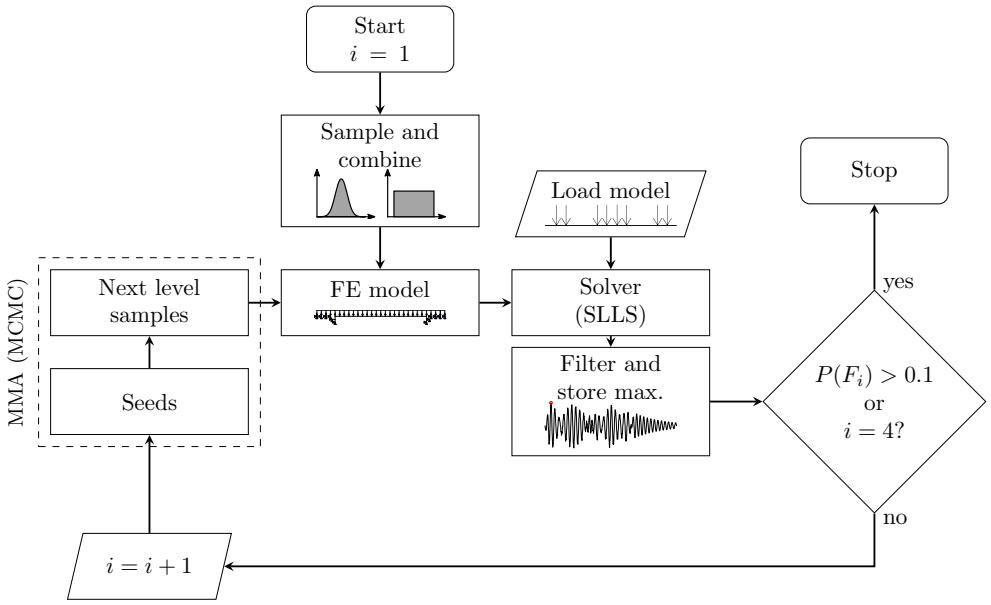

Figure 4.3: Application of subset simulation.

4.3.2 *Critical speed algorithm*

Although the application of subset simulation is associated with considerable savings in computation time, this only applies to the estimation of probabilities for a given running speed. That is, the question remains for which speed or set of speeds the probabilities must be calculated. Simulating in coarse intervals of 10 km/h is incompatible with the sensitivity of most dynamic calculations concerning speed. Conversely, a finer 1 km/h interval is not feasible given all the possible values in a usual speed interval.

Hence, an algorithm is proposed here to efficiently assess the critical speed, summarized in Figure 4.4. The objective of this procedure is to avoid wasting computational resources that would be misused by calculating probabilities of failure lower than 10^{-5}. When the search cycle is initialized, the running speed v is set to its initial value (the lowest in the given speed range). After the initial analysis (i.e. the crude Monte Carlo simulation in $i = 1$), if the cut-off y^* is lower than a chosen threshold value y_t, the speed is increased to the next value. Note that y_t must be chosen appropriately so that exceeding it represents a substantial likelihood that p_f is in the vicinity of 10^{-4}. Initially, the speed increment is a coarse interval of 20 km/h. The cycle continues until the $y^* > y_t$ condition is satisfied. If the resulting p_f is greater than 10^{-4}, a finer speed cycle of 1 km/h increments is triggered, symbolized by the flag $\boxed{\text{F}}$. The running speed is brought back to the value immediately after the second-highest calculated speed ($v = v - 19$ km/h), and the cycle continues. During this phase, if $y^* < y_t$, flag $\boxed{\text{D}}$ is activated to store the information that at least one running speed was discarded during the finer cycle. The first time that a $p_f > 10^{-4}$ is found, the current v is classified as a suitable candidate. If $\boxed{\text{D}}$ is off, no previous speed was discarded in $F1$ (i.e., the speed or speeds immediately before were calculated but turned out to be in the magnitude of

10^{-5} or lower), and the candidate is immediately accepted as v_{crit}. Otherwise, a $v = v - 1$ reverse search cycle is activated to check the previously discarded speed value until v_{crit} is confirmed.

For the proposed algorithm to be viable in terms of computational savings, it is imperative that the N, p_0, and y_t parameters are properly set. Unoptimized parameters may lead to inefficient use of simulation capacity for the following reasons:

- spending unnecessary time calculating v_{crit} candidates that result in $p_f \approx 0$;
- increased amount of entries in the $v = v - 1$ reverse search cycle
- insufficient dispersion in $i = 1$ results, jeopardizing further levels.

Hence, a sensitivity study is performed with the objective of setting appropriate parameters. The metrics adopted are the time required to go from v=140 km/h to v_{crit} and the total sample size n_S required for the simulation. The results are presented in Section 4.5.

An example of a complete run of the algorithm is depicted in Figure 4.5 (in the graphics, the offset in the coloured dots is meant to improve clarity and does not denote a change in speed). In this case, the sample size N for each level is 100 and $p_0 = 0.1$, which means that in the sorted results, y^* is in the $100 \times 0.1 = 10$-th position. In simulations 1 to 7, y^* was lower than y_t (3 m/s^2 in this case), meaning that no simulation progressed beyond $i = 1$. In simulation 8, y^* is greater than y_t, causing the simulation to continue, resulting in a calculated p_f of 0.02. This result at 280 km/h initiates the finer speed increment cycle at 280-19=261 km/h. Simulations 9, 10 and 11 (261 km/h, 262 km/h, and 263 km/h, respectively) do not meet the y_t criterion. Simulation 12, at 264 km/h meets the criterion and returns $p_f = 5.1 \times 10^{-4}$, making it a suitable v_{crit} candidate. However, since there was at least one discarded speed, the algorithm runs simulation 13 at 263 km/h by fetching the stored $i = 1$ results and resuming the subset simulation. The resulting p_f is 1.2×10^{-4}, making this speed the new v_{crit} candidate. Simulation 14, at 262 km/h is also resumed, resulting in $p_f = 4 \times 10^{-5}$, confirming that 263 km/h as v_{crit} and finishing the algorithm run. It is worth noting that this application of the algorithm, with its iterative nature, allowed a critical speed to be found with a total sample size of 2,200 (100 per level, with a maximum of 400 per speed value). In contrast, running a similar procedure using crude Monte Carlo simulations would require a total sample size of over 1 million.

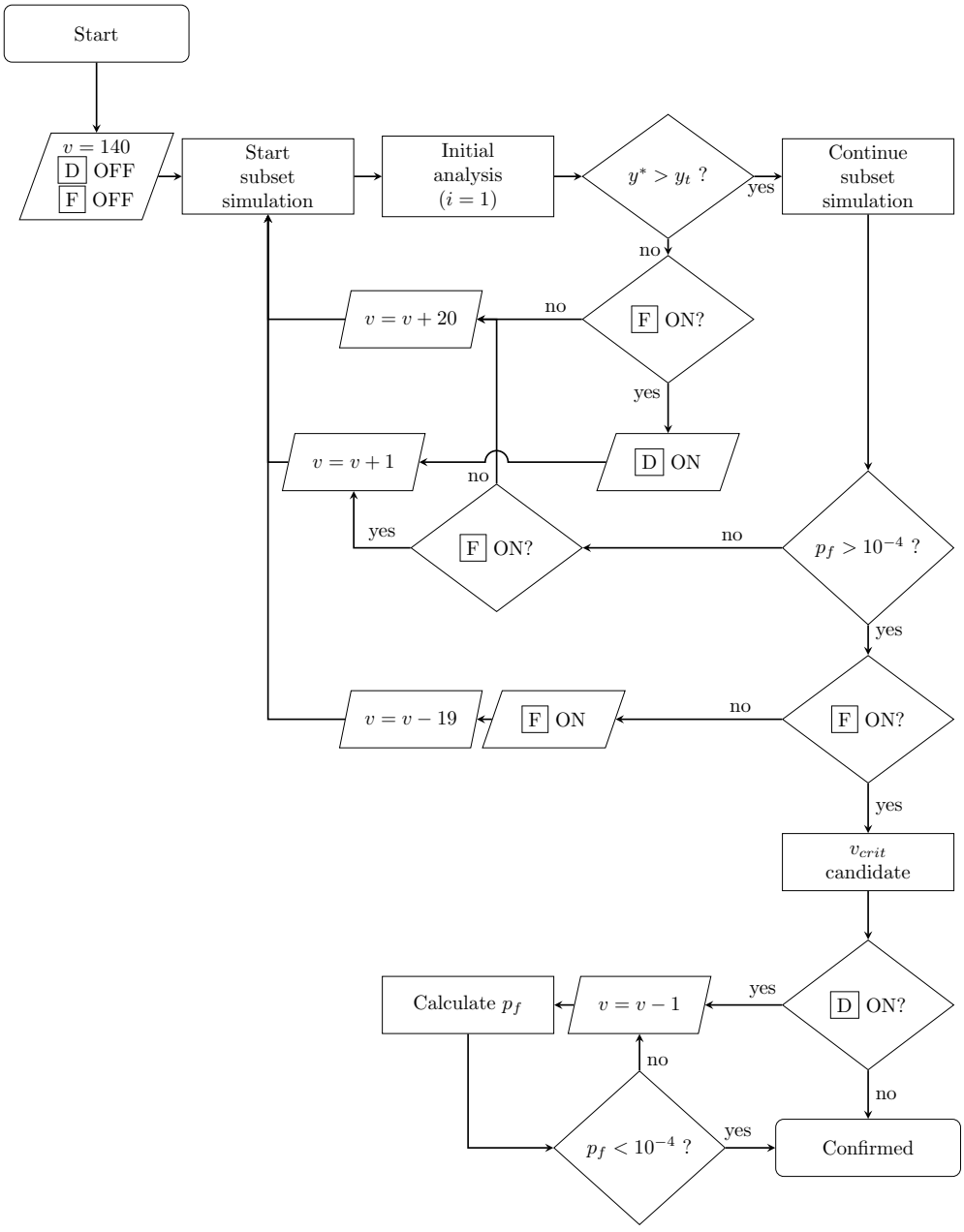

Figure 4.4: Algorithm to assess critical speed.

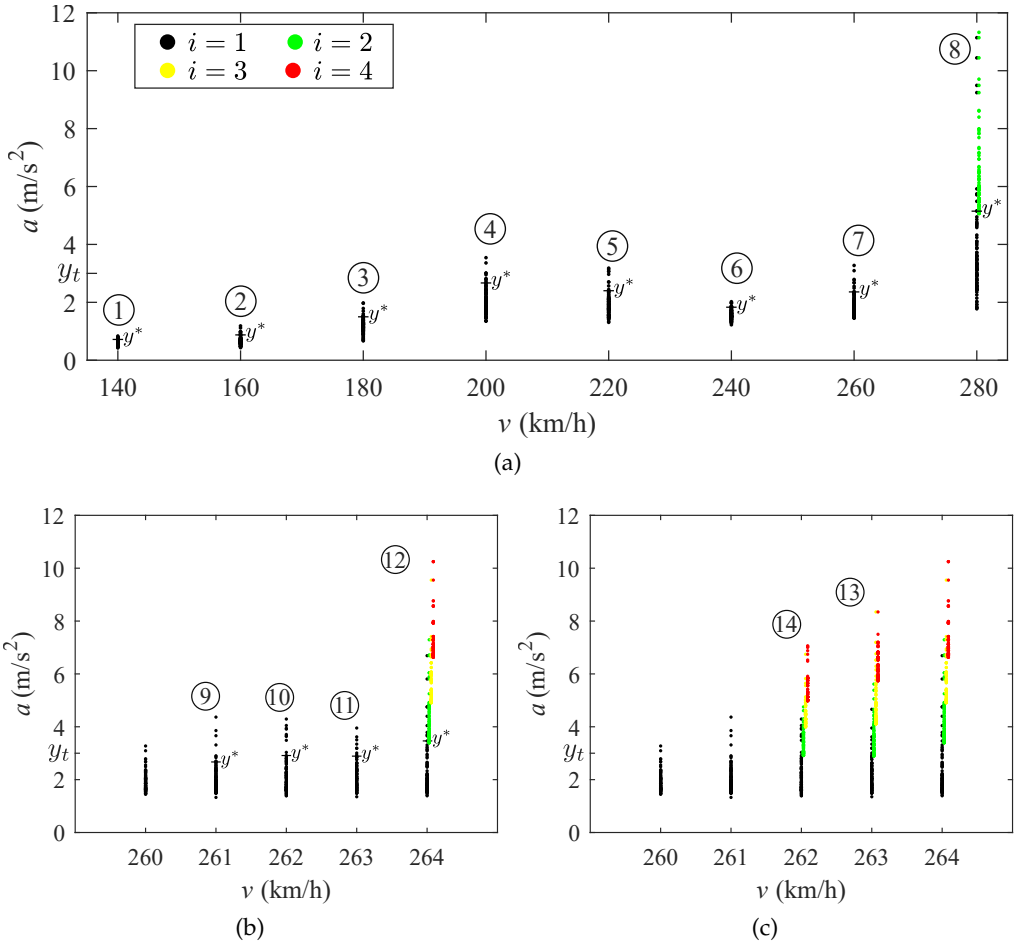

Figure 4.5: Example results from the application of the proposed algorithm. (a) Simulations 1 to 8; (b) simulations 9 to 12 (finer speed increment cycle); (c) simulations 13 and 14 ($v = v - 1$ reverse search cycle).

4.4 CASE STUDY BRIDGES

4.4.1 *General aspects*

The present case study is focused on four bridges of the Northern Line of the Portuguese Railway Network, which runs from Porto to Lisbon. The selected set of structures, located in the Aveiro, Leiria and Santarém districts, are representative of filler beam bridges, a characteristic construction solution of this line, which are simply supported concrete slabs directly cast on embedded steel profiles. The four bridges are presented in Table 4.1, where L_ϕ is the determinant span length. The reference numbers correspond to the locations in Figure 4.6.

The finite elements models are identical to the model presented in Section 3.4.1, substituting 14 of its deterministic material and geometrical properties by the random variables proposed by Rocha (2015), listed in Table 4.2. It is noted that the author attributes uniform distributions to the variables for which there is significant variability in existing studies' measurements. The bridge

dependant variables are introduced in the paragraphs for each bridge. These three variables follow normal distributions, with the mean equal to the nominal value taken from the project drawings and the standard deviation suggested by Rocha (2015). Other quantities of constant nature are the steel elasticity modulus E_S (210 GPa), the remaining mass (weight of the waterproofing, guard rails and gutters' box and covers) M_r (1.4 ton/m), the width of the sleeper underside l_b (0.3 m), the half sleeper effective support l_e (0.95 m), the sleeper spacing l_s (0.6 m), and the properties of the steel profiles (such as mass $M_{profile}$, moment of inertia $I_{profile}$ and height of the centre of gravity $y_{profile}$).

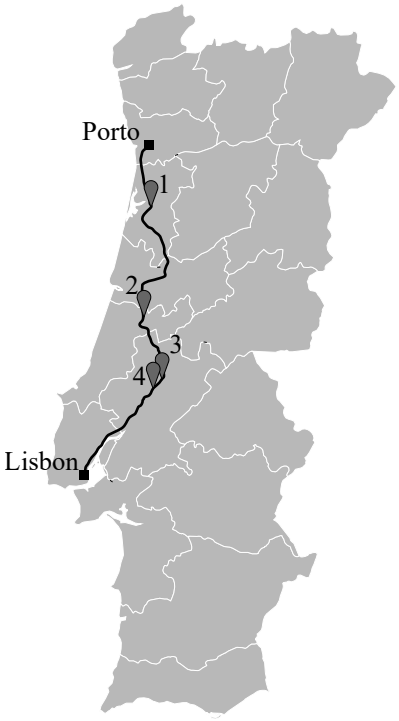

Figure 4.6: Location of the bridges in the Northern Line of the Portuguese Railway Network.

REF.	NAME	SPANS	L_ϕ (m)	TRACKS
1	Canelas bridge	6	6×11.5	2
2	Melga bridge	1	23.78	2
3	Cascalheira underpass	1	10.92	2
4	Braço do Cortiço underpass	1	7.02	2

Table 4.1: List of case study bridges.

Out of the presented variables, only the track shear stiffness, rail pad stiffness, sleeper mass, concrete elasticity modulus and structural damping are applied directly in the ANSYS®environment. For the first three, this is achieved by setting the stiffness or mass parameters of the finite elements, while the damping value is used to set Rayleigh factors, using Equation 2.25 and Equation 2.26 with the frequencies of the first and second vertical vibration modes. Since the deck

is modelled with 2D beam elements, the remaining structural random variables and constants are combined to provide the beam's mass M_{deck} (including the remaining mass M_r and the masses of the steel profiles and concrete, as well as the ballast weight that is supported by the structure) and the moment of inertia of the transformed composite section I_{deck}. The vertical stiffness of the ballast layer K_b is calculated with Equation 3.1, while the vertical and horizontal stiffnesses of the supports, $K_{s,v}$ and $K_{s,h}$, correspond to Equation 3.4 and Equation 3.5, respectively. Figure 4.7 illustrates how these random variables and constants are combined to produce ANSYS®-ready variables.

STRUCTURE VARIABLES (GAUSSIAN)	μ	σ
Reinforced concrete density ρ_C	2.5 t/m^3	0.1 t/m^3
Concrete elasticity modulus E_C	36.1 GPa	2.888 GPa
Structural damping ξ	2%	0.3%
Slab thickness t_{slab}	*Bridge dependant*	
Slab width b_{slab}	*Bridge dependant*	
Area of the steel profiles A_S	*Bridge dependant*	
TRACK VARIABLES (UNIFORM)	a	b
Ballast density ρ_b	1.5 t/m^3	2.1 t/m^3
Ballast elasticity modulus E_b	80 MPa	160 MPa
Ballast layer height h_b	300 mm	600 mm
Load distribution angle α	15°	35°
Sleeper mass m_s	220 kg	325 kg
Rail pad stiffness k_p	100 kN/mm	600 kN/mm
Track shear stiffness k_t	1×10^4 kN/m/m	3×10^4 kN/m/m
SUPPORT VARIABLES (UNIFORM)	a	b
G_n	0.75 MPa	1.5 MPa

Table 4.2: Structure, track, and support random variables (adapted from Rocha (2015)).

4.4.2 *Canelas bridge*

The cross-section and view of the first span of the Canelas bridge can be seen in Figure 3.4, since it is the case study from Chapter 3. In the same chapter, Figure 3.6 depicts the FE model and the deformed shape of the first vertical bending mode. The bridge dependant variables for this struc-

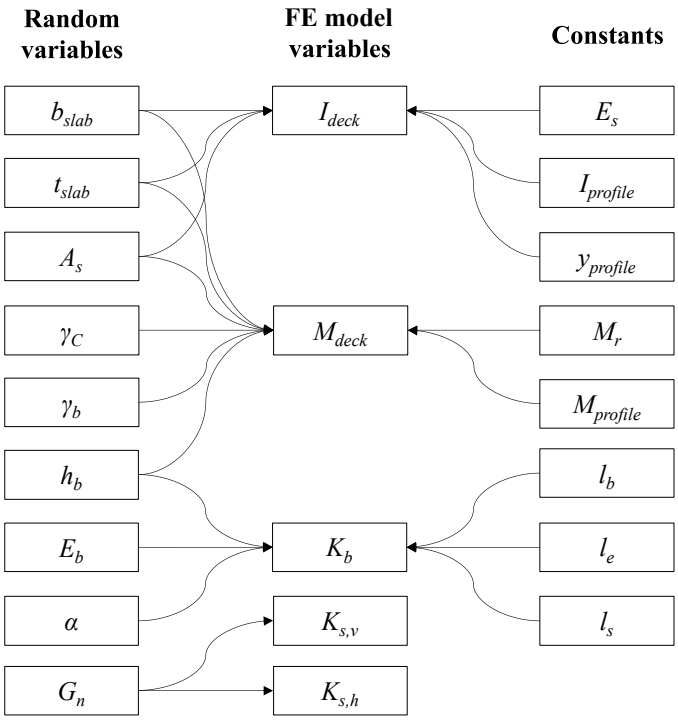

Figure 4.7: Relation of the random variables and constants to the FEM models.

ture are defined as $t_{slab} \sim N\left(0.7, 0.01^2\right)$ m, $b_{slab} \sim N\left(4.475, 0.005^2\right)$ m and $A_S \sim N\left(0.01975, 0.00079^2\right)$ m^2.

4.4.3 *Melga bridge*

With almost 24 m in length, the Melga bridge (Figure 4.8) is the longest of the set. It consists of a single simply supported span with HEB800 profiles. Both its decks, independent of each other, support a single track. The bridge dependant variables are defined as $t_{slab} \sim N\left(0.871, 0.01^2\right)$ m, $b_{slab} \sim N\left(4.20, 0.005^2\right)$ m and $A_S \sim N\left(0.03342, 0.00079^2\right)$ m^2, with the constants being the same as in the Canelas bridge. The FE model developed for this bridge is shown in Figure 4.9 where the deformed shape of the first mode can be seen. With mean values for the variables, the corresponding frequency is 2.80 Hz.

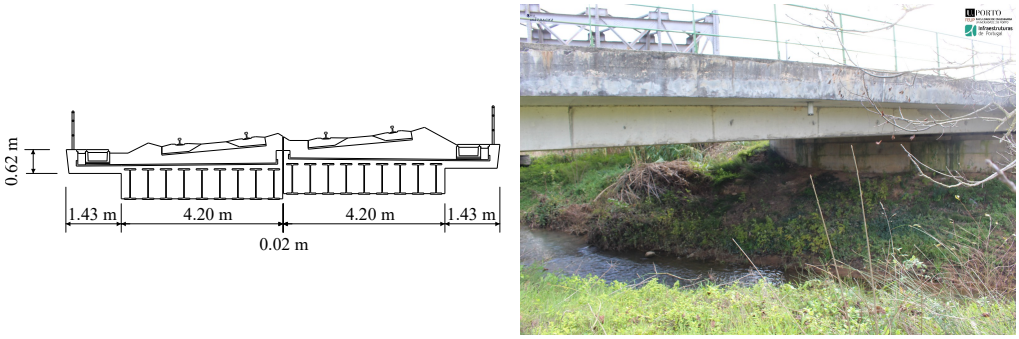

(a) (b)

Figure 4.8: Melga bridge. (a) cross-section (unit: m); (b) view of the deck.

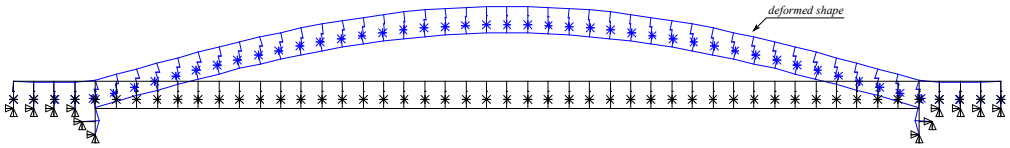

Figure 4.9: Finite elements model of the Melga bridge (in blue, the deformed shape of the first vertical bending mode).

4.4.4 *Cascalheira underpass*

The Cascalheira underpass (Figure 4.10) consists of a single simply supported span with embedded HEB500 steel profiles. It is composed of two independent decks, each carrying one track. The bridge dependant variables are defined as $t_{slab} \sim N\left(0.703, 0.01^2\right)$ m, $b_{slab} \sim N\left(4.08, 0.005^2\right)$ m and $A_S \sim N\left(0.01975, 0.00079^2\right)$ m^2, with the constants being the same as in the previous bridges. The FE model and its first vertical bending modal shape (corresponding to a modal frequency of 9.45 Hz) are represented in Figure 4.11, for a scenario where the variables are input with their mean values.

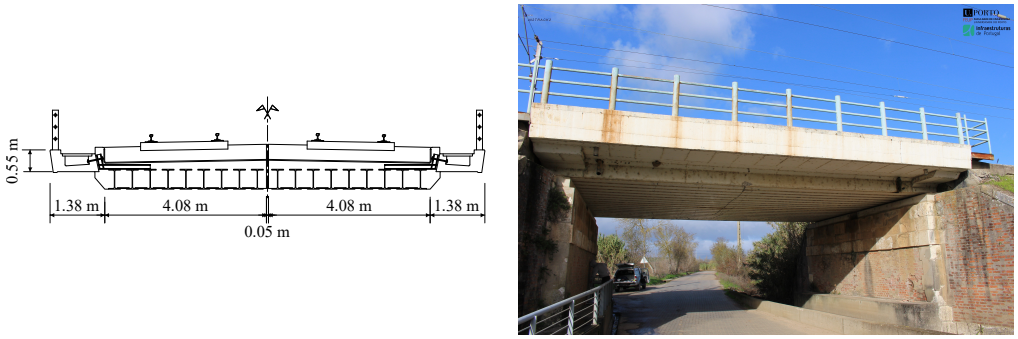

(a) (b)

Figure 4.10: Cascalheira underpass. (a) cross-section (unit: m); (b) view of the deck.

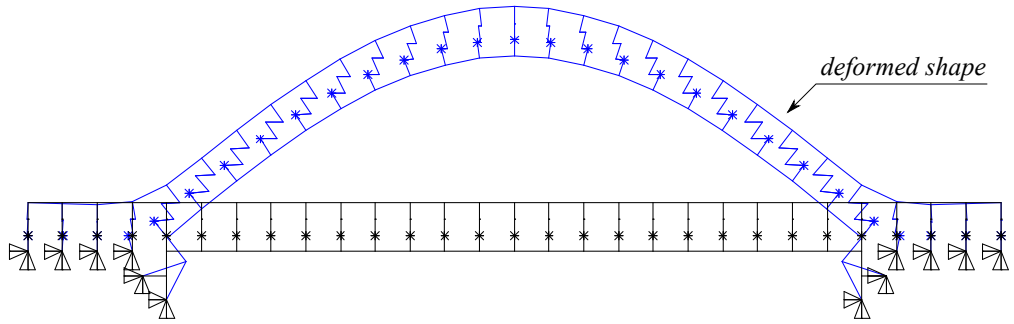

Figure 4.11: Finite elements model of the Cascalheira underpass (in blue, the deformed shape of the first vertical bending mode).

4.4.5 *Braço do Cortiço underpass*

The shortest of the set, the Braço do Cortiço underpass (Figure 4.12), is a single simply supported span with two independent decks of a single track each. It is embedded with HEB300 profiles, and its bridge dependant variables are $t_{slab} \sim N\left(0.445, 0.01^2\right)$ m, $b_{slab} \sim N\left(4.055, 0.005^2\right)$ m and $A_S \sim N\left(0.01491, 0.00079^2\right)$ m^2. As with the other structures, the constant values are the same. Taking average values for all the random variables, the first vertical bending mode is calculated as 17.86 Hz, and its shape can be seen in Figure 4.13.

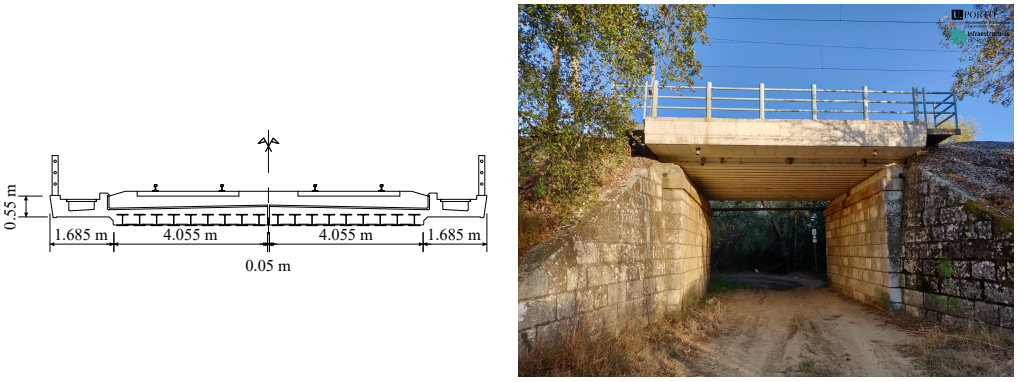

(a) (b)

Figure 4.12: Braço do Cortiço underpass. (a) cross-section (unit: m); (b) view of the deck.

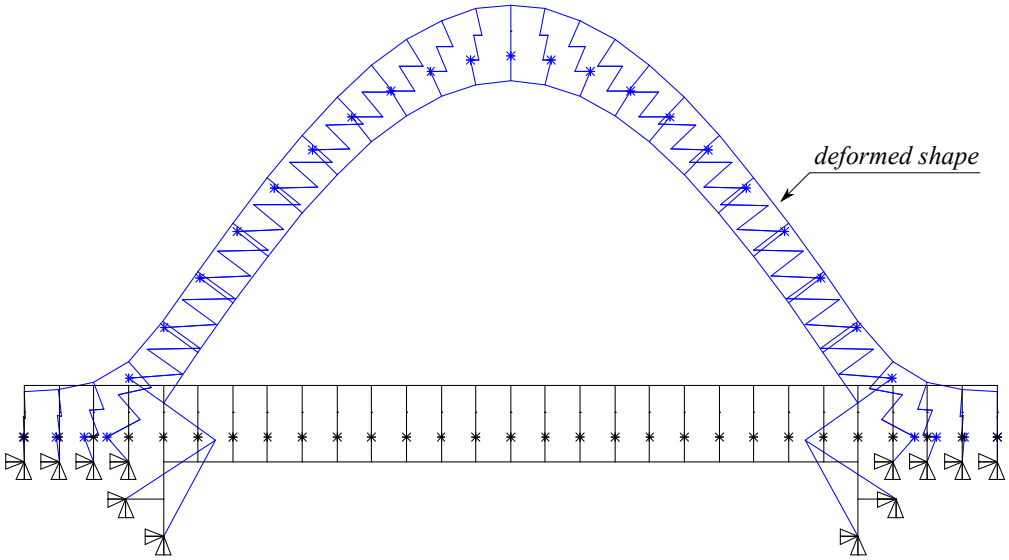

Figure 4.13: Finite elements model of the Braço do Cortiço underpass (in blue, the deformed shape of the first vertical bending mode).

4.4.6 *Dynamic response envelopes*

Plots of the dynamic response of the four bridge models are shown in Figure 4.14. The solid curves illustrate the response of the models when all random variables are considered at their mean values ($\mathcal{X}$), while the areas filled in blue and green indicate the envelopes of the dynamic responses when the most influential variables are set at lower ($\mathcal{Y}$ lower) or upper ($\mathcal{Y}$ upper) bounds, respectively. The curves represent the maximum of the 10 HSLM-A load configurations for each train speed value.

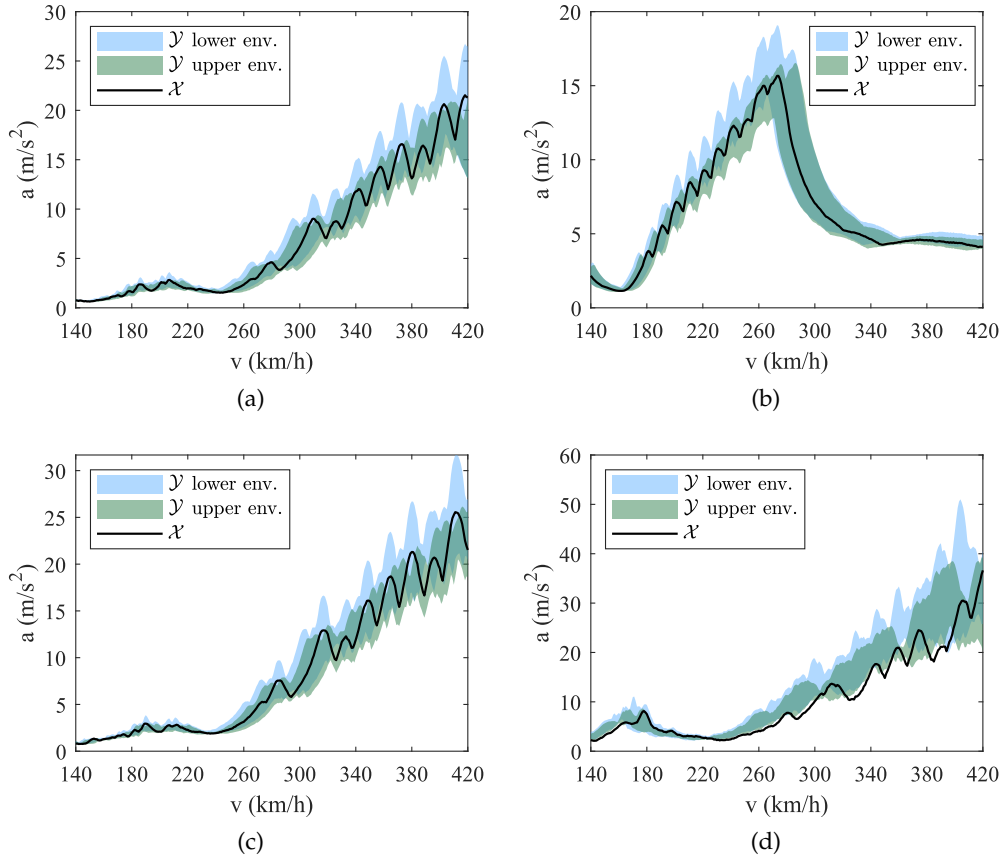

Figure 4.14: Dynamic response envelopes considering all random variables with mean values ($\mathcal{X}$) and the envelopes of lower and upper bounds of the most influential variables ($\mathcal{Y}$). (a) Canelas bridge; (b) Melga bridge; (c) Cascalheira underpass; (d) Braço do Cortiço underpass.

4.5 OPTIMIZATION OF THE ALGORITHM FOR EFFICIENT ASSESSMENT OF CRITICAL SPEEDS

4.5.1 *Optimization of the threshold value y_t*

The Canelas bridge and the HSLM-A3 train were selected to perform the optimization study of the critical speed algorithm. The first parameter to be studied was the threshold value y_t in $i = 1$, which controls whether a speed value is discarded. For this part of the study, the sample size and the intermediate probability were fixed at $N = 100$ and $p_0 = 0.1$, and y_t varied between 2.0 m/s^2, 2.5 m/s^2, 3.0 m/s^2 and 3.5 m/s^2. Table 4.3 lists the time and the total sample size needed to complete the algorithm, as well as the resulting v_{crit}. It can be seen that using the values of 3.0 m/s^2 and 3.5 m/s^2 resulted in the least computational expense. However, further analysis of the simulation results revealed that the stricter 3.5 m/s^2 limit caused the algorithm to skip $v = 264$ km/h, which would have produced a suitable p_f and therefore a lower (and valid) v_{crit} candidate. Conversely, while it is true that using lower threshold values prevents prematurely discarding of candidate speeds, this

option also leads to increased time expenditure, as additional time is spent calculating candidates that are far from the final one. The threshold value $y_t = 3.0$ m/s^2 is henceforth kept as optimal.

The parametric analyses' results can be further illustrated by comparing the complementary CDF of a simulation corresponding to a critical speed to the complementary CDF of its equivalent Monte Carlo simulation with $N = 100000$, as shown in Figure 4.15. In the figures, the circles highlight the acceleration value (i.e., that simulation's y^* values) at the intermediate level, while the asterisk indicates the final calculated p_f. It can be seen that there is a close correspondence for the scenarios with y_t=2.5 m/s^2 and y_t=3.0 m/s^2, where not only is the calculated p_f in the same vicinity (of 10^{-4}), but the intermediate levels also follow the trend of the corresponding Monte Carlo simulation.

y_t	2.0 m/s^2	2.5 m/s^2	3.0 m/s^2	3.5 m/s^2
time (h)	3:34	2:58	1:48	1:37
n_S	4200	3400	2200	2100
v_{crit} (km/h)	266	264	263	267

Table 4.3: Variation of the first level threshold y_t (HSLM-A3, $p_0 = 0.1$, $N = 100$).

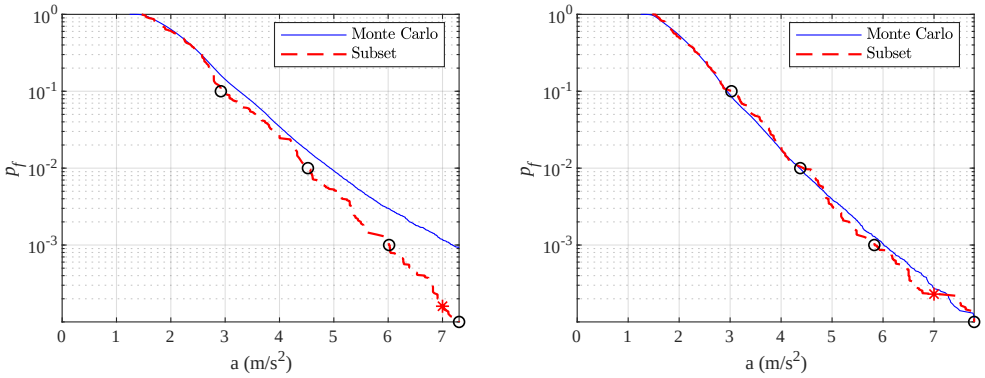

Figure 4.15: Complementary CDF of the subset simulations (HSLM-A3, $p_0 = 0.1$, $N = 100$) and corresponding Monte Carlo simulations with $N = 100000$. (a) y_t=2.0 m/s^2, v_{crit}=266 km/h; (b) y_t=2.5 m/s^2, v_{crit}=264 km/h.

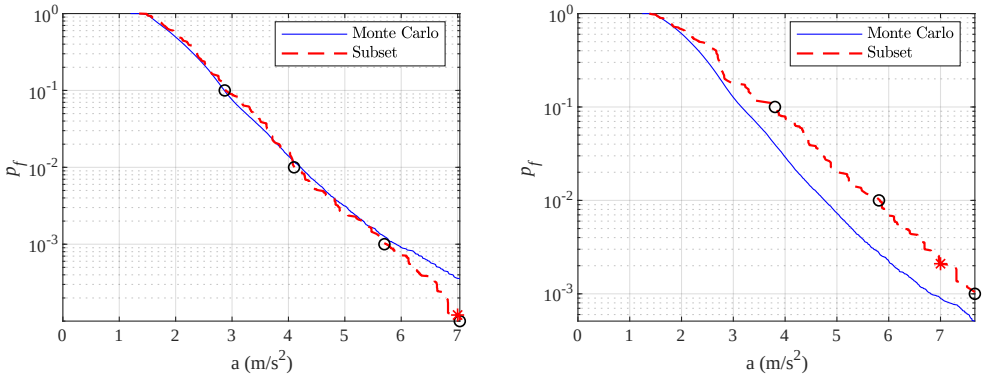

Figure 4.15: (continued) Complementary CDF of the subset simulations (HSLM-A3, $p_0 = 0.1$, $N = 100$) and corresponding Monte Carlo simulations with $N = 100000$. (c) y_t=3.0 m/s^2, v_{crit}=263 km/h; (d) y_t=3.5 m/s^2, v_{crit}=267 km/h.

4.5.2 *Optimization of the intermediate probability p_0*

Using the aforementioned y_t value and a fixed sample size $N = 100$, the optimal intermediate probability is examined by varying p_0 between 0.05, 0.1 and 0.2. As shown in Table 4.4, adopting an intermediate probability of 0.1 allowed the algorithm to converge in the shortest time and with the smallest total sample size. The effect of using $p_0 = 0.2$ was similar to that of having a high y_t, i.e. given the intermediate probability, the cut-off on the ordered results' list is made at a lower value. This makes it harder for y^* to achieve y_t, which in turn makes for a longer $v = v - 1$ reverse search cycle. As for the lower value, 0.05, the resulting additional computing time would only be justifiable if the target p_f was lower than 10^{-4}. Concerning the complementary CDF comparisons in Figure 4.16, it is noticed that the simulation with p_0=0.2 corresponds to a larger deviation when compared to the Monte Carlo assessments. Conversely, the same trends are closer for p_0=0.2, albeit at a higher computational cost.

p_0	0.05	0.1	0.2
time (h)	2:49	1:48	2:37
n_S	2700	2200	3700
v_{crit} (km/h)	264	263	265

Table 4.4: Variation of the intermediate probability p_0 (HSLM-A3, $y_t = 3.0$ m/s^2, $N = 100$).

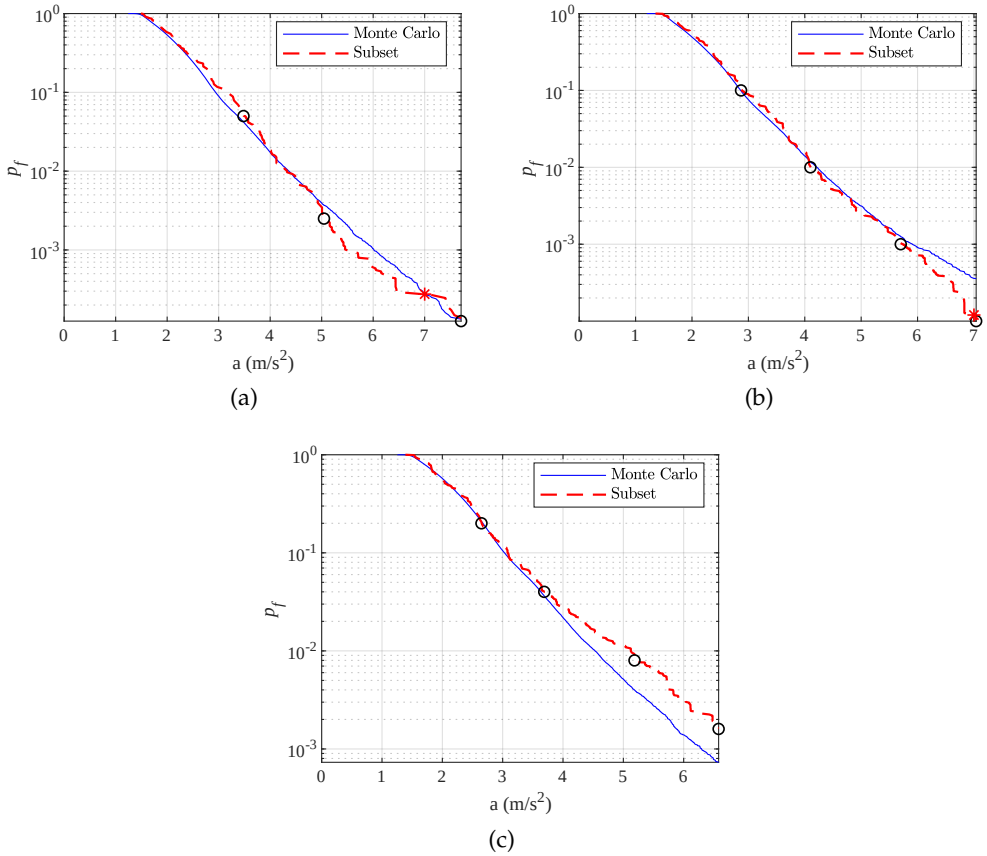

Figure 4.16: Complementary CDF of the subset simulations (HSLM-A3, $y_t = 3.0$ m/s^2, $N = 100$) and corresponding Monte Carlo simulations with $N = 100000$. (a) p_0=0.05, v_{crit}=264 km/h; (b) p_0=0.1, v_{crit}=263 km/h; (c) p_0=0.2, v_{crit}=265 km/h.

4.5.3 *Optimization of the sample size N*

Regarding the sample size, the comparison of N between 50, 100, 150 and 200 is calculated with fixed $y_t = 3.0$ and $p_f = 0.1$. Unsurprisingly, Table 4.5 reveals that it takes more time to compute larger sample sizes, while the smallest size, 50, corresponds to the least amount of time and smallest total sample size. However, with an intermediate probability of 0.1, each level of a subset simulation with $N = 50$ provides only 5 elements to generate the samples of the following level. As a result, the number of failed candidate states in the MMA increases, introducing inefficacy when scaling the method by artificially limiting the dispersion of the results. Observing the complementary CDFs in Figure 4.17, it is worth noting that there is an increased unevenness for $N = 50$, even if the resulting critical speed is the same as for $N = 100$. The larger sample sizes of $N = 150$ and $N = 200$ lead to similar results while consuming more computation time.

Given that the various applications lead to v_{crit} in close proximity, the final adopted values are $y_t = 3.0$m/s^2, $p_0 = 0.1$, and $N = 100$.

N	50	100	150	200
time (h)	1:01	1:48	3:26	2:52
n_S	1050	2200	6200	4000
v_{crit} (km/h)	263	263	267	265

Table 4.5: Variation of the sample size N (HSLM-A3, $y_t = 3.0$, $p_0 = 0.1$).

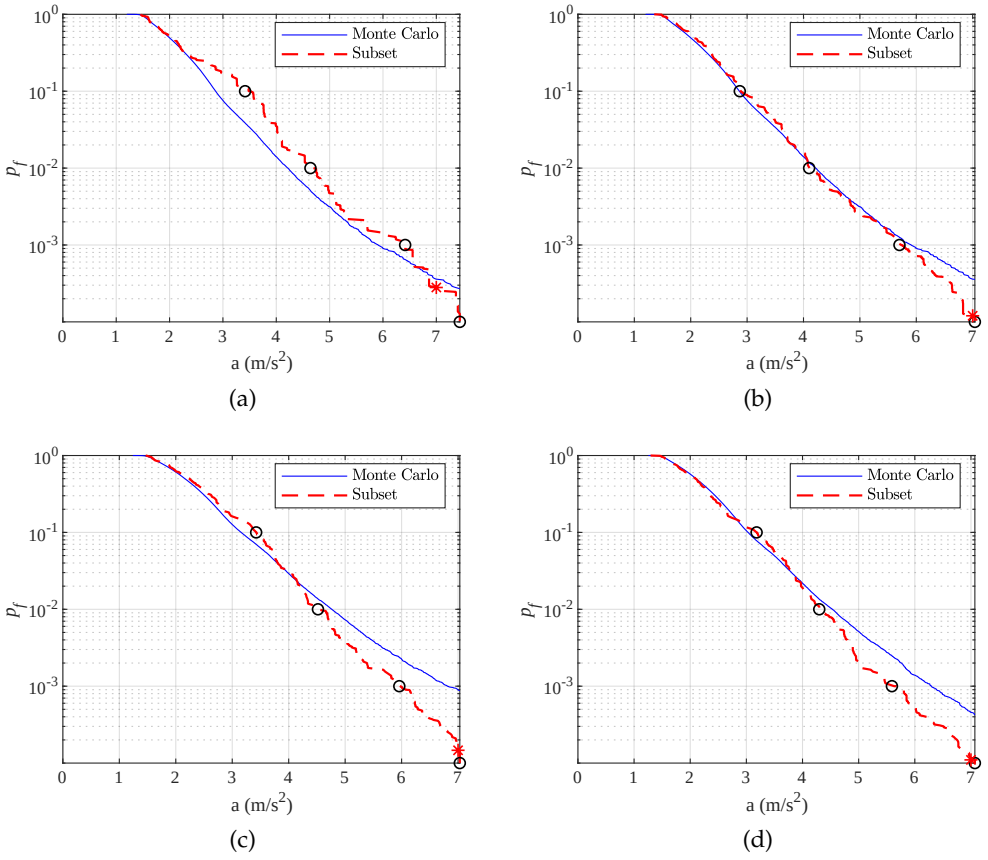

Figure 4.17: Complementary CDF of the subset simulations (HSLM-A3, $y_t = 3.0$ m/s^2, p_0=0.1) and corresponding Monte Carlo simulations with $N = 100000$. (a) N=50, v_{crit}=263 km/h; (b) N=100, v_{crit}=263 km/h; (c) N=150, v_{crit}=267 km/h; (c) N=200, v_{crit}=265 km/h.

4.6 SIMULATION RESULTS

4.6.1 *Calculated critical speeds*

The current section represents the application of the first step of the methodology. After setting the optimal factors in the algorithm, the critical speeds on each bridge are calculated for each HSLM-A train model. The individual critical speeds $v_{crit,i}$ are listed in Table 4.6. The final critical speed values, given by Equation 4.3, are highlighted in the same Table.

	$v_{crit,i}$ (km/h)			
HSLM	Canelas bridge	Melga bridge	Cascalheira underpass	Braço do Cortiço underpass
A1	414	N/A	250	244
A2	361	175	269	156
A3	263	173	263	255
A4	274	179	277	146
A5	284	185	284	264
A6	293	192	287	263
A7	298	194	289	244
A8	314	202	301	282
A9	316	205	261	252
A10	325	214	254	255

Table 4.6: Critical speeds for every HSLM-A.

4.6.2 *Assessment of the scenarios for bridge design*

The present section showcases the application of the second step of the methodology, where the scenarios for bridge design are defined as two sets of instructions on how to assign values to several random variables. The selection of the variables to be included in the definition of the scenarios is achieved through a sensitivity analysis, where the importance of each variable is assessed with Equation 4.4. Here, the study is performed for the Canelas bridge, using the 10 HSLM-A load configurations and a running speed interval from 140 km/h to 420 km/h. The response envelopes are depicted in Figure 4.18, where the line in full represents the response vector $\mathcal{X}$ and the dotted and dash-dotted lines represent the response vectors $\mathcal{Y}$ when each random variable is set to its lower or upper bound, respectively.

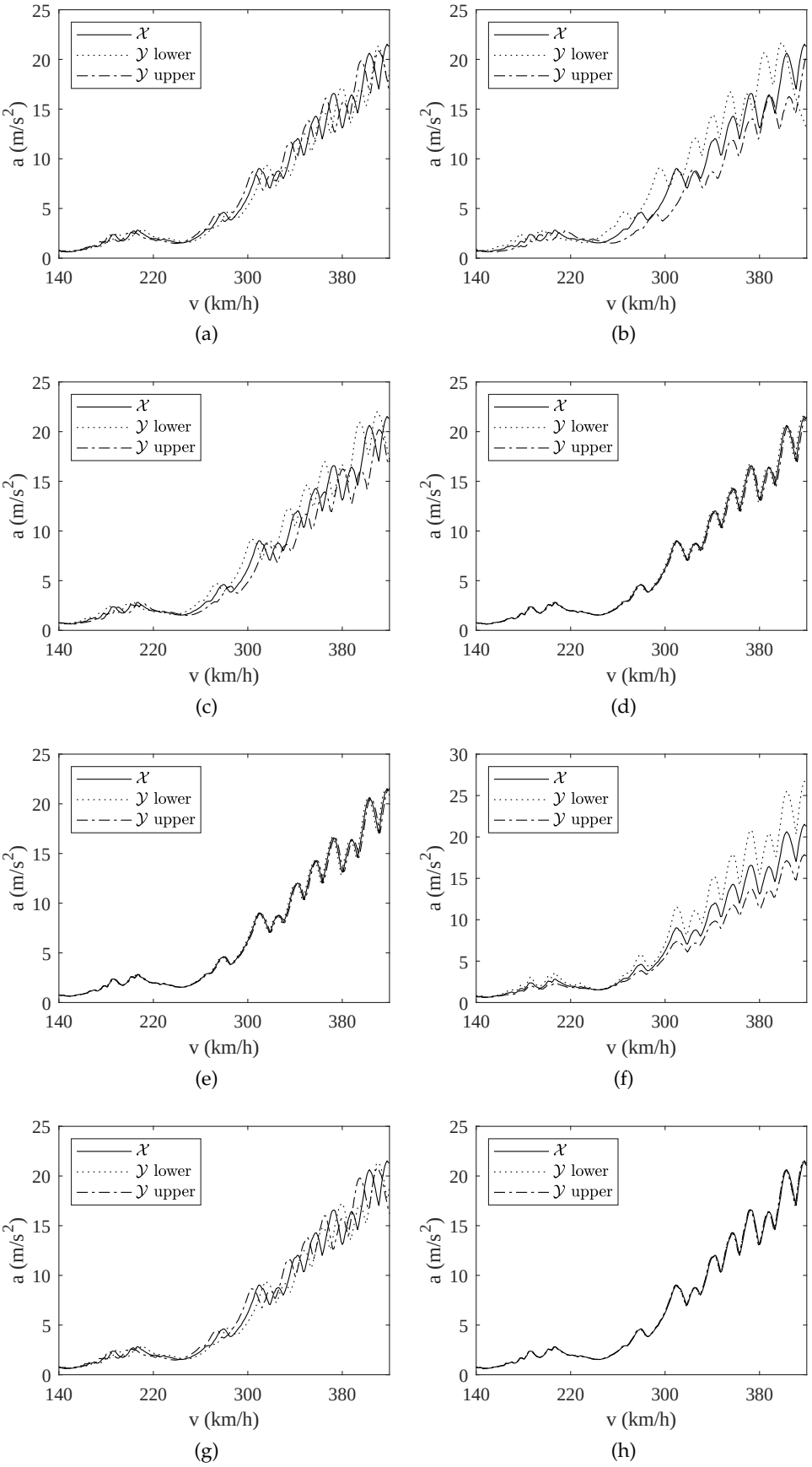

Figure 4.18: Individual influence of the random variables. (a) ρ_C; (b) E_C; (c) t_{slab}; (d) b_{slab}; (e) A_S; (f) ξ; (g) ρ_b; (h) E_b.

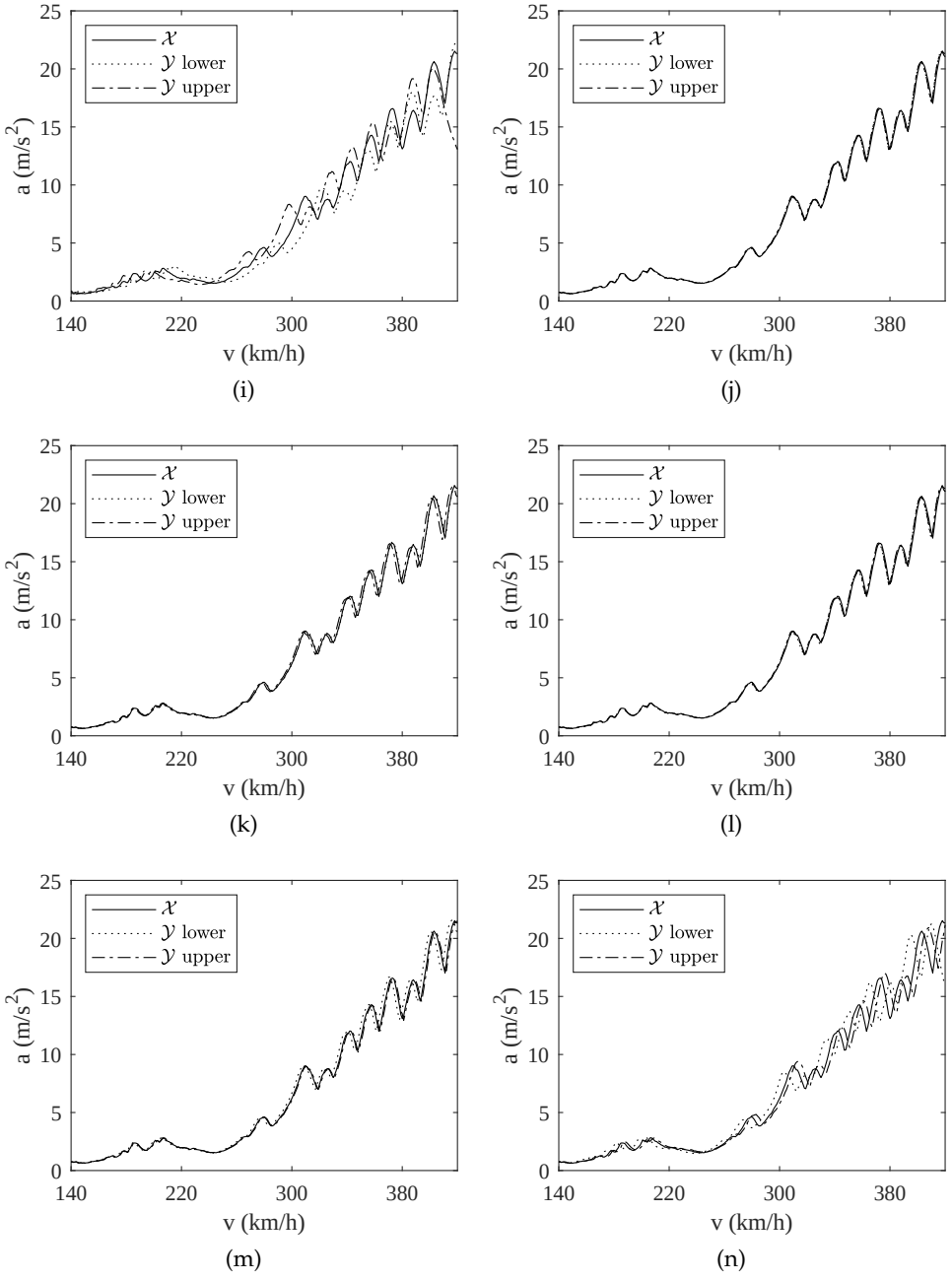

Figure 4.18: (continued) Individual influence of the random variables. (i) h_b; (j) α; (k) m_s; (l) k_p; (m) k_t; (n) G_n.

The calculated variance values are listed in Table 4.7. It can be seen that the variables that control most of the structural mass (thickness and density of both the slab and the ballast layer) and the concrete stiffness are of remarkable importance. Structural damping and support stiffness also account for a considerable portion of the problem. Due to the clear difference in the results, the variables that score a variance result (from Equation 4.4) greater than 1 are selected for the definition of the design scenarios.

VARIABLE	VARIANCE	
	$\mathcal{Y}$ lower envelope	$\mathcal{Y}$ upper envelope
Reinforced concrete density ρ_C	1.06	1.08
Concrete elasticity modulus E_C	2.63	1.46
Slab thickness t_{slab}	1.56	1.43
Slab width b_{slab}	0.06	0.06
Area of the steel profiles A_S	0.06	0.06
Structural damping ξ	2.29	1.13
Ballast density ρ_b	1.04	1.21
Ballast elasticity modulus E_b	0.02	0.02
Ballast layer height h_b	0.66	1.56
Load distribution angle α	0.02	0.02
Sleeper mass m_s	0.01	0.12
Rail pad stiffness k_p	0.03	0.02
Track shear stiffness k_t	0.20	0.03
Neoprene shear modulus G_n	1.29	0.53

Table 4.7: Sensitivity analysis of the variables' relative influence.

Consequently, the deterministic scenarios S1 and S2 are proposed in Table 4.8. In accordance with the EN 1991-2, there are two estimates of mass (upper and lower bound), defined by thickness and density (t_{slab}, h_b, ρ_C, ρ_b), combined with a single estimate (lower bound) of stiffness (E_C, G_n) and structural damping (ξ).

SCENARIO	E_c, ξ	ρ_C, t_{slab}	ρ_b, h_b	G_n
S1	$\mu - 1.64\sigma$	$\mu - 1.64\sigma$	min.	min.
S2	$\mu - 1.64\sigma$	$\mu + 1.64\sigma$	max.	min.

Table 4.8: Scenarios for bridge design.

Using the definitions of Table 4.8 and setting the remaining random variables to their mean values, the dynamic design response can be obtained. Figure 4.19, Figure 4.20, Figure 4.21 and Figure 4.22 represent the response envelopes of

the deterministic scenarios for the Canelas, Melga, Cascalheira and Braço do Cortiço bridges, respectively. It is worth noting that these bridges were originally designed for a running speed of 160 km/h, hence the large acceleration values at higher speeds. The methodology being used in this chapter may allow for higher permissible deck accelerations, which can possibly allow for higher running speeds. Such a study is helpful in addressing the sustainability of existing infrastructure by considering the need to deploy newer, faster, and longer trains to operators' rolling stock rather than replacing existing bridges.

Analyzing the local maxima on the plotted data, it is clear that S1 (with its lower bound estimate of the random variables controlling the structural mass) produces the highest acceleration values, albeit at higher speeds. Conversely, the upper estimates in S2 correspond to lower acceleration peaks, but avoid overestimating the resonant speeds. These observations help to validate the purpose of the scenarios, which corresponds to the Eurocode expects. The design acceleration values a_{Ed} are to be found in these curves at v_{crit}.

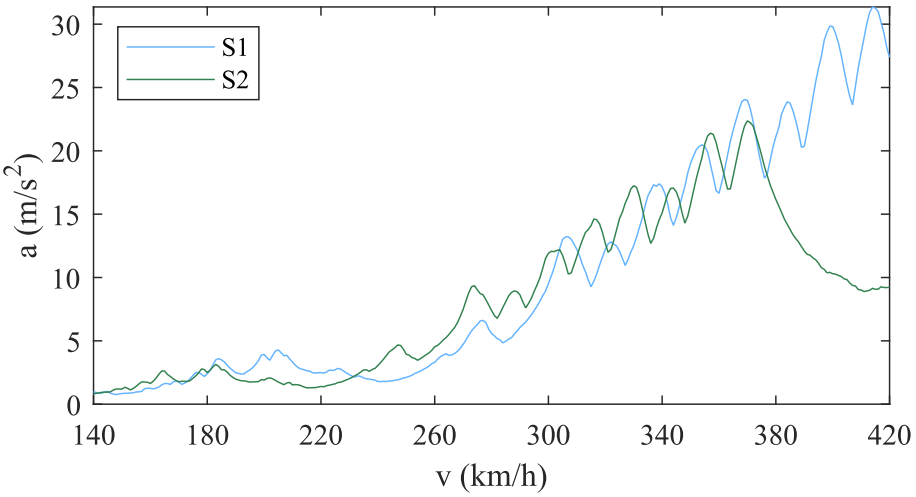

Figure 4.19: Design scenario response envelopes for the Canelas bridge.

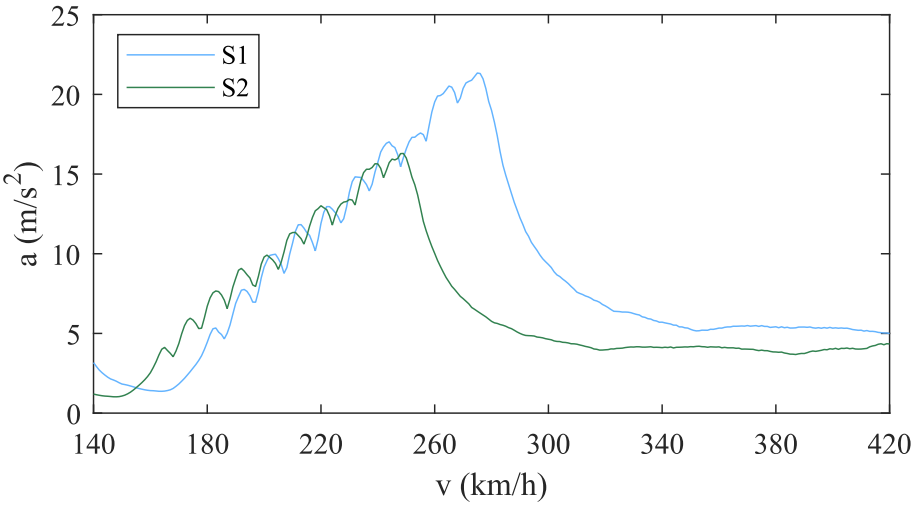

Figure 4.20: Design scenario response envelopes for the Melga bridge.

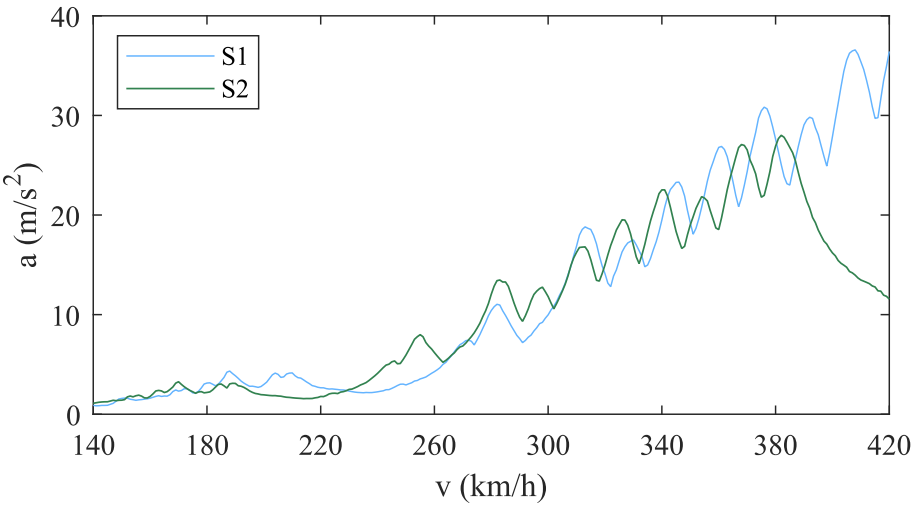

Figure 4.21: Design scenario response envelopes for the Cascalheira underpass.

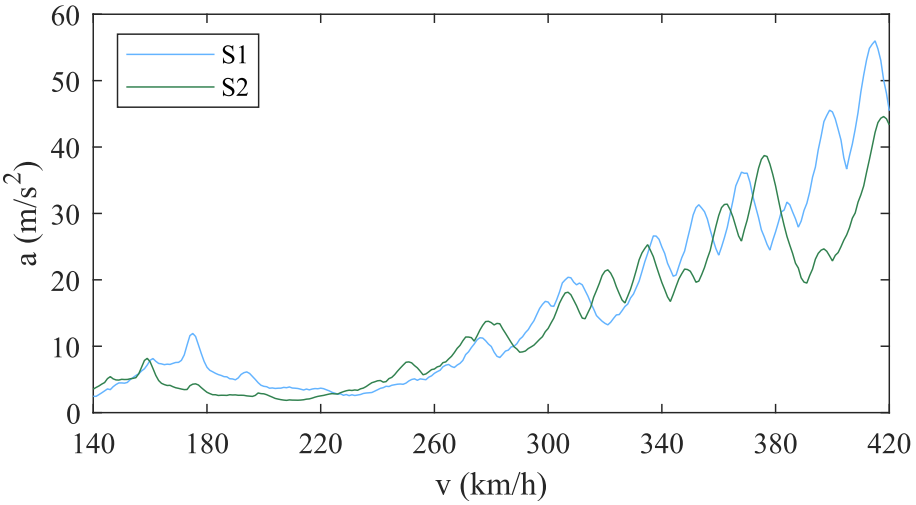

Figure 4.22: Design scenario response envelopes for the Braço do Cortiço underpass.

4.6.3 *Design acceleration and safety factors*

The third and final step of the methodology is performed in this section. Knowing the critical speeds and the envelopes of the design scenarios, the design accelerations a_{Ed} can be found, as illustrated in Figure 4.23. The values are given in Table 4.9, together with the safety factors, according to Equation 4.5.

From the results, it can be observed that a bridge design made with the current Eurocode limit of 3.5 m/s^2 (i.e. with the safety factor of 2.0) would either limit the maximum allowable running speed or result in heavier, more robust cross-sections. Conversely, the present approach suggests that safety would be ensured up to the calculated critical speeds within the target probability of failure.

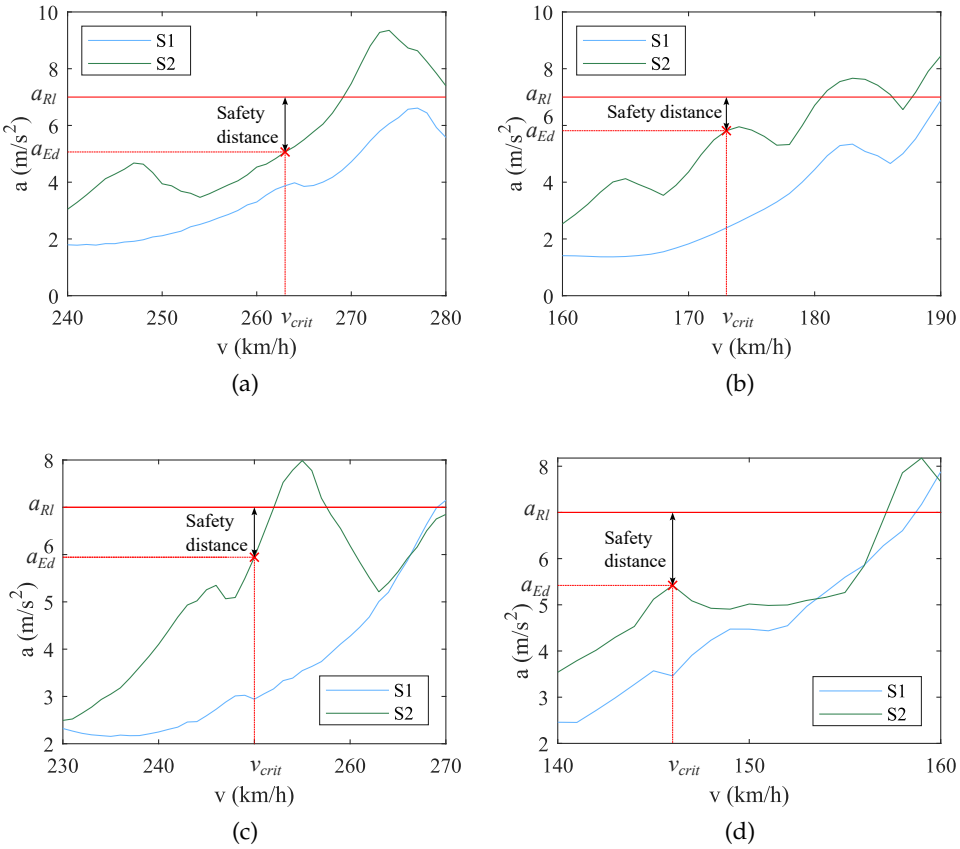

Figure 4.23: Critical speeds and design phase accelerations. (a) Canelas bridge; (b) Melga bridge; (c) Cascalheira underpass; (d) Braço do Cortiço underpass.

BRIDGE	v_{crit} (km/h)	a_{Ed} $\left(\mathrm{m/s^2}\right)$	γ_{bt}
Canelas bridge	263	5.07	1.38
Melga bridge	173	5.81	1.20
Cascalheira underpass	250	5.94	1.18
Braço do Cortiço underpass	146	5.42	1.29

Table 4.9: Critical speeds, design accelerations and partial safety factors.

4.7 NORMATIVE RECOMMENDATION

The research conducted in this chapter suggests that the current normative limit in the Eurocode may be over-conservative. A revised version of the EN 1990 could, therefore, allow higher deck acceleration limits. Nonetheless, this study is performed on existing bridges that are currently in operation. The design allowance could be different in new structures.

Currently, the Eurocode EN 1990 is a single document that applies both to new and existing structures. The second generation of Eurocodes is presently being developed and will be available in 2027 after the votes of the CEN-CENELEC national members. The current version (CEN, 2023a) already constitutes an improvement on the original (CEN, 2005). However, in the new norms, the EN 1990 is likely going to be separated into two parts (one focusing new structures and the other for existing structures), as demonstrated by the existence of the draft European standards prEN 1990-1 and prEN 1990-2 (Catarino et al., 2024). Therefore, the normative recommendation from this thesis is twofold:

RECOMMENDATION FOR NEW STRUCTURES: maintain the 3.5 m/s^2 deck acceleration limit for ballasted track railway bridges. Even though the new structures could be less robust, the increase in capacity does not come at a significant cost. ERRI D 192/RP 5 (1996) indicates, for instance, that a 40% increase in the design loads accounts for 2.2% higher construction cost. This approach ensures future-proofing, making allowance in new bridges for dynamic effects whose existence may still be unknown.

RECOMMENDATION FOR EXISTING STRUCTURES: allow a higher deck acceleration limit depending on case-specific safety assessments. Adopting a safety factor of 1.4 would result in a permissible acceleration of $7/1.4 = 5 m/s^2$. For reference, the same value is permitted by the RSSB (2024) GEGN8616 guidance, and such factor is in line with the safety factor of 1.38 found with a surrogate model approach (Allahvirdizadeh et al., 2024a) and with the German factor of 1.3 for soil loading capacity (Zacher and Baeßler, 2008). This approach underscores sustainability, as it enables new, faster, and heavier rolling stock to operate in the lines where the bridges already exist, extending their lifecycle without jeopardizing structural safety.

4.8 CONCLUDING REMARKS

In this chapter, the permissible acceleration limit in ballasted track bridges is addressed by defining a design phase acceleration. Two design scenarios are proposed where the design acceleration is found at a critical speed. This speed is assessed using a newly proposed algorithm to overcome the computational challenges associated with low probabilities of failure. The main conclusions of this study can be summarized according to the research questions proposed in Section 4.1:

1. The employment of subset simulation is cost effective when estimating low probabilities of failure. However, it still depends on knowing where

to start in the speed range. By using an appropriate first level threshold value, sample size, and intermediate probability, a simple decision-making algorithm can aid in rapidly going through the speed range.

2. The EN 1991-2 dictates how stiffness, damping, and mass must be estimated but does not specify how they are to be achieved. By describing the geometric and material properties of a bridge with basic random variables, it is possible to sample these variables and construct two design scenarios. An expedited sensitivity analysis is sufficient to highlight the most contributing variables;

3. The study of four real ballasted track structures revealed that a bridge can be designed so that its deck can experience an acceleration value greater than 3.5 m/s^2 without being associated with a probability of failure greater than 10^{-4}. Considering that the physical acceleration limit is kept at 7 m/s^2, this means that the safety factor, computed as the ratio between it and the allowable acceleration, can be set lower than 2.0;

Considering that the calculated design acceleration values are greater than 3.5 m/s^2 (or, in other words, that the associated safety factors are less than 2.0), it can be concluded that the normative limits are, at least, conservative. Therefore, a revision of the normative acceleration limit for ballasted track railway bridges may include the discussion of higher permissible limits.

5

PROBLEM 3: ANALYSIS OF THE DECK ACCELERATION CRITERION ON BALLASTLESS TRACK BRIDGES

5.1 INITIAL CONSIDERATION

The Eurocode EN 1990 (CEN, 2023a) stipulates a deck acceleration criterion to ensure traffic safety on railway bridges. On ballastless track bridges, the norm limits vertical deck acceleration to 5 m/s^2. This value is based on an arbitrarily attributed safety factor of 2 and on the assumption that a deck acceleration of 1 g compromises running safety. The empirical nature of these assumptions has led to scientific discussion, as presented in Section 2.2.5.3. The IN2TRACK3 (2021) project began studying the relation between deck acceleration and derailment, and the InBridge4EU (2023) project is currently formulating suitable normative recommendations, as mentioned towards the end of the current chapter.

Since the mechanics that govern wheel-rail contact (and, by extension, the possibility of loss of contact and occurrence of derailment) are complex and also depend on lateral components, this chapter proposes to study the risk of derailment considering three-dimensional TTBI models, with the purpose of comparing derailment criteria against calculated deck acceleration values, to make a critical analysis of the traffic stability criteria stipulated in the EN 1990. To overcome the knowledge gaps, the following research questions are proposed:

1. Do deck acceleration values above the normative limit correspond to derailment?
2. Are both lateral and vertical dynamics indispensable to assess running safety, or do vertical dynamics suffice?
3. How important is the influence of track quality, compared with the deck vibrations reached in resonance?
4. Can deck acceleration be an indicator of the passengers' riding comfort?

The present chapter is based on the work presented in Ferreira et al. (2024a) (Appendix C), starting with the statement of a methodology in Section 5.2. A set of bridges, train models, and rail irregularity profiles are described in Section 5.3. The results and discussion of the parametric analyses, including the study of increased irregularity profiles, of the influence of the bridge and the relation to running comfort, are shown in Section 5.4. The normative recommendations are summarized in Section 5.5, and the main conclusions, according to the proposed research questions, are listed in Section 5.6.

5.2 METHODOLOGY

There are several criteria that can be used to assess train running safety, varying according to different derailment mechanisms and countries. These criteria (presented in Section 2.2.4) are based on the relation between the wheel-rail contact forces that can only be accessed through TTBI models.

Among the available derailment criteria, the two used in the present study (Nadal and Unloading) are two of the most commonly used in the analysis of train running safety. The Nadal index ξ_N can be obtained through Equation 2.6, where Y and Q are the time histories from the lateral and vertical contact forces, respectively, in each wheel. The European TSI (European Comission, 2002) specifies a safety limit of 0.8 for this index.

Regarding the unloading index ξ_U, it can be calculated with Equation 2.10, where Q_0 is the wheel's static load. The stricter limit of 0.6, stipulated in the European norm related to the testing and simulation of railway vehicles EN 14363 (CEN, 2016) is considered in this chapter for the unloading index. According to the same norm, before computing the aforementioned derailment criteria, the time histories of both vertical and lateral contact forces should be low pass filtered with a cut-off frequency of 20 Hz using a filter of order 4. In this thesis, a Butterworth filter is adopted. Henceforth, the limits for the Nadal and Unloading criteria, as well as the acceleration limit, are referred to respectively as N_{lim}, U_{lim} and a_{lim}.

The methodology employed in this chapter involves conducting a parametric study on a set of 5 single-track slab bridges (presented in Section 5.3.1) with spans ranging between 10 m and 30 m, with trains running at speeds ranging between 150 km/h and 400 km/h. For each analysis, the maxima of the derailment indicators (Unloading and Nadal) and the maximum deck acceleration at midspan were registered. Each bridge is paired with 1 out of 10 possible HSLM-A universal trains (whose modelling is detailed in Section 5.3.2), i.e. only the most critical HSLM-A train for each bridge (the train that conditions the bridge design in terms of deck acceleration in the speed range) is considered in the analysis.

To study the effect of track irregularities, each bridge is simulated with a finite number of realizations of irregularity profiles (detailed in Section 5.3.3), corresponding to a smooth track, a high quality track, and an Alert Limit track. Therefore, the parametric study amounts to a total of 1430 3D TTBI dynamic simulations, conducted using the numerical tool developed and validated by Montenegro et al. (2015). This number corresponds to the 5 bridges being tested with 11 different irregularities profiles (5 realizations of a higher quality track, 5 of lower quality track and 1 smooth track profile) with trains running at 26 possible speed values (10 km/h intervals of the speed range).

The methodology is complemented with a study of 10 additional profiles (Section 5.4.4) where the track irregularities are increased above the normative Alert Limit and with the study of a rigid bridge (Section 5.4.5), to address the effects caused by the structure's vibration. Lastly, a study of whether deck acceleration can be considered an indicator of riding comfort is presented in Section 5.4.6.

5.3 NUMERICAL MODELLING

5.3.1 *Bridge models*

The characteristics of the bridges used for the present chapter were obtained from the work by Arvidsson and Andersson (2017) where, for simply supported single-span slab bridges, five models are proposed, with spans ranging from 10 m to 30 m and cross-sections designed to provide results near the Eurocode's acceleration limit when considering a design speed of 320 km/h (and consequently a maximum speed of 1.2×320 km/h, as per the EN 1991-2 (CEN, 2023b)).

For this work, the cross-sectional dimensions were obtained considering an elasticity modulus of 34 GPa and a Poisson's ratio of 0.2. The 3D models were developed with the Finite Element Method (FEM) using the commercial software ANSYS® (2018), using the following element types

- BEAM188: Timoshenko beam elements to model the deck, the track slab and the rails;
- COMBIN14: spring-dashpots to model the track elements, namely the mortar bed between the deck and the track slab, the subgrade bed in the adjacent track to the bridge and the rail fastenings

The bridge deck is modelled with beam elements located at its centre of gravity. From there, the track slab (which is also comprised of beam elements) is connected with an array of spring-dashpot elements that discretize the concrete-asphalt (CA) mortar bed. Above the slab, pairs of rigid elements reach the transversal coordinates of the rails, connecting to them through spring-dashpot elements that represent the fasteners and pads. The track slab is made up of modular sections with gaps at the abutments.

The properties of these bridges are presented in Table 5.1, including the span L, linear mass m, stiffness EI, the natural frequency of the first bending mode n_0, cross-sectional width b and height h. Damping is taken into account through the Rayleigh proportional matrix with damping ratios (taken from EN 1991-2 (CEN, 2023b) for all cases) set to the first two vertical bending modes of the bridge deck.

L (m)	m (ton/m)	EI (GN m^2)	n_0 (Hz)	b (m)	h (m)
10	15.4	12.5	14.3	8.1522	0.6426
15	21.2	36	9.2	7.3128	1.0336
20	25.4	65.1	6.4	7.0075	1.3184
25	33.1	152.0	5.4	6.7193	1.8333
30	36.7	211.0	4.2	6.6324	2.0744

Table 5.1: Properties of the simply supported slab bridges used in the 3D TTBI analysis (adapted from Arvidsson et al. (2018)).

Regarding the track elements, their vertical mechanical properties (stiffness and damping) were adopted from Arvidsson et al. (2018), while the lateral and longitudinal characteristics were adopted from previous 3D TTBI models developed by Montenegro et al. (2020, 2022) and Neto et al. (2021). The properties of the slabs and UIC60 rails (density ρ, modulus of elasticity E, area A, moment of inertia I, height h, width b, and gauge) are listed in Table 5.2 and the properties of the fasteners and elastic bed in Table 5.3, where x, y, and z indicate the longitudinal, transversal, and vertical directions, respectively.

PROPERTY	SLAB	RAILS
ρ $\left(\mathrm{kg/m^3}\right)$	2400	7850
E (GPa)	34	210
A $\left(\mathrm{m^2}\right)$	0.96	7.676×10^{-3}
I $\left(\mathrm{m^4}\right)$	7.2×10^{-3}	30.038×10^{-6}
h (m)	0.3	—
b (m)	3.2	—
gauge (m)	—	1.435

Table 5.2: Properties of the slabs and UIC60 rails.

	Direction		
FASTENERS	x	y	z
Stiffness (MN/m)	40	40	22.4
Damping (kNs/m)	40	40	5.47
Rotational stiffness (kN m/rad)	45	45	45
Spacing (m)	0.588		
ELASTIC BED			
Mortar modulus $\left(\mathrm{MN/m^3}\right)$	1×10^5		
Mortar damping $\left(\mathrm{kNs/m^2}\right)$	34.58		
Subgrade modulus $\left(\mathrm{MN/m^3}\right)$	100		
Subgrade damping $\left(\mathrm{kNs/m^3}\right)$	34.58		

Table 5.3: Properties of the fasteners and elastic bed (with values from Arvidsson et al. (2018), ERRI D 202/RP 11 (1997), Ling et al. (2019), and Shi et al. (2016)).

A schematic representation of the FE models is shown in Figure 5.1, alongside a characteristic 3D view of the ANSYS® model. While the deck and track slab's properties can be reduced to single beams to enable the coupling of a three-dimensional vehicle model, each rail has to be modelled separately, thus justifying the configuration of rigid elements that can be seen in the same figure.

Lastly, each bridge's first vertical bending modal shapes and frequencies can be seen in Figure 5.2.

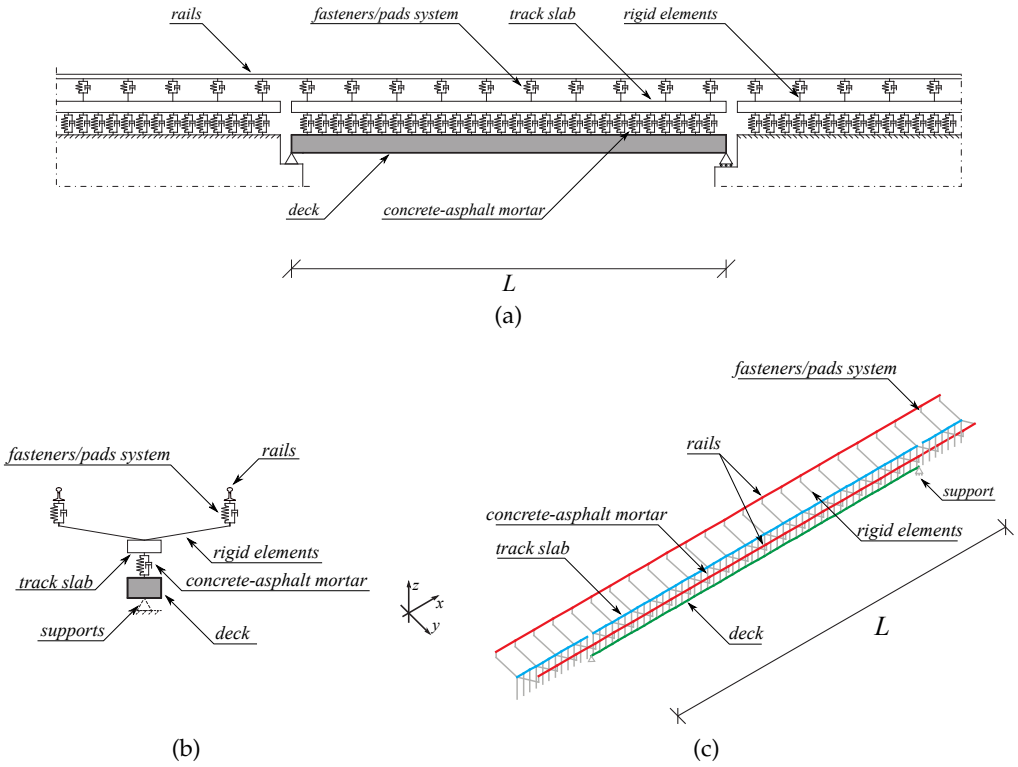

Figure 5.1: Finite elements model of the slab bridges. (a) Schematic representation (lateral view); (b) Schematic representation (transversal); (c) 3D view.

10 m bridge
$n_0 = 14.27$ Hz

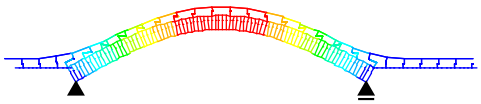

15 m bridge
$n_0 = 9.19$ Hz

20 m bridge
$n_0 = 6.38$ Hz

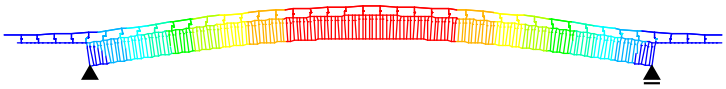

25 m bridge
$n_0 = 5.44$ Hz

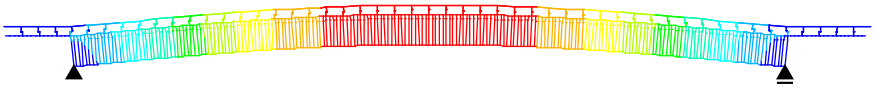

30 m bridge
$n_0 = 4.24$ Hz

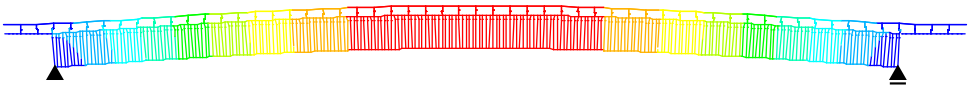

Figure 5.2: First vertical bending modes of the FE bridge models.

5.3.2 *Train models*

The train models used in this chapter for loading are 3D vehicles aimed to represent the High-Speed Load Model A (presented in Section 2.2.1.3). This approach was selected since the HSLM envelope is intended to cover a wide range of possible running trains. The HSLM-A is a moving load model with axle distances and loads whose geometric configuration resembles articulated trains, without any suspension or vehicle body data explicitly provided by the norm (CEN, 2023b). Therefore, the relevant information regarding the vertical dynamic behaviour was retrieved from Arvidsson et al. (2018) for each of the 10 HSLM-A trains. The authors of that study adjusted the car body masses to correspond to the axle loads (ranging from 17 to 21 tonnes/axle) and the primary and secondary suspensions' characteristics to produce realistic bounce frequencies. In contrast, the lateral and longitudinal suspensions were adopted from typical three-dimensional trains found in the literature (Goicolea, 2014; Lee and Kim, 2010). Table 5.4 lists the symbols used to describe the train model parameters, and a thorough list of the values can be consulted in Table 5.5 and Table 5.6.

MECHANICAL PROPERTIES				
		Moments of inertia		
	Mass	Roll	Pitch	Yaw
Car body	m_{cb}	$I_{cb,x}$	$I_{cb,y}$	$I_{cb,z}$
Bogie	m_b	$I_{b,x}$	$I_{b,y}$	$I_{b,z}$
Wheelset	m_w	$I_{w,x}$	—	$I_{w,z}$
SUSPENSION PROPERTIES				
		Direction		
		x	y	z
Primary	Stiffness	$k_{p,x}$	$k_{p,y}$	$k_{p,z}$
	Damping	$c_{p,x}$	$c_{p,y}$	$c_{p,z}$
Secondary	Stiffness	$k_{s,x}$	$k_{s,y}$	$k_{s,z}$
	Damping	$c_{s,x}$	$c_{s,y}$	$c_{s,z}$

Table 5.4: Train model parameters symbols.

		INTERMEDIATE COACHES			
Parameter	Unit	A1	A2	A3	A4
m_{cb}	kg	27,160	33,280	29,200	31,240
$I_{cb,y}$	kg m^2	0.91×10^6	1.41×10^6	1.19×10^6	1.51×10^6
$I_{b,y}$	kg m^2	1240	3650	1240	2700
		END COACHES			
Parameter	Unit	A1	A2	A3	A4
m_{cb}	kg	40,740	49,910	43,800	46,850
$I_{cb,y}$	kg m^2	1.02×10^6	1.52×10^6	1.37×10^6	1.69×10^6
$I_{b,y}$	kg m^2	1240	3650	1240	2700
		POWER CARS			
Parameter	Unit	A1	A2	A3	A4
m_{cb}	kg	54,320	66,550	58,400	62,470
$I_{cb,y}$	kg m^2	1.33×10^6	1.62×10^6	1.43×10^6	1.53×10^6
$I_{b,y}$	kg m^2	2700	2700	2700	2700
		COMMON PARAMETERS			
Parameter	Unit	A1	A2	A3	A4
$k_{p,z}$	kN m	1,410	1,320	1,380	1,350
$c_{p,z}$	kN m/s	20	19	20	19
$k_{s,z}$	kN m	640	820	700	760
$c_{s,z}$	kN m/s	39	50	43	46

Table 5.5: Varying parameters of the HSLM trains.

		INTERMEDIATE COACHES		
Parameter	Unit	A5	A6	A7
m_{cb}	kg	27,160	29,200	31,240
$I_{cb,y}$	kg m^2	1.31×10^6	1.53×10^6	1.77×10^6
$I_{b,y}$	kg m^2	1,240	1,240	1,240
		END COACHES		
Parameter	Unit	A5	A6	A7
m_{cb}	kg	40,740	43,800	46,850
$I_{cb,y}$	kg m^2	1.54×10^6	1.82×10^6	2.12×10^6
$I_{b,y}$	kg m^2	1,240	1,240	1,240
		POWER CARS		
Parameter	Unit	A5	A6	A7
m_{cb}	kg	54,320	58,400	62,470
$I_{cb,y}$	kg m^2	1.33×10^6	1.43×10^6	1.53×10^6
$I_{b,y}$	kg m^2	2,700	2,700	2,700
		COMMON PARAMETERS		
Parameter	Unit	A5	A6	A7
$k_{p,z}$	kg	1,410	1,380	1,350
$x_{p,z}$	kg m^2	20	20	19
$k_{s,z}$	kg m^2	640	700	760
$c_{s,z}$	kg m^2	39	43	46

Table 5.5: (continued) Varying parameters of the HSLM trains.

		INTERMEDIATE COACHES		
Parameter	Unit	A8	A9	A10
m_{cb}	kg	31,240	35,310	35,310
$I_{cb,y}$	kg m^2	1.98×10^6	2.32×10^6	2.49×10^6
$I_{b,y}$	kg m^2	1,900	1,240	1,240
		END COACHES		
Parameter	Unit	A8	A9	A10
m_{cb}	kg	46,850	52,970	52,970
$I_{cb,y}$	kg m^2	2.36×10^6	2.83×10^6	3.06×10^6
$I_{b,y}$	kg m^2	1,900	1,240	1,240
		POWER CARS		
Parameter	Unit	A8	A9	A10
m_{cb}	kg	62,470	70,630	70,630
$I_{cb,y}$	kg m^2	1.53×10^6	1.72×10^6	1.72×10^6
$I_{b,y}$	kg m^2	2,700	2,700	2,700
		COMMON PARAMETERS		
Parameter	Unit	A8	A9	A10
$k_{p,z}$	kg	1,350	1,280	1,280
$x_{p,z}$	kg m^2	19	19	19
$k_{s,z}$	kg m^2	760	880	880
$c_{s,z}$	kg m^2	46	53	53

Table 5.5: (continued) Varying parameters of the HSLM trains.

PARAMETER	UNIT	VALUE
$I_{cb,x}$	kg m^2	119,328
$I_{cb,z}$	kg m^2	1,957,888
m_b	kg	3,500
$I_{b,x}$	kg m^2	2,835
$I_{b,z}$	kg m^2	4,235
m_w	kg	2,000
$I_{w,x}$	kg m^2	1,000
$I_{w,z}$	kg m^2	1,000
$k_{p,x}$	kN m	12,500
$k_{p,y}$	kN m	120,000
$c_{p,x}$	kN m/s	9
$c_{p,y}$	kN m/s	27.9
$k_{s,x}$	kN m	2,500
$k_{s,y}$	kN m	240
$c_{s,x}$	kN m/s	30
$c_{s,y}$	kN m/s	30

Table 5.6: Constant parameters of the HSLM trains.

The 3D FE models were developed in the ANSYS® commercial software, using three of its available finite element types

- BEAM4: 3D elastic beams, to act as rigid beams;
- COMBIN14: 3D spring-damper elements, to model the suspension parameters;
- MASS21: 3D structural mass, to model all localized masses and rotational moments of inertia.

Each wheelset is connected to a primary suspension linked to the bogie via rigid beams. The bogies are connected to a secondary suspension that is, in turn, linked to the geometric centre of the car body. The HSLM is characteristically comprised of a power car at each end (with two bogies, independent of the rest of the train), an end coach attached to each power car (with an independent bogie and a shared bogie) and a succession of intermediate coaches that share bogies in the manner of an articulated train. The load model is symmetrical; therefore, the last intermediate coach shares a bogie with another end coach, which is followed by the final power car.

It is highlighted that the HSLM is a load model and not an actual train, presenting the challenge of articulating the intermediate coaches in the FE model. For this thesis, the solution achieved was to connect the secondary suspension to one of the carriages and then to couple the translational degrees of freedom of that suspension and the following carriage, allowing for free

rotation in every axis, effectively modelling a spherical joint. This approach is sufficient to analyse lateral and vertical forces at the level of the wheels, which is the intended purpose of the study. Figure 5.3 depicts lateral and front views of a schematic representation of the train model, while the corresponding FEM implementation can be seen in Figure 5.4.

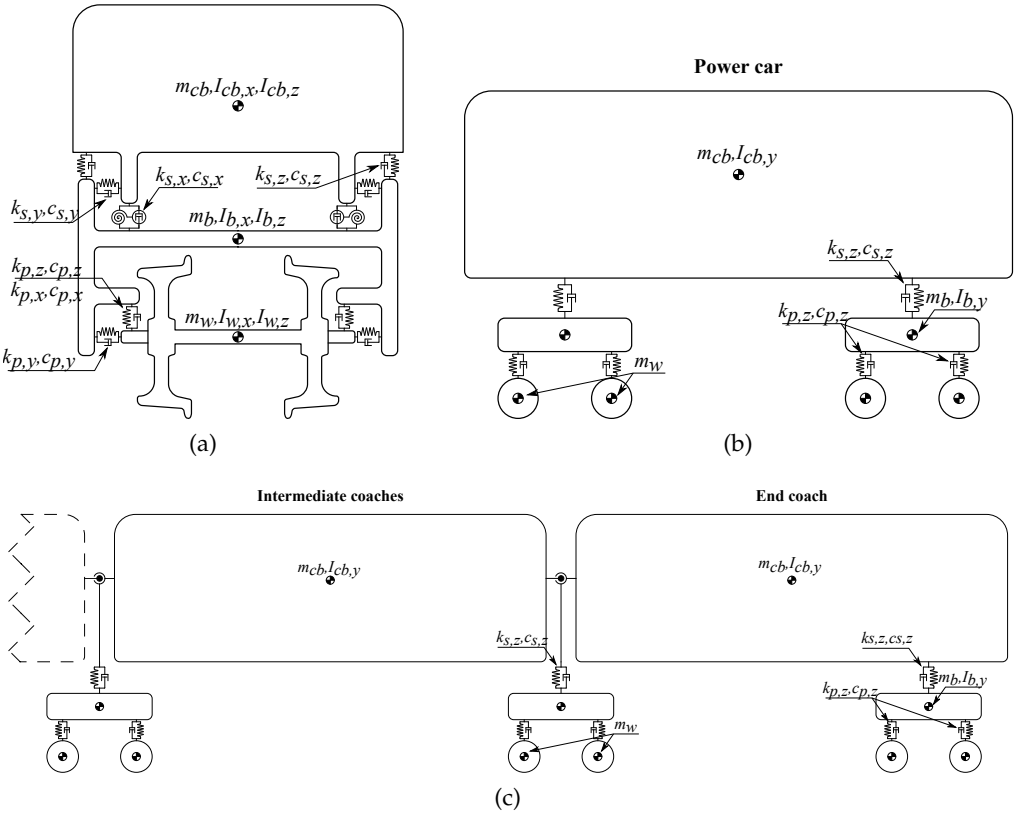

Figure 5.3: Schematic representation of the train model. (a) front view; (b) lateral view of the power car; (c) lateral view of the end and intermediate coaches.

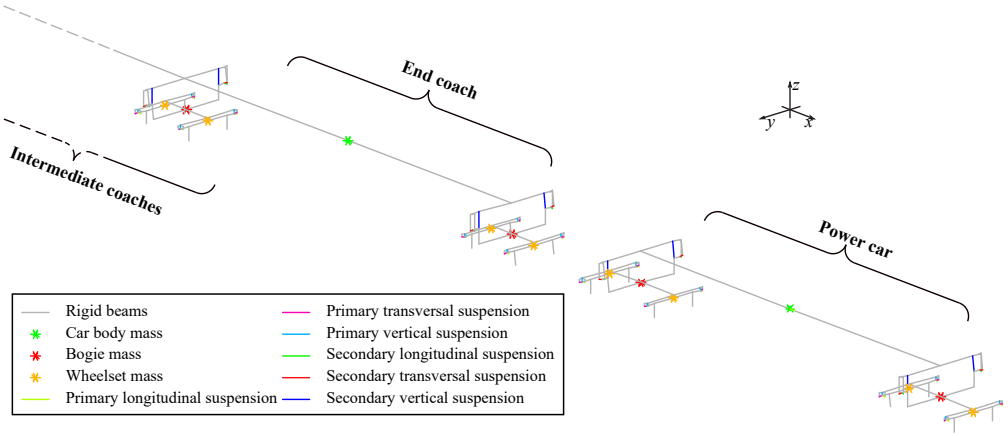

Figure 5.4: View of the train's FEM model.

5.3.3 *Track irregularities*

The track irregularity profiles employed in the present work were artificially generated based on the German Power Spectral Density (PSD) functions procedure described by Claus and Schiehlen (1998), where the irregularities r along the longitudinal development x are given by:

$$r(x) = \sqrt{2} \sum_{n=0}^{N-1} A_n \cos\left(\Omega_n x + \varphi_n\right) \tag{5.1}$$

where N is the number of frequencies Ω_n, φ_n is a random phase angle between 0 and 2π, and A_n are factors given by the same study. The wavelength interval 3-150 m was considered for generating the profiles, which includes the D1 (3-25 m), D2 (25-70 m), and D3 (70-150 m) ranges specified in the EN 13848-5 (CEN, 2015). Two track quality levels were considered:

LOWER TRACK QUALITY: With track quality factors for longitudinal (vertical) and alignment levels of $A_v = 6.00 \times 10^{-7}$ and $A_a = 2.70 \times 10^{-7}$, to obtain standard deviations in the D1 range compatible with the Alert Limit specified in CEN (2015) for speeds up to 300 km/h of $\sigma_{3-25,v}$ equal to 1.25 mm and $\sigma_{3-25,a}$ of 0.85 mm for the longitudinal and alignment profiles, respectively

HIGHER TRACK QUALITY: With track quality factors of $A_v = 0.60 \times 10^{-7}$ and $Aa = 0.35 \times 10^{-7}$, respectively, giving $\sigma_{3-25,v}$ equal to 0.40 mm and $\sigma_{3-25,a}$ of 0.30 mm, compatible with a well maintained track of the Chinese PSD (W. Zhai et al., 2015).

The rail irregularity profiles are generated for a total length of 2500 m with an interval of 0.25 m. Depending on the bridge span, each profile is offset so that one of its peaks coincides with the midspan point, increasing the likelihood of significant interaction forces occurring. Plots of example realizations of tracks' irregularities can be seen in Figure 5.5 for both quality levels in the lateral and vertical directions. An example of the alignment PSD is shown in Figure 5.6.

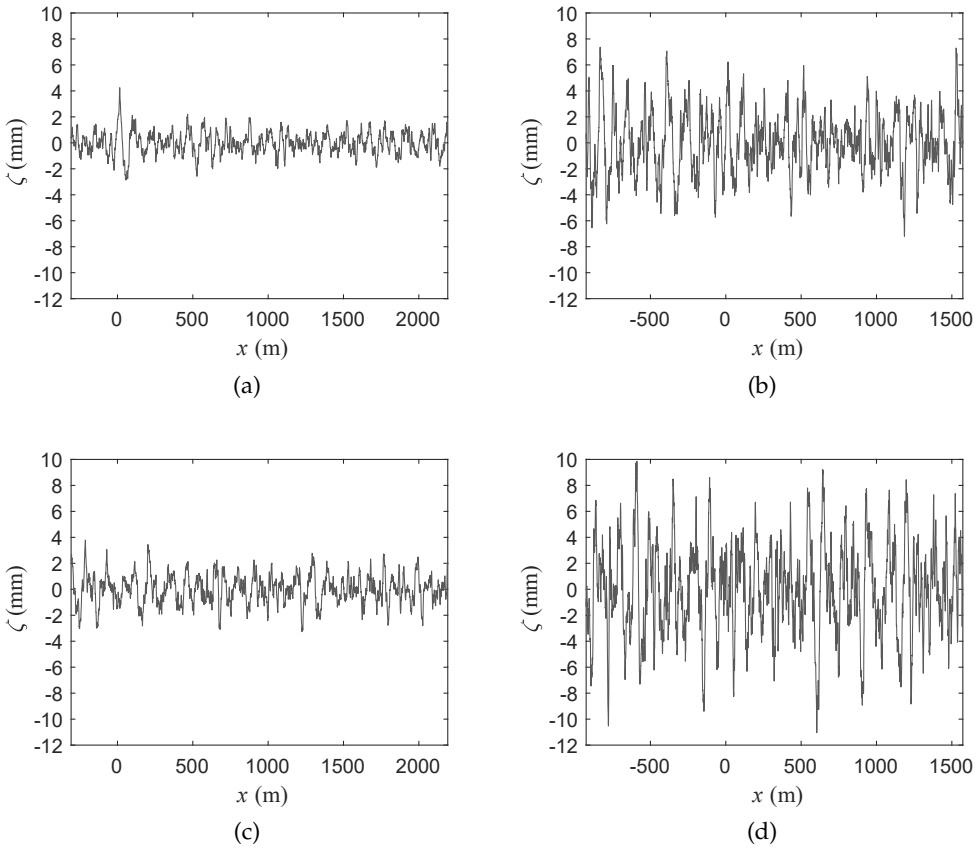

Figure 5.5: Example realization of tracks' irregularities in the vertical direction: (a) Well-maintained track, (b) Alert limit; lateral direction: (c) Well-maintained track, (d) Alert limit.

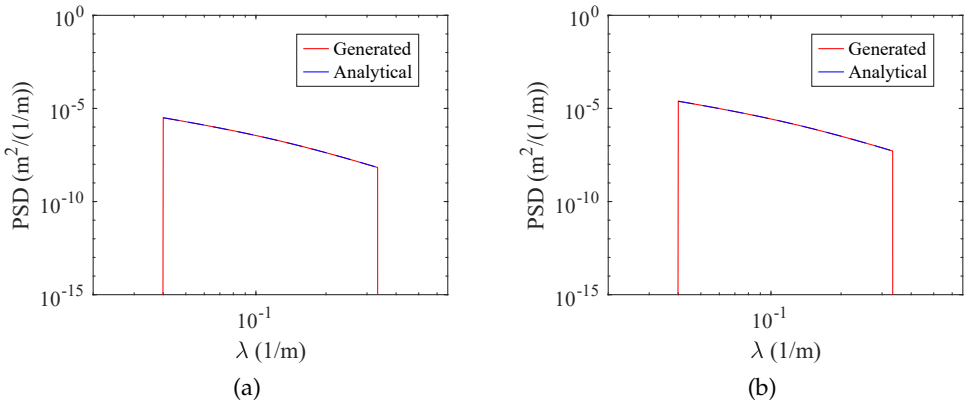

Figure 5.6: Example PSD of the alignment irregularities: (a) Well-maintained track, (b) Alert limit.

5.4 DYNAMIC ANALYSIS

5.4.1 *Train-bridge interaction*

The 3D TTBI dynamic analyses are carried out with the software "VSI — Vehicle Structure Interaction Analysis" (see Figure 5.7). This tool, capable of dealing with lateral dynamics, is implemented in MATLAB® (2018) and imports the structural matrices from the railway vehicle and bridge modelled in the FE package ANSYS® (2018). Then, the external excitations (which can be track irregularities, wind or seismic loads, among others) are imposed on the coupling system, and the corresponding dynamic responses are obtained. The interaction between the two sub-systems is accomplished by a specially developed contact finite element that considers the behaviour of the contact interface between wheel and rail. The contact formulation is divided into three main problems, namely the geometrical, the normal and the tangential contact problems. With the contact interface fully characterized, the equations of motion of the vehicle and bridge are complemented with constraint equations that couple these two structural systems. The full mathematical formulation and validation of the TTBI model can be seen in Neves et al. (2014) and Montenegro et al. (2015).

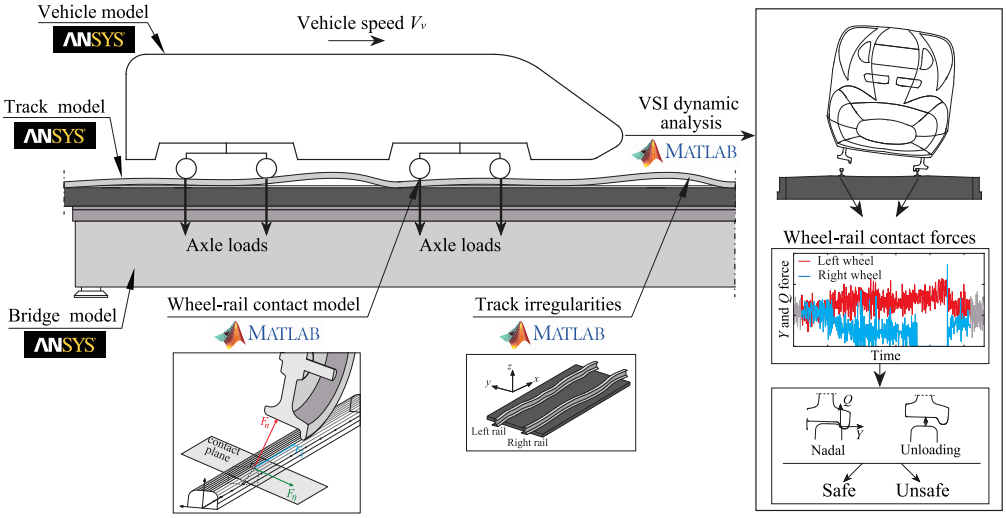

Figure 5.7: Framework of the tool for 3D TTBI dynamic analysis.

In VSI, the wheel-rail contact formulation relies on a specially developed contact element, implemented in MATLAB®, which is firstly used to evaluate the location of the contact point between wheel and rail, considering the relative movement between the vehicle and the structure. This first step, named the "geometrical contact problem", is accomplished with the parameterization of the surfaces of the contacting bodies, i.e., the wheel and rail. The potential contact point position is evaluated through the following nonlinear equations:

$$\begin{cases} \mathcal{T}_r \cdot \mathcal{D}_{wr} = 0 \\ \mathcal{T}_w \cdot \mathcal{N}_r = 0 \end{cases} \tag{5.2}$$

where $\mathcal{T}_r$ and $\mathcal{T}_w$ are the lateral tangent vectors to the rail and wheel surfaces, respectively, at the contact point, $\mathcal{N}_r$ is the normal vector to the rail surface at that same point, and $\mathcal{D}_{wr}$ is the vector that defines the relative position between the contact points in the wheel and rail surfaces directed at the wheel. However, as can be seen in Figure 5.8, the condition defined by Equation 5.2 is necessary but not sufficient to guarantee actual contact. Therefore, the following additional condition is added to the formulation to ensure that the two parametric surfaces intersect:

$$\mathcal{D}_{wr} \cdot \mathcal{N}_r \leq 0 \tag{5.3}$$

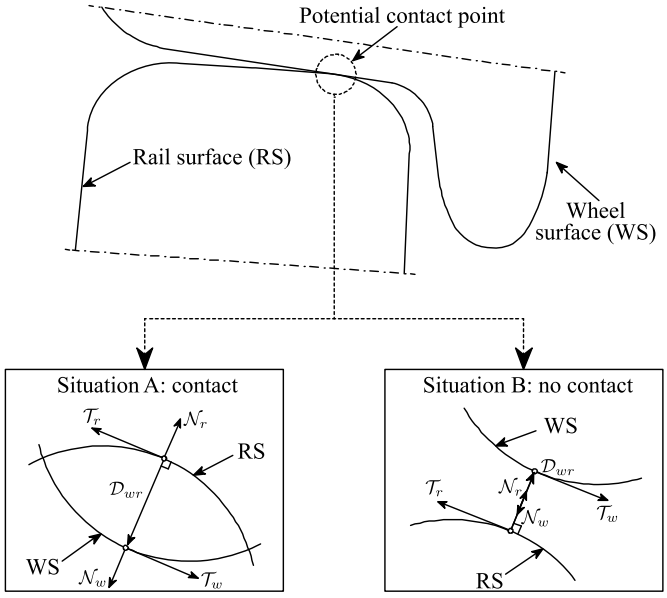

Figure 5.8: Possible situations after a valid solution of the nonlinear equations for contact search. (adapted from Montenegro et al. (2022))

Since $\mathcal{D}_{wr}$ is directed towards the wheel and $\mathcal{N}_r$ outside the rail surface, Equation 5.3 represents "Situation A" in Figure 5.8, in which contact occurs when the two vectors point in opposite directions. If this condition is not met (even though the solution for Equation 5.2 is valid), contact does not occur, as can be seen in "Situation B" in Figure 5.8. The deformation of the contact element is utilized to calculate the normal contact force and is given by:

$$d = \|\mathcal{D}_{wr}\| \tag{5.4}$$

For better and faster convergence, the results obtained in the previous iteration or step are used as an initial estimate for the solution of the nonlinear problem defined by Equation 5.2. It is noted that there may be multiple solutions for the equations if the contact point resides in the concave region between the wheel thread and flange. When this happens, an alternative contact point detection algorithm (described in detail by Montenegro et al. (2015)) is used.

The forces output in the contact interface are evaluated through the contact laws implemented in the contact finite element. Regarding the normal contact,

and according to the Hertz nonlinear theory, when two non-conforming bodies are compressed to each other, they deform in the region around the first contacting point, forming a contact patch with an elliptical format. The normal contact force F_n can thus be computed based on the deformation d of the contact element calculated in Equation 5.4 through:

$$F_n = K_h d^{\frac{3}{2}} \tag{5.5}$$

where K_h is a coefficient depending on the Young's modulus and Poisson ratio of the material from the contacting bodies and on their curvatures at the contact point.

After computing the normal forces, it is possible to evaluate the tangential forces on the contact interface that exist due to the rolling friction contact between wheel and rail. Contrary to the Coulomb friction, where the behaviour within the contact patch is homogenous (all points are adhering or slipping), when two compressing bodies are allowed to roll over each other, the contact area may share points in adhesion and in slippage simultaneously. Based on this, it is possible to compute the so-called creepages, which are the normalized relative velocities between wheel and rail at the contact point. Creepages are the main inputs for the tangential contact forces that play a major role in a vehicle's stability. The tangential creep forces in the longitudinal and lateral directions (F_ξ and F_η, see Figure 5.9) are precalculated and stored in a lookup table based on the USETAB algorithm (Kalker, 1996), to be later interpolated during the dynamic analysis as a function of the creepages and the semi axes ratio of the contact ellipse (details on how the table is built can be consulted in Montenegro et al. (2015)).

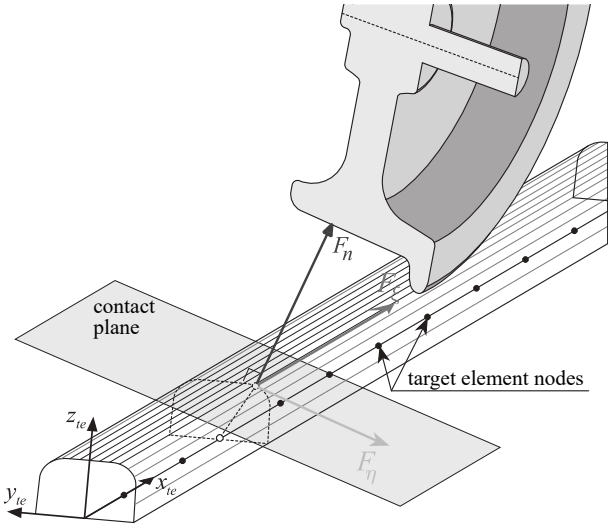

Figure 5.9: Normal and tangential contact forces in the interface between wheel and rail. (adapted from Montenegro et al. (2020))

The coupling between the vehicle and the bridge is accomplished through the Lagrange multipliers method, in which the governing equilibrium equations of motion are complemented with constraint equations that connect the two

sub-systems. These equations form a single system with displacements $\mathcal{A}$ and contact forces $\mathcal{X}$ (Lagrange multipliers) as unknowns that can be mathematically described as:

$$\begin{bmatrix} \mathcal{K} & \mathcal{D} \\ \mathcal{H} & 0 \end{bmatrix} \begin{bmatrix} \Delta\mathcal{A}^{i+1} \\ \Delta\mathcal{X}^{i+1} \end{bmatrix} = \begin{bmatrix} \Psi\left(\mathcal{A}^{t+\Delta t,i}, \mathcal{X}^{t+\Delta t,i}\right) \\ \mathcal{R} \end{bmatrix} \tag{5.6}$$

where $\mathcal{K}$ is the coupled effective stiffness matrix of the system, and $\mathcal{R}$ is the track irregularities vector that is interpolated in each timestep, depending on the position of the wheel. Due to the nonlinear nature of the problem, a formulation based on incremental displacements $\Delta\mathcal{A}$ and contact forces $\Delta\mathcal{X}$ is used, in which Ψ is the residual force vector. Finally, since node B from the contact element is located over non-nodal points from the track (the contact element is constantly moving), matrix $\mathcal{D}$ transforms the contact forces defined in the local coordinate system (CS) of the rail elements with the nodal forces in the global CS, while matrix $\mathcal{H}$ relates the nodal displacements of the rail elements in the global CS with the displacements of the non-nodal points from the rail elements where node B is located. $t + \Delta t$ indicates the current time step, while i and $i + 1$ refer, respectively, to the previous and current iteration.

5.4.2 *Critical train load model*

As stated in Section 5.2, only the most critical HSLM-A train for each case study bridge is taken into account for the study. The SLLS moving loads method, applicable to single-span simply supported bridges, was employed for this assessment, using the quantities listed in Table 5.1 and the load values and distances of the HSLM-A.

The maximum midspan acceleration a is estimated accounting for the resonant effects that occur due to the relation between the repeatability of the loads and the bridges' natural vibration frequencies. Each line of the graphics in Figure 5.10 corresponds to the maximum acceleration obtained from the response of each of the HSLM-A trains at different speeds on each bridge. The HSLM-A universal train (represented in blue) that causes an acceleration that exceeds the EN 1990 limit of 5 m/s^2 (at around 1.2×320 km/h) was chosen as the critical one for the bridge at matter.

Therefore, the critical HSLM-bridge pairs are:

- 10 m bridge: HSLM-A7
- 15 m bridge: HSLM-A7
- 20 m bridge: HSLM-A1
- 25 m bridge: HSLM-A3
- 30 m bridge: HSLM-A9

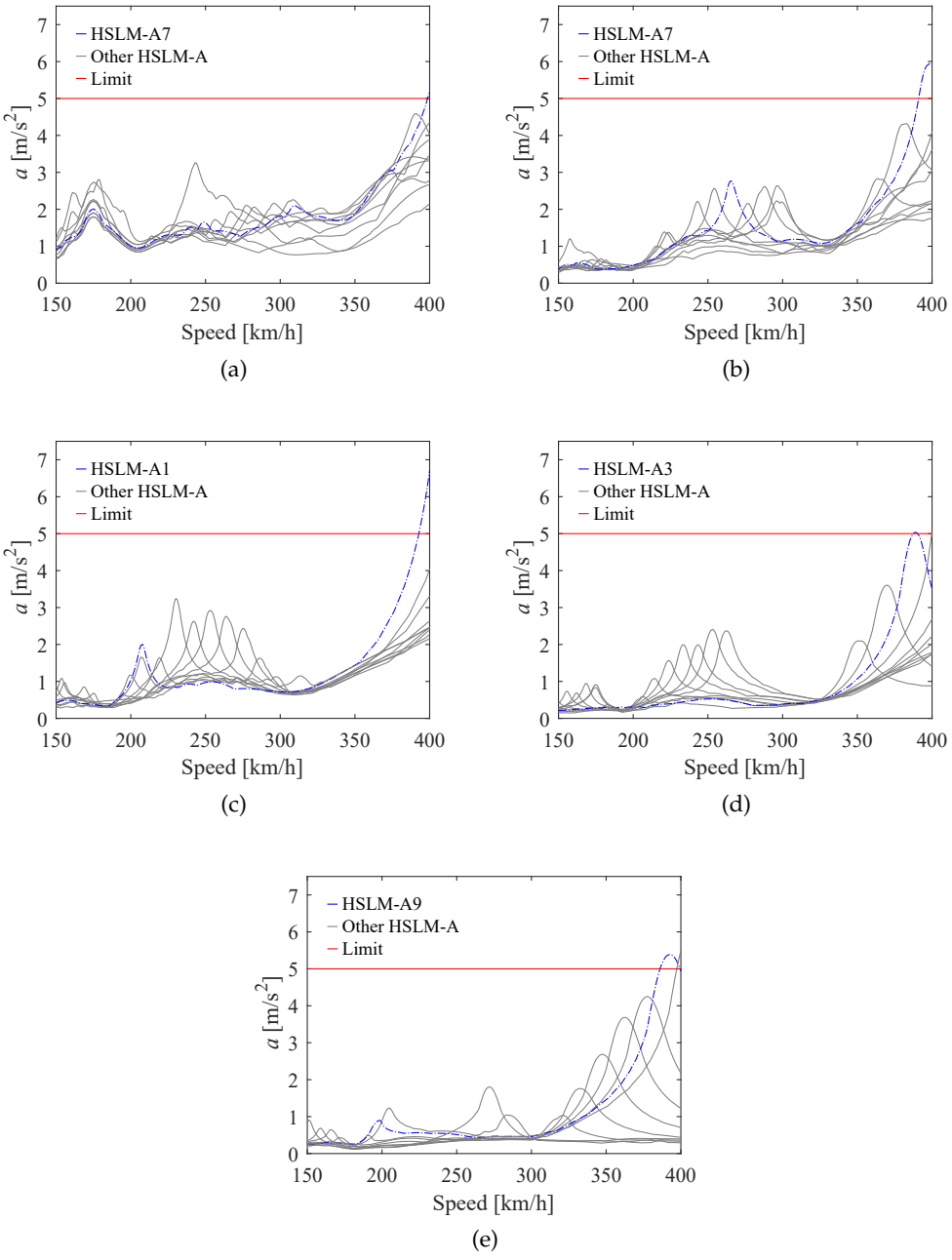

Figure 5.10: Maximum midspan deck acceleration and identification of the most critical HSLM-A train. (a) 10 m bridge; (b) 15 m bridge; (c) 20 m bridge; (d) 25 m bridge; (e) 30 m bridge.

5.4.3 *Analysis results*

The results of the parametric analyses introduced in Section 5.2 are presented hereinafter. Figure 5.11 depicts the envelopes of the maximum registered Unloading criteria, while the Nadal envelopes are presented in Figure 5.12. The displayed data points of the computed derailment criteria correspond, for each speed, to the worst-performing wheelset (while still on the bridge) of that particular simulation. The acceleration values can be seen in Figure 5.13, with each value representing the maximum absolute acceleration in the midspan of the bridge's deck.

The Nadal criterion measures no distinguishable features for a smooth track profile (i.e., with no vertical nor lateral rail irregularities imposed on the system). Due to the absence of lateral irregularities and other sources of transversal instability, this expected behaviour serves as a benchmark for the results. In fact, the vertical acceleration curves for smooth tracks show similarities to the moving loads assessment in both absolute value and location of resonance.

Concerning the track irregularities, either with high or low quality (Alert Limit level), the maximum values of ξ_U increase with speed, but the general shape of their trends remains the same (Figure 5.11). The same conclusion can be drawn from the accelerations' results. Notably, the Unloading criterion curves rise as the speed approaches 400 km/h, but they also show a less evident, yet present, peak around the sub-harmonic speeds.

In general, it is observed that ξ_N is unaffected by resonance phenomena, never following the trend of the acceleration or Unloading curves, but instead reflecting only the level of track condition (Figure 5.12). As the irregularities (including lateral) on the tracks get more prevalent, lateral forces become more present in each wheel, while vertical contact forces get diminished, thus increasing the criterion's values. However, even in scenarios of low-quality tracks (with Alert Limit irregularity profiles), the Nadal criterion remains fairly low and distant from its limit of 0.8.

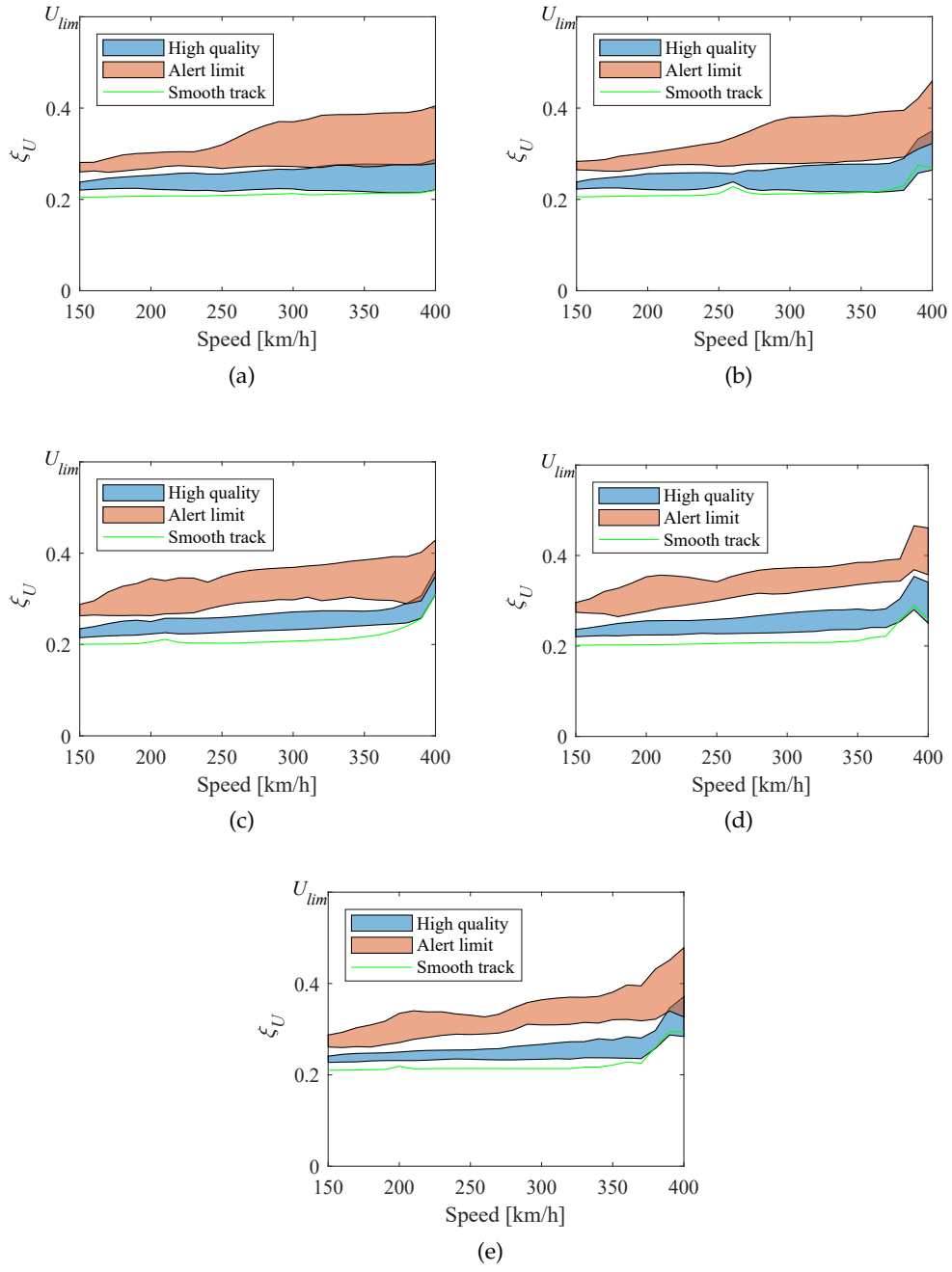

Figure 5.11: Unloading criterion envelopes. (a) 10 m bridge; (b) 15 m bridge; (c) 20 m bridge; (d) 25 m bridge; (e) 30 m bridge.

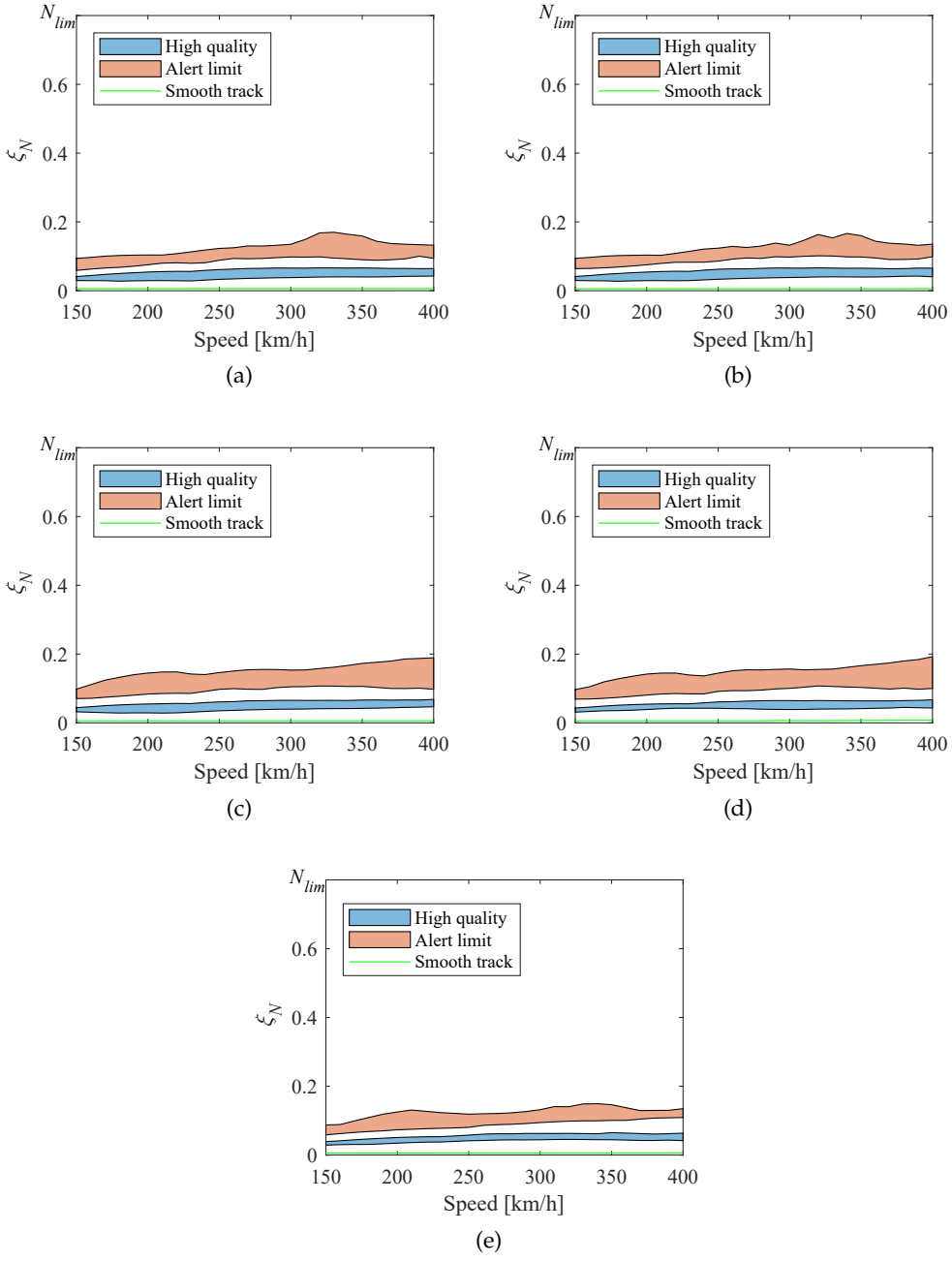

Figure 5.12: Nadal criterion envelopes. (a) 10 m bridge; (b) 15 m bridge; (c) 20 m bridge; (d) 25 m bridge; (e) 30 m bridge.

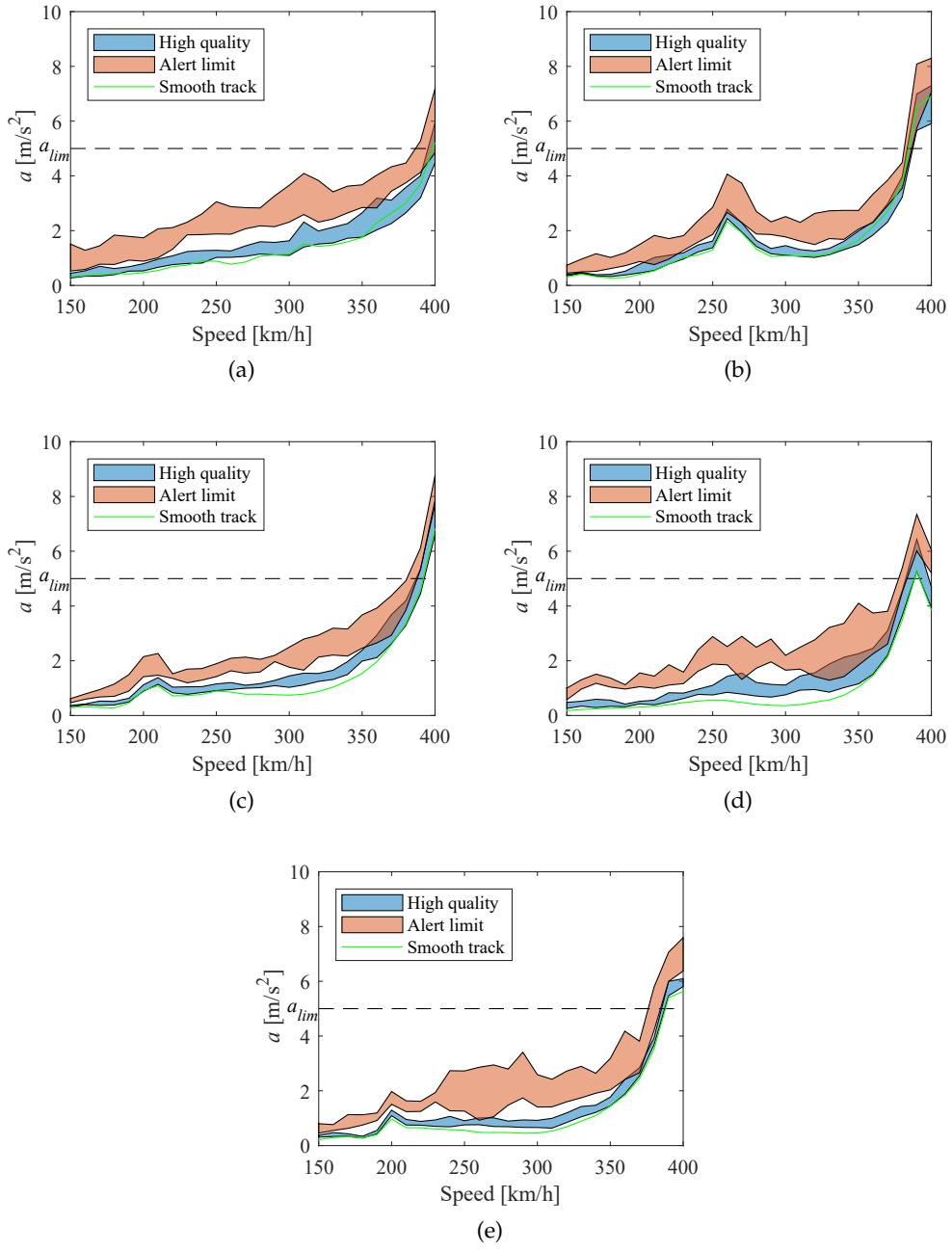

Figure 5.13: Acceleration envelopes. (a) 10 m bridge; (b) 15 m bridge; (c) 20 m bridge; (d) 25 m bridge; (e) 30 m bridge.

The maximum registered vertical acceleration for each bridge is registered in Table 5.7 for the high-quality track realizations and in Table 5.8 for the Alert Limit irregularity profiles. Both tables present the two concomitant criteria, i.e., the maximum value of the worst-performing wheelset that stems from the realization of rail irregularity leading to the maximum acceleration. From the observation of these results, there appears to be no correlation between acceleration levels above the normative limit of 5 m/s^2 and derailment indicators. Considering, for example, the worst-case scenario of track condition, an assessment based on the normative limit would conclude that the acceleration limit is surpassed. However, the maximum value of the unloading factor, in that case (for all studied bridges), is below 0.38 for high-quality tracks and 0.48 for Alert Limit tracks, which is far from the limit of 0.6. Therefore, since deck acceleration does not seem to condition derailment at such low values, the results do not support the thesis of safety being limited by the calculation of vertical deck acceleration.

		CRITERIA	
BRIDGE	MAX. ACCEL. $\left(m/s^2\right)$	UNLOADING	NADAL
10 m	5.93	0.25	0.04
15 m	7.30	0.26	0.07
20 m	7.70	0.36	0.07
25 m	6.43	0.30	0.06
30 m	6.09	0.29	0.06

Table 5.7: Maximum registered acceleration values and concomitant criteria (high quality track).

		CRITERIA	
BRIDGE	MAX. ACCEL. $\left(m/s^2\right)$	UNLOADING	NADAL
10 m	7.18	0.28	0.10
15 m	8.30	0.38	0.13
20 m	8.77	0.39	0.10
25 m	7.35	0.37	0.12
30 m	7.59	0.36	0.11

Table 5.8: Maximum registered acceleration values and concomitant criteria (Alert Limit track).

The existence of a correlation (or lack thereof) between acceleration and derailment indicators can be further explored by plotting all the pairs of data points and fitting a linear regression. This is presented in Figure 5.14a for the high quality track realizations and in Figure 5.14b for the Alert limit tracks, with the continuous black lines representing the fitted models. The displayed

coefficients of determination (r^2) show, for both cases, that the Unloading criterion is the one that follows acceleration the closest. Even so, the relation is insufficient to infer safety conditions from analyzing acceleration alone since several data points above the acceleration limit do not cross U_{lim}. This observation is even more evident when considering lateral forces for derailment, i.e. acceleration values from close to 0 m/s^2 to almost 8 m/s^2 hardly translate into any ξ_N values. It is also noteworthy that the gap between the criteria's r^2 values is narrower for the worst track conditions, which highlights the importance of the level of irregularities.

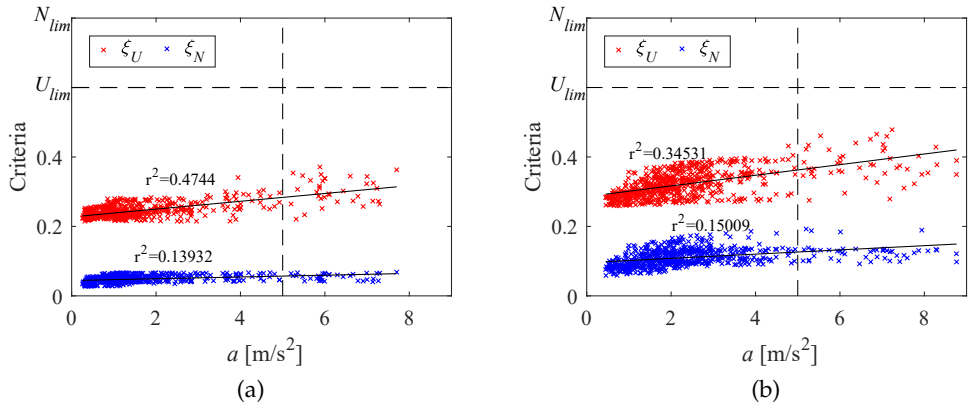

Figure 5.14: Relation between acceleration and derailment criteria (all bridges, every speed). (a) every realization of a high quality track; (b) every realization of an Alert Limit track.

5.4.4 *Influence of increased irregularities*

Results from Section 5.4.3 have shown that the derailment criteria are distant from their limits even at resonance. While deck acceleration is sensitive to both running speed and track condition, the Nadal and Unloading criteria are less influenced by the bridge's dynamic effects. An additional set of dynamic analyses was devised to sustain this observation further. These included generating new realizations of track irregularities, increasing both the vertical and alignment standard deviations in the 3 m to 25 m wavelength range, totalling 10 new profiles: 5 with a 50% increase over the Alert limit's σ_{3-25} (named Alert $\times$1.5) and 5 with 100% increase over the Alert limit's σ_{3-25} (named Alert $\times$2). This set of analyses was conducted on the 25 m bridge, with the HSLM-A3 model at 390 km/h, since this combination provided the most evident resonant situation.

Figure 5.15 presents the results from the increased irregularities simulations as boxplots superimposed on zoomed-in sections of Figure 5.11d, Figure 5.12d and Figure 5.13d. These figures allow for a comparison of 5 scenarios: smooth track, high quality track, Alert Limit, 50% increase of the Alert Limit and 100% increase. It can be seen that there is a direct relation between a worse track and higher derailment criteria: maximum values registered include 0.704

for Unloading and 0.505 for Nadal. As for acceleration, a maximum value of 8.168 m/s^2 is measured.

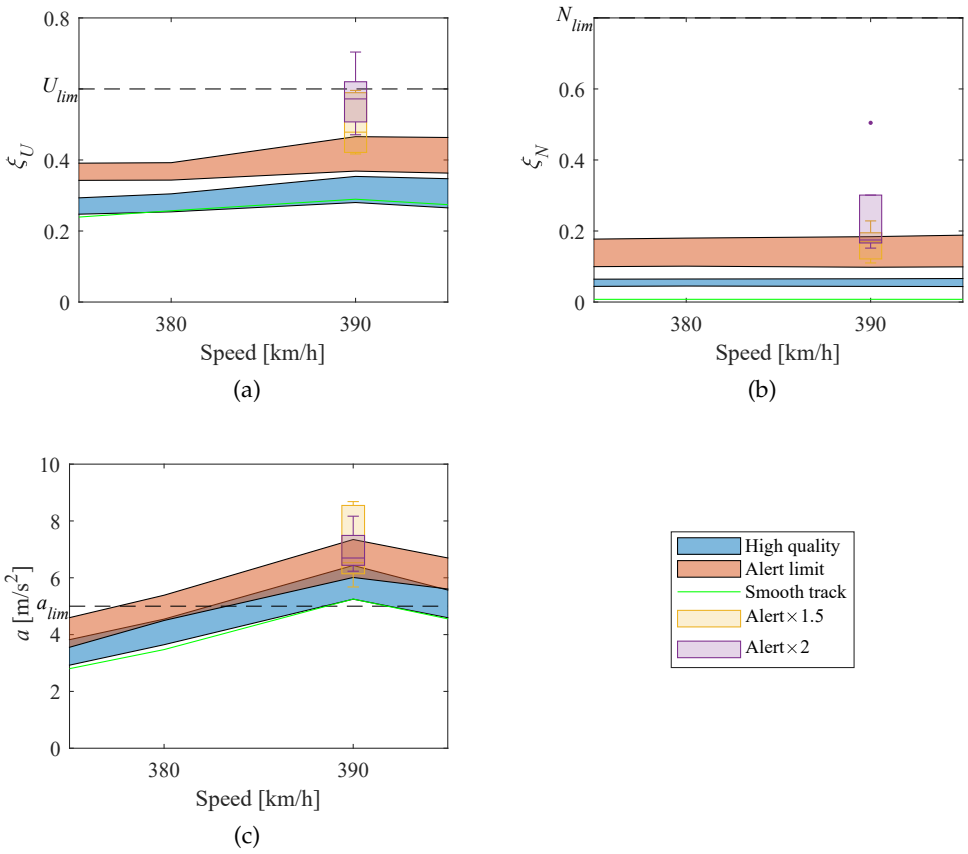

Figure 5.15: Criteria for increased irregularities (25 m bridge). (a) Unloading; (b) Nadal; (c) Acceleration.

The results presented strengthen the observation that derailment criteria, compared to deck accelerations, are more permeable to track conditions. It was necessary to increase Alert limit conditions up to double the standard deviation to register ξ_N values above 0.5 and ξ_U values greater than U_{lim}. On the other hand, acceleration was already greater than the normative 5 m/s^2 limit, even for a smooth track. Worsening the irregularity profiles increased the maximum acceleration. Still, it is worth noting that there is far more overlap between the different realizations' results on acceleration when compared to the derailment criteria, i.e., track condition plays a less relevant part in determining deck acceleration.

5.4.5 *Influence of the bridge vibration*

From the general and increased irregularities analyses, it can be inferred that track condition constitutes the predominant factor in assessing running safety. Even though the occurrence of resonance is relevant for deck acceleration, vibration from the bridge seems to have an imperceptible effect on the variation of wheel-rail contact forces and, therefore, on the derailment criteria. For this

reason, the present section presents the results of additional dynamic analyses of the same critical load model and speed as of the 25 m bridge, replacing it with a rigid bridge. These simulations consider the 21 available profiles, i.e. the same employed in Section 5.4.4. Figure 5.16a and Figure 5.16b depict the distribution of results regarding the Unloading and Nadal criteria, respectively.

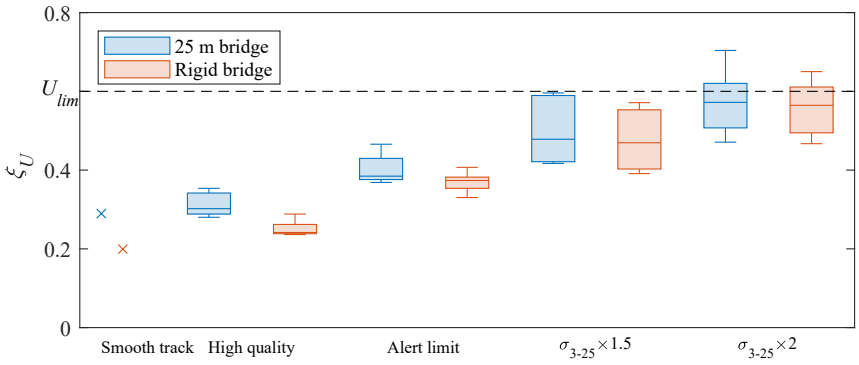

(a)

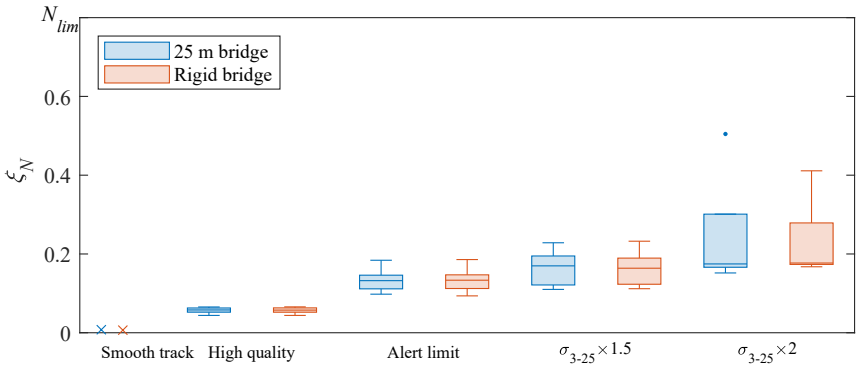

(b)

Figure 5.16: Influence of the bridge vibration. (a) Unloading criterion; (b) Nadal criterion.

The results indicate that regardless of considering the bridge's dynamic effects, the performance of derailment indicators is controlled by the track's condition. As quality decreases, so does the influence of the bridge vibration. To assess the fitness of using just the plain track model as a predictor (ξ_U^* and ξ_N^*) of the criteria, the sums of squared errors can be computed (using all available realizations) as:

$$\sum_{i=1}^{21} (\xi_U - \xi_U^*)^2 = 0.0419 \tag{5.7}$$

$$\sum_{i=1}^{21} (\xi_N - \xi_N^*)^2 = 0.0092 \tag{5.8}$$

Given that the scale of the criteria is between 0 and 1, the fact that the sums of squared errors are lower than 1% makes them negligible. It can be concluded

that regardless of the train model being subjected to bridge vibration, the relation between contact forces is already conditioned by the track quality.

5.4.6 *Effect on riding comfort*

Results in the previous sections suggest that deck acceleration does not accurately relate to derailment criteria. Since running safety appears to be conditioned by track condition rather than the amount of bridge vibration, a revision of the Eurocode could result in removing the acceleration limit. However, even if the maximum deck acceleration does not portray running safety, its value should nevertheless be limited if it can be taken as an indicator for other measurements, such as riding comfort.

The present subsection measures passenger riding comfort by calculating the vertical acceleration at coach level b_v. Using the same case study bridges and track irregularity profiles, time-histories are obtained for each carriage for the entire run (before, during, and after crossing the bridge) at every speed (Figure 5.17a). These responses are band-pass filtered (0.4 Hz to 10 Hz, cut off at -3 dB), according to the "Ride characteristics" requirements in the EN 14363 (CEN, 2016) (Figure 5.17b). The response section corresponding to the bridge crossing is isolated, and the maximum absolute value is stored (Figure 5.17c).

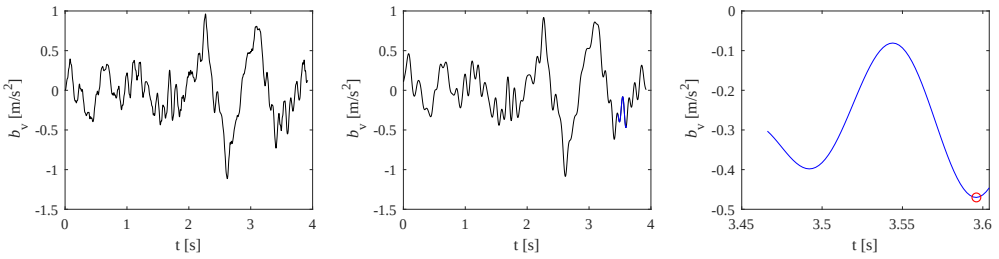

Figure 5.17: Visualization of the riding comfort assessment methodology. (a) Entire time-history; (b) Filtered response (bridge section in blue); (c) Maximum absolute.

The envelopes containing the maximum coach acceleration are illustrated in Figure 5.18. The dataset comprises the results from each run's worst-performing coach. In the figures, the "Very good", "Good", and "Acceptable" thresholds correspond to the limits introduced in Section 2.2.1.1. Similarly to the derailment criteria's analysis, it is observed that there is a clear separation concerning the track's quality, with the Alert limit tracks corresponding to the worst coach acceleration values. For high quality tracks, the thinner envelopes indicate less dispersion in results, with their lower limits generally following the smooth tracks' results. In all five bridges, the Alert limit irregularities cause the riding comfort to cross the "Very good" line, with the 30 m bridge even demonstrating a crossing of the "Acceptable" line (albeit at very high speeds). A better maintained high quality track is not only less permeable to speed differences but also a guarantee of higher riding comfort.

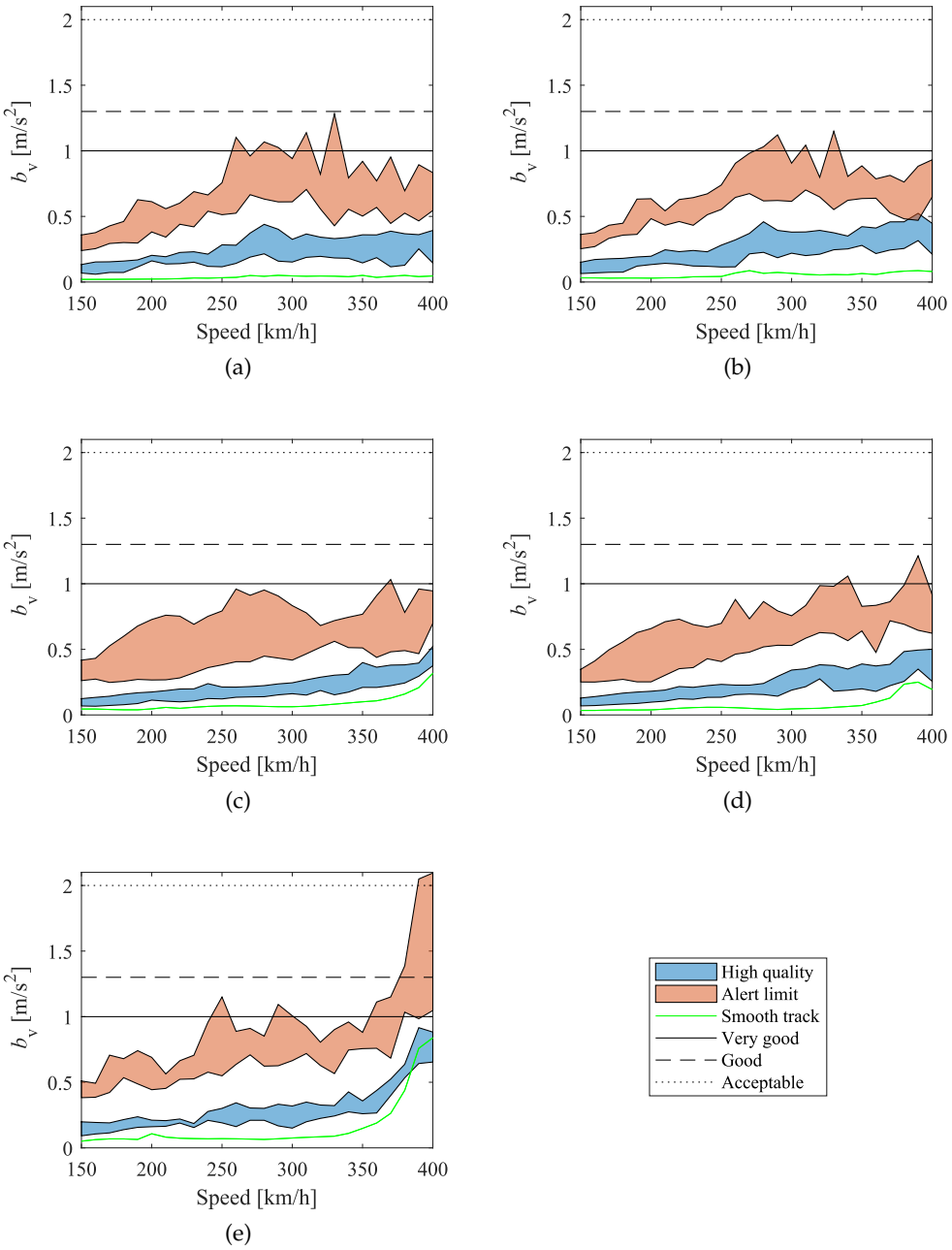

Figure 5.18: Coach acceleration envelopes. (a) 10 m bridge; (b) 15 m bridge; (c) 20 m bridge; (d) 25 m bridge; (e) 30 m bridge.

The possible correlation between deck and coach acceleration is further investigated by plotting the pairs of results (Figure 5.19) and calculating the coefficients of determination. There is less dispersion in the high quality track results, which makes for a larger correlation than in the alert limit track results. Nonetheless, in high quality tracks, deck accelerations around or above the normative limit of 5 m/s^2 do not increase coach acceleration. In fact, at 0.92 m/s^2, the maximum registered coach acceleration does not even cross the "Very good" 1 m/s^2 threshold. Conversely, in alert limit irregularity tracks, there are several instances where a deck acceleration of 6 m/s^2 can correspond either to a very low coach acceleration (0.47 m/s^2) or up to values above (2.10 m/s^2) the "Acceptable" threshold of 2 m/s^2. The correlation is insufficient to justify using deck acceleration as an indicator of passenger riding comfort.

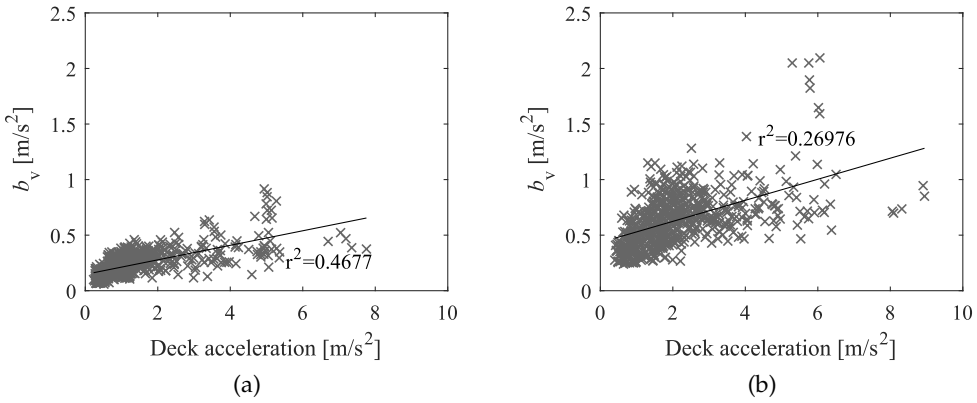

Figure 5.19: Relation between deck acceleration and coach acceleration (all bridges, every speed). (a) every realization of a high quality track; (b) every realization of an Alert Limit track.

5.5 NORMATIVE RECOMMENDATION

The current Eurocode EN 1990 (CEN, 2023a) limits the maximum vertical deck acceleration to "prevent track instability, for traffic safety reasons". This relation is contested by the research presented in the present chapter, which consistently suggests that vertical deck acceleration is unrelated to the assessment of running safety, concerning the occurrence of derailment. Not only is the current Eurocode limit of 5 m/s^2 not associated with any safety threshold, but deck acceleration itself, as an indicator, is insufficiently correlated to any variation in derailment criteria. Contrarily, track quality is a more relevant factor, demonstrating that the effect of rails' unevenness across hundreds of meters is far greater than the effect of the bridge's vibration. It could be argued, however, that deck acceleration should still have a limiting value related to other non-safety-related phenomena. In this regard, this thesis evaluates whether riding comfort correlates with deck acceleration, yet the results do not point in that direction.

As mentioned in Section 4.7, although the current Eurocode EN 1990 is a single document, in the upcoming second generation of Eurocodes, the norm will consist of two distinct parts, separating new from existing structures. Therefore, the normative recommendation for this matter is:

RECOMMENDATION FOR NEW AND EXISTING STRUCTURES: considering the lack of correlation between deck acceleration and derailment, remove the criterion presented in Section A.2.9.4.2.1 of the EN 1990 (CEN, 2023a) which limits the deck acceleration for ballastless track railway bridges to 5 m/s^2.

It is observed that dynamic assessment is still necessary since other limiting aspects exist, such as support uplift, slab separation, deflection control, fatigue assessment, or relative rotation. Additionally, it should be noted that some acceleration limit could still exist due to the presence of loosely supported non-structural components or to prevent malfunctioning pantograph-catenary interaction (for instance, Matsuoka et al. (2022) highlights the possible fatigue damage in overhead wires caused by excessive vibrations). However, such a limit should be clearly identified in the Eurocode as being due to the mentioned reasons and not because of traffic safety.

5.6 CONCLUDING REMARKS

The present chapter addressed the pertinence of utilizing an acceleration limit as a conditioning factor for the dynamic design of railway bridges. Multiple realizations of two track quality levels were tested on a wide range of running speeds for five different bridges with train models representative of the HSLM-A. A comparative analysis of increased irregularities, as well as of the influence of the bridge vibration under resonance, was also presented to further sustain the observations. Acceleration at coach level was studied, evaluating its relation to deck acceleration.

Referring to the research questions listed in Section 5.1, the main conclusions to be drawn can be outlined as follows:

1. Ballastless railway bridges can experience acceleration values above the normative limit of 5 m/s^2 without it corresponding to a surpassing of derailment criteria, which does not support the thesis of using deck acceleration as a limiting factor for running safety.

2. Even though both the Unloading and the Nadal criteria present a low correlation with acceleration, the former does indicate a closer relation. Vertical dynamics are, therefore, indispensable in assessing train running safety in scenarios where the Unloading criterion is conditioning. 3D analyses should be considered in scenarios where substantial lateral loads may contribute to the lateral instability of the train.

3. Across different running speeds, the Nadal criterion is shown to be close to constant, depending on the track quality, with the Unloading criterion being slightly more telling of the occurrence of resonance, while the

acceleration values are greatly dependent on the train's speed. Results show that both derailment criteria are greatly influenced by the level of track quality, with bridge vibration being imperceptible for wheel-rail contact forces. For the study of derailment, track quality is far more relevant than the vibration experienced on the bridge.

4. The correlation between deck and coach acceleration across multiple bridges and running speeds is not strong enough to confidently infer the level of passenger riding comfort from the analysis of deck vertical acceleration.

Considering the presented conclusions, it is observed that the current normative limit might be over-conservative. In the case of future discussion and research work leading to the acceleration criterion being discarded, different limiting criteria should be tested and evaluated.

6 CONCLUSIONS AND FUTURE WORKS

6.1 CONCLUSIONS

The work developed in this thesis is intended to contribute towards the discussion around the permanent improvement of the Eurocodes. The three problems presented (constituting the three core chapters of this work) were selected due to concerns expressed not only by the scientific community but also by regulatory bodies. Therefore, these aspects established pertinent research opportunities, motivating the objectives stated in Section 1.3.

From the documents explored in the literature review, it was made evident that there was a scarcity of studies evaluating the HSLM's limits of validity in comparison to the model's envelope. In Annex E of the EN 1991-2, the lack of definition of distances relevant to the HSLM also presented an opportunity. Furthermore, the clarification of the same norm's dispositions regarding estimates of mass and damping remained to be addressed. At the same time, the seemingly arbitrary reasoning behind the definition of deck acceleration limits in the EN 1990 had been questioned in studies. The quantification of permissible acceleration related to design scenarios for ballasted tracks was still fairly insufficient in the literature. In the case of ballastless tracks, a gap was identified in the inclusion of lateral dynamics in the assessment of running safety.

The evaluation of the HSLM's limits of validity was derived from the study of six sets of randomly generated articulated, conventional, and regular train load model configurations, with some abiding by the limits of Annex E of the EN 1991-2 and others having distances outside the range, which totalled more than 17 million dynamic analyses. For this quantity to be feasible, it was crucial to develop a tool to expedite the test of load models. The Single Load Linear Superposition method was developed and validated, achieving a computation time saving of 92%. This allowed any number of load models to be tested when provided with a bridge's response from a single moving load. The study of randomly generated load model configurations showed that it is possible for a load model abiding by the limitations of Annex E of EN 1991-2 to not be covered by the HSLM's envelope. This is verified for some articulated trains but primarily for conventional and regular trains. The Eurocode's insufficient description of the distance between the centres of adjacent vehicle bogies further hinders this evaluation. For trains that do not necessarily comply with the Annex's limits, it is found that the HSLM-A is partially suited to encompass some of them. This sort of future-proofing is useful for allowing new, longer trains to join current rolling stock fleets that operate on lines containing bridges designed with the EN 1991-2 HSLM in mind.

As for the improvement of the safety factor for deck acceleration in ballasted bridges, the methodology devised came with the challenge of finding critical

speeds associated with probabilities of failure of 10^{-4}. While the difficulty of a single probabilistic analysis can be circumvented by employing subset simulation, developing a procedure to find the critical speeds without unnecessary computational expenditure was necessary. After optimizing the simulations' parameters and proper stopping criteria, the proposed algorithm made it possible to compute a critical speed within a 1 km/h interval using a sample size of 2200, when an equivalent series of Monte Carlo simulations would entail a sample size of more than 1 million. Another gap addressed in this context was the EN 1991-2's dispositions regarding upper and lower bounds estimates of mass and stiffness. Following a sensitivity analysis, two design scenarios are defined, using Gaussian and uniform distributions for the description of structural and track variables. By comparing the physical acceleration limit associated with track instability with the design acceleration calculated at critical speeds, it was found, in four case study bridges, that a ballasted bridge can be designed for a permissible deck acceleration greater than 3.5 m/s^2 without crossing a target probability of failure greater than 10^{-4}. This means that the implied safety factor of 2.0 present in the EN 1990 is over-conservative. Considering that the new EN 1990 will distinguish new structures from existing ones, the normative recommendation from this thesis is to keep the limit for the design of new bridges (for future-proofing) and allow higher accelerations in the assessment of existing bridges. This finding can be applied to engineering practice by allowing a train that potentially causes deck accelerations above 3.5 m^2 to operate in high-speed lines containing ballasted bridges.

The acceleration limit for ballastless tracks appears to be based on an assumption relating deck accelerations around 1 g with unsafe conditions for running trains. For this part of the study, the identified fail condition was derailment, addressed through the calculation of derailment criteria for which it was necessary to calculate contact forces, deeming insufficient the usage of the HSLM as a moving loads model. Therefore, a 3D parametric model adaptation of the HSLM was developed, based on the distances and loads of the HSLM-A, suited to replicate its effects in simulations where metrics such as lateral wheel-rail contact forces are required. Considering varying quality levels of rail irregularities in five case study bridges with spans between 10 m and 30 m, the results consistently showed that a bridge could present deck acceleration values above 5 m/s^2 and not correspond to surpassing derailment criteria. The correlation between the two metrics is insufficient to justify limiting deck acceleration due to running safety. Deck acceleration was also found not to be an indicator of riding comfort. Therefore, the normative recommendation from this thesis is to remove the acceleration limit for ballastless bridges in the EN 1990. A practical application can be allowing deck accelerations to be higher than 5 m/s^2, provided proper track conditions, which is found to be the determinant aspect.

The developed tools and the methodologies tested for the fulfilment of this thesis' objectives were paramount to conclude the normative recommendations. The Eurocodes are documents that reflect the continuous research in several fields related to Civil Engineering to ensure the best practices in the industry. As society's needs for high-speed rail transportation grow, so must the norms

evolve. The research presented in this thesis can hopefully assist a Eurocode revision in extending the lifecycle of railway bridges.

6.2 RECOMMENDATIONS FOR FURTHER RESEARCH

Throughout the tasks undertaken for this present thesis, a few opportunities showed up that, while outside the scope of the present work, can constitute useful scientific work. Research is a continuous and collaborative work that draws on experience and leaves opportunities for the future. Therefore, the topics that follow are recommendations for further work in the fields of high-speed railway bridge dynamics:

- Develop a load model alternative to the HSLM (or add new universal trains to it) that encompasses the current limits of the norm, and that makes allowance for future trains.
- Complement the study of the HSLM's limitations, focusing on integral portal frames and metallic truss bridges. Evaluate the differences caused by bridges with physical characteristics associated with varying damping scenarios.
- Study the probability of simultaneous train crossings in opposing directions in double-track bridges where there is no independence between the tracks. Consider that while the effect of two concurrent trains can be critical, the probability of that event occurring may be within a reasonable reliability target.
- For slab track bridges, evaluate the existence of a correlation between deck acceleration and the possibility of slab separation.
- Apply the methodology for studying the safety factor for deck acceleration in ballasted track bridges considering the acceleration limit as a random variable, constructed using information from ongoing experimental studies.
- For the study of running safety in ballastless bridges, add a pier-supported bridge model with varying pier lateral stiffness, subjected to wind action, to increase the possible lateral instability of the trains.
- Enhance the normative criteria for structural damping through the statistical study of existing results from experimental campaigns and simulations.
- Study the validity of the Eurocode's usage of deck deflection as an indicator of passenger comfort, which currently depends on the number of spans.
- Evaluate the pertinence of the 1.2 Hz lower limit for lateral bridge vibration, especially considering the effects on high-pier viaducts.

APPENDIX A: ARTICLE FROM PROBLEM 1

The work by Ferreira et al. (2024b), on which Chapter 3 is based, is reproduced in this appendix.

G. Ferreira, P. Montenegro, J. R. Pinto, A. A. Henriques, and R. Calçada (2024b). "A discussion about the limitations of the Eurocode's high-speed load model for railway bridges." In: *Railway Engineering Science* 32.2, pp. 211–228. ISSN: 2662-4745. DOI: 10.1007/s40534-023-00321-5

Railway Engineering Science (2024) 32(2):211–228
https://doi.org/10.1007/s40534-023-00321-5

A discussion about the limitations of the Eurocode's high-speed load model for railway bridges

Gonçalo Ferreira[1] · Pedro Montenegro[1] · José Rui Pinto[1] · António Abel Henriques[2] · Rui Calçada[1]

Received: 9 December 2022 / Revised: 17 August 2023 / Accepted: 21 September 2023 / Published online: 28 February 2024

Abstract
High-speed railway bridges are subjected to normative limitations concerning maximum permissible deck accelerations. For the design of these structures, the European norm EN 1991-2 introduces the high-speed load model (HSLM)—a set of point loads intended to include the effects of existing high-speed trains. Yet, the evolution of current trains and the recent development of new load models motivate a discussion regarding the limits of validity of the HSLM. For this study, a large number of randomly generated load models of articulated, conventional, and regular trains are tested and compared with the envelope of HSLM effects. For each type of train, two sets of 100,000 load models are considered: one abiding by the limits of the EN 1991-2 and another considering wider limits. This comparison is achieved using both a bridge-independent metric (train signatures) and dynamic analyses on a case study bridge (the Canelas bridge of the Portuguese Railway Network). For the latter, a methodology to decrease the computational cost of moving loads analysis is introduced. Results show that some theoretical load models constructed within the stipulated limits of the norm can lead to effects not covered by the HSLM. This is especially noted in conventional trains, where there is a relation with larger distances between centres of adjacent vehicle bogies.

Keywords High-speed load model · Dynamic analysis · High-speed railways · Train signature · Railway bridges · Deck acceleration

1 Introduction

The evaluation of running safety on bridges has been a widely studied topic in the last years [1–3]. In particular, the design of high-speed railway bridges must fulfil, among others, several safety and serviceability normative criteria related to the dynamic behaviour of the structure under railway traffic. Among those criteria, particular attention should be given to the one related to the maximum deck accelerations specified in the European norm EN 1990-Annex A2 [4], since it often conditions the bridge design. This criterion stipulates a maximum deck acceleration of 3.5 and 5.0 m/s^2 for bridges with ballasted and non-ballasted tracks, respectively. While the former comes from the test rig experiments described in [5, 6], in which it was concluded that for accelerations above $0.7g$ the ballast layer loses its interlocking capabilities, leading to the instability of the ballast track and consequent higher probability of derailment, the latter is related to the fact that for accelerations above 1g there is a higher risk of uplift effects of bearings and train wheels. Then, according to the recommendation proposed by Ref. [7], a safety factor of 2 is applied to these values, leading to the above-mentioned limits stipulated by the norm.

To generalize the design of railway bridges subjected to important dynamic effects caused by the train passages, usually those designed for speeds greater than 200 km/h, the European Commission's regulation on the Technical Specifications for Interoperability [8] stated that these structures must be checked through the high-speed load model (HSLM)

✉ Gonçalo Ferreira
goncalo.ferreira@fe.up.pt

Pedro Montenegro
paires@fe.up.pt

António Abel Henriques
aarh@fe.up.pt

Rui Calçada
ruiabc@fe.up.pt

[1] CONSTRUCT-LESE, Faculty of Engineering, University of Porto, Rua Dr. Roberto Frias, 4200-465 Porto, Portugal

[2] CONSTRUCT-LABEST, Faculty of Engineering, University of Porto, Rua Dr. Roberto Frias, 4200-465 Porto, Portugal

specified in the European norm EN 1991-2 [9]. This load model, which dated from 1999 and was proposed in Ref. [10], was built based on the idea of separating the dynamic response of the train from the response of the bridge to facilitate the comparison of the dynamic loading effects caused by different trains. Such separation led to the definition of a train spectrum, called train signature, which was successfully obtained through a method called decomposition of the excitation at resonance (DER method). However, many other authors continue to contribute to the development of this type of train spectra for analysing the structural response under railway traffic. Vestroni and Vidoli [11] developed an approach based on a non-dimensional representation of the bridge response and Fourier transform of the train loads. Matsuoka et al. [12] defined the train spectrum of the Italian ETR-1000 train to study the influence of local deck vibrations on the assessment of the maximum accelerations in a steel–composite high-speed railway bridge. Auersch [13] studied resonant effects in railway bridges using modal force excitation techniques and train axle sequence spectra.

The first approach for defining an all-encompassing load model to be adopted by the norms, however, was not the HSLM, but the UNIV-A model, also developed by the ERRI committee. This load model took the properties of the Eurostar articulated train as a basis, with an individual axle load of 170 kN, and considered a variation of the coach length between 18 and 27 m [14]. The objective was to guarantee that the signature envelope of this model could cover the effects caused by both articulated (Eurostar and Thalys 2) and conventional (ICE2 and ETR) trains. However, this model proved to be insufficient to cover the effects of the Virgin and Talgo trains, namely for the excitation wavelengths λ of 24 m for the former and between 12.5 and 14.0 m for the latter. Such drawback led to the development of the current HSLM, composed of two sets of models, namely the HSLM-A, which consists of 10 load schemes to be used in the design of continuous bridges or simply supported structures with spans greater than 7 m, and the HSLM-B, which comprises a series of equally spaced 170 kN point forces to be used in the design of simply supported bridges with spans less than 7 m.

Although the HSLM continues to be the most complete load model currently existing, its limits of validity have been recently discussed by some authors. Based on such discussion, the following research questions may arise:

1. Is the current HSLM suited to represent future (and existing) trains that do not necessarily respect its limits?
2. How well do the 10 HSLM-A train configurations cover the dynamic effects of all possible articulated, conventional and regular trains that they are meant to do?
3. Does the lack of definition of some HSLM limiting parameters, such as the distance between the centres of bogies between adjacent vehicles d_{BS} in conventional trains, affect the evaluation of these same limits?

The first question is related to the fact that the current limits of validity of the HSLM defined in Annex E of EN 1991-2 [9] (hereinafter referred to as Annex E) are not broad enough to cover new and future trains. An example of such limitation is the recent introduction into service of the German high-speed train ICE4 with a coach length D of 28.75 m [15], which has been reported to cause acceleration responses on railway bridges that are not covered by the HSLM envelope: Reiterer et al. [16] observed that the ICE4 can produce vertical deck acceleration more than double than the HSLM-A. This problem is currently leading to new proposals for load models for railway dynamic analysis, in which two international consortia, one from the European Project In2Track3 [17] and another from the German Federal Railway Authority [18, 19], stand out. Both works are focused on the definition of alternative load models that may cover the effects of recent and future trains characterized by design parameters outside the ranges of variations of the current HSLM, but that were adopted by vehicle manufactures due to competition and economic reasons. In both approaches, the authors assess the train signature envelopes, as well as bridge responses obtained with dynamic numerical finite element (FE) analysis. Regarding the latter, Vorwagner et al. [19] reported that their study covers a wide range of train configurations and bridge characteristics, totalling around more than 17 million dynamic analyses. Such scale brings with it concerns about the computational cost associated with performing dynamic analysis on FE models. Envisaging the possibility of train manufacturers designing new high-speed trains that do not fully meet the geometric limits stipulated by Annex E due to economic reasons (avoiding short length coaches, for example), Unterweger et al. [20] investigated the most critical parameters that need to be fulfilled to ensure that the new vehicle is in line with the HSLM. The authors performed a study with eight fictitious trains characterized by limit values specified in Annex E, or slightly outside those limits ($D = 16$ m, $D = 28.5$ m, the spacing of axles within a bogie $d_{BA} = 1.5$, and $d_{BA} = 5.4$), to assess which properties most contribute to larger responses in a set of single-span railway bridges. They proposed a methodology to identify the most critical bridges, in terms of length and first natural frequency, to reduce the number of bridges that must be investigated with the introduction in the network of new and more aggressive trains, and concluded that, from all train parameters ranges stipulated by Annex E, only a few are critical for

the bridge response, mainly the distance d_{BA}, for which a small variation in its value may strongly affect the resonance phenomena.

Although the lack of coverage of the HSLM regarding new trains is already being studied by the scientific community, the studies related to the two remaining questions are still scarce in literature. Museros et al. [21] assessed the effects caused by articulated trains that fulfil the validity limits of the HSLM stipulated by the Annex E. They concluded that the limitation that defines the ratio between the coach length D over the axle spacing within a bogie d_{BA} should be close to an integer value is not important, while only very few cases of articulated trains defined within the premises of Annex E would lead to an exceedance in the vertical acceleration limits. However, the limits of validity regarding conventional or regular trains were outside the scope of this work and, since only articulated trains were studied, no conclusions regarding the lack of information about the d_{BS} distance were drawn.

While some attention is given in the present work to the issues raised in the first aforementioned question, by systematically checking how the HSLM covers, or not, the effects caused by trains defined within a wider parameter interval than that defined in the norm [9], the main focus and novelty of this article are more concentrated on answering the other two questions. Regarding the second one, the effects caused by a vast set of randomly generated train load models with properties within the limits specified in Annex E, both articulated, conventional and regular, are compared with those caused by the HSLM. Such comparison is performed both in terms of analytical signature envelopes of both sets, as well as with a complete numerical dynamic analysis carried out in a specific case study bridge to explicitly compute its maximum acceleration response and compare it with the HSLM acceleration envelopes. To increase the computational efficiency, an optimized method to perform moving load dynamic analyses is also proposed in this regard. Moreover, the lack of definition regarding some geometrical parameters in Annex E raised in the third question, especially the distance d_{BS} in conventional trains, is also addressed in this work to analyse how this issue may affect the validity of the HSLM.

It is therefore clear that the answers to the second and third questions raised above remain barely explored in the literature, which represents a gap of knowledge in this particular field. Hence, the findings obtained from this study aim to contribute to the identification of the main limitations of the current load models used to design high-speed railway bridges, as well as to open new research paths to improve these models, particularly by proposing a simplified methodology that can expedite dynamic calculations on different sets of wavelengths. The article is structured in five sections, in which the methodology to compare the HSLM effects with those caused by the theoretical trains randomly generated through the procedure stipulated in Annex E is presented in Sect. 2, while the numerical models used in this work are described in Sect. 3. Section 4 is dedicated to the results obtained in the preliminary analysis performed with the train signature technique and in the complete dynamic analysis carried out with the case study bridge. Finally, in Sect. 5, the main conclusions from this work are summarized and recommendations for future work are proposed.

2 Methods for dynamic assessment

The present section goes over the methodologies employed in this study, starting with an overview of the concept of train signatures and proceeding to introduce a procedure used for speeding up the process of dynamic analysis. At the end, an explanation of the numerical work can be found.

2.1 Train signatures

The decomposition of excitation at resonance (DER) method was introduced in Ref. [10] and applies to simple spans, under the following conditions:

- Inertial interaction is ignored.
- Only the first vibration mode is considered.
- The response is decomposed into a Fourier series, retaining only the resonance term.
- The results are independent of time.

Using this method, the maximum mid-span acceleration $\ddot{y}$ can be given as a product of a constant factor C_t, a function for the influence line $A(\cdot)$ and the train spectrum $G(\cdot)$:

$$\ddot{y} \leq C_t A\left(\frac{L}{\lambda}\right) G(\lambda). \tag{1}$$

For a bridge with a first frequency f_0, generalized stiffness K, span L and linear mass m, the constant factor is given by

$$C_t = \frac{8\pi f_0^2}{K} = \frac{4}{mL\pi}. \tag{2}$$

Given the excitation wavelength λ, the influence line function is taken as

$$A\left(\frac{L}{\lambda}\right) = \left| \frac{\cos\left(\frac{\pi L}{\lambda}\right)}{\left(\frac{2L}{\lambda}\right)^2 - 1} \right|. \tag{3}$$

Regarding the train, with N loads P_k at coordinates x_k at position k, on a bridge with damping ratio ξ, its spectrum is given by

$$G(\lambda) \cong \underset{i=1,\, N-1}{\mathrm{MAX}} \frac{1}{\xi x_i} \left[\sqrt{\left(\sum_{k=0}^{i} P_k \cos\left(\frac{2\pi x_k}{\lambda}\right) \right)^2 + \left(\sum_{k=0}^{i} P_k \sin\left(\frac{2\pi x_k}{\lambda}\right) \right)^2} \left(1 - \mathrm{e}^{-2\pi\xi \frac{x_i}{\lambda}}\right) \right]. \tag{4}$$

The DER method is sensitive to some of its errors, namely due to:

- High wavelengths and short trains influence on the resonance criteria.
- Values of zero of the influence line.
- Overestimation of the response for high damping coefficients.

Nonetheless, the method can also be used to approximate the maximum mid-span displacement y, given the first angular frequency ω_0 and the static displacement given by the train loads y_{stat}, as

$$y \cong y_{\mathrm{stat}} + \frac{\ddot{y}_{\max}}{\omega_0^2}. \tag{5}$$

One major aspect of the application of this methodology is that it introduces the concept of train signature. Since the train spectrum does not allow a separate assessment of the train effect from the bridge response, given its dependence on the damping coefficient, the train signature $S_0(\lambda)$ is the result of

$$S_0(\lambda) = \lim_{\xi \to 0} G(\lambda), \tag{6}$$

and as such

$$S_0(\lambda) = \underset{i=1,\, N-1}{\mathrm{MAX}} \frac{1}{\xi x_i} \left[\sqrt{\left(\sum_{k=0}^{i} P_k \cos\left(\frac{2\pi x_k}{\lambda}\right) \right)^2 + \left(\sum_{k=0}^{i} P_k \sin\left(\frac{2\pi x_k}{\lambda}\right) \right)^2} \right]. \tag{7}$$

These signatures allow for fast comparisons between the different train effects. Knowing the signatures of the trains in operation on a given line, a new train can be deemed as either apt or inapt for running on that line, by simply comparing the new vehicle signature to the previous ones.

2.2 Single load linear superposition (SLSS)

The fulfilment of the present study objectives is dependent on the ability to perform several thousand dynamic analyses in varying scenarios. Whether considering the random variation of a train geometrical configuration or the randomness of bridge characteristics, there are advantages in simplifying the dynamic analysis process. In the scope of this work, the metric being evaluated in ballasted bridges is the vertical deck acceleration, and therefore dynamic analyses with moving loads are sufficient. In this approach, different train models are described as a series of individual axle loads and the distances between them—e.g. how the HSLM is represented. Generally, the first step in such an analysis is to determine the individual nodal loads, for each axle load and rail node. Instead, the proposed procedure (SLLS) considers the dynamic effects caused by a single moving load, of an arbitrary positive value P, travelling at the desired speed v. The resulting response (such as an acceleration or displacement time-history) is then scaled to the corresponding axle load and added to the total response, with a time offset related to the speed and the distance between axles.

As an example, a simple load model is considered, comprising four axle loads of 147.15 kN each, with a regular spacing of 3 m, running at a speed of 200 km/h. The overall effect is evaluated on the mid-span displacement of a 12 m simply supported bridge. Figure 1a depicts the displacement caused by a single load, while Fig. 1b illustrates the same response, multiplied and offset. The dashed line in Fig. 1c represents the sum of these effects and the bold line is the response of a separate calculation, on which the entire load model was set to run over the bridge model. The dotted line illustrates the difference between the two approaches, and its maximum absolute value is 3.6312×10^{-6} m.

The main advantage of implementing this approach is time reduction since the number of necessary time steps can be greatly reduced (the total running length corresponds only to the bridge model length, instead of the sum of the

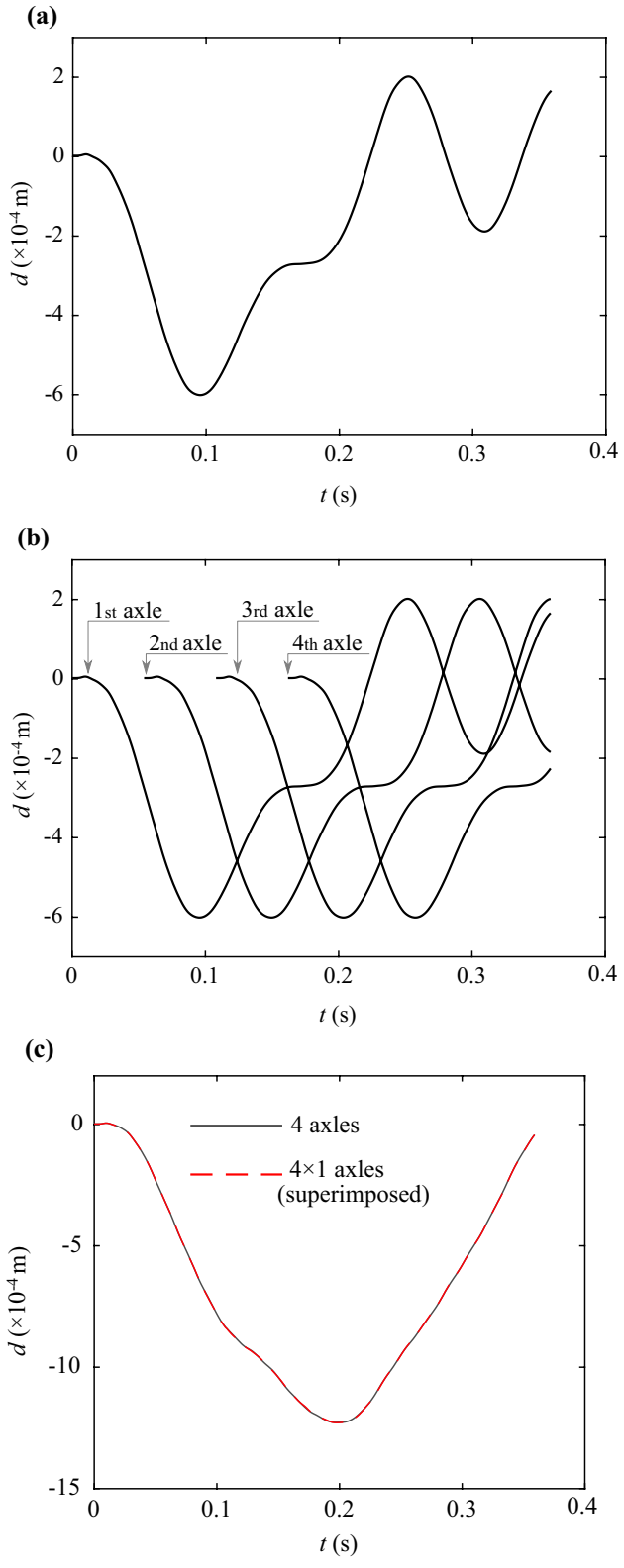

Fig. 1 Mid-span displacement of a single load and combined effect: **a** single load; **b** four axles; **c** combined response

bridge and train lengths). Also, by calculating the isolated response of an axle load, any load model response can be replicated by scaling and superimposing the known effects. The offset in the combination of actions can reproduce different axle spacings and the scaling can even be adjusted to different values in the same load model, e.g. where the loads of the power car are superior. Furthermore, if after the calculation of the effects for several load models on a bridge a new load model is required to be taken into consideration, there is no need for additional dynamic analysis, since the dynamic equations only have to be accessed once per speed value in order to save the single axle response.

The limitations of this methodology have to do with the moving load analysis, limiting its applicability to scenarios where there are no nonlinear aspects, such as wheel–rail contact. This leaves out train-bridge interaction analysis and the evaluation of criteria related to contact forces or car body acceleration. For the scope of the present work, this means that the discussed superposition method is applicable to the assessment of deck acceleration on ballasted tracks.

An example application is presented in Fig. 2, for the HSLM-A1 train. A single load $P = 170$ kN moves at a speed $v = 200$ km/h causing the mid-span displacement seen in Fig. 2a. On a commercially available 4-core computer, this operation took 149.751 s to complete, and the SLLS response, presented in Fig. 2b, was computed in 0.121 s. In comparison, the full load model of the HSLM-A1 that produces the response seen in the same figure took 34 min to be calculated.

2.3 Methodology application

The methodology proposed in this section addresses the questions listed in Sect. 1, having the goal of evaluating the HSLM-A coverage of trains made possible by Annex E of the EN 1991-2 and also of other trains whose properties fall outside those limits, to account for possible future vehicles. This methodology consists firstly in creating two sets of randomly generated load model configurations—"set *A*" abiding by the EN 1991-2 limits and "set *B*" employing wider limits—for each of the three train types, as detailed in Sect. 3.2 (sets A_a and B_a for articulated trains, A_c and B_c for conventional trains and A_r and B_r for regular trains). Afterwards, the dynamic signatures of all randomly generated trains and HSLM-A trains can be calculated, using Eq. (7). Then, to validate the conclusions, the dynamic response of all random trains is obtained for an example bridge. Since the SLLS approach is being used, only one dynamic analysis needs to be carried out since all different moving loads results can be derived from the single load

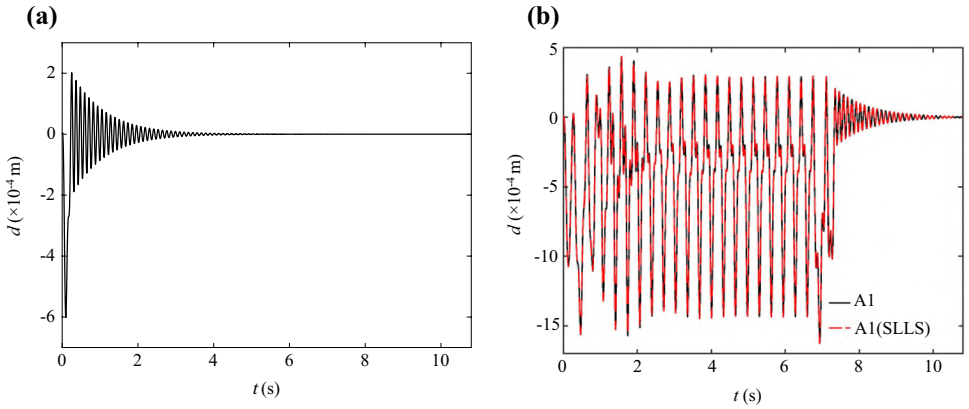

Fig. 2 Mid-span displacement of a single load and combined effect of HSLM-A1: **a** single load; **b** HSLM-A1

response. The same procedure is done for the 10 HSLM-A trains, thus allowing for a comparison to be established, using the maximum vertical deck acceleration as a metric. In this work, the selected example is the Canelas bridge (presented in Sect. 3.1), the sample size for the randomly generated sets is 100,000, the variable distribution is uniform and the speed range is from 140 to 420 km/h, with 10 km/h intervals (assuming a maximum line speed of 350 km/h, the EN 1991-2 defines the maximum design speed as 1.2 times that value, which gives $1.2 \times 350 = 420$). The samples for the random variables (D, d_{BA} d_{BS}, e_C, D_{IC} and D_L) are generated using a random number suited for uniform distributions, scaled to the limits detailed in Sect. 3.2.

A representative diagram of this methodology is presented in Fig. 3. The single load dynamic response is computed with a custom-built moving loads analysis application using [22].

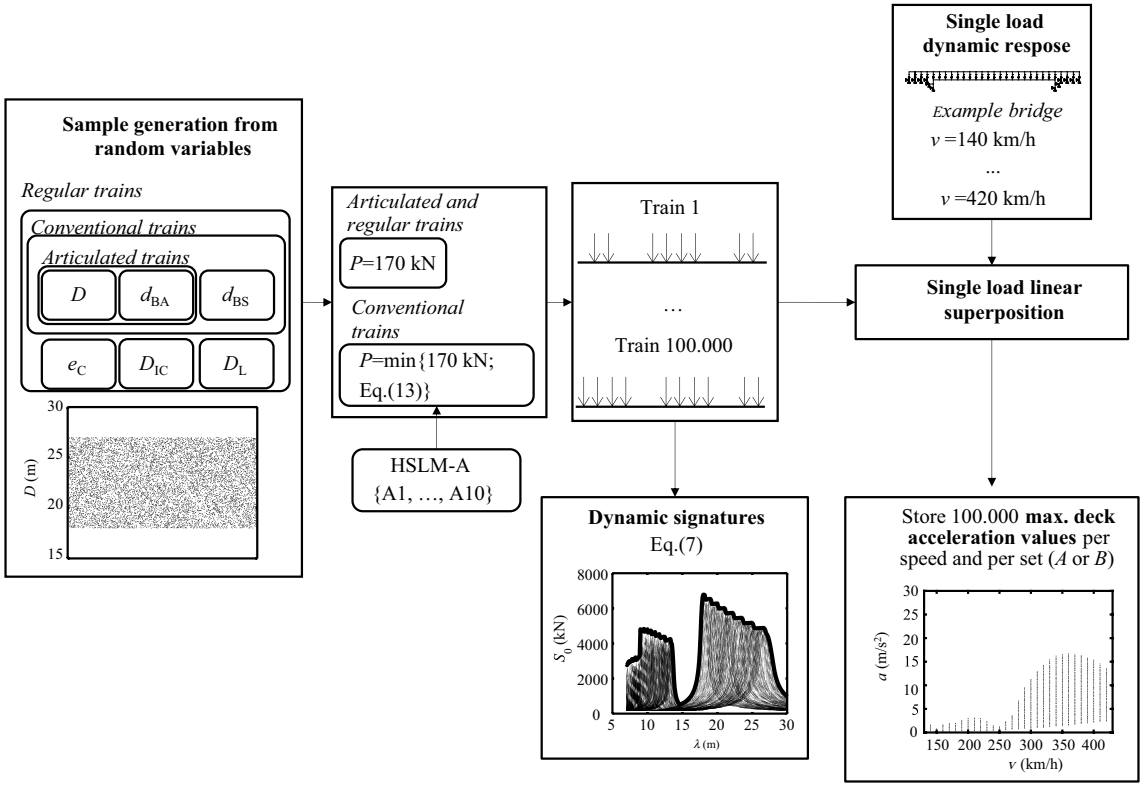

Fig. 3 Overview of the methodology to assess the HSLM limits of validity

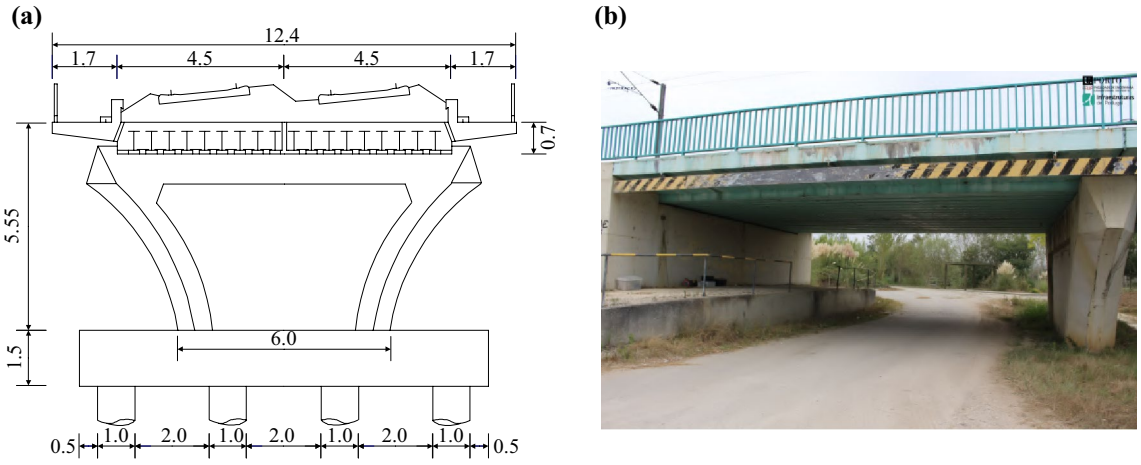

Fig. 4 Canelas bridge (unit: m): **a** cross section (adapted from [24]); **b** view of the first span

Table 1 Material and geometrical properties of the finite element model

Property name	Symbol	Value	Unit
Reinforced concrete density	γ_C	2.5	t/m^3
Concrete elasticity modulus	E_C	36.1	GPa
Slab thickness	t_{slab}	0.7	m
Slab width	b_{slab}	4.475	m
Area of the steel profiles	A_s	0.01975	m^2
Structural damping	ξ	2%	-
Ballast density	γ_b	1.8	t/m^3
Ballast elasticity modulus	E_b	120	MPa
Ballast height	h_b	450	mm
Load distribution angle	α	25	°
Sleeper mass	m_s	272.5	kg
Rail pad stiffness	k_p	350	kN/mm
Track shear stiffness	k_l	2×10^4	kN/m/m
Neoprene shear modulus	G_n	0.975	MPa
Steel elasticity modulus	E_S	210	GPa
Permanent loads	m_p	1.4	ton/m
Width of the sleeper underside	l_b	0.3	m
Half sleeper effective support	l_e	0.95	m
Sleeper spacing	l_s	0.6	m

3 Numerical modelling

3.1 Case study railway bridge

An existing bridge was selected as a case study. The Canelas bridge (Fig. 4) (built in 1996 on the Portuguese Railway Network's Northern Line) was chosen, given the already available information, regarding both experimental [23, 24] and numerical studies [25]. This filler beam structure comprises 6 simply supported 12 m spans, each formed by 2 independent decks constituted of concrete slabs directly cast on 9 embedded rolled steel profiles (HEB500). Each deck carries a ballasted track with UIC60 rails and is supported by a set of neoprene bearings.

To evaluate vertical deck acceleration, a 2D model of a single deck has been developed using [26] Parametric Design language, which allows the employment of several element types, specifically:

- COMBIN14: spring-dashpot elements, used in the track (for shear stiffness and for the separate representation of the ballast and rail pads stiffness) and in the bearing supports (in the vertical and horizontal directions, accounting for their flexibility).
- MASS21: mass point elements, used for the localized mass of the sleepers.
- BEAM3: beam elements, used to represent the rails and the deck.

The material and geometrical properties used in the model are listed in Table 1. In the model, the structural damping value is used to set Rayleigh factors (using the frequencies of the first and second vertical vibration modes) and the vertical stiffness of the ballast layer K_b is calculated in order to incorporate load distribution effects as proposed by [27]

$$K_{\mathrm{b}} = \begin{cases} K_{\mathrm{b}} = \dfrac{2(l_{\mathrm{e}} - l_{\mathrm{b}})\tan\alpha}{\ln\left[\left(\dfrac{l_{\mathrm{e}}}{l_{\mathrm{b}}}\right)(l_{\mathrm{b}} + 2h_{\mathrm{b}}\tan\alpha)/(l_{\mathrm{e}} + 2h_{\mathrm{b}}\tan\alpha)\right]} & \text{if } h_{\mathrm{b}}\tan\alpha \le \dfrac{l_{\mathrm{s}}}{2} \\ K_{\mathrm{b}} = \dfrac{K_{\mathrm{b1}}K_{\mathrm{b2}}}{K_{\mathrm{b1}} + K_{\mathrm{b2}}} & \text{if } h_{\mathrm{b}}\tan\alpha > \dfrac{l_{\mathrm{s}}}{2} \end{cases}, \tag{8}$$

where

$$K_{\mathrm{b1}} = \frac{2(l_{\mathrm{e}} - l_{\mathrm{b}})\tan\alpha}{\ln\left[(l_{\mathrm{e}}l_{\mathrm{s}})/(l_{\mathrm{b}}(l_{\mathrm{e}} + l_{\mathrm{s}} - l_{\mathrm{b}}))\right]}E_{\mathrm{b}}, \tag{9}$$

and

$$K_{\mathrm{b2}} = \frac{l_{\mathrm{s}}(l_{\mathrm{s}} - l_{\mathrm{b}} + 2l_{\mathrm{e}} + 2h_{\mathrm{b}}\tan\alpha)\tan\alpha}{l_{\mathrm{b}} - l_{\mathrm{s}} + 2h_{\mathrm{b}}\tan\alpha}E_{\mathrm{b}}. \tag{10}$$

Furthermore, the effect of load degradation underneath the sleepers was found to have a negligible effect on the global response of the deck. The stiffness of the spring elements representing the supports in both the vertical $K_{\mathrm{s,v}}$ and horizontal $K_{\mathrm{s,h}}$ directions includes all nine bearings (each comprised of two neoprene layers of 0.25 m × 0.15 m × 0.004 m and four neoprene layers of 0.25 m × 0.15 m × 0.008 m) on each end of the deck, and it was calculated according to [28, 29],

$$K_{\mathrm{s,v}} = \frac{n_{\mathrm{b}}}{\sum_{i=1}^{n_{\mathrm{l}}} \dfrac{t_i^3}{3G_{\mathrm{n}}a^3bf_1f_2}}, \tag{11}$$

$$K_{\mathrm{s,h}} = \frac{n_{\mathrm{b}}abG_{\mathrm{n}}}{\sum_{i=1}^{n_{\mathrm{l}}} t_i}, \tag{12}$$

where n_{b} is the number of bearings, n_{l} is the number of neoprene layers in each bearing, t_i is each of the layer thickness, a is the smaller dimension (0.15 m), b is the largest dimension (0.25 m), f_1 is a form factor dependent on a and b, and f_2 is a factor for dynamic loading, which depends on G_{n}.

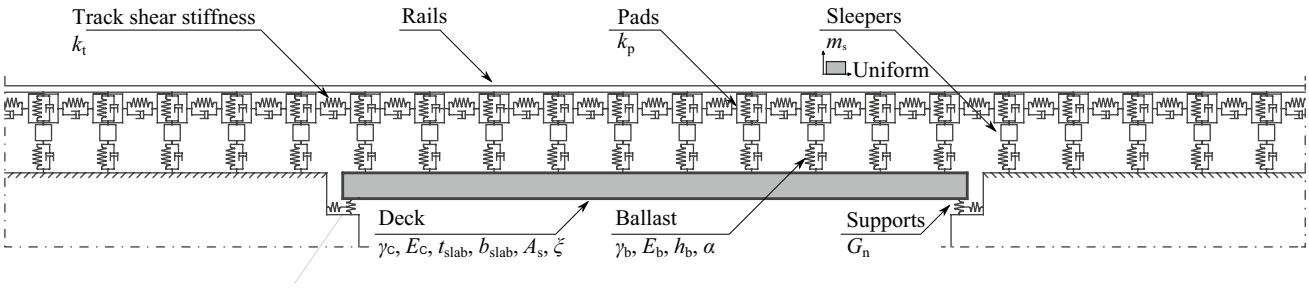

Fig. 5 Schematic representation of the filler beam bridge finite elements models and their random variables

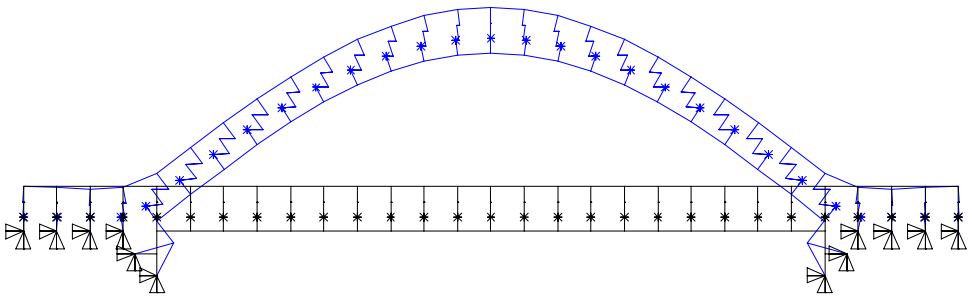

Fig. 6 Finite element model of the Canelas bridge (with the deformed shape of the first vertical bending mode)

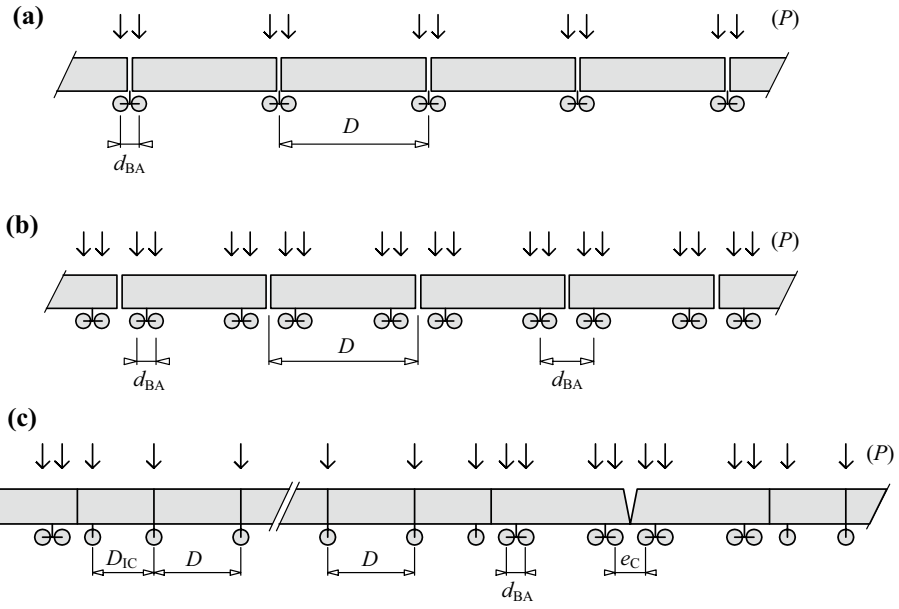

Fig. 7 Train type configurations (adapted from [9]): **a** articulated train; **b** conventional train; **c** regular train

Table 2 Random variables—articulated trains

Variable	Set A_a		Set B_a	
	Minimum (m)	Maximum (m)	Minimum (m)	Maximum (m)
D	18	27	15	30
d_{BA}	2.5	3.5	2	4

Table 3 Random variables—conventional trains

Variable	Set A_c		Set B_c	
	Minimum (m)	Maximum (m)	Minimum (m)	Maximum (m)
D	18	27	15	30
d_{BA}	2.5	3.5	2	4
d_{BS}	5.5	8.5	5.5	8.5

Figure 5 shows a schematic representation of the finite element model, which is shown in Fig. 6, alongside the deformed shape of the first vertical bending mode, corresponding to an eigenfrequency of 8.60 Hz (which is in the proximity of the 8.70 Hz experimentally assessed by Ref. [23]) In the figure, it can be seen that two additional track segments of 2.3 m were added on both sides of the deck. These extensions serve the purpose of providing a transition space where the moving loads can begin crossing the deck without being subjected to an abrupt change in track stiffness.

Table 4 Random variables—regular trains

Variable	Set A_r		Set B_r	
	Minimum (m)	Maximum (m)	Minimum (m)	Maximum (m)
D	10	14	8	16
d_{BA}	2.5	3.5	2	4
D_{IC}	8	11	6	13
e_C	7	10	5	12
d_{BS}	5.5	8.5	5.5	8.5
D_L	15.5	18.5	15.5	18.5

3.2 Load model configuration

Annex E of the EN 1991-2 lists the HSLM-A's limits of validity, concerning articulated, conventional and regular trains. Figure 7 illustrates the three types of trains, where:

- P is the individual axle load;
- D is the coach length or distance between regularly repeating axles;
- d_{BA} is the distance between axles of the same bogie;
- d_{BS} is the distance between the centres of adjacent vehicle bogies;
- D_{IC} is the intermediate coach length (regular trains);
- e_c is the distance between consecutive axles on the coupling of two trainsets (regular trains).

P is limited to 170 kN or, for conventional trains, the lesser of 170 kN and the value that comes from Eq. (13), where

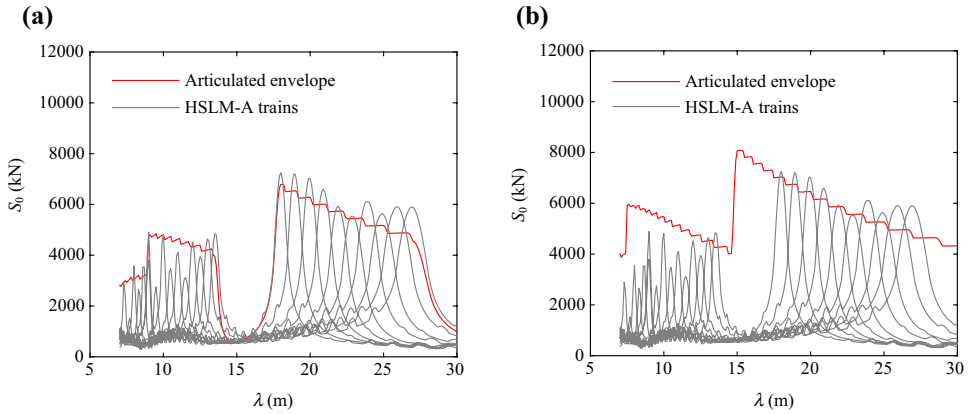

Fig. 8 Dynamic signatures of articulated trains: **a** set A_a; **b** set B_a

P_{HSLMA}, d_{HSLMA} and D_{HSLMA} are the corresponding properties of the Universal Trains. This can be a single Universal Train if D matches an existing D_{HSLMA} or two Universal trains otherwise, selecting the two whose D_{HSLMA} values are just greater and just lesser than D. D should be between 18 and 27 m for articulated and conventional trains or between 10 and 14 m for regular trains, while D_{BA} lies between 2.5 and 3.5 m.

While the norm lacks in providing limits for d_{BS}, it states that D/d_{BA} and $\left(d_{BS} - d_{BA}/d_{BA}\right)$ should not approach integer values and that d_{BS} must be in accordance with Eq. (13). D_{IC} must be between 8 and 11 m and e_C between 7 and 10 m. In addition, there are also limits for total train weight (10000 kN), length (400 m) and unsprung axle mass (2 tonnes).

$$4P\cos\left(\frac{\pi d_{BS}}{D}\right)\cos\left(\frac{\pi d_{BA}}{D}\right) \leq 2P_{HSLMA}\cos\left(\frac{\pi d_{HSLMA}}{D_{HSLMA}}\right). \quad (13)$$

For articulated trains, the sets of random variables are listed in Table 2, where set A_a contains the variables as defined in the norm and set B_a has the wider limits, intended to represent the influence of future (and existing) trains that do not necessarily respect the norm limits. The point load value P is set to its maximum allowed of 170 kN, since the highest value corresponds to the maximum acceleration registered.

The variables for conventional trains are presented in Table 3. As previously discussed, there are no set limits for variable d_{BS}, and for that reason, its values on set A_c (which stem from the real trains of types A, D and F on [7]) remain unaltered on set B_c. Since the maximum allowed value of P for conventional trains is the lesser of 170 kN and the value resulting from Eq. (13), all randomly generated samples must undergo that check.

Regarding regular trains, the random variables are itemized in Table 4. An additional variable D_L is here defined to represent the length of the first and last coaches of each trainset. Its limits are the same in both set A_r and set B_r due to the same reason considered for variable d_{BS} (which for regular trains represents the distance between the centremost bogies of the first and last coache and the closest axle of the intermediate coach). In both sets, P has a value of 170 kN.

4 Results discussion

Following the methodology described in Sect. 2.3, the obtained results are here presented—firstly concerning the dynamic signatures (calculated directly from the sampled distances), followed by the response of the case study bridge. For each type of train, the influence of the individual variables is evaluated by assessing selected samples from set B.

4.1 Preliminary analysis based on train signatures

Given that the case study bridge is a simply supported span, in order to study the HSLM-A the dynamic signatures that follow are presented for wavelengths starting at 7 m, as per the EN 1991-2. Figure 8 represents the envelope of articulated trains' signatures, for both sets, as the line in red. Each of the 10 light grey lines represents one of the HSLM-A universal trains. It can be seen that the load model provides good coverage of the complying articulated trains, particularly above wavelengths of 6 m, while the sampled set B_a yields higher spectra.

For conventional trains, the dynamic signatures represented in Fig. 9 also show a better coverage for set A_c than for set B_c. It appears to be, however, a lack of coverage in wavelengths up to 12 m, even for set A_c. This finding motivates

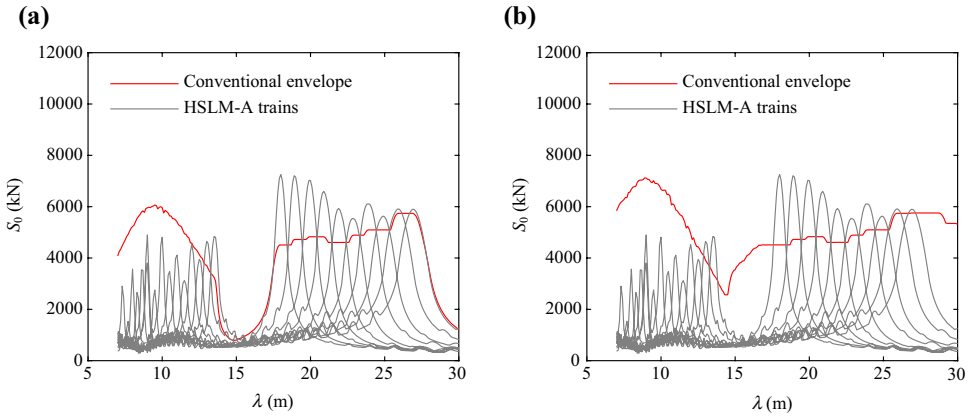

Fig. 9 Dynamic signatures of conventional trains: **a** set A_c; **b** set B_c

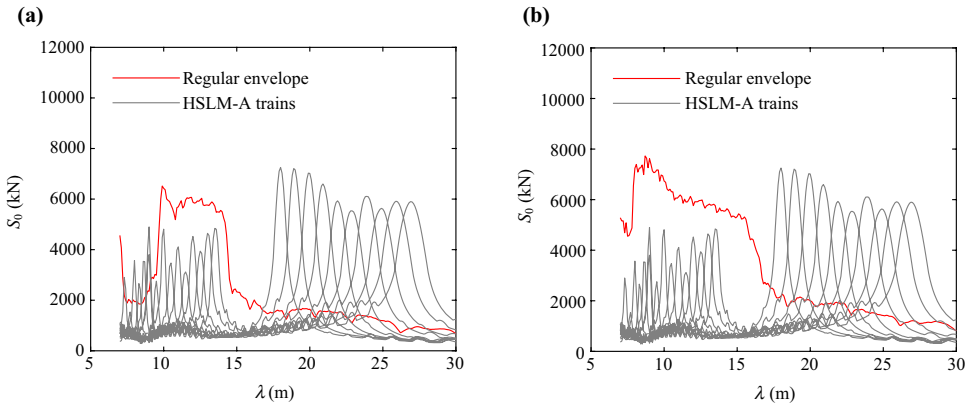

Fig. 10 Dynamic signatures of regular trains: **a** set A_r; **b** set $\mathbf{B}_r$

looking into the dynamic analyses to understand whether or not this is due to the influence of any of the variables.

As for regular trains, in Fig. 10, the shown dynamic signatures lead to a similar conclusion regarding the difference between sets A_r and B_r, particularly in the fact that even in set A_r lower wavelengths (up to 17 m) can lead to results above the HSLM-A's. On the other hand, the larger difference to the HSLM-A dynamic signatures in the 17–30 m range is noted, in comparison to the previously discussed articulated and conventional train types.

4.2 Numerical analysis

The following results represent the entirety of stochastic dynamic analyses performed on the case study bridges, with the same randomly generated train configurations that constitute sets A and B for the 3 types of trains. The goal is to validate the conclusions obtained from the signature analysis regarding the HSLM coverage and to better understand which variables contribute the most to the presence of extreme values. The present section reflects a total of 17.4 dynamic million analyses, i.e. the product of the sample size (100.000), number of speed values (29) and number of sets of random variables (6 sets: A_a, B_a, A_c, B_c, A_r, B_r).

4.2.1 Articulated trains

The results from the dynamic analyses regarding articulated trains are represented in Fig. 11, for both sets, where each dot represents the maximum vertical deck acceleration calculated for each sampled train. The line in full, which remains unaltered in both sets, is the envelope of the 10 HSLM-A universal train responses, as per the graph in Fig. 3. Observing the results, it can be seen that the sample set generated within the norm's limits is adequately covered by the HSLM, apart from a few outliers (which is in accordance with the findings by Museros et al. [21]). As expected, the resulting values from set B_a are not covered by the load model, especially in higher velocities. This finding is unfavourable towards the first question listed in Sect. 1, although it is stated that this matter is not the main focus of the present study.

To better understand the independent influence of each variable, Figs. 12 and 13 present selections of results from set B_a, alternately highlighting a variable's influence when

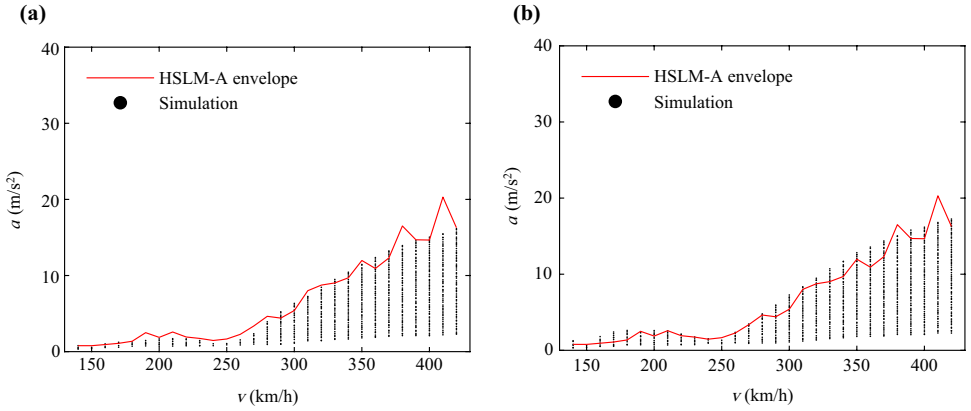

Fig. 11 Dynamic response of articulated trains: **a** set A_a; **b** set B_a

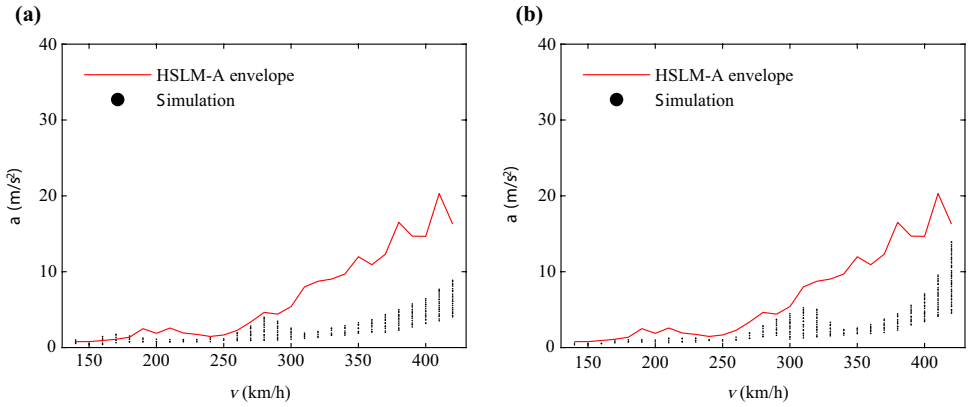

Fig. 12 Articulated trains—selected results from set B_a highlighting variable D: **a** 15 m ≤ D ≤ 18 m, 2.5 m ≤ d_{BA} ≤ 3.5 m, **b** 27 m ≤ D ≤ 30 m; 2.5 m ≤ d_{BA} ≤ 3.5 m

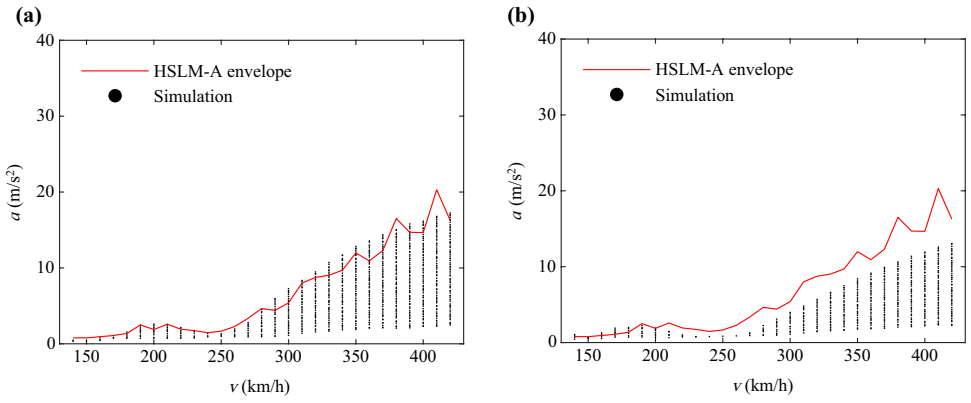

Fig. 13 Articulated trains—selected results from set B_a highlighting variable d_{BA}. **a** 18 m ≤ D ≤ 27 m, 2 m ≤ d_{BA} ≤ 2.5 m; **b** 18 m ≤ D ≤ 27 m, 3.5 m ≤ d_{BA} ≤ 4 m

it is taken above or below the stated limits of validity while selecting the complying values for the other variables. From Fig. 12, it can be seen that there is a similar contribution from simulated trains whose coach length is inferior to the limit and due to those that are above it.

As for the distance between axles (Fig. 13), while its lower values lead to higher results, its consequences are not as notorious. In fact, as D decreases, resonant effects become more noticeable in the bridge taken as the example in this study.

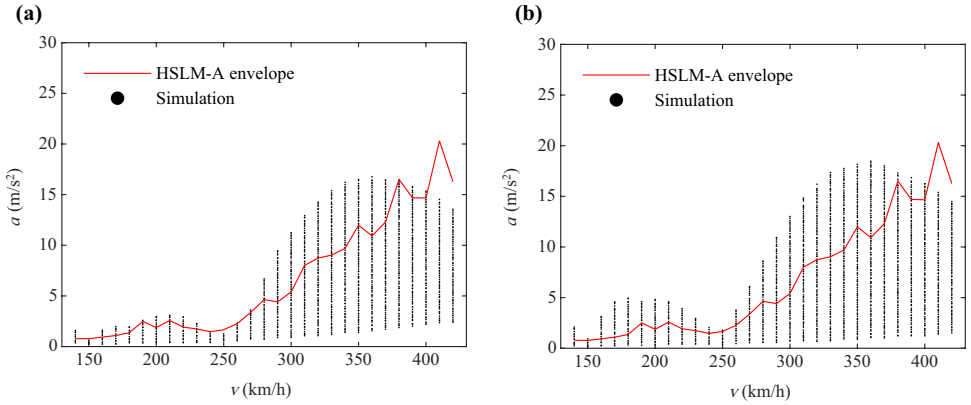

Fig. 14 Dynamic response of conventional trains: **a** set A_c; **b** set B_c

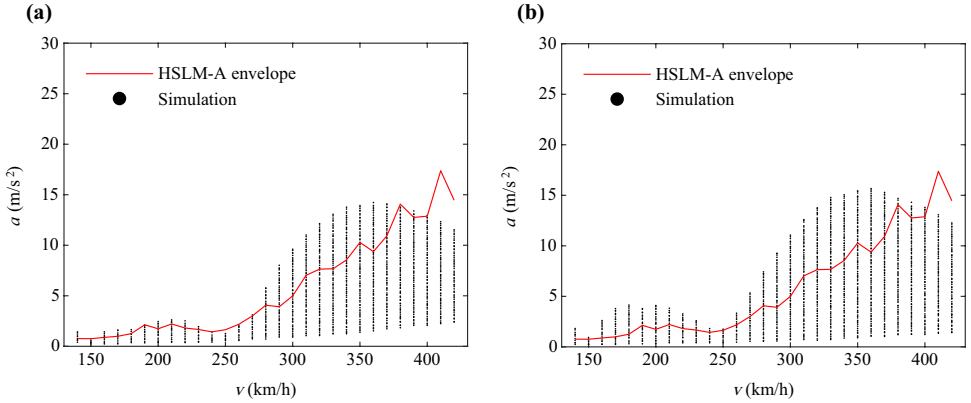

Fig. 15 Dynamic response of conventional trains (with additional damping): **a** set A_c; **b** set B_c

4.2.2 Conventional trains

The results of the dynamic analyses with conventional trains are shown in Fig. 14. In it, it is noted that even set A_c, which is in accordance with the normative limits, hosts load model configurations that cause dynamic effects greater than those produced by the HSLM-A universal trains. The lack of coverage discussed with the dynamic signatures is once more present in a corresponding range of wavelengths. In fact, considering that the frequency of the first vertical bending mode for the bridge is 8.60 Hz, the wavelength range corresponding to the 280 to 370 km/h speed range is 9.04 to 11.95 m.

Sets A_c and B_c were selected to infer the effects of including additional damping in the dynamic analyses. For that, a new single load was generated from the FE model of the Canelas bridge, considering a total structural damping ξ_{total} of

$$\xi_{total} = \xi + \Delta\xi = 2\% + \frac{0.0187L - 0.00064L^2}{1 - 0.0441L - 0.0044L^2 + 0.000255L^3}\% = 2\% + 0.476\% = 2.476\%. \quad (14)$$

The results of the dynamic analyses, as well as the HSLM envelopes generated with additional damping, are shown in Fig. 15. Both the simulations distribution and the envelopes present themselves as scaled-down versions of the responses without additional damping of Fig. 14. The relation between the randomly generated train load models and the HSLM is maintained, and the issue raised before (i.e. load configurations in set A_c that surpass the HSLM-A envelope) is still observable.

As before, it can be seen that the exceedingly higher values on the highest speeds correspond to the lowest values of D (Fig. 16). On the other hand, it is the higher values of d_{BA} that result in lower acceleration peaks (Fig. 17). In fact, the only scenario where the outlying values between 280 and 370 km/h tend to disappear is the scenario considering d_{BA} values above the allowed limit. To better understand this phenomenon, Fig. 18 shows the distribution of variable d_{BS} from simulations whose dynamic response is superior to that of the HSLM, for two example speed values within the 280–370 km/h range. It is visible that the outlying simulated trains correspond to increasingly higher values

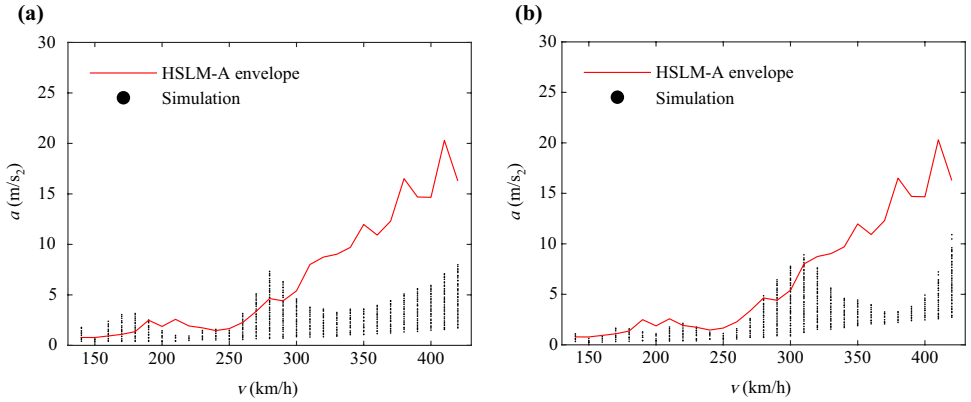

Fig. 16 Conventional trains—selected results from set B_c highlighting variable D: **a** 15 m ≤ D ≤ 18 m, 2.5 m ≤ d_{BA} ≤ 3.5 m; **b** 27 m ≤ D ≤ 30 m, 2.5 m ≤ d_{BA} ≤ 3.5 m

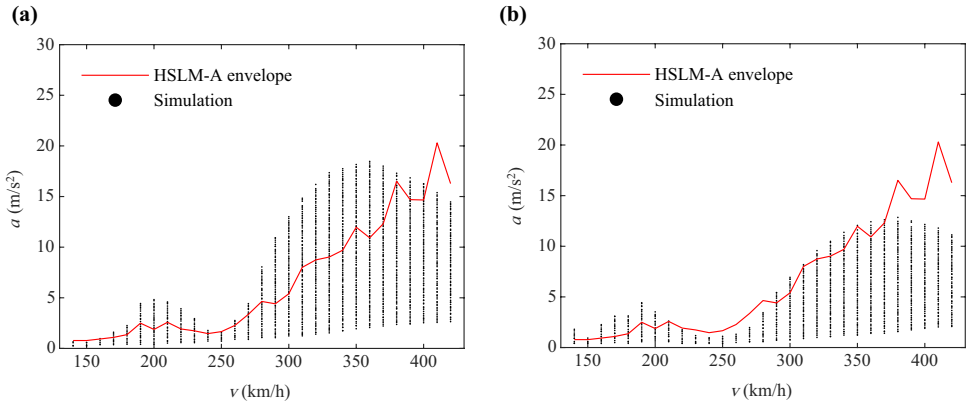

Fig. 17 Conventional trains—selected results from set B_c highlighting variable d_{BA}: **a** 18 m ≤ D ≤ 27 m, 2 m ≤ d_{BA} ≤ 2.5 m; **b** 18 m ≤ D ≤ 27 m, 3.5 m ≤ d_{BA} ≤ 4 m

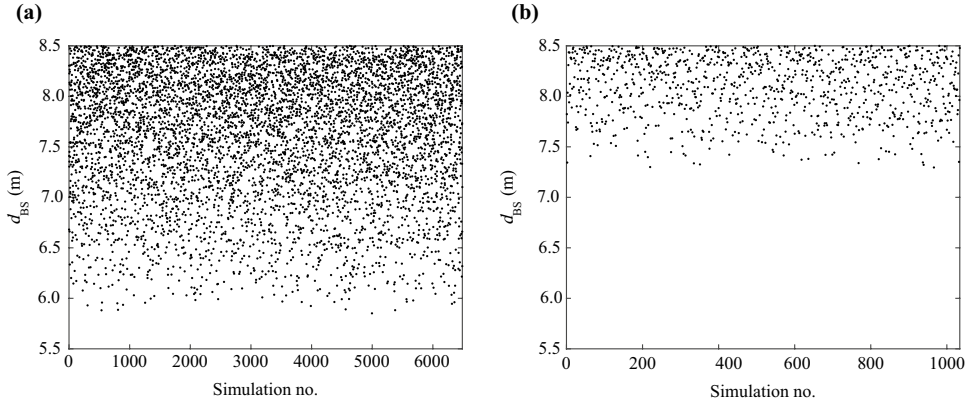

Fig. 18 Dynamic response of conventional trains—distribution of variable d_{BS} on simulations above the HSLM envelope, from set B_c: **a** 300 km/h; **b** 350 km/h

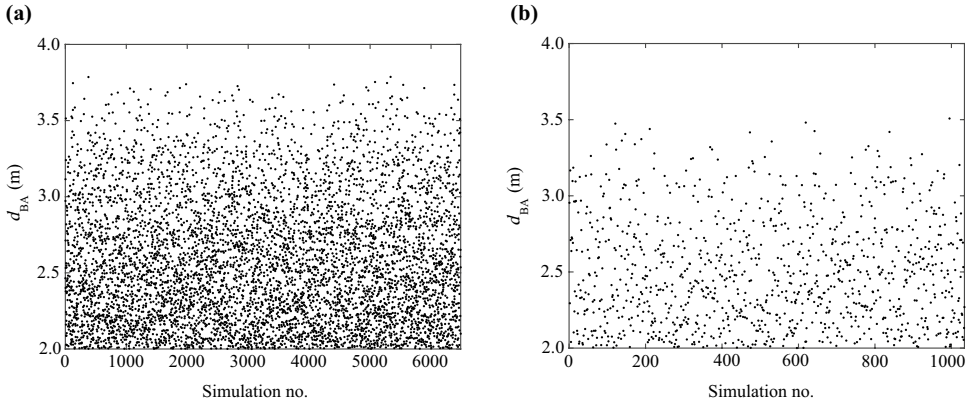

Fig. 19 Dynamic response of conventional trains—distribution of variable d_{BA} on simulations above the HSLM envelope, from set B_c: **a** 300 km/h; **b** 350 km/h

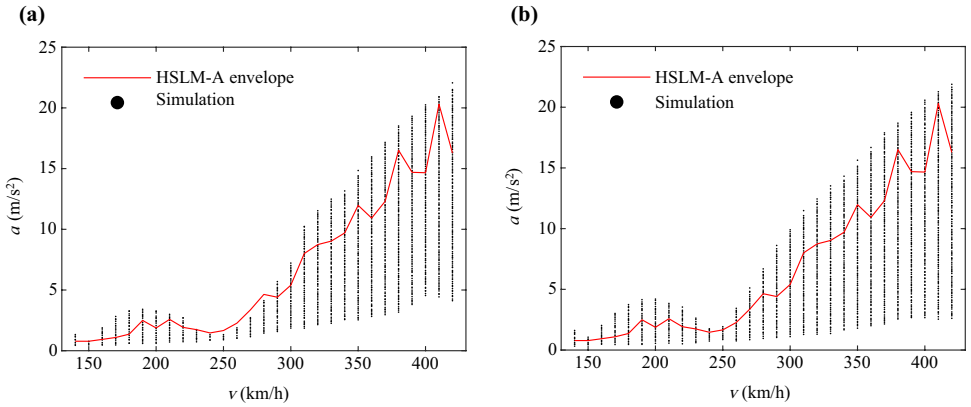

Fig. 20 Dynamic response of regular trains: **a** set A_r; **b** set B_r

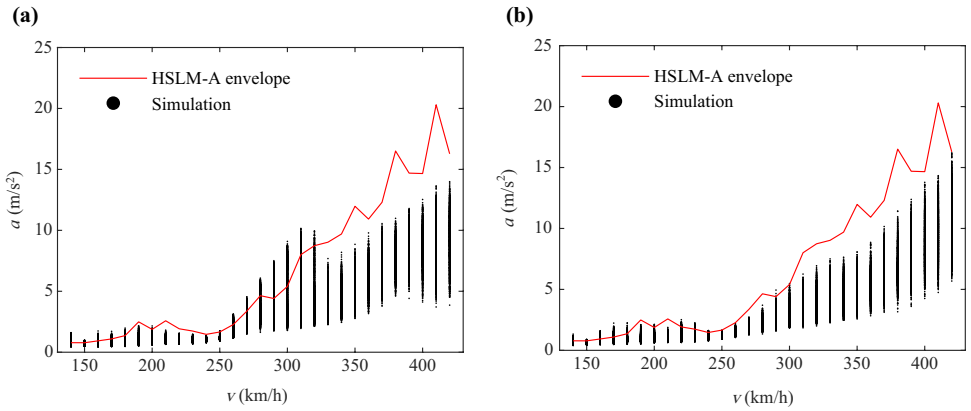

Fig. 21 Regular trains—selected results from set B_r highlighting variable D: **a** 8 m ≤ D ≤ 10 m, 2.5 m ≤ d_{BA} ≤ 3.5 m, 8 m ≤ D_{IC} ≤ 11 m, 7 m ≤ e_C ≤ 10 m; **b** 14 m ≤ D ≤ 16 m, 2.5 m ≤ d_{BA} ≤ 3.5 m, 8 m ≤ D_{IC} ≤ 11 m,7 m ≤ e_C ≤ 10 m

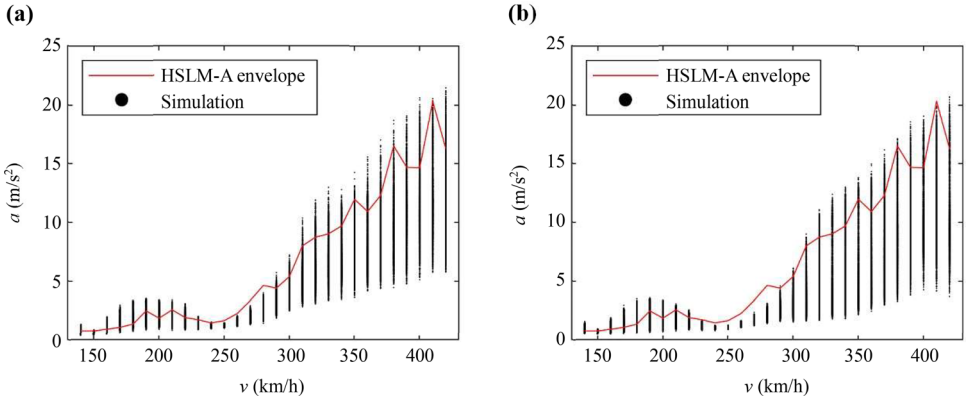

Fig. 22 Regular trains—selected results from set B_r highlighting variable d_{BA}: **a** 10 m ≤ D ≤ 14 m, 2 m ≤ d_{BA} ≤ 2.5 m, 8 m ≤ D_{IC} ≤ 11 m, 7 m ≤ e_C ≤ 10 m; **b** 10 m ≤ D ≤ 14 m, 3.5 m ≤ d_{BA} ≤ 4 m, 8 m ≤ D_{IC} ≤ 11 m, 7 m ≤ e_C ≤ 10 m

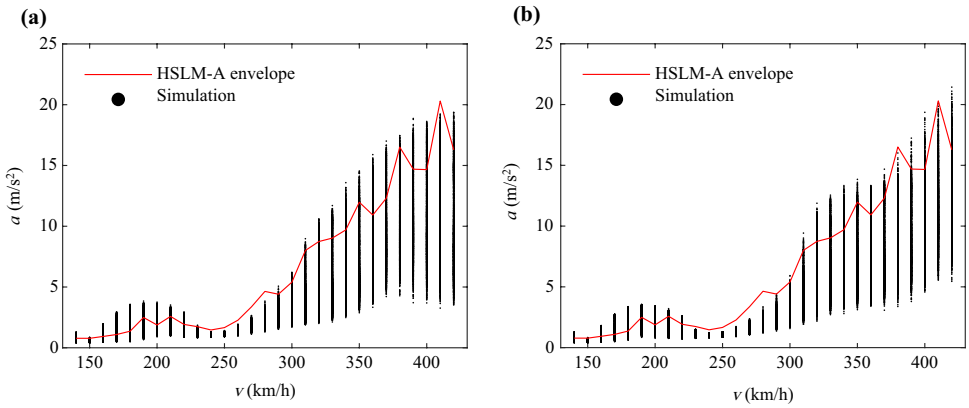

Fig. 23 Regular trains—selected results from B_r highlighting variable D_{IC}: **a** 10 m ≤ D ≤ 14 m, 2.5 m ≤ d_{BA} ≤ 3.5 m, 6 m ≤ D_{IC} ≤ 8 m, 7 m ≤ e_C ≤ 10 m; **b** 10 m ≤ D ≤ 14 m, 2.5 m ≤ d_{BA} ≤ 3.5 m, 11 m ≤ D_{IC} ≤ 13 m, 7 m ≤ e_C ≤ 10 m

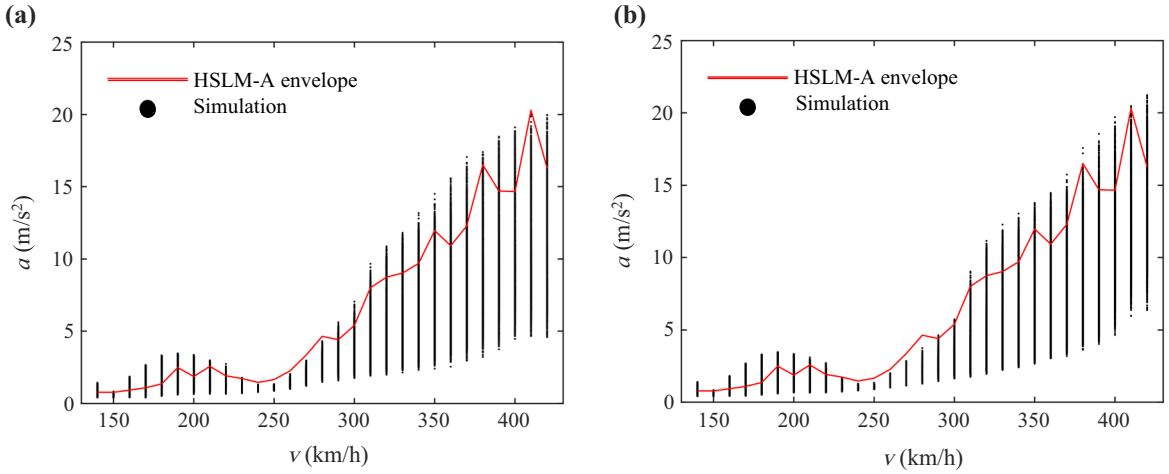

Fig. 24 Regular trains—selected results from set B_r highlighting variable e_C: **a** 10 m ≤ D ≤ 14 m, 2.5 m ≤ d_{BA} ≤ 3.5 m, 8 m ≤ D_{IC} ≤ 11 m, 5 m ≤ e_C ≤ 7 m; **b** 10 m ≤ D ≤ 14 m, 2.5 m ≤ d_{BA} ≤ 3.5 m, 8 m ≤ D_{IC} ≤ 11 m, 10 m ≤ e_C ≤ 12 m

of this variable. This observation underlines the pertinence of the third question listed in Sect. 1 since the Eurocode could be clearer in defining limits for this distance. When looking at the distribution of variable d_{BA} from the same samples (illustrated in Fig. 19), a concentration on lower values appears. Therefore, it can be concluded that the most aggressive scenarios correspond to higher d_{BS} and lower d_{BA}. Indeed, as d_{BS} increases (approaching D), the regularity of the moving loads grows, contributing to dynamic effects. As for d_{BA}, as it decreases, the effect of the pair of moving loads approaches that of a single double-load.

4.2.3 Regular trains

The dynamic responses of sets A_r and B_r for regular trains are presented in Fig. 20. While both sets contain train load configurations that result in acceleration values above the HSLM-A's, set A_r distributions tend to follow the trend of the envelope more closely throughout the entire speed range. From the individual variable influence, in this case there is some variability caused by D (Fig. 21), while variable d_{BA} (Fig. 22) is the less influential. The same can be observed for the D_{IC} (Fig. 23) and e_C (Fig. 24) variables, although it should be highlighted that the former only controls four load distances and the latter a single one.

5 Conclusion

The conclusions of this study are summarized according to the questions listed in Sect. 1 as follows:

1. With the extended limits considered in this study, it can be said that the HSLM-A is partially suited to represent some future trains, given the similarity in the results for both sets A and B on speeds up to 400 km/h (of the selected example bridge), or wavelengths excluding the 15–17 m range. Nevertheless, this should not be thought of as a lack of the load model readiness but more of as an indicator of the need for future-proofing.
2. The 10 HSLM-A universal trains do not cover the dynamic effects of some theoretical train load models that can be constructed abiding by the EN 1991-2 limits of validity. This happens in some limit cases of articulated trains, but it is most prevalent in conventional and regular trains, although it should be noted that the last two train types are lacking in the definition of some variables. In conventional trains, there is a relation between the non-complying trains and the increasing distance between centres of adjacent vehicle's bogies—as this variable increases, the effect of consecutive bogies acts progressively more as individual loads and less as pairs, which in turn leads to higher vertical acceleration levels, due to the contribution that the loads repetition has to resonant effects.
3. The definition of variable d_{BS} in the norm is insufficient and this constitutes an obstacle to the evaluation of the HSLM's limits of validity, which is made more apparent when this variable's importance is noted. There is also a challenge in defining the two distances, not mentioned in the norm, necessary to characterize regular trains.

It is therefore understood that there is some margin for improvement in Annex E of the EN 1991-2, not only by providing better definitions of some distances but also by adjusting the HSLM-A's universal trains. In this regard, future work should focus on parametric studies for the definition of the proposed load models, including equivalent train–track–bridge interaction models with replication of the HSLM's effects. The methodology applied in this work to assess the dynamic response of the case study bridge and the efficiency of the HSLM in covering the effects of different trains can be utilized and replicated for a number of different high-speed railway bridges. The present study draws the conclusion that there are issues with the current load model from the analysis of a case study filler beam bridge, and therefore, a future publication should include integral portal frames, composite concrete-steel structures and metallic truss bridges, in different spans lengths. In addition, the probability of trains crossing on a bridge and the effects of such phenomenon are also considered for future work.

Acknowledgements This work was financially supported by the Portuguese Foundation for Science and Technology (FCT) through the PhD scholarship PD/BD/143007/2018. The authors would like also to acknowledge the financial support of the projects IN2TRACK2—Research into enhanced track and switch and crossing system 2 and IN2TRACK3—Research into optimised and future railway infrastructure funded by European funds through the H2020 (SHIFT2RAIL Innovation Programme) and of the Base Funding—UIDB/04708/2020 of the CONSTRUCT—Instituto de I &D em Estruturas e Construções—funded by national funds through the FCT/MCTES (PIDDAC).

References

1. Zhang N, Zhou Z, Wu Z (2022) Safety evaluation of a vehicle-bridge interaction system using the pseudo-excitation method. Railw Eng Sci 30(1):41–56
2. Gong W, Zhu ZY, Liu R et al (2020) Running safety assessment of a train traversing a three-tower cable-stayed bridge under spatially varying ground motion. Railw Eng Sci 28(2):184–198
3. Montenegro PA, Carvalho H, Ribeiro D et al (2021) Assessment of train running safety on bridges: a literature review. Eng Struct 241:112425
4. Commité European de Normalisation (2005) Eurocode 0—Basis of structural design—Annex A2: applications for bridges (normative). Brussels
5. Zacher M, Baeßler M (2008) Dynamic behaviour of ballast on railway bridges. In: Dynamics of high-speed railway bridges. CRC Press, London
6. European Rail Research Institute (1999) Rail bridges for speeds > 200 km/h: Confirmation of values against experimental data, ERRI D 214/RP 8. Utrecht
7. European Rail Research Institute (1999) Rail bridges for speeds > 200 km/h: Final report, ERRI D 214/RP 9. Utrecht
8. European Commission (2014) Commission Regulation (EU) No 1299/2014 of 18 November 2014 on the technical specifications for interoperability relating to the 'infrastructure' subsystem of the rail system in the European Union Text with EEA relevance. http://data.europa.eu/eli/reg/2014/1299/oj/eng
9. Commité European de Normalisation (2003) Eurocode 1—part 2: Actions on structures—traffic load on bridges. Brussels
10. European Rail Research Institute (1999) Rail bridges for speeds > 200 km/h: Calculations for bridges with simply supported beams during the passage of a train ERRI D 214/RP 6. Utrecht
11. Vestroni F, Vidoli S (2007) Closed-form solutions for the structural response to train loads. J Sound Vib 303(3):691–706
12. Matsuoka K, Collina A, Somaschini C et al (2019) Influence of local deck vibrations on the evaluation of the maximum acceleration of a steel-concrete composite bridge for a high-speed railway. Eng Struct 200:109736
13. Auersch L (2021) Resonances of railway bridges analysed in frequency domain by the modal-force-excitation, bridge-transfer and axle-sequence spectra. Eng Struct 249:113282
14. Marvillet D, Tartary JP (2003) Bridges, high speed and dynamic calculation - short version. In: IABSE Symposium: Structures for High-Speed Railway Transportation, Antwerp, pp 80–81
15. Bernhard G, Josef F (2021) A redesigned approach to the additional damping method in the dynamic analysis of simply supported railway bridges. Eng Struct 241:112415
16. Reiterer M, Firus A, Vorwagner A et al (2021) Railway bridge dynamics: Development of a new high-speed train load model for dynamic analyses of train crossing. In: IABSE Congress Ghent 2021—Structural Engineering for Future Societal Needs, Ghent, pp 1633–1642
17. Andersson A, Allahvirdizadeh R, Albright A et al (2021) Report No. D5.6–Performed high-speed low-cost bridges I2T3 demonstrators. H2020-Sift2Rail-In2Track3 project: Research into optimised and future railway infrastructure (S2R-CFM-IP3-01-2020 Innovation Action). Tunnel and Bridge I2T2 Report-High speed low cost bridges-D5.2.5. Porto, Stockholm and Valencia
18. Reiterer M, Kohl AM, Vorwagner A et al (2022) Development of a new high-speed load model and validation on existing railway bridges. In: The 5th International Conference on Railway Technology: Research, Development and Maintenance, Montpellier
19. Vorwagner A, Kwapisz M, Flesch R et al (2021) FEM based approach for development of a new high-speed load model for railway bridges. In: IABSE Congress, Ghent 2021—Structural Engineering for Future Societal Needs, Ghent, pp 1614–1622
20. Harald U, Schörghofer DA, Taras A (2017) Critical bridges in high-speed railway lines: systematic identification for specific trains. In: 8th European Conference on Steel and Composite Structures (Eurosteel 2017), Copenhagen, pp 1427–1436
21. Museros P, Andersson A, Martí V et al (2021) Dynamic behaviour of bridges under critical articulated trains: signature and bogie factor applied to the review of some regulations included in EN 1991–2. Proc Instit Mech Eng Part F J Rail Rap Transit 235(5):655–675
22. MATLAB ® (2018) version 9.4.0.813654 (R2018a). The Mathworks, Inc., Natick
23. Bonifácio C, Ribeiro D, Calçada R et al (2014) Calibration and validation of the numerical model of a short-span railway bridge based on dynamic tests. In: Proceedings of the 9th International Conference on Structural Dynamics, Porto, pp 1315–1321
24. Pimentel R, Barbosa C, Costa N et al (2007) Characterization of railway traffic and its effects on a short span bridge by sing a hybrid fibre optic/electrical measurement system. In: Third European Workshop on Optical Fibre Sensors, Naples, pp 66193Y. International Society for Optics and Photonics
25. Rocha JM, Abel HA, Rui C (2016) Probabilistic assessment of the train running safety on a short-span high-speed railway bridge. Struct Infrastruct Eng 12(1):78–92
26. ANSYS®, (2018) Release 19.2. ANSYS Inc., Canonsburg, Pennsylvania
27. Zhai W, Wang K, Lin J (2004) Modelling and experiment of railway ballast vibrations. J Sound Vib 270(4):673–683
28. Manterola J (2006) Puentes: apuntes para su diseño, cálculo y construcción. Colegio de Ingenieros de Caminos, Canales y Puertos.
29. Rocha J (2015) Probabilistic methodologies for the safety assessment of short span railway bridges for high-speed traffic. Dissertation, Faculdade de Engenharia da Universidade do Porto

B

APPENDIX B: ARTICLE FROM PROBLEM 2

The work by Ferreira et al. (2025), on which Chapter 4 is based, is reproduced in this appendix.

G. Ferreira, Montenegro P., C. Adam, A. A. Henriques, and R. Calçada (2025). "Evaluation of the Eurocode's Safety Factor for Deck Acceleration Limit on Ballasted Track Railway Bridges." In: Submitted for publication

Evaluation of the Safety Factor in the Eurocode for Deck Acceleration Limit on Ballasted Railway Bridges

Gonçalo Ferreira[a], Pedro Montenegro[a], Christoph Adam[b], António Abel Henriques[c], Rui Calçada[a]

[a] *CONSTRUCT-iRAIL - Faculty of Engineering, University of Porto, Rua Dr. Roberto Frias, 4200-465, Porto, Portugal*
[b] *Universität Innsbruck, Unit of Applied Mechanics, Technikerstr. 13, 6020 Innsbruck, Austria*
[c] *CONSTRUCT-LABEST - Faculty of Engineering, University of Porto, Rua Dr. Roberto Frias, 4200-465, Porto, Portugal*

Abstract

Ballasted railway bridges are subject to dynamic excitation from passing trains, which can cause excessive vibrations in the ballast bed depending on the train speed, resulting in track instability. The Eurocode EN 1990 uses vertical deck acceleration as an indicator of safety, limited it to 3.5 m/s^2 for ballasted bridges. Since experimental studies show that ballast instability occurs at about 7.0 m/s^2, the normative limit seems to be arbitrarily based on a safety factor of 2.0. The present paper examines the suitability of a lower safety factor. The proposed methodology compares the physical acceleration limit with the design acceleration calculated at a critical speed corresponding to a failure probability of 10^{-4}. An algorithm for the efficient assessment of critical speeds based on subset simulation is introduced, together with a parametric study for its optimization. A sensitivity analysis of the random variables of ballasted bridges allows the definition of two design scenarios in accordance with the Eurocode EN 1991-2. Results from the application of the methodology to four case study bridges show that design accelerations greater than the limit defined in the Eurocode can be found in ballasted bridges within the target probability of failure, suggesting that the safety factor can be set lower than 2.0.

Keywords: Ballasted railway bridge, Eurocode, Deck acceleration, Safety factor, Subset simulation

1. Introduction

Railway bridges are subject to the dynamic effects of passing trains. In addition to the static loading, the repetitive cadence of the axle loads can induce a resonant response. When the dynamic actions cause excessive deck accelerations in ballasted track bridges, the ballast layer may lose stability. Excessive vibrations can compromise the interlocking capability of the ballast particles, leading to a loss of resistance in the load path from the rails, rail pads, sleepers, and ballast bed. Such issues require track maintenance, which can mean an interruption of train service, with a significant impact on rail operations. Ultimately, an unmaintained ballast track can be the cause of derailment. Section A.2 in Annex A of the Eurocode EN 1990 [1] uses vertical deck acceleration as an indicator, limited to 3.5 m/s^s in ballasted track bridges.

Concerns with the occurrence of instability in the ballast layer began with special test runs by the SNCF, noting issues corresponding to deck accelerations of 0.7 to 0.8 g [2]. A limit was then defined after tests commissioned by the European Rail Research Institute to validate the ENV European pre-standard. These tests were carried out at the German Federal Institute for Materials Research and Training and showed ballast instability at accelerations of 0.7 g. The fact that the Eurocode limit is close to 0.35 g indicates that a safety factor of 2 was applied. However, the reason for adopting this factor appears to be arbitrary, as noted by Zacher and Baeßler [3] when replicating the same experiments. The same authors propose the adoption of limits resulting from the consideration of a safety factor of 1.3. In a recent technical note, the European Union Agency for Railways (ERA) [4] lists the revision of acceleration limits as one of the research areas to be addressed in order to close the open points on the Technical Specification for Interoperability [5].

The importance of the ballast layer towards the overall bridge stiffness is addressed by Heiland et al. [6] after noticing differences between experimental and numerical assessment of natural frequencies. Using a small-scale test rig, the researchers found no significant changes in bending frequencies related to varying ballast stiffness. Given the inherent uncertainty in modeling characteristics, Stollwitzer et al. [7] developed a large-scale, 1:1 rig to investigate ballast stiffness. The findings regarding track stability indicate that momentary excessive vibration levels have almost no effect on ballast instability. Although isolated events may be harmless, their cumulative effect may be relevant. This issue is addressed by Menezes [8], which considers

the accumulated damage in a manner analogous to fatigue analysis, allowing an assessment of lifespan status with respect to lateral track stability. Mitigating the overall effects of acceleration is also a topic of study. A practical solution to control the amount of ballast bed vibration is the use of ballast mats, which have also been tested on bridges [9].

However, the study of a safety factor can involve a significant computational cost associated with performing multiple dynamic analyses on finite element models. Considering the random nature of some of the parameters, the analysis of railway bridges with uncertainty becomes a reliability assessment problem. In recent years, researchers have been working on techniques to solve these problems in a computationally efficient manner. Mao et al. [10] have employed the Probability Density Estimation Method (PDEM) as an alternative to the Monte Carlo method to determine vibrations in train-bridge interaction models. The authors found the random nature of the train load and the elasticity modulus of the concrete to be the most influential. The same method is used by Xu et al. [11] for assessing wind effects and by Xin et al. [12], who demonstrate with 3D interaction analysis that results with a sample size of 195 for the PDEM are similar to 3,000 or 5,000 Monte Carlo samples. In the same study, an approach to sensitivity analysis of input parameters is presented, with the authors concluding that the combination of different parameters controls sensitivity more than the individual effect of each parameter. Another method, the Response Surface Model (RSM), is utilized by Park and Towashiraporn [13] for risk assessment of railway bridges subjected to seismic actions.

One motive for the increase in the number of train-bridge simulations is probabilistic safety assessment, where it is necessary to compute very low probabilities of failure. Rocha et al. [14] evaluated the wheel unloading coefficient as a safety indicator, using the generalized Pareto distribution in conjunction with the Monte Carlo method. Concerning target probabilities in the order of 10^{-4} (a target from the Joint Commitee on Structural Safety (JCSS) [15]), the authors were able to estimate probabilities with a sample size of 20,000. Allahvirdizadeh et al. [16] present another approach to calculating the probability of exceedance of a limit state, employing the First-Order Reliability Method, which is suitable for problems that can be described analytically. A semi-probabilistic method comparable to FORM is devised by Grigoriou and Brühwiler [17], using data from a monitoring campaign. Salcher et al. [18] address the uncertainty of damping, temperature and of the material and geometric properties through line sampling and Latin

hypercube sampling. Later, Hirzinger et al. [19] add subset simulation and asymptotic sampling as alternative methods. To assess probabilities of failure in the order of 10^{-3} (considering a serviceability limit state), the authors find an equivalence between a Monte Carlo simulation and line sampling with a sample size two orders of magnitude smaller. To account for the effects of random rail irregularities, Salcher and Adam [20] compare a fitted analytical response on a small number of Monte Carlo trials to subset simulation. Another study on the probabilities of exceedance of bridge acceleration, by Hirzinger et al. [21], considers the speed range as another source of variability. The authors measure probabilities of failure using several metrics, including a weighted probability of failure.

Given the discrepancy between the normative limit and the experimentally assessed acceleration limit, the following research questions are posed:

- How can critical train speeds associated with low probabilities of failure be evaluated in a timely manner?
- How to set up scenarios to calculate the acceleration in the design phase?
- Can the safety factor (i.e., the ratio of the physical acceleration limit to the permissible value) be less than 2.0?

To address these issues, the present article proposes definitions for a safety factor, design scenarios, and critical speed in Section 2, followed by the introduction of an algorithm for their efficient assessment in Section 3. Four case study bridges are presented in Section 4. A parametric study to optimize the critical speed algorithm is given in Section 5, allowing the calculation of critical speeds in Section 6. In the same Section, after a sensitivity analysis of the random variables, two design scenarios are proposed, and the final safety factors are calculated. The main conclusions are listed in Section 7.

2. Methodology

This section describes the procedure for calculating safety factors for existing bridges and provides the necessary definitions. It is divided into three steps, which are outlined in Fig. 1 and developed in the following subsections. The first step (Section 2.1) is to determine the speed at which a load model causes an excessive deck acceleration. This first step involves probabilistic

analysis using bridge models constructed with random variables. After finding the critical speed (v_{crit}), the second step (Section 2.2) is to determine the acceleration value that can be calculated with fixed values for the variables (instead of probabilistic analysis). The instructions for setting the variables to perform a deterministic analysis are referred to as the design scenarios. Employing such scenarios is beneficial to ensure that trustworthy results are attainable in the engineering practice of bridge design with simple analyses. The third step (Section 2.3) is to locate in the design scenarios the acceleration value at the critical speed, here called "design acceleration" (a_{Ed}). The margin between this value and the physical limit of 7.0 m/s^2 (a_{Rl}) indicates the distance to safety. Therefore, the safety factor (γ_{bt}) can finally be estimated by dividing 7 by the design acceleration.

2.1. Step 1: Find the critical speed

This study of ballasted track bridges assesses failure due to track instability (loss of stability of the ballast layer), assuming that the 7.0 m/s^2 value for vertical deck acceleration is a physical value that acts as the safety threshold. Therefore, a failure event is considered to have occurred if a bridge deck experiences a vertical acceleration a greater than this limit (a_{Rl}) when subjected to any load model, at any given train speed. It is also assumed that the loss of stability can ultimately lead to derailment, and that this risk corresponds to Class 3 consequences as defined in the Probabilistic Model Code of the JCSS [15]. The authors consider that the relative cost of safety measures (extensive measurements through safety inspections over significant periods of time) is large. In the Probabilistic Model Code, this combination of consequence and cost corresponds to a target reliability index β of 3.7, which corresponds to probabilities of failure in the order of magnitude of 10^{-4}. The probability of failure p_f is therefore defined as:

$$p_f = P\left(a \geq a_{Rl}\right) \tag{1}$$

When testing a load model, different train speeds result in different maximum values of vertical deck acceleration. For this study, a critical speed is defined, for a given load model, as the lowest speed that causes the following condition:

$$p_f \geq 10^{-4} \tag{2}$$

The High-Speed Load Model (HSLM-A) [22], whose purpose is to represent the envelope of actions of real high-speed rolling stock traffic, is employed

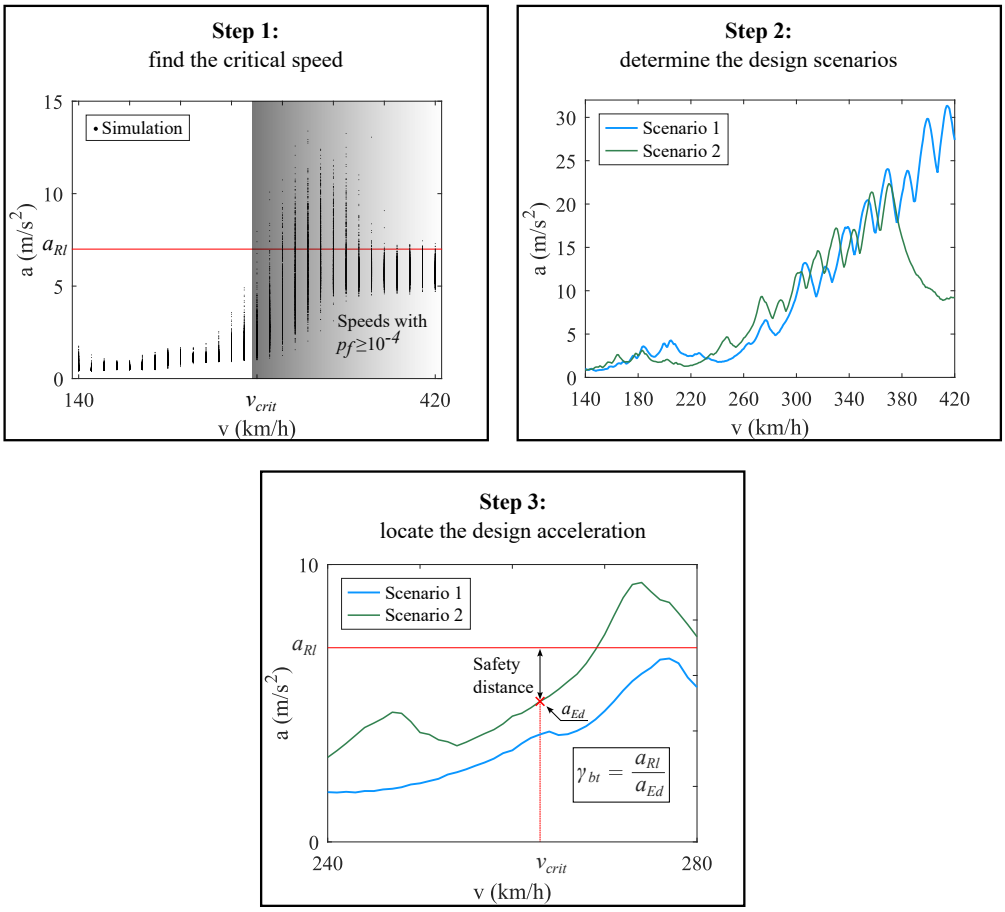

Figure 1: Overview of the methodology for estimation of safety factors for the deck acceleration criterion.

in this work. This load model, which is used for the design of high-speed railway bridges, is given as a set of 10 configurations of axle loads and spacings and is intended for moving load analysis. For a given bridge, critical speeds can be calculated for each of the 10 HSLM-A. These individual critical speeds $v_{crit,i}$ form a set. The minimum value of the set gives the critical speed v_{crit} of the bridge:

$$v_{crit} = \min\left(\{v_{crit,i}\}_{i=1}^{10}\right) \tag{3}$$

2.2. Step 2: Determine the design scenarios

The scenarios for bridge design are defined in this study as sets of deterministic values attributed to structural and track variables utilized to calculate the dynamic response of railway bridges. Two sets are defined, in accordance with the provisions of Eurocode EN 1991-2 [22], which requires a lower bound estimate of stiffness and structural damping and both upper and lower bound estimates of mass. This procedure is meant to maximize the acceleration response and to avoid overestimating the resonant speed. In spite of this statement being present in the Eurocode, the standard does not specify which variables are to be considered in the estimates, nor what constitutes upper or lower bounds. Since the current study utilizes either normal or uniform distributions, the bounds are proposed as follows:

Normal distributions: For variables with distribution $N(\mu, \sigma^2)$, adopt as bounds $\mu \pm 1.64\sigma$, corresponding to the 5% and 95% percentiles.

Uniform distributions: For uniformly distributed random variables $U(a, b)$, adopt the respective minima and maxima.

Regarding the selection of random variables to be included in the definition of scenarios, it should be noted that, depending on the complexity of the models employed, stiffness, damping, and mass can be related to more than one variable and even share variables. Therefore, it is necessary to perform a parametric study of the relative influence of each variable. The proposed methodology for such a study starts with setting all variables to their mean value and calculating the resulting deck acceleration envelope considering the 10 HSLM-A. The response vector is $\mathbf{X}$ for a given speed range with k speed values. Then, each variable is independently set to its upper or lower bound, resulting in a new response vector $\mathbf{Y}$ with the same length k. To evaluate the influence of each variable, the variance of the absolute difference between

the vectors is calculated as:

$$\mathrm{Var}\left(|\mathbf{X}-\mathbf{Y}|\right)=\frac{\sum_{i=1}^{k}\left(|\mathbf{X}_i-\mathbf{Y}_i|-\mathrm{E}\left(|\mathbf{X}_i-\mathbf{Y}_i|\right)\right)}{n-1} \tag{4}$$

Consequently, the most influential variables are included in the definition of the two design scenarios. Both scenarios use a lower bound on the variables that control stiffness and damping. The first scenario (S1) uses a lower bound estimate of mass, while the second (S2) uses an upper bound. The variables that are not considered influential enough after the parametric study are taken at their mean values. This step of the methodology concludes with the calculation of the response envelope of both scenarios under the effect of the 10 HSLM-A configurations.

2.3. Step 3: Locate the design acceleration

At this point, the maximum speed that can be considered safe is already known. The remaining question is how far away the design scenarios are from the actual failure events. The value on the envelope of the design scenarios at v_{crit} is here given the name of design acceleration a_{Ed}. The safety factor, henceforth referred to as γ_{bt}, is defined in this work as the ratio between the physical value a_{Rl} and the acceleration calculated in the design phase a_{Ed} and is given by:

$$\gamma_{bt}=\frac{a_{Rl}}{a_{Ed}}=\frac{7}{a_{Ed}} \tag{5}$$

3. Subset simulation application for the estimation of critical speed

3.1. Application basics

Monte Carlo simulation, while a highly reliable approach, implies an escalation in computational cost as the intended target probabilities of failure get lower. In fact, according to Bjerager [23], the appropriate sample size N to assess a probability of 10^{-4} would be:

$$\frac{1}{p_f}\leq N\leq\frac{10}{p_f}\Leftrightarrow 10,000\leq N\leq 100,000 \tag{6}$$

For moving loads analyses (as is the case in the present study) and less complex 2D finite element models, such a number would be feasible. However, any change in the train speed or load requires a new analysis, and therefore,

the search for critical speed can quickly grow to several hundred thousand (or millions) of dynamic analyses.

Therefore, subset simulation (introduced by Au and Beck [24]) is chosen to estimate the probabilities of failure. With this method, p_f is estimated as the conditional probability of reaching the unsafe region in a reliability problem through successive increments of intermediate failure events. The same authors calculate p_f as:

$$p_f = P(F_i) \prod_{i=1}^{m-1} P(F_{i+1}|F_i) \tag{7}$$

where F_i are m number of intermediate events (or levels) such that $F_1 \supset F_2 \supset \ldots F_m$. For the first level, $P(F_1)$ is estimated with a crude Monte Carlo simulation, provided a reasonable N. The resulting acceleration values are ordered from highest (belonging to F_1) to lowest (farthest from F_1), as illustrated in Fig. 2a. Given a selected arbitrary intermediate probability p_0, the $(p_0 \times N)$-th value is classified as the cut-off y^*. The states of the random variables corresponding to values greater than or equal to y^* are used as generators (x) to generate the sample of the next level $(\tilde{x})$, using the Modified Metropolis Algorithm (MMA) [25]. This ensures that the states of the variables of the resulting sample are inside F_1. It is visible, in the example in Fig. 2b, how every result in $i = 2$ is greater or equal to the cut-off that defines F_1. The process is repeated (Figs. 2c and 2d) until y^* is found inside F_m (i.e., $P(F_i) > p_0$). With $p_0 = 0.1$, probabilities of the order of magnitude of $10^{-4} = 0.1 \times 0.1 \times 0.1 \times 0.1$ are attainable with four levels ($F_m = F_4$). Note that in Fig. 2d, with $p_0 = 10$ and $N = 100$, $y*$ is in the 10th ordered position. Since in that example there are 13 results equal or greater than $y*$, $P(F_4) = 13/100 = 0.13 > p_0$, and as such, $p_f = 0.13 \prod_{i=1}^{4-1} 0.1 = 1.3 \times 10^{-4}$.

The diagram in Fig. 3 illustrates how subset simulation is applied in practice for this study. Initially, the random variables are sampled (using MATLAB® [26]) and combined with existing constant quantities to create the input for the FE model, which is created in ANSYS® [27]. The dynamic response is calculated for the desired load model (i.e., one of the 10 HSLM-A configurations) using the Single Load Linear Superposition (SLLS) method (introduced by Ferreira et al. [28]) because of its efficacy and ease of application. It is then filtered with a low-pass Type II Chebyshev filter, cut off at 60 Hz (although the EN 1990 only requires the consideration of frequencies up to 30 Hz, studies have highlighted the importance of extending

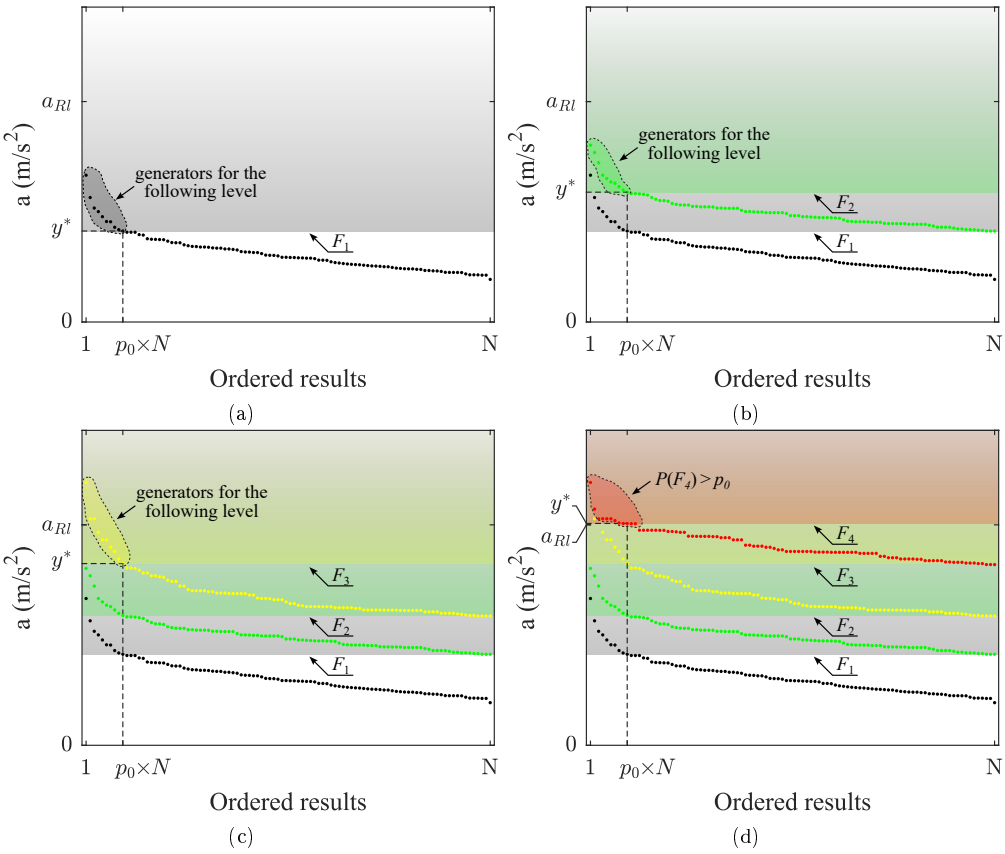

Figure 2: Visualization of subset simulation. (a) $i = 1$; (b) $i = 2$; (c) $i = 3$; (d) $i = 4$.

the frequency range [29]), and the maximum absolute acceleration is stored for each randomly generated bridge. After this crude Monte Carlo phase, if no stopping criterion is met, the level counter is increased, and the ordered results greater or equal to y^* are used as the seeds for the Markov Chain Monte Carlo (MCMC). The MMA implementation is based on Uribe [30]. In this work, the adopted proposal functions to obtain candidates η from the current state of a variable x_k are:

- for Gaussian distributed variables $N(\mu, \sigma^2)$: $\eta \sim N(x_k, \sigma^2)$;
- for uniformly distributed variables $U(a, b)$: $\eta \sim N\left(x_k, \dfrac{(b-a)^2}{12}\right)$;

With the samples of the next level, new FE models are obtained, and the dynamic responses for the new set are calculated. The process stops after the $P(F_i) > 0.1$ condition occurs (after which p_f can be estimated) or if $i = 4$ (i.e., if the subset simulation is already in the fourth level, any possible p_f would be lower than 10^{-4}, and therefore not worth further exploration for the purposes of this study).

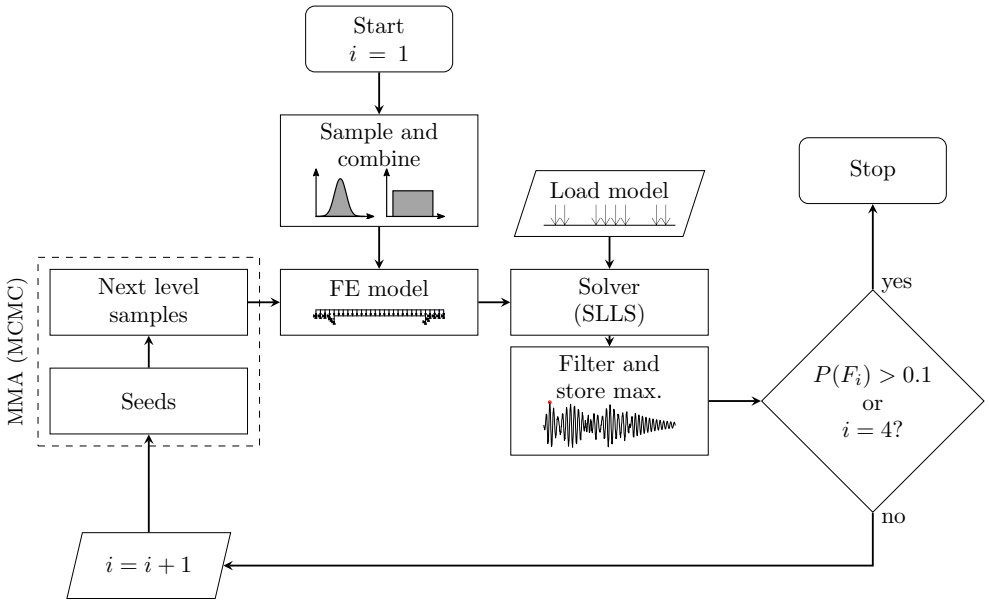

Figure 3: Application of subset simulation.

3.2. Critical speed algorithm

Although the application of subset simulation is associated with considerable savings in computation time, this only applies to the estimation of probabilities for a given train speed. That is, the question remains for which speed or set of speeds the probabilities must be calculated. Simulating in coarse intervals of 10 km/h is incompatible with the sensitivity of most dynamic calculations concerning speed. Conversely, a finer 1 km/h interval is not feasible given all the possible values in a usual speed interval.

Hence, an algorithm is proposed here to efficiently assess the critical speed, which is summarized in Fig. 4. The objective of this procedure is to avoid wasting computational resources that would be misused by calculating

probabilities of failure lower than 10^{-5}. When the search cycle is initialized, the train speed v is set to its initial value (the lowest in the given speed range). After the initial analysis (i.e., the crude Monte Carlo simulation in $i = 1$), if the cut-off y^* is lower than a chosen threshold value y_t, the speed is increased to the next value. Note that y_t must be chosen appropriately so that exceeding it represents a substantial likelihood that p_f is in the vicinity of 10^{-4}. Initially, the speed increment is a coarse interval of 20 km/h. The cycle continues until the $y^* > y_t$ condition is satisfied. If the resulting p_f is greater than 10^{-4}, a finer speed cycle of 1 km/h increments is triggered, symbolized by the flag $\boxed{\text{F}}$. The train speed is brought back to the value immediately after the second-highest calculated speed ($v = v - 19$ km/h), and the cycle continues. During this phase, if $y^* < y_t$, flag $\boxed{\text{D}}$ is activated to store the information that at least one train speed was discarded during the finer cycle. The first time that a $p_f > 10^{-4}$ is found, the current v is classified as a suitable candidate. If $\boxed{\text{D}}$ is off, no previous speed was discarded in $F1$ (i.e., the speed or speeds immediately before were calculated but turned out to be in the magnitude of 10^{-5} or lower), and the candidate is immediately accepted as v_{crit}. Otherwise, a $v = v - 1$ reverse search cycle is activated to check the previously discarded speed value until v_{crit} is confirmed.

An example of a complete run of the algorithm is depicted in Fig. 5 (in the graphics, the offset in the coloured dots is meant to improve clarity and does not denote a change in speed). In this case, the sample size N for each level is 100 and $p_0 = 0.1$, which means that in the sorted results, y^* is in the $100 \times 0.1 = 10$-th position. In simulations 1 to 7, y^* was lower than y_t (in this case 3 m/s^2), meaning that no simulation progressed beyond $i = 1$. In simulation 8, y^* is greater than y_t, causing the simulation to continue, resulting in a calculated p_f of 0.02. This result at 280 km/h initiates the finer speed increment cycle at 280-19=261 km/h. Simulations 9, 10 and 11 (261 km/h, 262 km/h, and 263 km/h, respectively) do not meet the y_t criterion. Simulation 12, at 264 km/h meets the criterion and returns $p_f = 5.1 \times 10^{-4}$, making it a suitable v_{crit} candidate. However, since there was at least one discarded speed, the algorithm runs simulation 13 at 263 km/h, by fetching the stored $i = 1$ results and resuming the subset simulation. The resulting p_f is 1.2×10^{-4}, making this speed the new v_{crit} candidate. Simulation 14, at 262 km/h is also resumed, resulting in $p_f = 4 \times 10^{-5}$, confirming that 263 km/h as v_{crit} and finishing the algorithm run. It is worth noting that this application of the algorithm, with its iterative nature,

allowed a critical speed to be found with a total sample size of 2,200 (100 per level, with a maximum of 400 per speed value). In contrast, performing a similar procedure using crude Monte Carlo simulations would require a total sample size of over 1 million.

For the proposed algorithm to be viable in terms of computational savings, it is imperative that the N, p_0, and y_t parameters are properly set. Unoptimized parameters may lead to inefficient use of simulation capacity for the following reasons:

- Waste of unnecessary time calculating v_{crit} candidates that result in $p_f \approx 0$
- Increased number of entries in the $v = v - 1$ reverse search cycle
- Inadequate dispersion in $i = 1$ results, jeopardizing further levels

Hence, a sensitivity study is performed with the objective of setting appropriate parameters. The metrics adopted are the time required to go from v=140 km/h to v_{crit} and the total sample size n_S required for the simulation. The results are presented in Section 5.

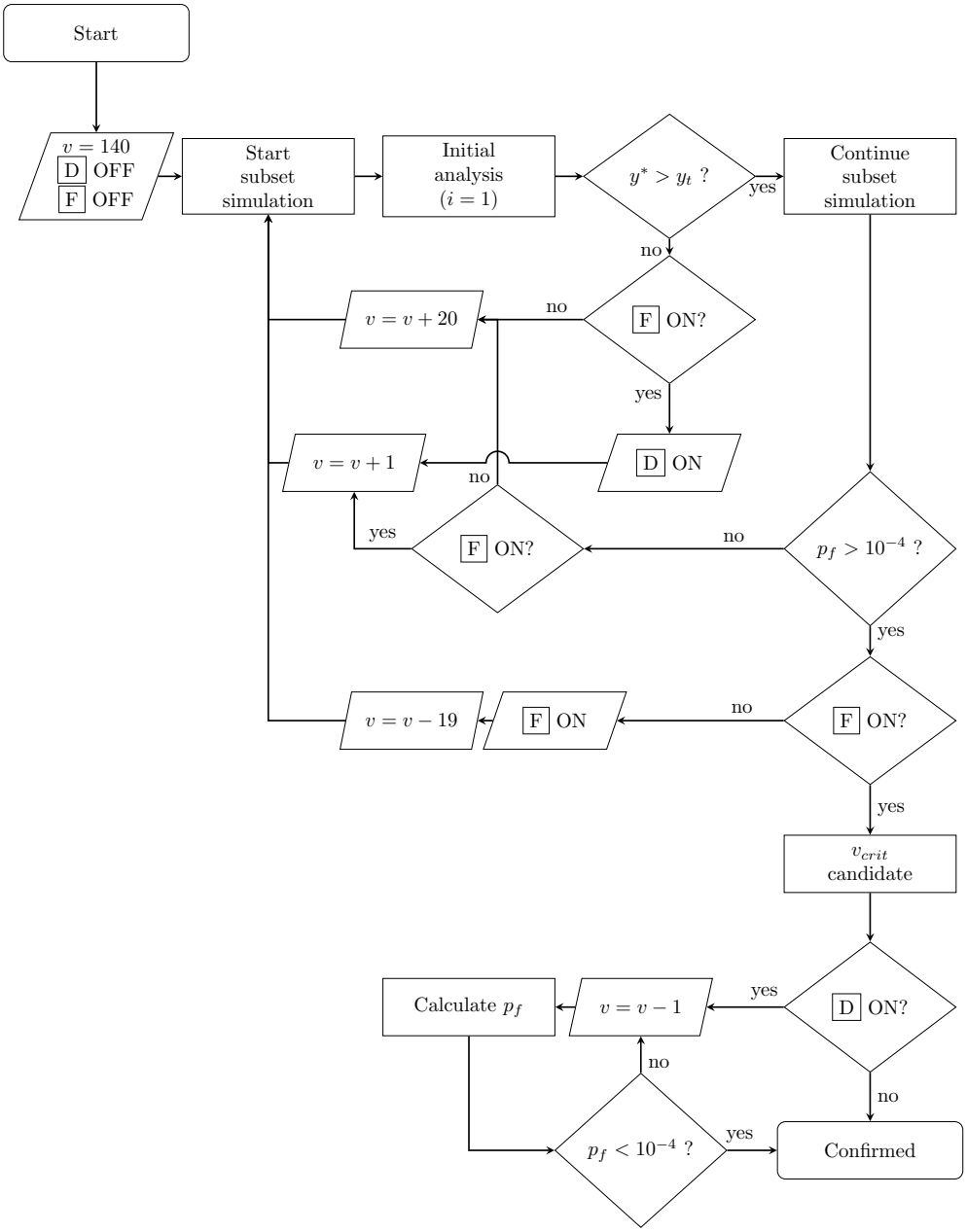

Figure 4: Algorithm to assess critical speed.

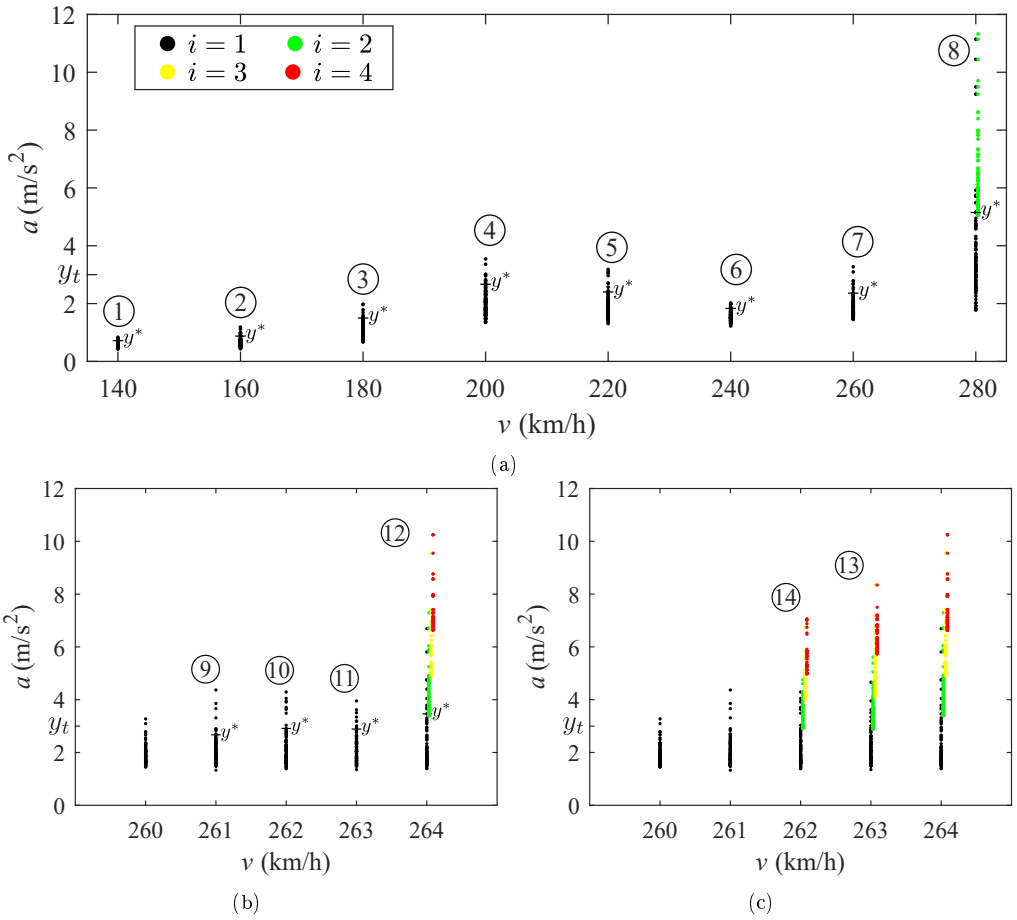

Figure 5: Example results from the application of the proposed algorithm. (a) Simulations 1 to 8; (b) simulations 9 to 12 (finer speed increment cycle); (c) simulations 13 and 14 ($v = v - 1$ reverse search cycle).

4. Application examples

4.1. Initial considerations

The proposed methodology is applied to four bridges of the Northern Line of the Portuguese Railway Network. The selected set of structures are representative of filler beam bridges, which is a characteristic construction solution of this line. This construction solution consists of simply supported concrete slabs directly cast on embedded steel profiles. Each double-track bridge comprises two independent decks (one for each track), built with directly cast concrete on rolled steel profiles. The track consists of UIC60 rails, wooden sleepers, and a ballast bed. The decks are supported by sets of neoprene bearings located directly under the nine steel profiles on each support.

Considering that the present study focuses on the vertical deck acceleration, and that the torsional effects on the eccentricities of the sections correspond to high frequencies that are outside of the scope of this work (and therefore negligible), the bridge decks can be represented by a single beam, and thus a two-dimensional modeling approach is sufficient to capture the dynamic behavior of the bridges using moving loads analysis. The finite element models used employ the modeling technique developed by Rocha [31], adapted for the ANSYS® [27] environment. In this technique, the ballast layer, rail pads, and supports are modeled with spring-dashpot elements (COMBIN14), while the rails and deck are discretized with beam elements (BEAM3). The localized masses of the sleepers are represented by mass elements (MASS21).

The random variables common to the four models are listed in Table 1, which is adapted from Rocha [31]. It is noted that the author attributes uniform distributions to the variables for which there is significant variability in existing studies' measurements. Each model has three bridge-dependent random variables, which are the thickness (t_{slab}) and width (b_{slab}) of the slab and the area of the steel profiles (A_S). These three variables follow normal distributions, with the mean equal to the nominal value taken from the project drawings and the standard deviation suggested by Rocha [31]. Other quantities of constant nature are the steel elasticity modulus E_S (210 GPa), the remaining mass (weight of the waterproofing, guard rails and gutters' box and covers) M_r (1.4 ton/m), the width of the sleeper underside l_b (0.3 m), the half sleeper effective support l_e (0.95 m), the sleeper spacing l_s (0.6 m), and the properties of the steel profiles (such as mass $M_{profile}$, moment of in-

ertia $I_{profile}$ and height of the center of gravity $y_{profile}$). The vertical stiffness of the ballast layer is calculated according to Zhai et al. [32], while the supports' vertical and horizontal stiffnesses use the equations given by Manterola [33] and Rocha [31]. Since the methodology utilizes the Single Load Linear Superposition [28] method to calculate the HSLM response, the model only needs to be subjected to a single moving load. The single load's response is calculated with direct integration, using Rayleigh damping matrices (set to the first and second vertical modes of vibration) for the structural damping of the models. A schematic representation of the typical model components is given in Fig. 6. The FE model implementation (exemplified by the Canelas bridge model, which has 546 degrees of freedom) can be seen in Fig. 7.

Table 1: Random variables of the structure, track, and support (adapted from [31]).

Structure variables (Gaussian)	μ	σ
Reinforced concrete density ρ_C	2.5 t/m^3	0.1 t/m^3
Concrete elasticity modulus E_C	36.1 GPa	2.888 GPa
Structural damping ξ	2%	0.3%
Track variables (Uniform)	min.	max.
Ballast density ρ_b	1.5 t/m^3	2.1 t/m^3
Ballast elasticity modulus E_b	80 MPa	160 MPa
Ballast layer height h_b	300 mm	600 mm
Load distribution angle α	15°	35°
Sleeper mass m_s	220 kg	325 kg
Rail pad stiffness k_p	100 kN/mm	600 kN/mm
Track shear stiffness k_t	1×10^4 kN/m/m	3×10^4 kN/m/m
Support variables (Uniform)	min.	max.
Neoprene shear modulus G_n	0.75 MPa	1.5 MPa

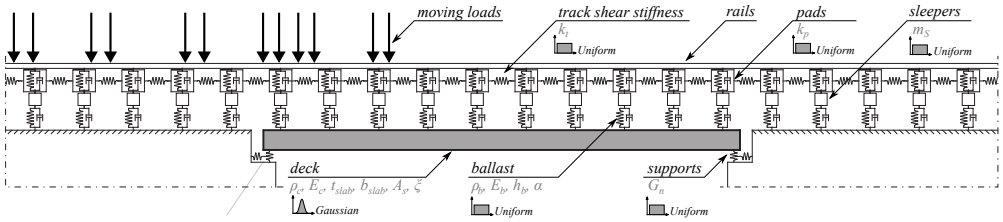

Figure 6: Schematic representation of the finite element model and random variables.

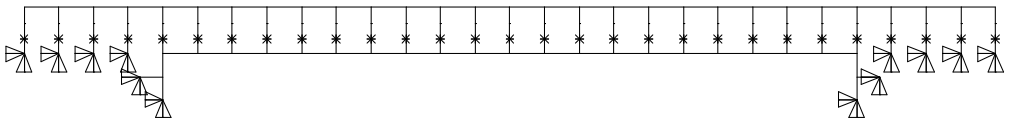

Figure 7: Finite element model of the Canelas bridge.

4.2. Case study bridges

4.2.1. Canelas bridge

The Canelas bridge, consisting of 6 spans, is the only multi-span structure of the set, although the spans are simply supported. Each span has a determinant length of 11.5 m. The cross-section and view of the first span of the Canelas bridge can be seen in Fig. 8. The steel profiles used are HEB500 and the bridge dependent variables for this structure are defined as $t_{slab} \sim N\left(0.7, 0.01^2\right)$ m, $b_{slab} \sim N\left(4.475, 0.005^2\right)$ m and $A_S \sim N\left(0.01975, 0.00079^2\right)$ m^2.

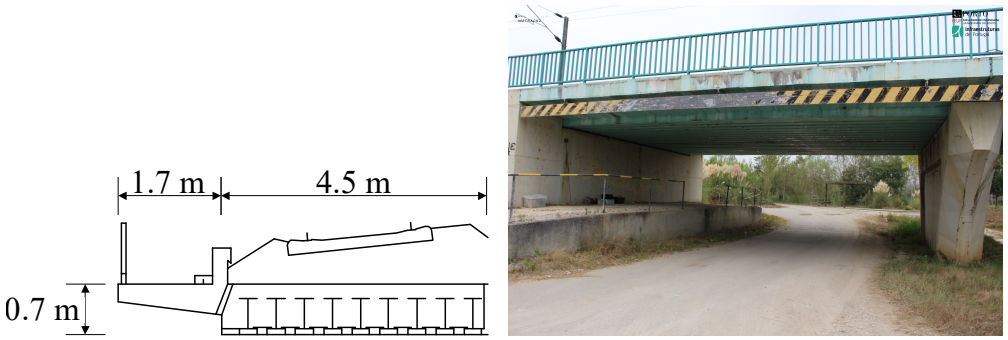

(a) (b)

Figure 8: Canelas bridge. (a) Cross-section (unit: m) (adapted from Pimentel et al. [34]); (b) view of the first span.

4.2.2. Melga bridge

With a determinant span length of 23.78 m, the Melga bridge (Fig. 9) is the longest of the set. It consists of a single simply supported span with HEB800 profiles. Both its decks, independent of each other, support a single track. The bridge dependent variables are defined as $t_{slab} \sim N\left(0.871, 0.01^2\right)$ m, $b_{slab} \sim N\left(4.20, 0.005^2\right)$ m and $A_S \sim N\left(0.03342, 0.00079^2\right)$ m^2.

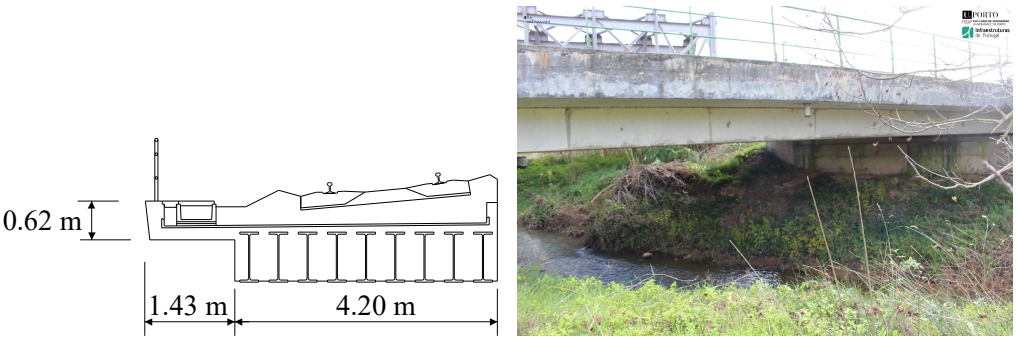

(a) (b)

Figure 9: Melga bridge. (a) Cross-section (unit: m); (b) view of the deck.

4.2.3. Cascalheira underpass

The Cascalheira underpass (Fig. 10) consists of a single simply supported span of 10.92 m determinant length, with embedded HEB500 steel profiles. It is composed of two independent decks, each carrying one track. The bridge dependent variables are defined as $t_{slab} \sim N\left(0.703, 0.01^2\right)$ m, $b_{slab} \sim N\left(4.08, 0.005^2\right)$ m and $A_S \sim N\left(0.03342, 0.00079^2\right)$ m^2.

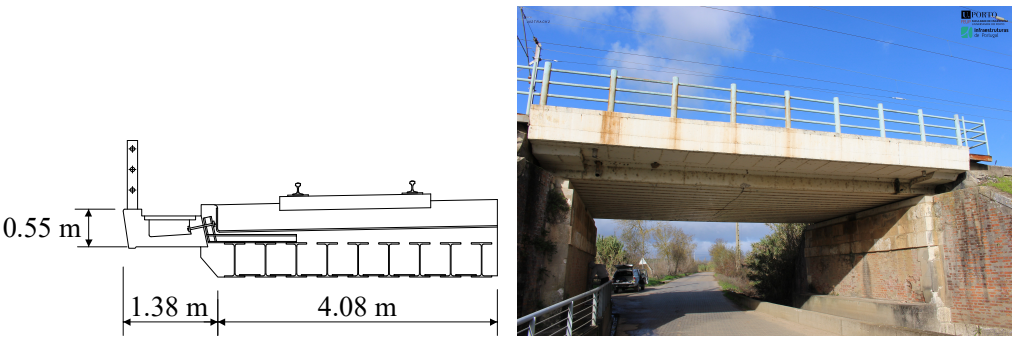

(a) (b)

Figure 10: Cascalheira underpass. (a) Cross-section (unit: m); (b) view of the deck.

4.2.4. Braço do Cortiço underpass

With a determinant span length of 7.02 m, the Braço do Cortiço underpass (Fig. 11) is the shortest of the set. This single simply supported span has two independent decks, each with a single track. This deck is embedded with HEB300 profiles and its bridge dependent variables are $t_{slab} \sim$

$N\,(0.445, 0.01^2)$ m, $b_{slab} \sim N\,(4.055, 0.005^2)$ m and $A_S \sim N\,(0.01491, 0.00079^2)$ m^2.

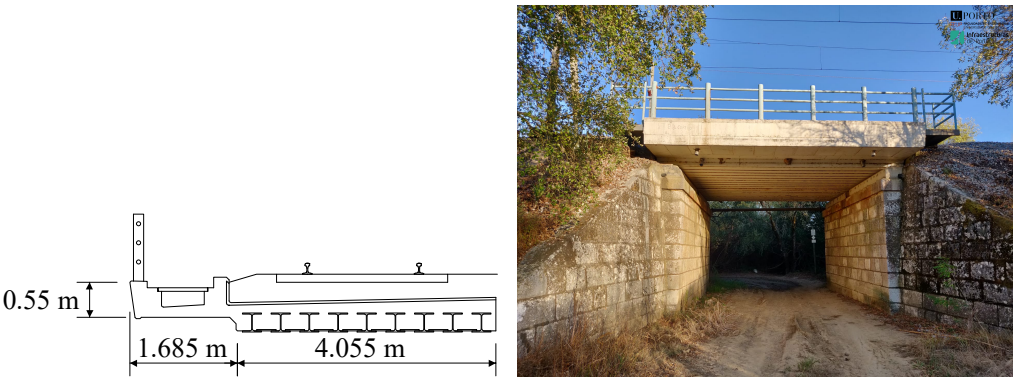

(a) (b)

Figure 11: Braço do Cortiço underpass. (a) Cross-section (unit: m); (b) view of the deck.

4.3. Dynamic response envelopes

Plots of the dynamic response of the four bridge models are shown in Fig. 12. The solid curves illustrate the response of the models when all random variables are considered at their mean values ($\mathbf{X}$), while the areas filled in blue and green indicate the envelopes of the dynamic responses when the most influential variables are set at lower ($\mathbf{Y}$ lower) or upper ($\mathbf{Y}$ upper) bounds, respectively. The curves represent the maximum of the 10 HSLM-A load configurations for each train speed value.

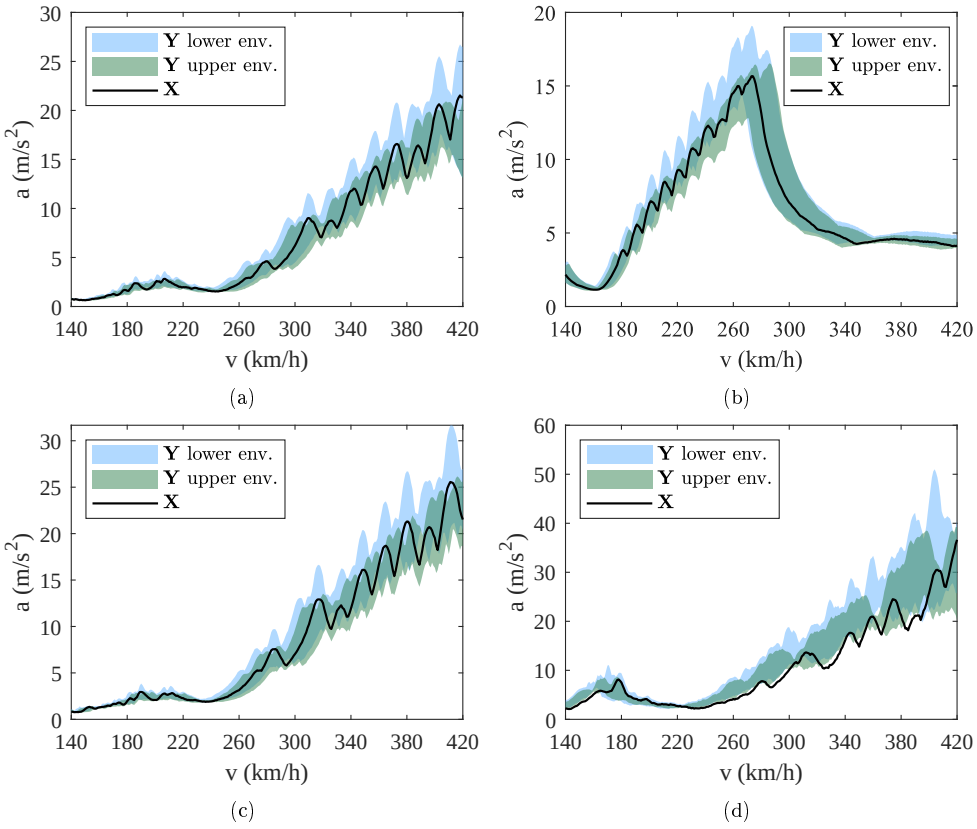

Figure 12: Dynamic response envelopes considering all random variables with mean values ($\mathbf{X}$) and the envelopes of lower and upper bounds of the most influential variables ($\mathbf{Y}$). (a) Canelas bridge; (b) Melga bridge; (c) Cascalheira underpass; (d) Braço do Cortiço underpass

5. Optimization of the algorithm for efficient assessment of critical speeds

5.1. Optimization of the threshold value y_t

The Canelas bridge and the HSLM-A3 train were selected to perform the optimization study of the critical speed algorithm. The first parameter to be studied was the threshold value y_t for the initial analysis in $i = 1$, which controls whether a speed value is discarded. For this part of the study, the sample size and the intermediate probability were fixed at $N = 100$ and $p_0 = 0.1$, and y_t varied between 2.0 m/s^2, 2.5 m/s^2, 3.0 m/s^2 and 3.5 m/s^2. Table 2 lists the time and the total sample size needed to complete the algorithm,

as well as the resulting v_{crit}. It can be seen that using the values of 3.0 m/s^2 and 3.5 m/s^2 resulted in the least computational expense. However, further analysis of the simulation results revealed that the stricter 3.5 m/s^2 limit caused the algorithm to skip $v = 264$ km/h, which would have produced a suitable p_f and therefore a lower (and valid) v_{crit} candidate. Conversely, while it is true that using lower threshold values prevents prematurely discarding of candidate speeds, this option also leads to increased time expenditure, as additional time is spent calculating candidates that are far from the final one. The threshold value $y_t = 3.0$ m/s^2 is henceforth kept as optimal.

Table 2: Variation of the first level threshold y_t (HSLM-A3, $p_0 = 0.1$, $N = 100$).

y_t	2.0 m/s^2	2.5 m/s^2	3.0 m/s^2	3.5 m/s^2
time (h)	3:34	2:58	1:48	1:37
n_S	4200	3400	2200	2100
v_{crit} (km/h)	266	264	263	267

5.2. Optimization of the intermediate probability p_0

Using the aforementioned y_t value and a fixed sample size $N = 100$, the optimal intermediate probability is examined by varying p_0 between 0.05, 0.1 and 0.2. As shown in Table 3, adopting an intermediate probability of 0.1 allowed the algorithm to converge in the shortest time and with the smallest total sample size. The effect of using $p_0 = 0.2$ was similar to that of having a high y_t, i.e., given the intermediate probability, the cut-off on the ordered results' list is made at a lower value. This makes it harder for y^* to achieve y_t, which in turn makes for a longer $v = v - 1$ reverse search cycle. As for the lower value, 0.05, the resulting additional computing time would only be justifiable if the target p_f was lower than 10^{-4}.

Table 3: Variation of the intermediate probability p_0 (HSLM-A3, $y_t = 3.0$, $N = 100$).

p_0	0.05	0.1	0.2
time (h)	2:49	1:48	2:37
n_S	2700	2200	3700
v_{crit} (km/h)	264	263	265

5.3. Optimization of the sample size N

Regarding the sample size, the comparison of N between 50, 100, 150 and 200 is calculated with fixed $y_t = 3.0$ and $p_f = 0.1$. Unsurprisingly, Table 4 reveals that it takes more time to compute larger sample sizes, while the smallest size, 50, corresponds to the least amount of time and smallest total sample size. However, with an intermediate probability of 0.1, each level of a subset simulation with $N = 50$ provides only 5 elements to generate the samples of the following level. As a result, the number of failed candidate states in the MMA increases, introducing inefficacy when scaling the method by artificially limiting the dispersion of the results.

Table 4: Variation of the sample size N (HSLM-A3, $y_t = 3.0$, $p_0 = 0.1$).

N	50	100	150	200
time (h)	1:01	1:48	3:26	2:52
n_S	1050	2200	6200	4000
v_{crit} (km/h)	263	263	267	265

Given that the various applications lead to v_{crit} in close proximity, the final adopted values are $y_t = 3.0\text{m/s}^2$, $p_0 = 0.1$, and $N = 100$.

6. Simulation results

6.1. Calculated critical speeds

The current section represents the application of the first step of the methodology. After setting the optimal factors in the algorithm, the critical speeds on each bridge are calculated for each HSLM-A train model. The individual critical speeds $v_{crit,i}$ are listed in Table 5. The final critical speed values, given by Eq. 3, are highlighted in the same table.

Table 5: Critical speeds for each HSLM-A train model.

HSLM	$v_{crit,i}$ (km/h)			
	Canelas bridge	Melga bridge	Cascalheira underpass	Braço do Cortiço underpass
A1	414	N/A	250	244
A2	361	175	269	156
A3	263	173	263	255
A4	274	179	277	146
A5	284	185	284	264
A6	293	192	287	263
A7	298	194	289	244
A8	314	202	301	282
A9	316	205	261	252
A10	325	214	254	255

6.2. Assessment of scenarios for bridge design

The present section showcases the application of the second step of the methodology, where the scenarios for bridge design are defined as two sets of instructions on how to assign values to several random variables. The selection of the variables to be included in the definition of the scenarios is achieved through a sensitivity analysis, where the importance of each variable is assessed with Eq. 4. Here, the study is performed for the Canelas bridge, using the 10 HSLM-A load configurations and a train speed interval from 140 km/h to 420 km/h. The calculated variance values are listed in Table 6. It can be seen that there is a remarkable importance of the variables that control most of the structural mass (thickness and density of both the slab and the ballast layer) and of the concrete stiffness. Structural damping and support stiffness also account for a considerable portion. Due to the clear difference in the results, the variables that score a variance result (from Eq. 4) greater than 1 are selected for the definition of the design scenarios.

Consequently, the deterministic scenarios S1 and S2 are proposed in Table 7. In accordance with the EN 1991-2 [22], there are two estimates of mass (upper and lower bound), defined by thickness and density (t_{slab}, h_b, ρ_C, ρ_b), combined with a single estimate (lower bound) of stiffness (E_C, G_n) and structural damping (ξ).

Using the definitions of Table 7 and setting the remaining random variables to their mean values, the dynamic design response can be obtained.

Table 6: Sensitivity analysis of the relative influence of the variables.

	Variance	
Variable	$\mathbf{Y}$ lower envelope	$\mathbf{Y}$ upper envelope
Reinforced concrete density ρ_C	1.06	1.08
Concrete elasticity modulus E_C	2.63	1.46
Slab thickness t_{slab}	1.56	1.43
Slab width b_{slab}	0.06	0.06
Area of the steel profiles A_S	0.06	0.06
Structural damping ξ	2.29	1.13
Ballast density ρ_b	1.04	1.21
Ballast elasticity modulus E_b	0.02	0.02
Ballast layer height h_b	0.66	1.56
Load distribution angle α	0.02	0.02
Sleeper mass m_s	0.01	0.12
Rail pad stiffness k_p	0.03	0.02
Track shear stiffness k_t	0.20	0.03
Neoprene shear modulus G_n	1.29	0.53

Table 7: Scenarios for bridge design.

Scenario	E_c, ξ	ρ_C, t_{slab}	ρ_b, h_b	G_n
S1	$\mu - 1.64\sigma$	$\mu - 1.64\sigma$	min.	min.
S2	$\mu - 1.64\sigma$	$\mu + 1.64\sigma$	max.	min.

Fig. 13 represents the response envelopes of the deterministic scenarios for the case study bridges. It is worth noting that these bridges were originally designed for a train speed of 160 km/h, hence the large acceleration values at higher speeds. The methodology being used in this work may allow for higher permissible deck accelerations, which can possibly allow for higher train speeds. Such a study is helpful in addressing the sustainability of existing infrastructure by considering the need to deploy newer, faster, and longer trains to operators' rolling stock rather than replacing existing bridges.

Analyzing the local maxima on the plotted data, it is clear that S1 (with its lower bound estimate of the random variables controlling the structural mass) produces the highest acceleration values, albeit at higher speeds. Conversely, the upper estimates in S2 correspond to lower acceleration peaks, but avoid overestimating the resonant speeds. These observations help to validate the purpose of the scenarios, which corresponds to the Eurocode

expects. The design acceleration values a_{Ed} are to be found in these curves at v_{crit}.

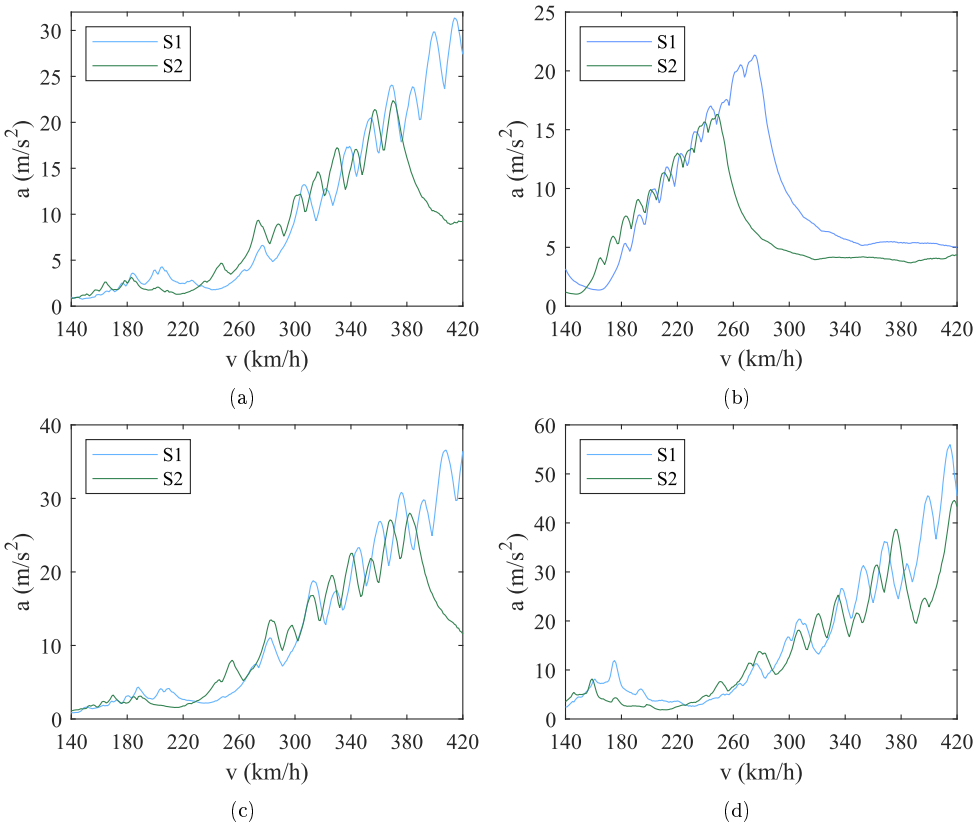

Figure 13: Design scenario response envelopes. (a) Canelas bridge; (b) Melga bridge; (c) Cascalheira underpass; (d) Braço do Cortiço underpass

6.3. Design acceleration and safety factors

The third and final step of the methodology is performed in this section. Knowing the critical speeds and the envelopes of the design scenarios, the design accelerations a_{Ed} can be found, as illustrated in Fig. 14. The values are given in Table 8, together with the safety factors, according to Eq. 5.

From the results, it can be observed that a bridge design made with the current Eurocode limit of 3.5 m/s^2 (i.e., with the safety factor of 2.0) would either limit the maximum allowable train speed or result in heavier, more robust cross-sections. Conversely, the present approach suggests that

safety would be ensured up to the calculated critical speeds within the target probability of failure.

Table 8: Design accelerations and safety factors.

Bridge	$a_{Ed}\ \left(\mathrm{m/s^2}\right)$	γ_{bt}
Canelas bridge	5.07	1.38
Melga bridge	5.81	1.20
Cascalheira underpass	5.94	1.18
Braço do Cortiço underpass	5.42	1.29

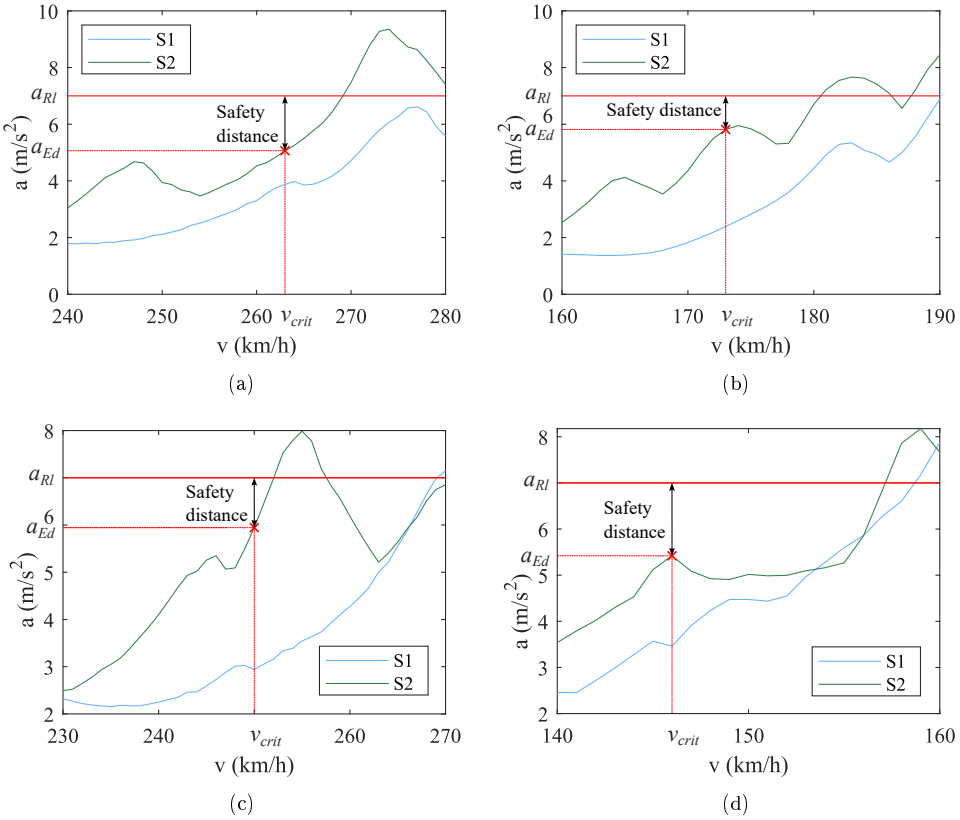

Figure 14: Critical speeds and design phase accelerations. (a) Canelas bridge; (b) Melga bridge; (c) Cascalheira underpass; (d) Braço do Cortiço underpass.

7. Conclusion

In this study, the permissible acceleration limit in ballasted track bridges is addressed by defining a design phase acceleration. Two design scenarios are proposed where the design acceleration is found at a critical speed. This speed is assessed using a newly proposed algorithm to overcome the computational challenges associated with low probabilities of failure. The main conclusions of this study can be summarized according to the research questions proposed in Section 1:

1. The employment of subset simulation is cost effective when estimating low probabilities of failure. However, it still depends on knowing where to start in the speed range. By using an appropriate first-level threshold value, sample size, and intermediate probability, a simple decision-making algorithm can aid in rapidly going through the speed range.
2. The Eurocode EN 1991-2 dictates how stiffness, damping, and mass must be estimated, but does not specify how they are to be achieved. By describing the geometric and material properties of a bridge with basic random variables, it is possible to sample these variables and construct two design scenarios. An expedited sensitivity analysis is sufficient to highlight the most contributing variables;
3. The study of four real ballasted track structures has revealed that a bridge can be designed so that its deck can experience an acceleration value greater than 3.5 m/s^2 without being associated with a probability of failure greater than 10^{-4}. Considering that the physical acceleration limit is kept at 7 m/s^2, this means that the safety factor, computed as the ratio between it and the allowable acceleration, can be set lower than 2.0.

Considering that the calculated design acceleration values are greater than 3.5 m/s^2 (or, in other words, that the associated safety factors are less than 2.0), it can be concluded that the normative limits are, at least, conservative. Therefore, a revision of the normative acceleration limit for ballasted track railway bridges may include the discussion of higher permissible limits. A future contribution to this topic should focus on the cost of maintaining the current limit, considering that the Eurocode could, for instance, have a lower limit for existing bridges while maintaining the current limit for new structures.

CRediT authorship contribution statement

Gonçalo Ferreira: Writing - original draft, Visualization, Investigation, Formal analysis. **Pedro Montenegro:** Writing - review & editing, Methodology, Conceptualization. **Christoph Adam:** Writing - review & editing, Conceptualization, Validation. **António Abel Henriques:** Writing review & editing, Methodology, Supervision. **Rui Calçada:** Conceptualization, Supervision, Resources.

Declaration of Competing Interest

The authors declare that they have no known competing financial interests or personal relationships that could have appeared to influence the work reported in this paper.

Data availability

Data will be made available on request.

Acknowledgements

The authors would like to acknowledge the financial support of:

- "InBridge4EU - Enhanced Interfaces and train categories for dynamic compatibility assessment of European railway bridges" project funded by European funds through Horizon Europe (Europe's Rail Joint Undertaking);
- Portuguese Foundation for Science and Technology (FCT) through the PhD scholarship PD/BD/143007/2018;
- Base Funding - UIDB/04708/2020 of the CONSTRUCT - Instituto de I&D em Estruturas e Construções - funded by national funds through the FCT/MCTES (PIDDAC).

A1

References

[1] CEN, Eurocode - Basis of Structural and Geotechnical Design, EN 1990, Commité European de Normalisation (CEN), Brussels, 2023.

[2] ERRI D 214/RP 9, Rail Bridges for Speeds > 200 Km/h, Final Report, European Rail Research Institute, Utrecht, 1999.

[3] M. Zacher, M. Baeßler, Dynamic behaviour of ballast on railway bridges, in: Dynamics of High–Speed Railway Bridges. Selected and Revised Papers from the Advanced Course on 'Dynamics of High–Speed Railway Bridges', Porto, Portugal, 20–23 September 2005, CRC Press, 2008, pp. 125–142.

[4] European Union Agency for Railways (ERA), ERA1193-TD-01-2022 - ERA technical note on work needed for closing TSI open points on bridge dynamics, 2022. URL: https://rail-research.europa.eu:443/about-europes-rail/europes-rail-reference-documents/additional-technical-material/.

[5] European Comission, Consolidated text: Commission Decision of 30 May 2002 concerning the technical specification for interoperability relating to the infrastructure subsystem of the trans-European high-speed rail system referred to in Article 6(1) of Council Directive 96/48/EC (notified under document number C(2002) 1948) (Text with EEA relevance) (2002/732/EC), 2002. URL: https://eur-lex.europa.eu/eli/dec/2002/732/2002-09-12.

[6] T. Heiland, M. Hägle, T. Triantafyllidis, L. Stempniewski, A. Stark, Stiffness contributions of ballast in the context of dynamic analysis of short span railway bridges, Construction and Building Materials 360 (2022) 129536. URL: https://www.sciencedirect.com/science/article/pii/S0950061822031920. doi:10.1016/j.conbuildmat.2022.129536.

[7] A. Stollwitzer, L. Bettinelli, J. Fink, Vertical Track-Bridge Interaction in Railway Bridges with Ballast Superstructure: Experimental Analysis of Dynamic Stiffness and Damping Behavior, International Journal of Structural Stability and Dynamics (2024). doi:10.1142/S0219455425400085.

[8] J. Menezes, Modelling of the Dynamic Behaviour of Ballast on Railway Bridges, Master's thesis, Faculdade de Engenharia da Universidade do Porto, Porto, Portugal, 2024. URL: https://repositorio-aberto.up.pt/handle/10216/162090.

[9] B. Hou, D. Wang, B. Wang, X. Chen, J. Pombo, Vibration Reduction in Ballasted Track Using Ballast Mat: Numerical and Experimental Evaluation by Wheelset Drop Test, Applied Sciences 12 (2022) 1844. URL: https://www.mdpi.com/2076-3417/12/4/1844. doi:10.3390/app12041844.

[10] J. Mao, Z. Yu, Y. Xiao, C. Jin, Y. Bai, Random dynamic analysis of a train-bridge coupled system involving random system parameters based on probability density evolution method, Probabilistic Engineering Mechanics 46 (2016) 48–61. URL: https://www.sciencedirect.com/science/article/pii/S0266892016300972. doi:10.1016/j.probengmech.2016.08.003.

[11] Z. Xu, G. Dai, Y. F. Chen, H. Rao, Z. Huang, Extreme response analysis of train-track-bridge-wind interaction system based on in-situ monitoring wind data, Structural Safety 100 (2023) 102288. URL: https://www.sciencedirect.com/science/article/pii/S0167473022000959. doi:10.1016/j.strusafe.2022.102288.

[12] L. Xin, X. Li, Y. Zhu, M. Liu, Uncertainty and sensitivity analysis for train-ballasted track–bridge system, Vehicle System Dynamics 58 (2020) 453–471. URL: https://doi.org/10.1080/00423114.2019.1584678. doi:10.1080/00423114.2019.1584678.

[13] J. Park, P. Towashiraporn, Rapid seismic damage assessment of railway bridges using the response-surface statistical model, Structural Safety 47 (2014) 1–12. URL: https://www.sciencedirect.com/science/article/pii/S0167473013000787. doi:10.1016/j.strusafe.2013.10.001.

[14] J. M. Rocha, A. A. Henriques, R. Calçada, Probabilistic assessment of the train running safety on a short-span high-speed railway bridge, Structure and Infrastructure Engineering 12 (2016) 78–92. URL: https://doi.org/10.1080/15732479.2014.995106. doi:10.1080/15732479.2014.995106.

A3

[15] JCSS, Probabilistic Model Code, JCSS-OSTL/DIA/VROU -10-11-2000, Joint Commitee on Structural Safety (JCSS), 2001. URL: https://www.jcss-lc.org/jcss-probabilistic-model-code/.

[16] R. Allahvirdizadeh, A. Andersson, R. Karoumi, Reliability assessment of the dynamic behavior of high-speed railway bridges using first order reliability method, in: 11th International Conference on Structural Dynamics, volume 2, Athens, Greece, 2020, pp. 3438–3450.

[17] V. Grigoriou, E. Brühwiler, Monitoring-based safety verification at the Ultimate Limit State of fracture of the RC slab of a short span railway underpass, Structural Safety 60 (2016) 16–27. URL: https://www.sciencedirect.com/science/article/pii/S0167473016000138. doi:10.1016/j.strusafe.2016.01.002.

[18] P. Salcher, H. Pradlwarter, C. Adam, Reliability of high-speed railway bridges with respect to uncertain characteristics, in: 9th European Conference on Structural Dynamics, Porto, Portugal, 2014.

[19] B. Hirzinger, C. Adam, P. Salcher, M. Oberguggenberger, On the optimal strategy of stochastic-based reliability assessment of railway bridges for high-speed trains, Meccanica 54 (2019) 1385–1402. URL: https://doi.org/10.1007/s11012-019-00999-0. doi:10.1007/s11012-019-00999-0.

[20] P. Salcher, C. Adam, Estimating Exceedance Probabilities of Railway Bridge Vibrations in the Presence of Random Rail Irregularities, International Journal of Structural Stability and Dynamics 20 (2020) 2041005. URL: https://www.worldscientific.com/doi/abs/10.1142/S0219455420410059. doi:10.1142/S0219455420410059.

[21] B. Hirzinger, C. Adam, M. Oberguggenberger, P. Salcher, Approaches for predicting the probability of failure of bridges subjected to high-speed trains, Probabilistic Engineering Mechanics 59 (2020) 103021. URL: https://www.sciencedirect.com/science/article/pii/S0266892020300060. doi:10.1016/j.probengmech.2020.103021.

[22] CEN, Eurocode 1 - Actions on Structures - Part 2: Traffic Loads on Bridges and Other Civil Engineering Works, EN 1991-2, Commité European de Normalisation (CEN), Brussels, 2023.

[23] P. Bjerager, Methods for Structural Reliability Computations, in: F. Casciati, J. B. Roberts (Eds.), Reliability Problems: General Principles and Applications in Mechanics of Solids and Structures, International Centre for Mechanical Sciences, Springer, 1991, pp. 89–135. URL: https://doi.org/10.1007/978-3-7091-2616-5_3. doi:10.1007/978-3-7091-2616-5_3.

[24] S.-K. Au, J. L. Beck, Estimation of small failure probabilities in high dimensions by subset simulation, Probabilistic Engineering Mechanics 16 (2001) 263–277. URL: https://www.sciencedirect.com/science/article/pii/S0266892001000194. doi:10.1016/S0266-8920(01)00019-4.

[25] K. M. Zuev, Subset Simulation Method for Rare Event Estimation: An Introduction, in: M. Beer, I. A. Kougioumtzoglou, E. Patelli, I. S.-K. Au (Eds.), Encyclopedia of Earthquake Engineering, Springer, 2013, pp. 1–25. URL: https://doi.org/10.1007/978-3-642-36197-5_165-1. doi:10.1007/978-3-642-36197-5_165-1.

[26] MATLAB®, Academic Research, 2018.

[27] ANSYS®, Release 19.2, ANSYS Inc., 2018.

[28] G. Ferreira, P. Montenegro, J. Pinto, A. Henriques, R. Calçada, A discussion about the limitations of the Eurocode's high-speed load model for railway bridges, Railway Engineering Science 32 (2024) 211–228. doi:10.1007/s40534-023-00321-5.

[29] C. C. d. S. Horas, Comportamento Dinâmico de Pontes Com Tabuleiro Pré-Fabricado Em Vias de Alta Velocidade, Master's thesis, Faculdade de Engenharia da Universidade do Porto, Porto, Portugal, 2011. URL: https://repositorio-aberto.up.pt/handle/10216/66380.

[30] F. Uribe, Monte Carlo and subset simulation example, 2016. URL: https://www.mathworks.com/matlabcentral/fileexchange/57947-monte-carlo-and-subset-simulation-example.

[31] J. M. Rocha, Probabilistic Methodologies for the Safety Assessment of Short Span Railway Bridges for High-Speed Traffic, Ph.D. thesis, Faculdade de Engenharia da Universidade do Porto, Porto, Portugal, 2015. URL: https://repositorio-aberto.up.pt/handle/10216/83809.

[32] W. M. Zhai, K. Y. Wang, J. H. Lin, Modelling and experiment of railway ballast vibrations, Journal of Sound and Vibration 270 (2004) 673–683. URL: https://www.sciencedirect.com/science/article/pii/S0022460X0300186X. doi:10.1016/S0022-460X(03)00186-X.

[33] J. Manterola, Puentes: apuntes para su diseño, cálculo y construcción, Colegio de Ingenieros de Caminos, Canales y Puertos, Madrid, Spain, 2006.

[34] R. Pimentel, C. Barbosa, N. Costa, D. Ribeiro, L. A. Ferreira, F. M. Araújo, R. Calçada, Characterization of railway traffic and its effects on a short span bridge by using a hybrid fibre optic/electrical measurement system, in: Third European Workshop on Optical Fibre Sensors, International Society for Optics and Photonics, 2007. URL: https://www.spiedigitallibrary.org/conference-proceedings-of-spie/6619/66193Y/Characterization-of-railway-traffic-and-its-effects-on-a-short/10.1117/12.738786.short. doi:10.1117/12.738786.

C

APPENDIX C: ARTICLE FROM PROBLEM 3

The work by Ferreira et al. (2024a), on which Chapter 5 is based, is reproduced in this appendix.

G. Ferreira, P. Montenegro, A. Andersson, A. A. Henriques, R. Karoumi, and R. Calçada (2024a). "Critical analysis of the current Eurocode deck acceleration limit for evaluating running safety in ballastless railway bridges." In: *Engineering Structures* 312, p. 118127. ISSN: 0141-0296. DOI: 10.1016/j.engstruct.2024.118127

Engineering Structures 312 (2024) 118127

Contents lists available at ScienceDirect

Engineering Structures

journal homepage: www.elsevier.com/locate/engstruct

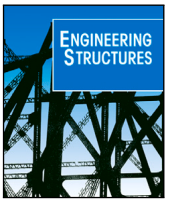

Critical analysis of the current Eurocode deck acceleration limit for evaluating running safety in ballastless railway bridges

Gonçalo Ferreira [a,*], Pedro Montenegro [a], Andreas Andersson [b,c], António Abel Henriques [d], Raid Karoumi [b], Rui Calçada [a]

[a] CONSTRUCT-LESE - Faculty of Engineering, University of Porto, Rua Dr. Roberto Frias, 4200-465, Porto, Portugal
[b] Division of Structural Engineering and Bridges, KTH Royal Institute of Technology, Stockholm, Sweden
[c] The Swedish Transport Administration (Trafikverket), Solna, Sweden
[d] CONSTRUCT-LABEST - Faculty of Engineering, University of Porto, Rua Dr. Roberto Frias, 4200-465, Porto, Portugal

ARTICLE INFO

Keywords:
Ballastless railway bridges
Derailment
Running safety
Deck acceleration
Eurocodes

ABSTRACT

The assessment of running safety of railway bridges is conditioned by the Eurocode EN 1990 A2 by limiting vertical deck acceleration. On ballastless track bridges, this value is 5 m/s^2. The background for this value is not clear, and it is believed that it originates in the application of an arbitrary safety factor of 2 on accelerations around 1 g to avoid loss of wheel–rail contact. However, studies show that the level of acceleration may not be directly related to the occurrence of derailment. In this work, this idea is expanded by assessing both vertical and lateral dynamics, comparing acceleration values with the Unloading and Nadal derailment criteria. The parametric study is comprised of a set of five representative single-track slab bridges with spans between 10 m and 30 m with two levels of track irregularities, corresponding to a well-maintained track and an Alert limit situation. A three-dimensional articulated FE model based on the load properties of the EN 1991-2 High-Speed Load Model A is presented, crossing the bridges at running speeds from 150 km/h to 400 km/h. Despite the complexity of the models, a large amount (1461) of full 3D train–track–bridge interaction dynamic analyses are performed, to produce a data set representative of the phenomenon. Results show a weak correlation between the criteria and deck acceleration (maximum r^2 of 0.47 for Unloading and 0.15 for Nadal). Additionally, track quality is shown to be a more conditioning factor for derailment when compared to resonance. This work contributes to discussing the thesis of using deck acceleration as an indicator of running safety, considering lateral dynamics.

1. Introduction

The design of civil engineering structures is governed by norms that ensure safe practices and standard construction. The Eurocodes are essential tools used daily across Europe, but they are not impermeable to change, as they are frequently discussed and are currently under revision [1]. Railway infrastructures are, in many ways conditioned by these norms, and railway bridges are no exception. The abundance of these structures (there are an estimated 300,000 in Europe [2]) makes the study of running safety an extensively studied topic in recent years [3–5].

Concerning the dynamic assessment of running safety, the current European code EN 1990 A2 [6] stipulates a deck acceleration criterion to ensure traffic safety on railway bridges. According to this Eurocode, the vertical deck acceleration on ballasted bridges should be limited to 3.5 m/s^2 to avoid ballast instability, while in non-ballasted ones, the limit is slightly higher, 5 m/s^2. Identical values can be found in the Chinese norm [7], albeit the calculation of derailment indexes is often required [3]. A different approach can be found in the Japanese norm [8], where safety is assessed by limiting deflection according to the number of spans, running speed, and track type. As for the origin of the aforementioned values, the ballasted track limit is based on the tests performed at the German Federal Institute for Materials Research and Training (BAM) in which the track instability occurred for accelerations from 7 m/s^2, commissioned by the European Rail Research Institute [9] to validate the then European pre-standard (ENV). Conversely, the non-ballasted track limit is likely based on the fact that the wheel may detach from the rail from accelerations of 1 g. In fact, when [10] replicated the BAM tests, they noted that the ballastless track's limit had not been proofed either numerically or experimentally.

Comparing these values to the limits inscribed in the norm, it seems like a safety factor equal to 2.0 was adopted to guarantee a safety

* Corresponding author.
E-mail address: gcferreira@fe.up.pt (G. Ferreira).

https://doi.org/10.1016/j.engstruct.2024.118127
Received 10 February 2024; Received in revised form 9 April 2024; Accepted 26 April 2024
Available online 28 May 2024

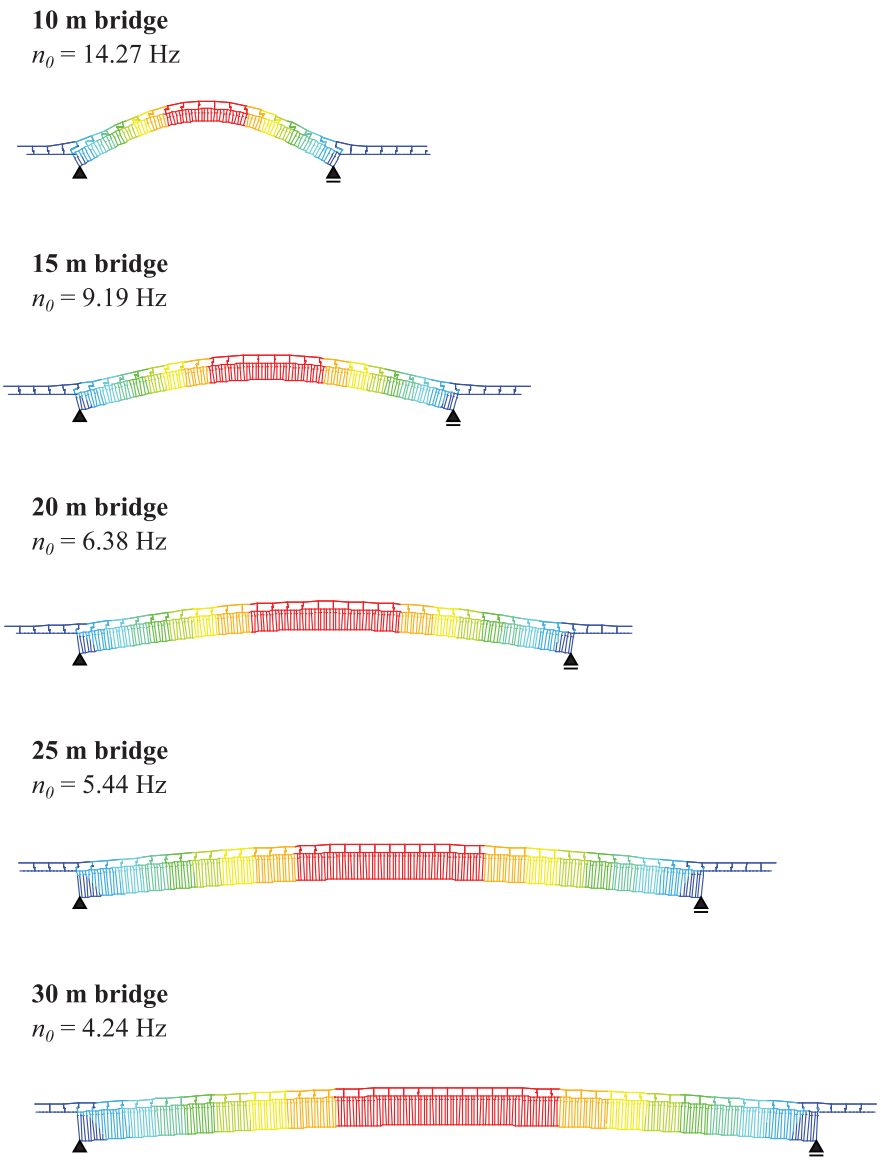

Fig. 1. Bending modes of the FE bridge models.

margin. However, the validity of such a margin was not originally based upon a probabilistic method, which has led to the proposal of alternatives [11] and studies that give a certain percentage allowance over the limit [12]. In fact, while the limit for ballasted tracks is connected with a physical phenomenon, the limit for ballastless (or slab) tracks is seemingly based on the assumption that a train experiencing accelerations upwards of 1 g on a bridge is at risk. Yet, preliminary studies showed that, for the particular case of non-ballasted bridges, when the deck acceleration reaches 1 g, it does not necessarily lead to wheel detachments [13], i.e. the fact that a point is subjected to 1 g acceleration does not imply the lifting of the entire train's mass. Therefore, it is important to define recommendations to define a more accurate design criterion based on advanced train–track–bridge interaction (TTBI) simulations that can explicitly assess the risk of derailment and ensure traffic safety. The track itself exerts influence since, as [14] note, neglecting the rails can lead to an underestimation of results at high speeds and the level of track irregularities is connected with the derailment coefficient [15].

Other studies on the performance of high-speed ballastless track bridges have focused on dynamic assessment, such as [16] finding deck accelerations above the normative limit on shorter spans. Contributions have also been made to the evaluation of deck acceleration, with [17] and [18] focusing on the effects of local deck vibrations, or [19] and [20] proposing faster computational methods. Different authors have also approached the safety of ballastless bridges under seismic actions [21–24], while the previously mentioned research [13] did not consider the lateral dynamics in the train–bridge interaction analysis, and focused solely on vertical dynamics. Other studies on ballastless bridges addressed the issues caused by settlement in subgrade-bridge transition zones [25,26] and running comfort [27]. Since the mechanics that govern wheel–rail contact (and, by extension, the loss of contact and derailment) are complex and also depend on lateral components, this work proposes to study the risk of derailment considering three-dimensional TTBI models with the purpose of comparing derailment criteria against calculated deck acceleration values to make a critical analysis of the traffic stability criteria stipulated in EN1990-A2 that has been questioned lately by the regulatory bodies [28] and addressed in recent EU research projects [29]. To overcome the gaps, the following research questions are presented:

1. Do deck acceleration values above the normative limit correspond to derailment?
2. Are both lateral and vertical dynamics indispensable to assess running safety or do vertical dynamics suffice?

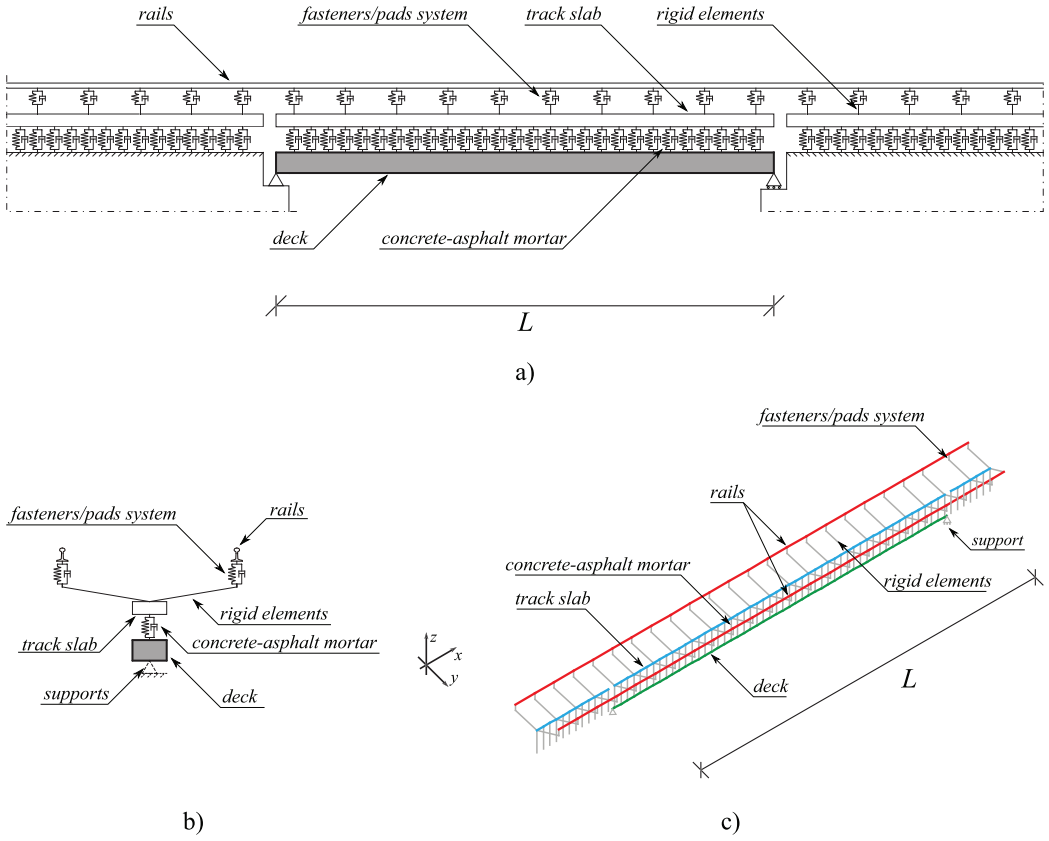

Fig. 2. Finite element model. (a) Schematic representation (lateral); (b) Schematic representation (transversal); (c) 3D view.

3. How important is the influence of track quality, compared with the deck vibrations reached in resonance?

To properly address these questions, the present paper describes a set of bridges, train models, and irregularity profiles in Section 2. This is followed by a statement of the parametric analyses in Section 3, along with a presentation of the safety indexes employed and the critical train models for each bridge. Section 4 shows the results and discussion of the parametric analyses, including the study of increased irregularity profiles and the influence of the bridge. The main conclusions are listed in Section 5.

2. Numerical modelling

2.1. Bridge models

For the present study, the bridges' characteristics were obtained from the work by [30] where, for simply supported single-span slab bridges, five models are proposed, with spans ranging from 10 m to 30 m and cross-sections designed to provide results near the Eurocode's acceleration limit when considering a design speed of 320 km/h (and consequently a maximum speed of 1.2×320 km/h, as per the EN 1991-2 [31]). In the present work, the cross-sectional dimensions were obtained considering an elasticity modulus of 34 GPa and a Poisson's ratio of 0.2. The 3D models were developed with the Finite Element Method (FEM) using the commercial software ANSYS [32], using mainly BEAM188 Timoshenko beam elements to model the deck, the track slab and the rails and COMBIN14 spring–dashpots to model the track elements, namely the mortar bed between the deck and the track slab, the subgrade bed in the adjacent track to the bridge and the rail fastenings. The bridge deck is modelled with beam elements located at its centre of gravity. From there, the track slab (which is also comprised of beam elements) is connected with an array of spring–dasphot elements that discretize the concrete-asphalt (CA) mortar bed. Above the slab, pairs of rigid elements reach the transversal coordinates of the rails, connecting to them through spring–dasphot elements that represent the fasteners and pads. The track slab is made up of modular sections, with gaps at the abutments. The properties of these bridges are presented in Table A.3, including the span L, linear mass m, stiffness EI, the natural frequency of the first bending mode n_0, cross-sectional width b and height h. Damping is taken into account through the Rayleigh proportional matrix with damping ratios (taken from EN 1991-2 [31] for all cases) set to the first two vertical bending modes of the bridge deck. Regarding the track elements, their vertical mechanical properties (stiffness and damping) were adopted from [13], while the lateral and longitudinal characteristics were adopted from previous 3D TTBI models developed by the authors [33–35]. The properties of the slabs and UIC60 rails (density ρ, modulus of elasticity E, area A, moment of inertia I, height h, width b, and gauge) are listed in Table A.4 and the properties of the fasteners and elastic bed in Table A.5. While the deck and track slab's properties can be reduced to single beams, to enable the coupling of a three-dimensional vehicle model, each rail has to be modelled separately, thus justifying the configuration of rigid elements that can be seen in the same figure. The finite element models were developed in ANSYS [32] software, and are represented by a characteristic 3D view. The first vertical bending modal shapes and frequencies of each bridge can be seen in Fig. 1 and a schematic representation of the typical FE model is shown in Fig. 2.

2.2. Train models

For loading, this study uses 3D vehicle models aimed to represent the EN 1991-2 [31] High-Speed Load Model A (HSLM-A), which is a moving load model with axle distances and loads whose geometric configuration resembles articulated trains, without any suspension or vehicle body data. The relevant information regarding vertical dynamic behaviour was retrieved from [13], for each of the 10 HSLM-A trains,

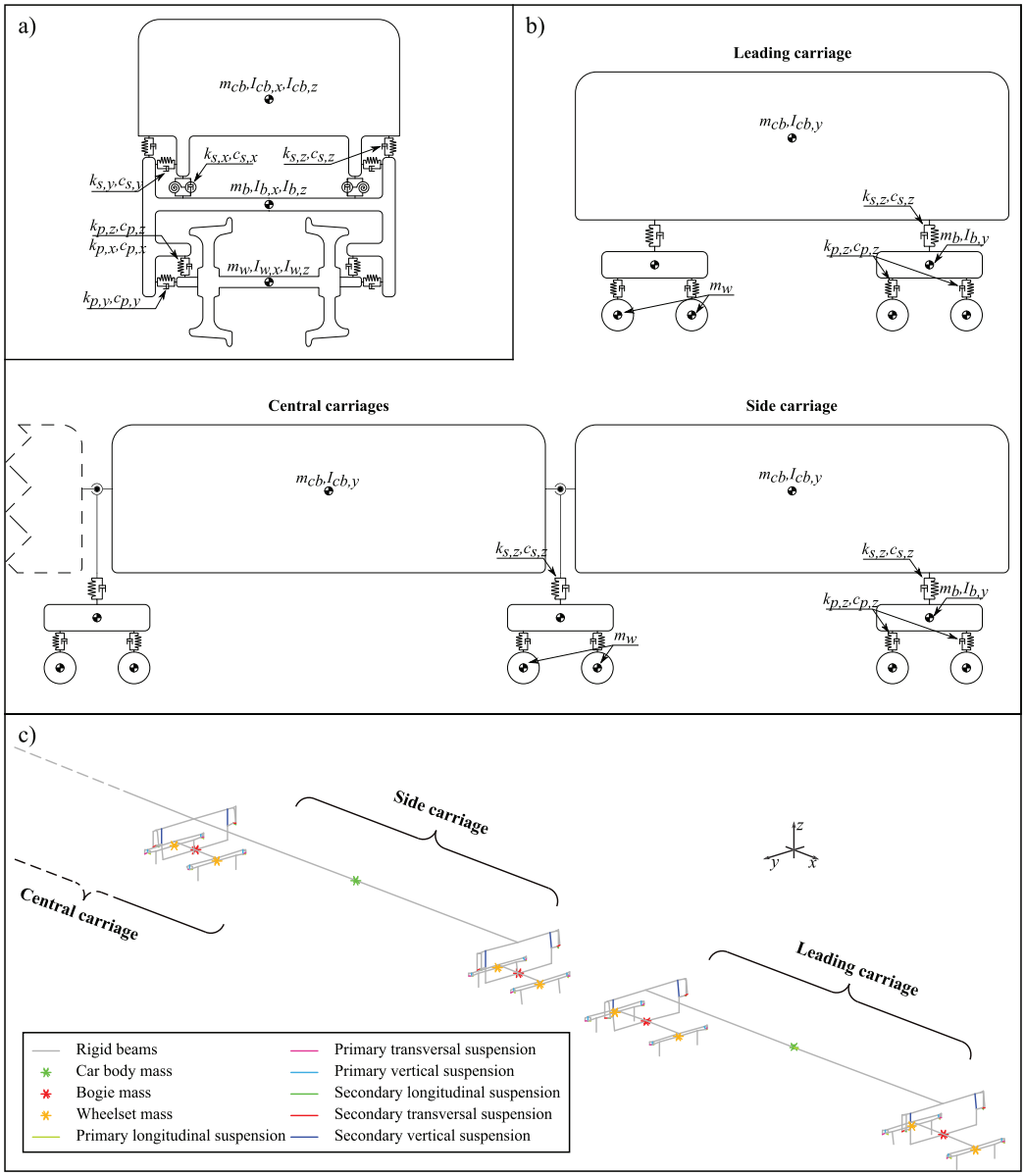

Fig. 3. Train model. (a) Schematic representation (lateral view); (b) Schematic representation (front view); (c) FE model.

where the authors adjusted the car body masses to correspond to the axle loads (ranging from 17 to 21 ton/axle) and the primary and secondary suspensions characteristics produce realistic bounce frequencies. In contrast, the lateral and longitudinal suspensions were adopted from typical three-dimensional trains found in the literature [36,37]. Table B.6 lists the symbols used to describe the train model parameters and a thorough list of the values can be consulted in Appendix B.

The 3D FE models were developed in the ANSYS [32] commercial software, using three of its available finite element types: BEAM4 (3D elastic beam) to act as rigid beams, COMBIN14 (3D spring–damper) to model the suspension parameters and MASS21 (3D structural mass) to model all localized masses and rotational moments of inertia. Each wheelset is connected to a primary suspension linked to the bogie via rigid beams. The bogies are connected to a secondary suspension that is in turn linked to the geometric centre of the car body. The HSLM is characteristically comprised of a leading carriage (with two bogies, independent from the rest of the train), a side carriage (with an independent bogie and a shared bogie) and a succession of central carriages that share bogies in the manner of an articulated train. The load model is symmetrical; therefore, the last central carriage shares a bogie with another side carriage, which is followed by the final leading carriage. It is highlighted that the HSLM is a load model and not an actual train, presenting the challenge of articulating the central carriages in the FE model. In the present work, the solution achieved was to connect the secondary suspension to one of the carriages and then to couple the translational degrees of freedom of that suspension and the following carriage, allowing for free rotation in every axis, effectively modelling a spherical joint. This approach is sufficient to analyse lateral and vertical forces at the level of the wheels, which is the intended purpose of the study. Fig. 3 depicts lateral and front views of a schematic representation of the train model, as well as the FE implementation.

2.3. Track irregularities

The track irregularity profiles employed in the present work were artificially generated based on the German Power Spectral Density (PSD) functions procedure described by [38], where the irregularities

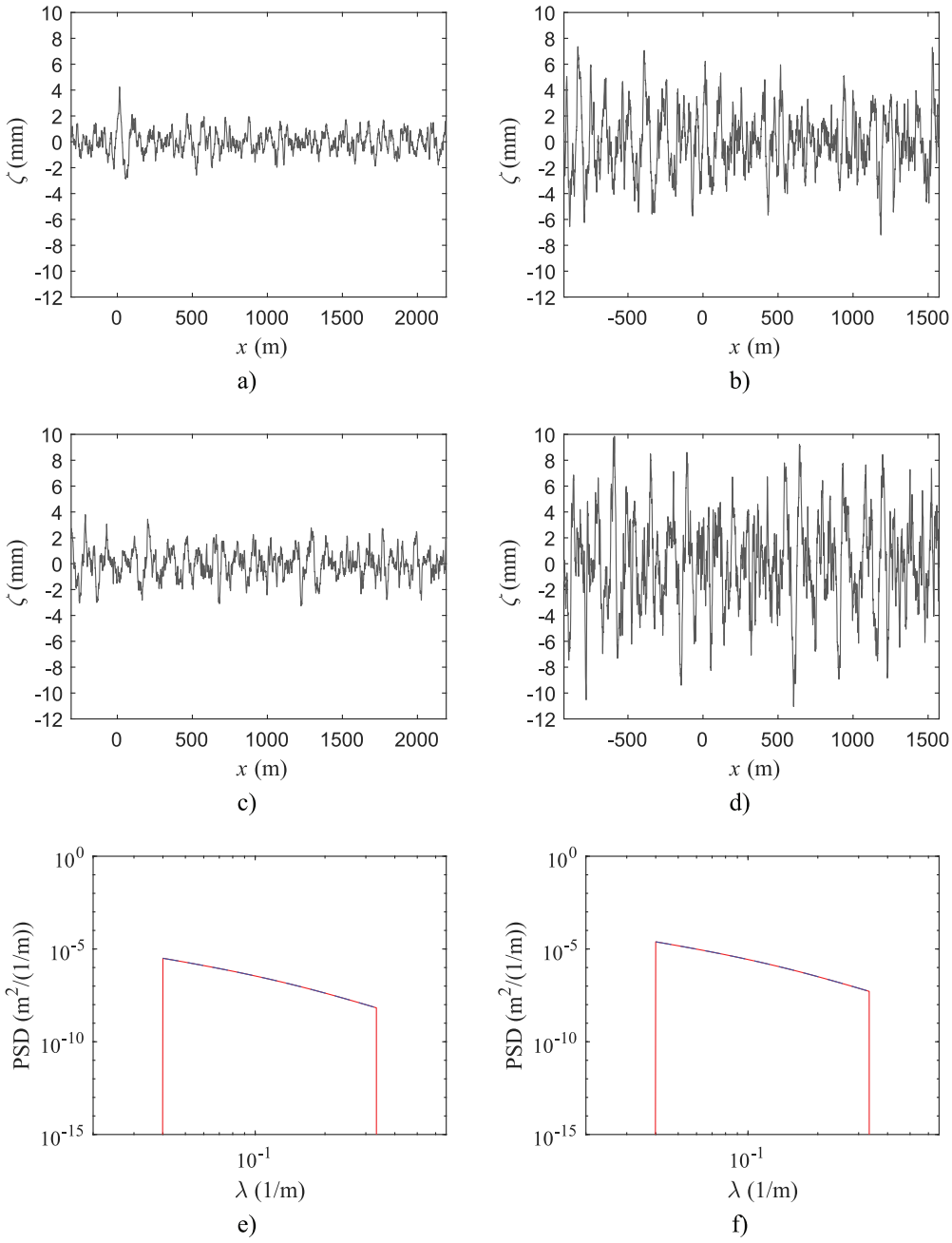

Fig. 4. Example realization of tracks' irregularities in the vertical direction: (a) Well-maintained track, (b) Alert limit; lateral direction: (c) Well-maintained track, (d) Alert limit. PSD of the alignment irregularities: (e) Well-maintained track, (f) Alert limit.

r along the longitudinal development x are given by:

$$r(x) = \sqrt{2} \sum_{n=0}^{N-1} A_n \cos\left(\Omega_n x + \varphi_n\right) \tag{1}$$

where N is the number of frequencies Ω_n, φ_n is a random phase angle between 0 and 2π and A_n are factors given by the same study.

The wavelength interval 3–150 m was considered in the generation, which includes the D1 (3–25 m), D2 (25–70 m) and D3 (70–150 m) ranges specified in [39]. Two track quality levels were considered:

(i) a lower track quality whose track quality factors for longitudinal (vertical) and alignment levels were $A_v = 6.00 \times 10^{-7}$ and $A_a = 2.70 \times 10^{-7}$, to obtain standard deviations in the D1 range compatible with the Alert Limit specified in [39] for speeds up to 300 km/h of $\sigma_{3-25,v}$ equal to 1.25 mm and $\sigma_{3-25,a}$ of 0.85 mm for the longitudinal and alignment profiles, respectively;

(ii) a higher track quality, with track quality factors of $A_v = 0.60 \times 10^{-7}$ and $A_a = 0.35 \times 10^{-7}$, respectively, giving $\sigma_{3-25,v}$ equal to 0.40 mm and $\sigma_{3-25,a}$ of 0.30 mm, compatible with a well-maintained track of the Chinese PSD [40].

Plots of example realizations of tracks' irregularities can be seen in Fig. 4 for both quality levels in the lateral and vertical directions, as well as the alignment PSD.

2.4. Train bridge interaction

The 3D TTBI dynamic analyses are carried out with the in-house software "VSI — Vehicle Structure Interaction Analysis" (see Fig. 5). This tool, capable of dealing with lateral dynamics, is implemented in MATLAB [41] and imports the structural matrices from the railway vehicle and bridge modelled in the FE package ANSYS [32]. Then,

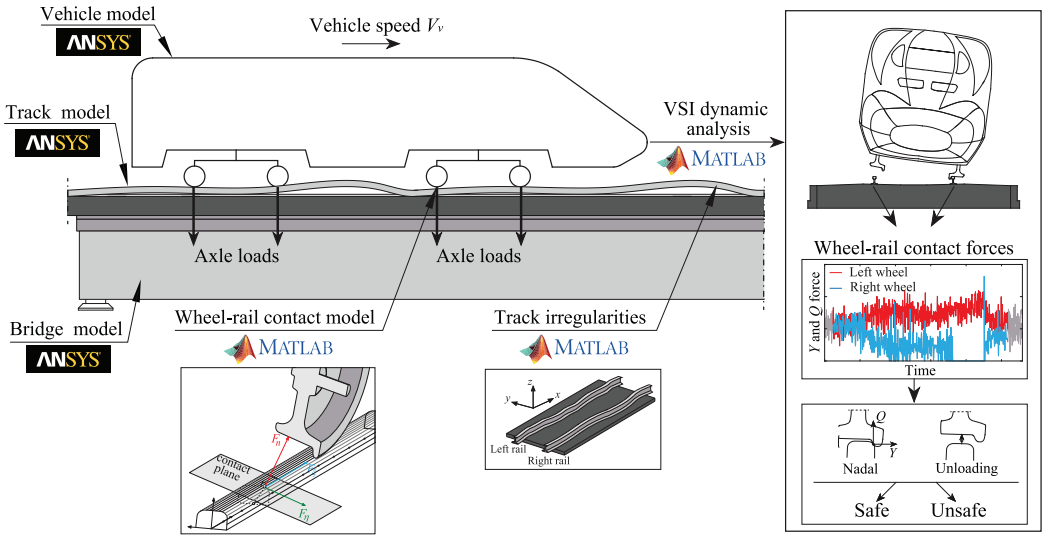

Fig. 5. Framework of the tool for 3D TTBI dynamic analysis.

the external excitations (track irregularities, wind or seismic loads, among others) are imposed on the coupling system, and the corresponding dynamic responses are obtained. The interaction between the two sub-systems is accomplished by a specially developed contact finite element that considers the behaviour of the contact interface between wheel and rail. The contact formulation is divided into three main problems, namely the geometrical, the normal and the tangential contact problems. With the contact interface fully characterized, the equations of motion of the vehicle and bridge are complemented with constraint equations that couple these two structural systems. The full mathematical formulation and validation of the TTBI model are presented in previous publications [33,42–44], where the description of the wheel–rail contact model and the governing equilibrium equations of the dynamic system can be consulted.

3. Running safety analysis

3.1. Initial consideration

A parametric study has been performed for a set of 5 single-track slab bridges with spans ranging between 10 m and 30 m with trains running at speeds ranging between 150 km/h and 400 km/h. For each analysis, the maxima of the derailment indicators (Unloading and Nadal) and the maximum deck acceleration at midspan were registered. Only the most critical HSLM-A train for each bridge, i.e., the train that conditions the bridge design in terms of deck acceleration in the speed range, is considered in the analysis.

To complete this study, 1461 3D train–track–bridge interaction dynamic simulations were conducted using the numerical tool developed and validated by [42]. This corresponds to the 5 bridges being tested with 11 different irregularities profiles (5 realizations of a higher quality track, 5 of lower quality track and 1 smooth track profile) with trains running at 26 speed values (10 km/h intervals of the speed range), accounting for 1430 analyses. Given that the resulting derailment indexes were within the safety limits, 10 additional profiles were generated, with track irregularities increased above the normative Alert limit. Finally, a comparison with a rigid bridge is made, with 21 more analyses.

3.2. Running safety indexes

There are several criteria that can be used to assess train running safety, varying according to derailment mechanism and country. These criteria (for which a summary can be found in [3]) are based on relationships between the wheel–rail contact forces that can only be accessed through TTBI models.

Among the available derailment criteria, the two used in the present study (Nadal and Unloading) are two of the most commonly used in the analysis of train running safety. The Nadal index ξ_N can be obtained through the following equation:

$$\xi_N = \frac{Y}{Q} \tag{2}$$

where Y and Q are the time histories from the lateral and vertical contact forces, respectively, in each wheel. The European Technical Specifications for Interoperability [45] specified a safety limit of 0.8 for this index. Regarding the unloading index ξ_U, this can be defined as:

$$\xi_U = 1 - \frac{Q}{Q_0} \tag{3}$$

where Q_0 is the wheel's static load. The criterion may also be analysed individually for each wheel. The European norm related to the testing and simulation of railway vehicles, EN 14363 [46], stipulates a limit of 0.6 for the unloading index. According to the same norm, before computing the aforementioned derailment criteria, the time histories of both vertical and lateral contact forces should be low pass filtered with a cut-off frequency of 20 Hz using a filter of order 4. In the present study, a Butterworth filter was adopted. Henceforth, the limits for the Nadal and Unloading criteria, as well as the acceleration limit, are referred to respectively as N_{lim}, U_{lim} and a_{lim}.

3.3. Selection of critical train model

As mentioned before, only the most critical HSLM-A train for each case study bridge has been considered in the study. A simple moving loads method, applicable to single span simply supported bridge, was employed for this assessment, using the quantities listed in Table A.3 and the load values and distances of the HSLM-A. The maximum midspan acceleration a is estimated accounting for the resonant effects that occur due to the relation between the repeatability of the loads and the bridges' natural vibration frequencies. Each line of the graphics in Fig. 6 corresponds to the maximum acceleration obtained from the response of each of the HSLM-A trains at different speeds on each bridge. The HSLM-A universal train (represented in blue) that causes an acceleration that exceeds the EN 1990-A2 [6] limit of 5 m/s^2 (at around 1.2×320 km/h) was chosen as the critical one for the bridge at matter.

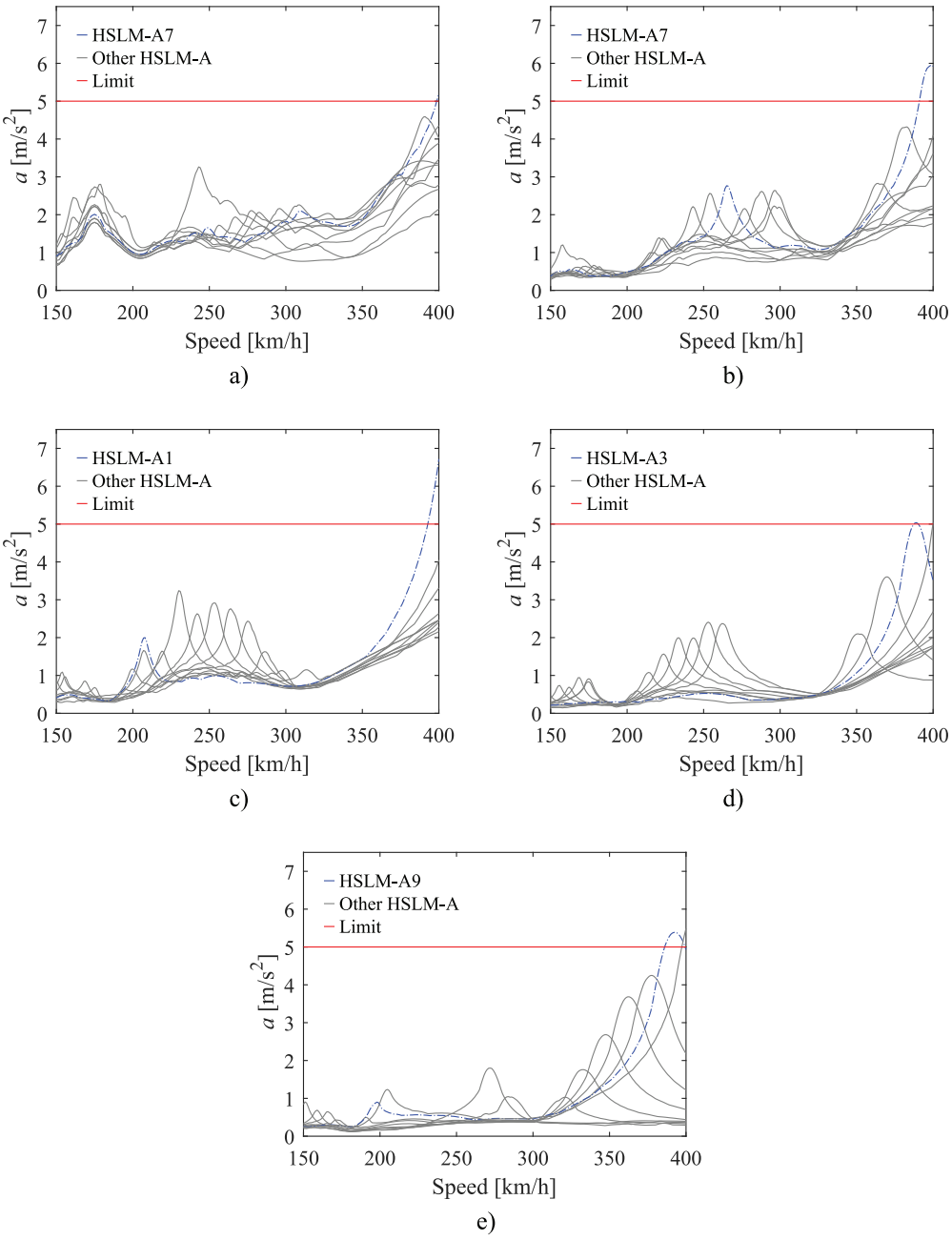

Fig. 6. Maximum midspan deck acceleration and identification of the most critical HSLM-A train. (a) 10 m bridge; (b) 15 m bridge; (c) 20 m bridge; (d) 25 m bridge; (e) 30 m bridge. (For interpretation of the references to colour in this figure legend, the reader is referred to the web version of this article.)

4. Simulation results and discussion

4.1. General 3D analyses

The results of the parametric analyses presented in Section 3.1 are presented hereinafter. Fig. 7 depicts the envelopes of the maximum registered Unloading criteria, while the Nadal envelopes are presented in Fig. 8. The displayed data points of the computed derailment criteria correspond, for each speed, to the worst-performing wheelset (while still on the bridge) of that particular simulation. The acceleration values can be seen in Fig. 9, with each value representing the maximum absolute acceleration in the midspan of the bridge's deck.

For a smooth track profile (i.e. with no vertical nor lateral rail irregularities imposed on the system), the Nadal criterion measures no distinguishable features. Due to the absence of lateral irregularities and other sources of transversal instability, this behaviour is expected, serving as a benchmark for the results. In fact, the vertical acceleration curves for smooth tracks show similarities to the moving loads assessment in both absolute value and location of resonance.

Concerning the track irregularities, either with high or low quality (alert limit level), the maximum values of ξ_U increase with speed, but the general shape of their trends remains the same (Fig. 7). The same conclusion can be drawn from the accelerations' results. It is noteworthy that the Unloading criterion curves rise as the speed approaches 400 km/h, but they also show a less evident, yet present, peak around the subharmonic speeds.

In general, it is observed that ξ_N is unaffected by resonance phenomena, never following the trend of the acceleration or Unloading

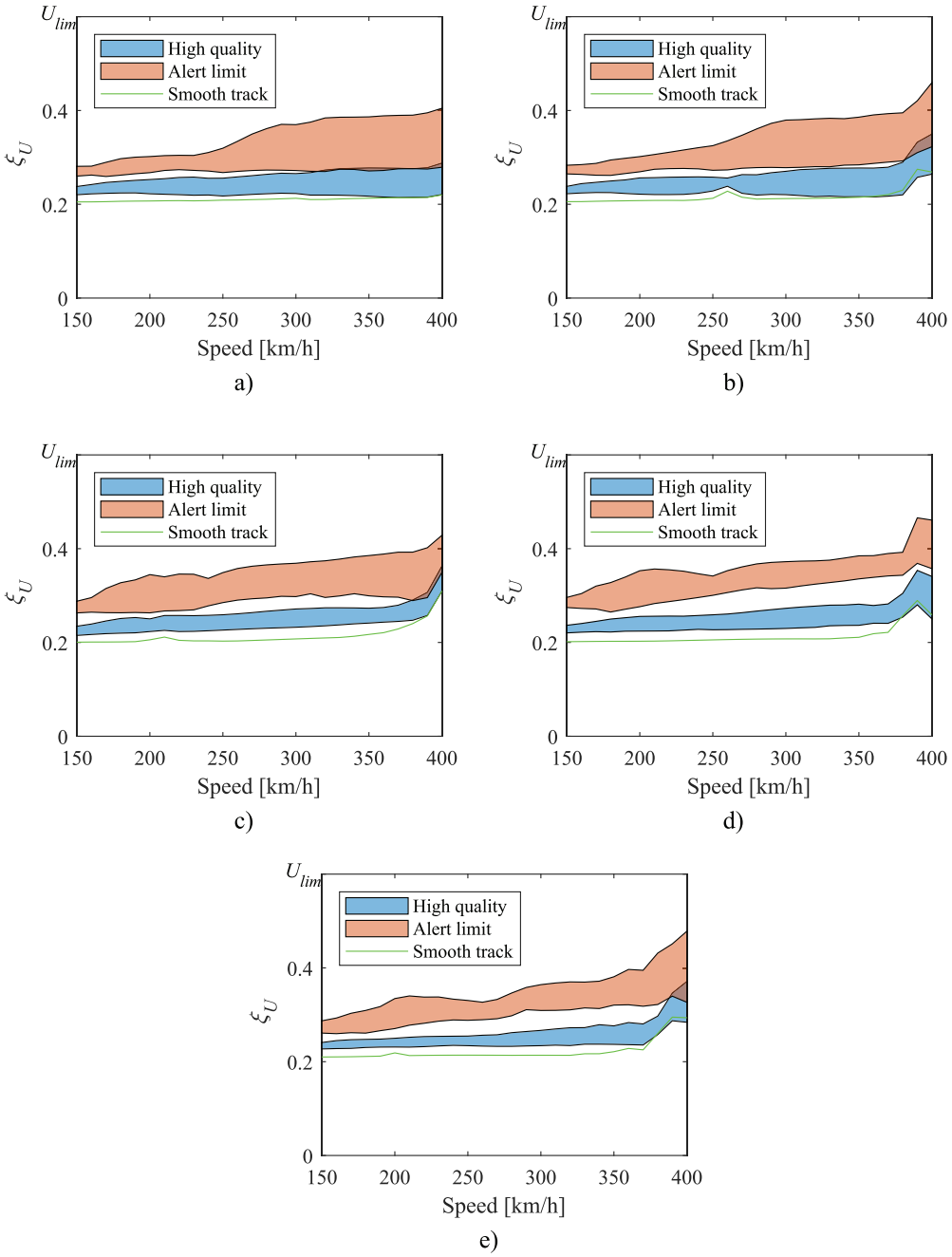

Fig. 7. Unloading criterion envelopes. (a) 10 m bridge; (b) 15 m bridge; (c) 20 m bridge; (d) 25 m bridge; (e) 30 m bridge.

curves but instead reflecting only the level of track condition (Fig. 8). As the irregularities (including lateral) on the tracks get more prevalent, lateral forces become more present in each wheel, while vertical contact forces get diminished, thus increasing the criterion's values. However, even in scenarios of low-quality tracks (with alert limit irregularity profiles), the Nadal criterion remains fairly low and distant from its limit of 0.8.

The maximum registered vertical acceleration for each bridge is registered in Table 1 for the high-quality track realizations and in Table 2 for the alert limit irregularity profiles (Fig. 9). Both tables present the two concomitant criteria, i.e., the maximum value of the worst-performing wheelset that stems from the realization of rail irregularity leading to the maximum acceleration. From the observation of these results, there appears to be no correlation between acceleration levels above the normative limit of 5 m/s^2 and derailment indicators. Considering, for example, the worst-case scenario of track condition, an assessment based on the normative limit would conclude that the acceleration limit is surpassed. However, the maximum value of the unloading factor, in that case (for all studied bridges), is below 0.38 for high-quality tracks and 0.48 for alert limit tracks, which is far from the limit of 0.6. Therefore, since deck acceleration does not seem to condition derailment at such low values, the results do not support the thesis of safety being limited by the calculation of vertical deck acceleration.

The existence of a correlation (or lack thereof) between acceleration and derailment indicators can be further explored by plotting all the pairs of data points and fitting a linear regression. This is presented in Fig. 10(a) for the high quality track realizations and in Fig. 10(b) for

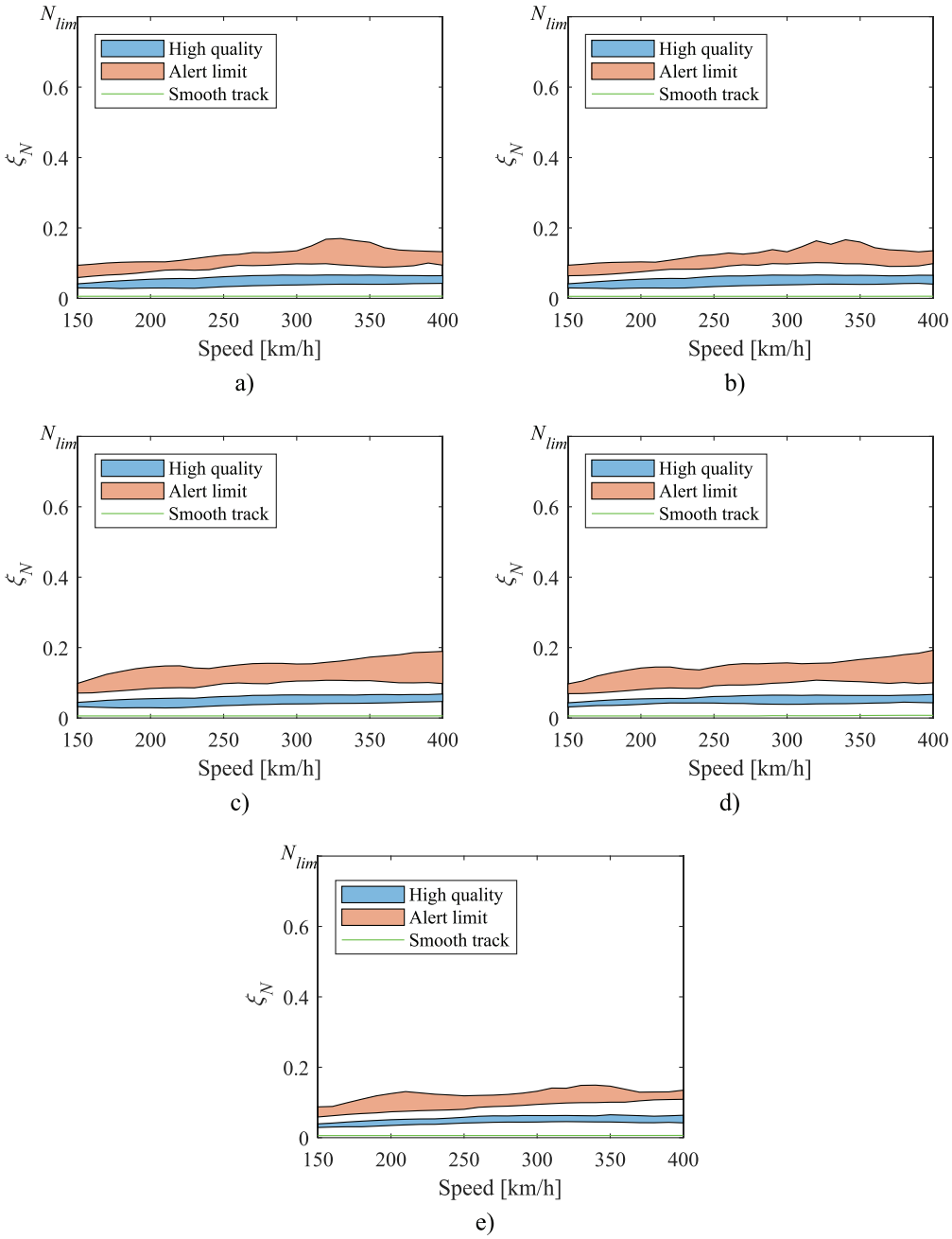

Fig. 8. Nadal criterion envelopes. (a) 10 m bridge; (b) 15 m bridge; (c) 20 m bridge; (d) 25 m bridge; (e) 30 m bridge.

Table 1
Maximum registered acceleration and concomitant criteria (high quality).

		Criteria	
Bridge	Max. accel. (m/s^2)	Unloading	Nadal
10 m	5.93	0.25	0.04
15 m	7.30	0.26	0.07
20 m	7.70	0.36	0.07
25 m	6.43	0.30	0.06
30 m	6.09	0.29	0.06

Table 2
Maximum registered acceleration and concomitant criteria (alert limit).

		Criteria	
Bridge	Max. accel. (m/s^2)	Unloading	Nadal
10 m	7.18	0.28	0.10
15 m	8.30	0.38	0.13
20 m	8.76	0.39	0.10
25 m	7.35	0.37	0.12
30 m	7.59	0.36	0.11

the Alert limit tracks, with the continuous black lines representing the fitted models. The displayed coefficients of determination (r^2) show, for both cases, that the Unloading criterion is the one that follows acceleration the closest. Even so, the relation is insufficient to infer safety conditions from analysing acceleration alone, for several data points above the acceleration limit do not cross U_{lim}. This observation is even more evident when considering lateral forces for derailment, i.e. acceleration values from close to 0 m/s^2 to almost 8 m/s^2 hardly

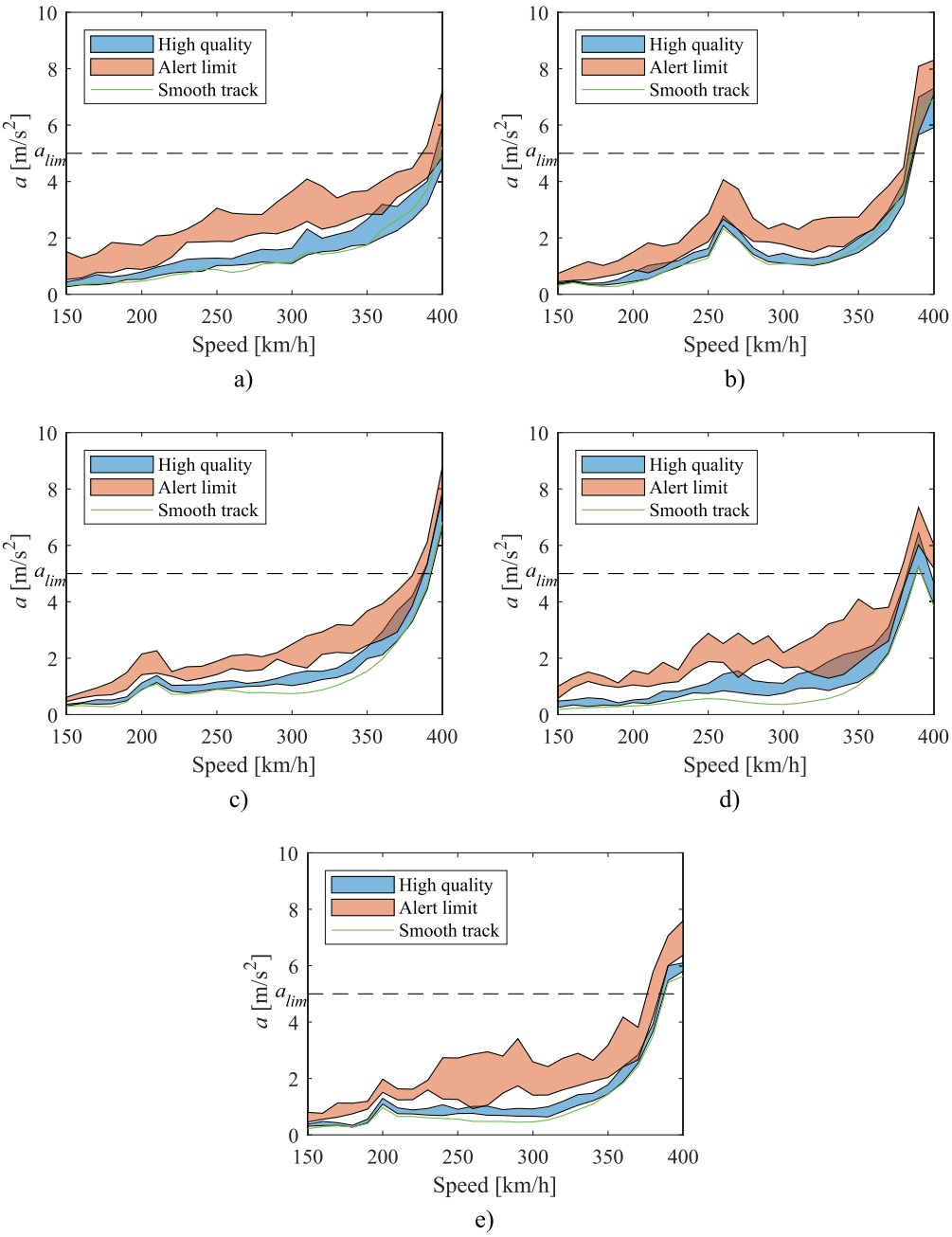

Fig. 9. Acceleration envelopes. (a) 10 m bridge; (b) 15 m bridge; (c) 20 m bridge; (d) 25 m bridge; (e) 30 m bridge.

translate into any ξ_N values. It is also noteworthy that the gap between the criteria's r^2 values is narrower for the worst track conditions, which highlights the importance of the level of irregularities.

4.2. Analysis with track irregularities increased above the normative Alert limit

Results from the previous section have shown that even at resonance, the derailment criteria are distant from their limits. While deck acceleration is sensitive to both running speed and track condition, the Nadal and Unloading criteria are less influenced by the bridge's dynamic effects. To further sustain this observation, an additional set of dynamic analyses was devised. These included generating new realizations of track irregularities, increasing both the vertical and alignment standard deviations in the 3 to 25 m wavelength range, totalling 10 new profiles: 5 with a 50% increase over the alert limit ($\sigma_{3-25}\times 1.5$) and 5 with 100% increase ($\sigma_{3-25}\times 2$). This set of analyses was conducted on the 25 m bridge, with the HSLM-A3 model at 390 km/h, since this combination provided the clearest resonant situation.

Fig. 11 presents the results from the increased irregularities simulations as boxplots superimposed on zoomed-in sections of Figs. 7(d), 8(d) and 9(d). These figures allow for a comparison of 5 scenarios: smooth track, high quality track, alert limit, 50% increase of the alert limit and 100% increase. It can be seen that there is a direct relation between a worse track and higher derailment criteria: maximum values registered

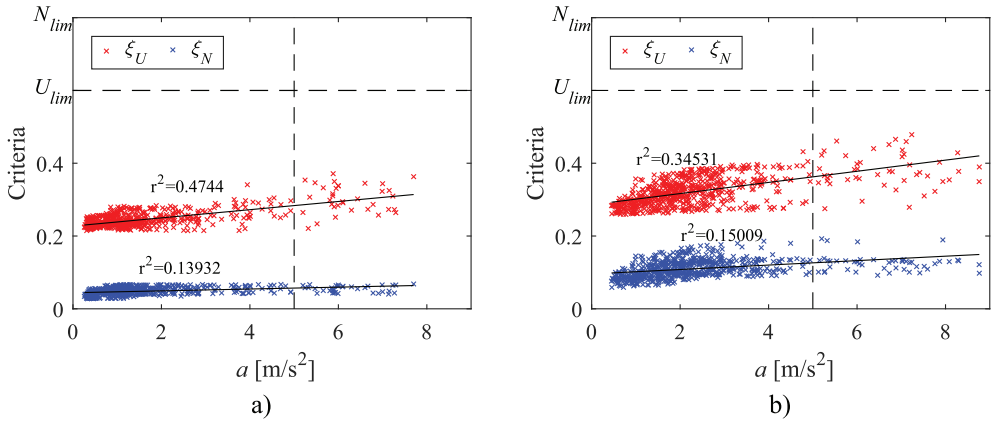

Fig. 10. Relation between acceleration and derailment criteria (all bridges, every speed). (a) every realization of a high quality track; (b) every realization of an Alert limit track.

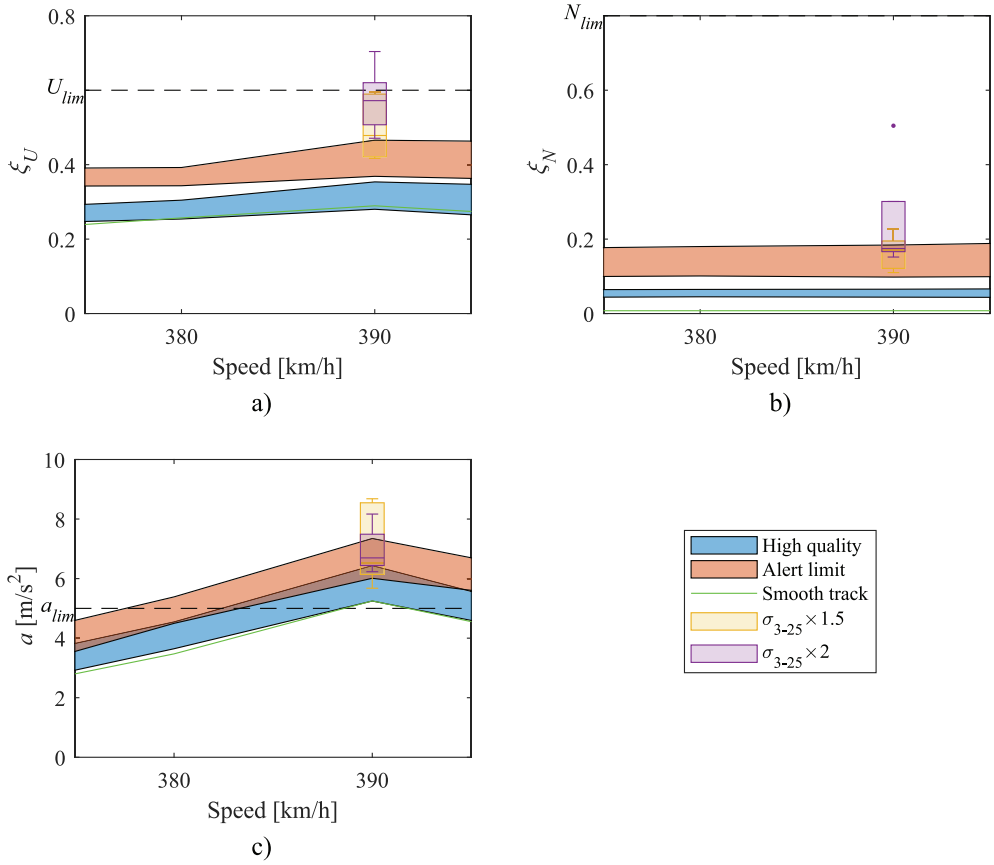

Fig. 11. Criteria for increased irregularities (25 m bridge). (a) Unloading; (b) Nadal; (c) Acceleration.

include 0.704 for Unloading and 0.505 for Nadal. As for acceleration, a maximum value of 8.168 m/s^2 is measured.

The results presented strengthen the observation that derailment criteria, compared to deck accelerations, are more permeable to track conditions. It was necessary to increase Alert limit conditions up to double the standard deviation to register ξ_N values above 0.5 and ξ_U values greater than U_{lim}. On the other hand, acceleration was already greater than the normative 5 m/s^2 limit, even for a smooth track. Worsening the irregularity profiles increased the maximum acceleration, but it is worth noting that there is far more overlapping of the different realizations' results on acceleration when compared to the derailment criteria, i.e. track condition plays a less relevant part in determining deck acceleration.

4.3. Influence of the bridge vibration

From both the general analyses and the increased irregularities analyses, it can be inferred that track condition constitutes the predominant factor in assessing running safety. Even though the occurrence of resonance is relevant for deck acceleration, vibration from the bridge

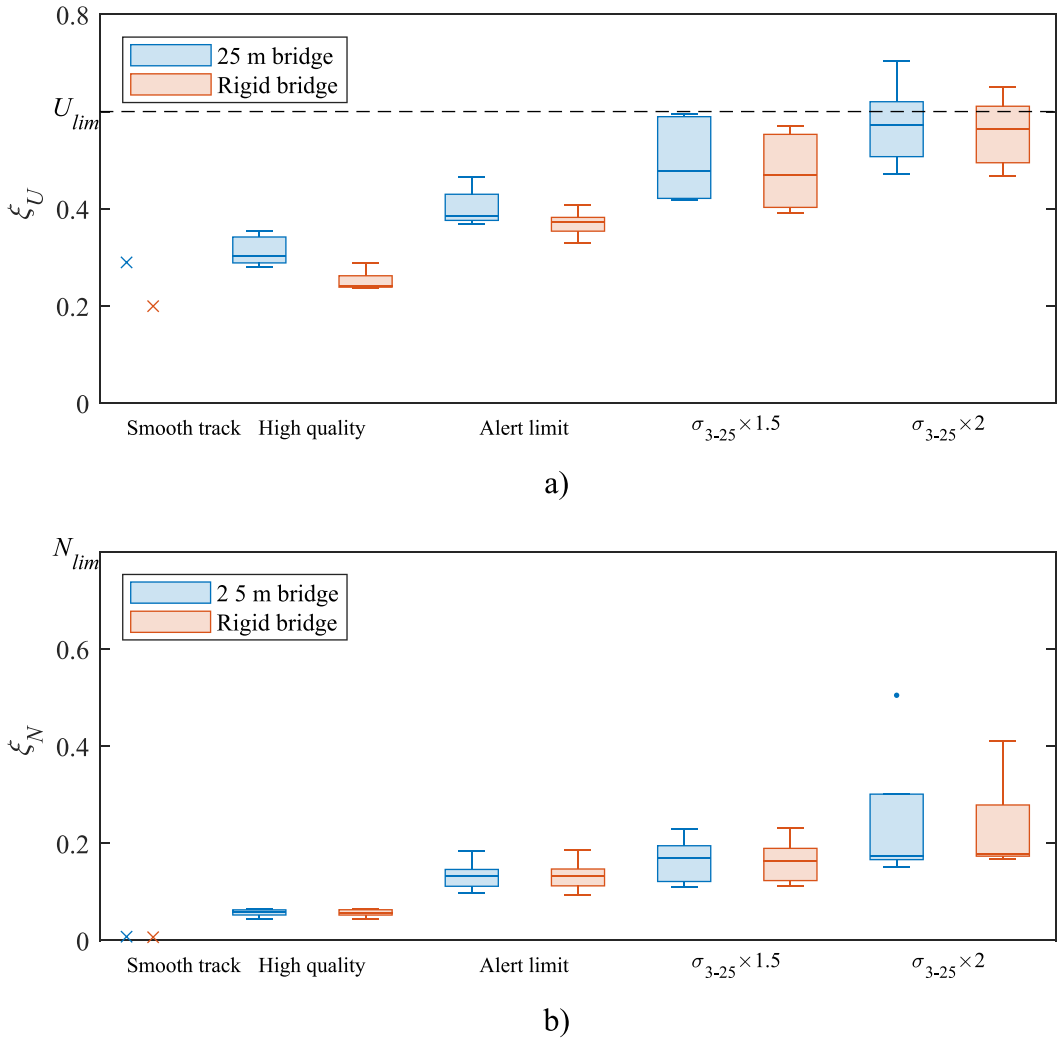

Fig. 12. Influence of the bridge vibration. (a) Unloading criterion; (b) Nadal criterion.

seems to have an imperceptible effect on the variation of wheel–rail contact forces, and, therefore, on the derailment criteria. For this reason, the present section presents the results of additional dynamic analyses of the same critical load model and speed as of the 25 m bridge, replacing it with a rigid bridge. These simulations considered the 21 available profiles, i.e. the same employed in the previous section. Fig. 12 presents the distribution of results regarding the Unloading and Nadal criteria, respectively.

The results indicate that whether or not considering the bridge's dynamic effects, the performance of derailment indicators is controlled by track condition. As quality decreases, so does the influence of the bridge vibration. To assess the fitness of using just the plain track model as a predictor (ξ_U^* and ξ_N^*) of the criteria, the sums of squared errors can be computed (using all available realizations) as:

$$\sum_{i=1}^{21}\left(\xi_U-\xi_U^*\right)^2=0.0419 \tag{4}$$

$$\sum_{i=1}^{21}\left(\xi_N-\xi_N^*\right)^2=0.0092 \tag{5}$$

Given that the scale of the criteria is between 0 and 1, the fact that the sums of squared errors are lower than 1% makes them negligible. It can be concluded that regardless of the train model being subjected to bridge vibration, the relation between contact forces is already conditioned by the track quality.

5. Conclusion

The present study addressed the pertinence of utilizing an acceleration limit as a conditioning factor for the dynamic design of railway bridges. Multiple realizations of two track quality levels were tested on a wide range of running speeds, for five different bridges with train models representative of the HSLM-A. A comparative analysis of increased irregularities, as well as of the influence of the bridge vibration under resonance, was also presented, to further sustain the observations. Referring to the research questions listed in Section 1, the main conclusions of this work can be outlined as follows:

1. Ballastless railway bridges can experience acceleration values above the normative limit of 5 m/s^2 without corresponding to a surpassing of derailment criteria, which does not support the thesis of using deck acceleration as a limiting factor for running safety.
2. Even though both the Unloading and the Nadal criteria present a low correlation with acceleration, the former does indicate a closer relation. Vertical dynamics are, therefore, indispensable in assessing train running safety and the Unloading criterion is conditioning in regular operation scenarios. 3D analyses should be considered in scenarios where important lateral loads may contribute to the lateral instability of the train.
3. Across different running speeds, the Nadal criterion is shown to be close to constant, depending on the track quality, with the Unloading criterion being slightly more telling of the occurrence of

Table A.3
Properties of the simply supported slab bridges used in the 3D TTBI analysis.
Source: Adapted from [13].

L (m)	m (ton/m)	EI (GN m^2)	n_0 (Hz)	b (m)	h (m)	Slenderness ratio[a]
10	15.4	12.5	14.3	8.1522	0.6426	481.9
15	21.2	36	9.2	7.3128	1.0336	1136.5
20	25.4	65.1	6.4	7.0075	1.3184	2061.1
25	33.1	152.0	5.4	6.7193	1.8333	3295.2
30	36.7	211.0	4.2	6.6324	2.0744	4779.8
Constant	E (GPa)	ν	G (GPa)			
–	34	0.2	1.4167			

[a] GAL^2/EI

resonance, while the acceleration values are greatly dependent on the train's speed. Results show that both derailment criteria are greatly influenced by the level of track quality, with bridge vibration being imperceptible for wheel–rail contact forces. For the study of derailment, track quality is far more relevant than the vibration experienced on the bridge.

Considering the presented conclusions, it is observed that the current normative limit might be over-conservative. In the case of future discussion and research work leading to the acceleration criterion being discarded, different limit criteria should be tested and evaluated in further studies. Furthermore, the study of pier lateral stiffness in pier-supported bridges, subject to wind action, is left for a future publication.

CRediT authorship contribution statement

Gonçalo Ferreira: Writing – original draft, Visualization, Investigation, Formal analysis. **Pedro Montenegro:** Writing – review & editing, Methodology, Conceptualization. **Andreas Andersson:** Writing – review & editing, Conceptualization. **António Abel Henriques:** Writing – review & editing, Supervision. **Raid Karoumi:** Supervision, Resources, Conceptualization. **Rui Calçada:** Supervision, Resources.

Declaration of competing interest

The authors declare that they have no known competing financial interests or personal relationships that could have appeared to influence the work reported in this paper.

Data availability

Data will be made available on request.

Acknowledgements

The authors would like to acknowledge the financial support of :

- "InBridge4EU — Enhanced Interfaces and train categories for dynamic compatibility assessment of European railway bridges" project funded by European funds through Horizon Europe (Europe's Rail Joint Undertaking);
- "IN2TRACK3 — Research into optimised and future railway infrastructure" project funded by European funds through the H2020 (SHIFT2RAIL Innovation Programme);
- Base Funding — UIDB/04708/2020 of the CONSTRUCT - Instituto de I&D em Estruturas e Construções - funded by national funds through the FCT/MCTES (PIDDAC), Portugal.

Appendix A. Bridge model parameters

See Tables A.3–A.5.

Table A.4
Properties of the slabs and UIC60 rails.

	Slab	Rails
ρ (kg/m^3)	2400	7850
E (GPa)	34	210
A (A^2)	0.96	7.676×10^{-3}
I (m^4)	7.2×10^{-3}	30.038×10^{-6}
h (m)	0.3	–
b (m)	3.2	–
gauge (m)	–	1.435

Table A.5
Properties of the fasteners and elastic bed (with values from [13,47,48]) and [49].

Fasteners			
	Longitudinal	Transversal	Vertical
Stiffness (MN/m)	40	40	22.4
Damping (kNs/m)	40	40	5.47
Rotational stiffness (kN m/rad)	45	45	45
Spacing (m)		0.588	
Elastic bed			
Mortar modulus (MN/m^3)		1×10^5	
Mortar damping (kNs/m^2)		34.58	
Subgrade modulus (MN/m^3)		100	
Subgrade damping (kNs/m^2)		34.58	

Table B.6
Train model parameters symbols.

Mechanical properties				
		Moments of inertia		
	Mass	Roll	Pitch	Yaw
Car body	m_{cb}	$I_{cb,x}$	$I_{cb,y}$	$I_{cb,z}$
Bogie	m_b	$I_{b,x}$	$I_{b,y}$	$I_{b,z}$
Wheelset	m_w	$I_{w,x}$	–	$I_{w,z}$
Suspension properties				
		Longitudinal	Transversal	Vertical
Primary	Stiffness	$k_{p,x}$	$k_{p,y}$	$k_{p,z}$
	Damping	$c_{p,x}$	$c_{p,y}$	$c_{p,z}$
Secondary	Stiffness	$k_{s,x}$	$k_{s,y}$	$k_{s,z}$
	Damping	$c_{s,x}$	$c_{s,y}$	$c_{s,z}$

Appendix B. Train model parameters

The values for the train model parameters (compiled from [13,36], and [37]) are listed in Tables B.7 and B.8.

Table B.7
Varying train model parameters.

		Central carriages									
Parameter	Unit	A1	A2	A3	A4	A5	A6	A7	A8	A9	A10
m_{cb}	kg	27 160	33 280	29 200	31 240	27 160	29 200	31 240	31 240	35 310	35 310
$I_{cb,y}$	kg·m^2	0.91×10^6	1.41×10^6	1.19×10^6	1.51×10^6	1.31×10^6	1.53×10^6	1.77×10^6	1.98×10^6	2.32×10^6	2.49×10^6
$I_{b,y}$	kg·m^2	1240	3650	1240	2700	1240	1240	1240	1900	1240	1240
		Side carriages									
Parameter	Unit	A1	A2	A3	A4	A5	A6	A7	A8	A9	A10
m_{cb}	kg	40 740	49 910	43 800	46 850	40 740	43 800	46 850	46 850	52 970	52 970
$I_{cb,y}$	kg·m^2	1.02×10^6	1.52×10^6	1.37×10^6	1.69×10^6	1.54×10^6	1.82×10^6	2.12×10^6	2.36×10^6	2.83×10^6	3.06×10^6
$I_{b,y}$	kg·m^2	1240	3650	1240	2700	1240	1240	1240	1900	1240	1240
		Leading carriages									
Parameter	Unit	A1	A2	A3	A4	A5	A6	A7	A8	A9	A10
m_{cb}	kg	54 320	66 550	58 400	62 470	54 320	58 400	62 470	62 470	70 630	70 630
$I_{cb,y}$	kg·m^2	1.33×10^6	1.62×10^6	1.43×10^6	1.53×10^6	1.33×10^6	1.43×10^6	1.53×10^6	1.53×10^6	1.72×10^6	1.72×10^6
$I_{b,y}$	kg·m^2	2700	2700	2700	2700	2700	2700	2700	2700	2700	2700
		Central, side, and leading carriages									
Parameter	Unit	A1	A2	A3	A4	A5	A6	A7	A8	A9	A10
$k_{p,z}$	kN·m	1410	1320	1380	1350	1410	1380	1350	1350	1280	1280
$c_{p,z}$	kN·m/s	20	19	20	19	20	20	19	19	19	19
$k_{s,z}$	kN·m	640	820	700	760	640	700	760	760	880	880
$c_{s,z}$	kN·m/s	39	50	43	46	39	43	46	46	53	53

Table B.8
Constant train model parameters.

Parameter	Unit	Value
$I_{cb,x}$	kg·m^2	119328
$I_{cb,z}$	kg·m^2	1957888
m_b	kg	3500
$I_{b,x}$	kg·m^2	2835
$I_{b,z}$	kg·m^2	4235
m_w	kg	2000
$I_{w,x}$	kg·m^2	1000
$I_{w,z}$	kg·m^2	1000
$k_{p,x}$	kN·m	12.5×10^3
$k_{p,y}$	kN·m	120×10^3
$c_{p,x}$	kN·m/s	9
$c_{p,y}$	kN·m/s	27.9
$k_{s,x}$	kN·m	2500
$k_{s,y}$	kN·m	240
$c_{s,x}$	kN·m/s	30
$c_{s,y}$	kN·m/s	30

References

[1] CEN/TC250. N 3659 (Timeline for the evolution of the EN Eurocodes). 2023.
[2] Paulsson B, Olofsson J, Hedlund H, Bell B, Täljsten B, Elfgren L. Sustainable Bridges – Results from a European Integrated Research Project. In: Large structures and infrastructures for environmentally constrained and urbanised areas. 2010, p. 314–5. http://dx.doi.org/10.2749/222137810796024727, URL: https://structurae.net/en/literature/conference-paper/sustainable-bridges-results-from-a-european-integrated-research-project.
[3] Montenegro PA, Carvalho H, Ribeiro D, Calçada R, Tokunaga M, Tanabe M, et al. Assessment of train running safety on bridges: A literature review. Eng Struct 2021;241:112425. http://dx.doi.org/10.1016/j.engstruct.2021.112425, URL: https://www.sciencedirect.com/science/article/pii/S0141029621005757.
[4] Zhang N, Zhou Z, Wu Z. Safety evaluation of a vehicle–bridge interaction system using the pseudo-excitation method. Railw Eng Sci 2022;30(1):41–56. http://dx.doi.org/10.1007/s40534-021-00259-6.
[5] Allahvirdizadeh R, Andersson A, Karoumi R. Surrogate-assisted investigation on influence of epistemic uncertainties on running safety of high-speed trains on bridges. Probab Eng Mech 2024;75. http://dx.doi.org/10.1016/j.probengmech.2023.103559.
[6] CEN. Eurocode EN 1990: Basis of structural design. European Committee for Standardization; 2002.
[7] TB 10002-2017. Code for design on railway bridge and culvert. Beijing: People's Republic of China National Railway Administration (CNRA-PRC); 2017.
[8] Institute RTR. Outline of design standards for railway structures and commentary (displacement limits). Tokyo: Maruzen Co., Ltd.; 2006.
[9] ERRI D 214/RP 8. Rail bridges for speeds > 200 km/h: Confirmation of values against experimental data. Tech. rep., Utrecht: European Rail Research Institute; 1999.
[10] Zacher M, Baeßler M. Dynamic behaviour of ballast on railway bridges. In: Dynamics of high–speed railway bridges. selected and revised papers from the advanced course on 'dynamics of high–speed railway bridges', porto, Portugal, 20–23 September 2005. CRC Press; 2008, p. 125–42.
[11] Allahvirdizadeh R, Andersson A, Karoumi R. Estimating running safety factor of ballastless railway bridges using tail modelling. In: Acta polytechnica CTU proceedings, Vol. 36. 2022, p. 25–32, ISSN: 2336-5382.
[12] Moliner E, Martínez-Rodrigo MD, Museros P. Dynamic performance of existing double track railway bridges at resonance with the increase of the operational line speed. Eng Struct 2017;132:98–109. http://dx.doi.org/10.1016/j.engstruct.2016.11.031, URL: https://www.sciencedirect.com/science/article/pii/S0141029616312639.
[13] Arvidsson T, Andersson A, Karoumi R. Train running safety on non-ballasted bridges. Int J Rail Transp 2018;7:1–22.
[14] Yang YB, Yau JD. Resonance of high-speed trains moving over a series of simple or continuous beams with non-ballasted tracks. Eng Struct 2017;143:295–305.
[15] Cai X, Guo L, Hou B, Ren C. Influence of ballastless track complex irregularities on high-speed train. Beijing Jiaotong Daxue Xuebao (J Beijing Jiaotong Univ) 2016;40(1):12–9. http://dx.doi.org/10.11860/j.issn.1673-0291.2016.01.002.
[16] Schneider S, Marx S. Design of railway bridges for dynamic loads due to high-speed traffic. Eng Struct 2018;174:396–406. http://dx.doi.org/10.1016/j.engstruct.2018.07.030, URL: https://www.sciencedirect.com/science/article/pii/S0141029618300580.
[17] Matsuoka K, Collina A, Somaschini C, Sogabe M. Influence of local deck vibrations on the evaluation of the maximum acceleration of a steel-concrete composite bridge for a high-speed railway. Eng Struct 2019;200:109736.
[18] Yotsui H, Matsuoka K, Kaito K. Acceleration evaluation of a high-speed railway PC box girder bridge with slab track. In: Conference proceedings of the society for experimental mechanics series. 2024, p. 25–32. http://dx.doi.org/10.1007/978-3-031-36663-5_4, ISSN: 2191-5644.
[19] García-Macías E, Martínez-Castro AE. Hilbert transform-based semi-analytic meta-model for maximum response envelopes in dynamics of railway bridges. J Sound Vib 2020;487:115618. http://dx.doi.org/10.1016/j.jsv.2020.115618, URL: https://www.sciencedirect.com/science/article/pii/S0022460X20304491.
[20] Museros P, Moliner E, Martínez-Rodrigo MD. Free vibrations of simply-supported beam bridges under moving loads: Maximum resonance, cancellation and resonant vertical acceleration. J Sound Vib 2013;332(2):326–45. http://dx.doi.org/10.1016/j.jsv.2012.08.008, URL: https://www.sciencedirect.com/science/article/pii/S0022460X12006293.
[21] Chen L, Jiang L. Research on the dynamic response of high-speed railway train-ballastless track-bridge system and train running safety under earthquake. Zhongguo Tiedao Kexue (China Railw Sci) 2013;34(1):131–3. http://dx.doi.org/10.3969/j.issn.1001-4632.2013.01.20.
[22] Cao L, Yang C, Zhang J, Zeng P, Li S. Earthquake response of the train–slab ballastless track–subgrade system: A shaking table test study. J Vib Control 2021;27(17–18):1979–90. http://dx.doi.org/10.1177/1077546320951380.
[23] Chen Y, Jiang L, Lai Z, Li J. A novel evaluation of train running safety on the HSR bridges under earthquakes based on the observed track deformation rate. Eng Struct 2023;275:115260. http://dx.doi.org/10.1016/j.engstruct.2022.115260, URL: https://www.sciencedirect.com/science/article/pii/S0141029622013360.

[24] Liu X, Jiang L-z, Xiang P, Lai Z-p, Feng Y-l, Cao S-s. Dynamic response limit of high-speed railway bridge under earthquake considering running safety performance of train. J Central South Univ Technol 2021;28(3):968–80. http://dx.doi.org/10.1007/s11771-021-4657-2.

[25] He C, Chen Z, Zhai W. Mapping relationship between uneven settlement of subgrade and rail deformation in subgrade-bridge transition section and its dynamic application. Zhongguo Kexue Jishu Kexue (Sci Sin Technol) 2018;48(8):881–90. http://dx.doi.org/10.1360/N092017-00257.

[26] Chen H, Luo Q, Zhang L, Liu G, Chen J. Test analysis of vibration characteristics of high-speed railway on CRTS II slab ballastles strack bridge-subgrade transition. Zhendong yu Chongji (J Vib Shock) 2014;33(1):81–8.

[27] Lai Z, Jiang L, Zhou W, Yu J, Zhang Y, Liu X, et al. Lateral girder displacement effect on the safety and comfortability of the high-speed rail train operation. Veh Syst Dyn 2022;60(9):3215–39. http://dx.doi.org/10.1080/00423114.2021.1942507, Publisher: Taylor & Francis _eprint: https://doi.org/10.1080/00423114.2021.1942507.

[28] European Union Agency for Railways (ERA). ERA1193-TD-01-2022 - ERA technical note on work needed for closing TSI open points on bridge dynamics. 2022, URL: https://rail-research.europa.eu:443/about-europes-rail/europes-rail-reference-documents/additional-technical-material/.

[29] InBridge4EU – Enhancing European railway bridge standards. 2023, URL: https://inbridge4eu.eu/.

[30] Arvidsson T, Andersson A. Train–track–bridge interaction for non-ballasted railway bridges on high-speed lines. Tech. Rep. TRITA-BKN Report 165, Stockholm: KTH Royal Institute of Technology; 2017.

[31] CEN. Eurocode EN 1991-2: Actions of Structures - Part 2: Traffic Loads on Bridges. European Committee for Standardization; 2003.

[32] ANSYS®. Academic Research. 2018.

[33] Montenegro P, Carvalho H, Ortega M, Millanes F, Goicolea J, Zhai W, et al. Impact of the train-track-bridge system characteristics in the runnability of high-speed trains against crosswinds - part I: Running safety. J Wind Eng Ind Aerodyn 2022;224:104974. http://dx.doi.org/10.1016/j.jweia.2022.104974, URL: https://linkinghub.elsevier.com/retrieve/pii/S0167610522000794.

[34] Montenegro P, Barbosa D, Carvalho H, Calçada R. Dynamic effects on a train-bridge system caused by stochastically generated turbulent wind fields. Eng Struct 2020;211:110430. http://dx.doi.org/10.1016/j.engstruct.2020.110430, URL: https://linkinghub.elsevier.com/retrieve/pii/S0141029619338040.

[35] Neto J, Montenegro PA, Vale C, Calçada R. Evaluation of the train running safety under crosswinds - a numerical study on the influence of the wind speed and orientation considering the normative Chinese hat model. Int J Rail Transp 2021;9(3):204–31. http://dx.doi.org/10.1080/23248378.2020.1780965, URL: https://www.tandfonline.com/doi/full/10.1080/23248378.2020.1780965.

[36] Goicolea JM. Simplified Mechanical Description of AVE S-103 - ICE3 Velaro e High Speed Train. Tech. rep., School of Civil Engineering, Technical University of Madrid–UPM; 2014.

[37] Lee Y-S, Kim S-H. Structural analysis of 3D high-speed train–bridge interactions for simple train load models. Veh Syst Dyn 2010;48(2):263–81. http://dx.doi.org/10.1080/00423110902751912, Publisher: Taylor & Francis _eprint: https://doi.org/10.1080/00423110902751912.

[38] Claus H, Schiehlen W. Modeling and simulation of railway bogie structural vibrations. Veh Syst Dyn 1998;29(sup1):538–52. http://dx.doi.org/10.1080/00423119808969585, Publisher: Taylor & Francis _eprint: https://doi.org/10.1080/00423119808969585.

[39] EN 13848-5. Railway applications - Track - Track geometry quality - Part 5: Geometric quality assessment. Brussels: European Committee for Standarization (CEN); 2005.

[40] Zhai W, Liu P, Lin J, Wang K. Experimental investigation on vibration behaviour of a CRH train at speed of 350 km/h. Int J Rail Transp 2015;3(1):1–16. http://dx.doi.org/10.1080/23248378.2014.992819, Publisher: Taylor & Francis _eprint: https://doi.org/10.1080/23248378.2014.992819.

[41] MATLAB®. Academic Research. 2018.

[42] Montenegro P, Neves S, Calçada R, Tanabe M, Sogabe M. Wheel–rail contact formulation for analyzing the lateral train–structure dynamic interaction. Comput Struct 2015;152:200–14, Publisher: Elsevier. URL: https://www.sciencedirect.com/science/article/pii/S0045794915000139.

[43] Montenegro PA, Calçada R. Wheel–rail contact model for railway vehicle–structure interaction applications: Development and validation. Railw Eng Sci 2023;31(3):181–206. http://dx.doi.org/10.1007/s40534-023-00306-4.

[44] Neves SGM, Montenegro PA, Azevedo AFM, Calçada R. A direct method for analyzing the nonlinear vehicle–structure interaction. Eng Struct 2014;69:83–9. http://dx.doi.org/10.1016/j.engstruct.2014.02.027, URL: https://www.sciencedirect.com/science/article/pii/S0141029614001205.

[45] TSI. Technical specification for interoperability relating to the infrastructure subsystem of the trans-European high-speed rail system. Off J Eur Union 2008.

[46] EN 14363. Railway applications - Testing and Simulation for the acceptance of running characteristics of railway vehicles - Running Behaviour and stationary tests. Brussels: European Committee for Standarization (CEN); 2016.

[47] Ling L, Dhanasekar M, Wang K, Zhai W, Weston B. Collision derailments on bridges containing ballastless slab tracks. Eng Fail Anal 2019;105:869–82. http://dx.doi.org/10.1016/j.engfailanal.2019.07.042, URL: https://www.sciencedirect.com/science/article/pii/S1350630719303930.

[48] ERRI D 202/RP 11. Parametric Study and Sensitivity Analysis of CWERRI. Tech. rep., Utrecht: European Rail Research Institute; 1997.

[49] Shi H, Yu Z, Shi H. An Improved Method for Dynamic Modelling of a Slab Track on a High-Speed Railway. Madrid, Spain; 2016, p. 225–37. http://dx.doi.org/10.2495/CR160211, URL: http://library.witpress.com/viewpaper.asp?pcode=CR16-021-1.

BIBLIOGRAPHY

AAR (2015). *Manual of Standards and Recommended Practices: Section C, Part II - Design, Fabrication, and Construction of Freight Cars*. Washington, USA: Association of American Railroads.

Albuquerque, Carlos Miguel Correia (2008). "Comportamento Dinâmico de Pontes Com Tabuleiro Ortotrópico Em Vias de Alta Velocidade." Master's Thesis. Porto, Portugal: Faculdade de Engenharia da Universidade do Porto. URL: https://repositorio-aberto.up.pt/handle/10216/58939.

Allahvirdizadeh, R., A. Andersson, and R. Karoumi (2020). "Reliability Assessment of the Dynamic Behavior of High-Speed Railway Bridges Using First Order Reliability Method." *XI International Conference on Structural Dynamics*. Vol. 2. Athens, Greece, pp. 3438–3450. ISBN: 978-618-85072-1-0.

– (2022). "Estimating Running Safety Factor of Ballastless Railway Bridges Using Tail Modelling." *Acta Polytechnica CTU Proceedings* 36, pp. 25–32. ISSN: 2336-5382. DOI: 10.14311/APP.2022.36.0025. URL: https://ojs.cvut.cz/ojs/index.php/APP/article/view/8366.

– (2024a). "Partial Safety Factor Calibration Using Surrogate Models: An Application for Running Safety of Ballasted High-Speed Railway Bridges." *Probabilistic Engineering Mechanics* 75, p. 103569. ISSN: 0266-8920. DOI: 10.1016/j.probengmech.2023.103569. URL: https://www.sciencedirect.com/science/article/pii/S0266892023001583.

– (2024b). "Surrogate-Assisted Investigation on Influence of Epistemic Uncertainties on Running Safety of High-Speed Trains on Bridges." *Probabilistic Engineering Mechanics* 75. ISSN: 0266-8920. DOI: 10.1016/j.probengmech.2023.103559.

Andersson, A., R. Allahvirdizadeh, A. Albright, P. A. Montenegro, G. Ferreira, M. A. Peixer, P. Museros, R. Karoumi, and R. Calçada (2021). *Report No. D5.6 – Performed High-Speed Low-Cost Bridges I2T3 Demonstrators. H2020 - Sift2Rail - In2Track3 Project: Research into Optimised and Future Railway Infrastructure (S2R-CFM-IP3-01-2020 Innovation Action)Tunnel and Bridge I2T2 Report - High Speed Low Cost Bridges - Appendix D5.2.5*. Porto, Portugal, Stockholm, Sweden, and Valencia, Spain.

ANSYS® (2018). *Release 19.2*. Canonsburg, Pennsylvania, USA: ANSYS Inc.

Antolín, Pablo, Jose M. Goicolea, Javier Oliva, and Miguel A. Astiz (2012). "Nonlinear Train-Bridge Lateral Interaction Using a Simplified Wheel-Rail Contact Method Within a Finite Element Framework." *Journal of Computational and Nonlinear Dynamics* 7.041014. ISSN: 1555-1415. DOI: 10.1115/1.4006736. URL: https://doi.org/10.1115/1.4006736.

Arvidsson, T. and A. Andersson (2017). *Train-Track-Bridge Interaction for Non-Ballasted Railway Bridges on High-Speed Lines*. TRITA-BKN, Report 165. Stockholm, Sweden: KTH Royal Institute of Technology. URL: https://kth.diva-portal.org/smash/record.jsf?pid=diva2%3A1209473&dswid=-8418.

Arvidsson, T., A. Andersson, and R. Karoumi (2018). "Train Running Safety on Non-Ballasted Bridges." *International Journal of Rail Transportation* 7, pp. 1–22. URL: https://doi.org/10.1080/23248378.2018.1503975.

Au, Siu-Kui and James L. Beck (2001). "Estimation of Small Failure Probabilities in High Dimensions by Subset Simulation." *Probabilistic Engineering Mechanics* 16.4, pp. 263–277. ISSN: 0266-8920. DOI: 10.1016/S0266-8920(01)00019-4. URL: https://www.sciencedirect.com/science/article/pii/S0266892001000194.

Auersch, Lutz (2021). "Resonances of Railway Bridges Analysed in Frequency Domain by the Modal-Force-Excitation, Bridge-Transfer and Axle-Sequence Spectra." *Engineering Structures* 249, p. 113282. ISSN: 0141-0296. DOI: 10.1016/j.engstruct.2021.113282. URL: https://www.sciencedirect.com/science/article/pii/S0141029621014036.

Ayasse, Jean-Bernard and Hugues Chollet (2005). "Determination of the Wheel Rail Contact Patch in Semi-Hertzian Conditions." *Vehicle System Dynamics* 43.3, pp. 161–172. ISSN: 0042-3114. DOI: 10.1080/00423110412331327193. URL: https://doi.org/10.1080/00423110412331327193.

Baeßler, Matthias (2008). "Lageveränderungen des Schottergleises durch zyklische und dynamische Beanspruchungen." Doctoral Thesis. Technische Universität Berlin. URL: https://depositonce.tu-berlin.de/handle/11303/2207.

Bittner, M, L Fritsch, B Hirzinger, M Broggi, and M Beer (2024). "Efficient Time-Dependent Reliability Analysis for a Railway Bridge Model." *Journal of Physics: Conference Series* 2647.6, p. 062002. ISSN: 1742-6596. DOI: 10.1088/1742-6596/2647/6/062002. URL: https://dx.doi.org/10.1088/1742-6596/2647/6/062002.

Bjerager, P. (1991). "Methods for Structural Reliability Computations." *Reliability Problems: General Principles and Applications in Mechanics of Solids and Structures*. Ed. by F. Casciati and J. B. Roberts. International Centre for Mechanical Sciences. Vienna, Austria: Springer, pp. 89–135. ISBN: 978-3-7091-2616-5. DOI: 10.1007/978-3-7091-2616-5_3. URL: https://doi.org/10.1007/978-3-7091-2616-5_3.

Bonifácio, Cristiana, Diogo Ribeiro, Rui Calçada, and Raimundo Delgado (2014). "Calibration and Validation of the Numerical Model of a Short-Span Railway Bridge Based on Dynamic Tests." *Proceedings of the 9th International Conference on Structural Dynamics*. Porto, Portugal. ISBN: 978-972-752-165-4.

Bourinet, J. -M., F. Deheeger, and M. Lemaire (2011). "Assessing Small Failure Probabilities by Combined Subset Simulation and Support Vector Machines." *Structural Safety* 33.6, pp. 343–353. ISSN: 0167-4730. DOI: 10.1016/j.strusafe.2011.06.001. URL: https://www.sciencedirect.com/science/article/pii/S0167473011000555.

Bozzone, M., E. Pennestrì, and P. Salvini (2011). "Dynamic Analysis of a Bogie for Hunting Detection through a Simplified Wheel–Rail Contact Model." *Multibody System Dynamics* 25.4, pp. 429–460. ISSN: 1573-272X. DOI: 10.1007/s11044-010-9233-8. URL: https://doi.org/10.1007/s11044-010-9233-8.

Breitung, Karl (1984). "Asymptotic Approximations for Multinormal Integrals." *Journal of Engineering Mechanics* 110.3, pp. 357–366. ISSN: 0733-9399. DOI:

10.1061/(ASCE)0733-9399(1984)110:3(357). URL: https://ascelibrary.org/doi/abs/10.1061/%28ASCE%290733-9399%281984%29110%3A3%28357%29.

Broding, William C., F. W. Diederich, and Philip S. Parker (1964). "Structural Optimization and Design Based on a Reliability Design Criterion." *Journal of Spacecraft and Rockets* 1.1, pp. 56–61. ISSN: 0022-4650. DOI: 10.2514/3.27592. URL: https://arc.aiaa.org/doi/10.2514/3.27592.

Cai, X., L. Guo, B. Hou, and C. Ren (2016). "Influence of Ballastless Track Complex Irregularities on High-Speed Train." *Beijing Jiaotong Daxue Xuebao/Journal of Beijing Jiaotong University* 40.1, pp. 12–19. DOI: 10.11860/j.issn.1673-0291.2016.01.002.

Calçada, Rui (1995). "Efeitos Dinâmicos Em Pontes Resultantes Do Tráfego Ferroviário a Alta Velocidade." Master's Thesis. Porto, Portugal: Faculdade de Engenharia da Universidade do Porto. URL: https://repositorio-aberto.up.pt/handle/10216/12064.

Cao, L., C. Yang, J. Zhang, P. Zeng, and S. Li (2021). "Earthquake Response of the Train–Slab Ballastless Track–Subgrade System: A Shaking Table Test Study." *JVC/Journal of Vibration and Control* 27.17-18, pp. 1979–1990. ISSN: 1077-5463. DOI: 10.1177/1077546320951380.

Catarino, José Manuel, Júlio Appleton, João André, and Luís Oliveira Santo (2024). "2.ª Geração Do Eurocódigo – Bases Para o Projeto Estrutural e Geotécnico." *Revista Portuguesa de Engenharia de Estruturas*. III 25, pp. 23–30. ISSN: 183-8488. DOI: 10.34638/rpee-sIII-n25-003. URL: http://rpee.lnec.pt/Ficheiros/DOI/rpee_sIII_n25_03.htm.

CEN (2003). *Eurocode 1 - Part 2: Actions on Structures - Traffic Load on Bridges*. EN 1991-2. Brussels, Belgium: Commité European de Normalisation (CEN).

– (2005). *Eurocode: Basis of Structural Design*. EN 1990. Brussels, Belgium: Commité European de Normalisation (CEN).

– (2010). *Railway Applications - Aerodynamics - Part 6: Requirements and Test Procedures for Cross Wind Assessment*. EN 14067-6. Brussels, Belgium: Commité European de Normalisation (CEN).

– (2015). *Railway Applications; Track - Track geometry quality; Part 5: Geometric quality levels - Plain line*. EN 13848-5. Brussels, Belgium: Commité European de Normalisation (CEN).

– (2016). *Railway Applications - Testing and Simulation for the acceptance of running characteristics of Railway Vehicles - Running Behaviour and stationary tests*. EN 14363. Brussels, Belgium: Commité European de Normalisation (CEN).

– (2023a). *Eurocode - Basis of Structural and Geotechnical Design*. EN 1990. Brussels, Belgium: Commité European de Normalisation (CEN).

– (2023b). *Eurocode 1 - Actions on Structures - Part 2: Traffic Loads on Bridges and Other Civil Engineering Works*. EN 1991-2. Brussels, Belgium: Commité European de Normalisation (CEN).

CEN/TC 250 (2023). *N 3659 (Timeline for the Evolution of the EN Eurocodes)*. Letter.

Chen, G. and Zhai W.M. (2004). "A New Wheel/Rail Spatially Dynamic Coupling Model and Its Verification." *Vehicle System Dynamics* 41.4, pp. 301–322. ISSN: 0042-3114. DOI: 10.1080/00423110412331315178. URL: https://doi.org/10.1080/00423110412331315178.

Chen, H., Q. Luo, L. Zhang, G. Liu, and J. Chen (2014). "Test analysis of vibration characteristics of high-speed railway on CRTS II slab ballastles strack bridge-subgrade transition." *Zhendong yu Chongji/Journal of Vibration and Shock* 33.1, pp. 81–88. ISSN: 1000-3835.

Chen, L. and L. Jiang (2013). "Research on the dynamic response of high-speed railway train-ballastless track-bridge system and train running safety under earthquake." *Zhongguo Tiedao Kexue/China Railway Science* 34.1, pp. 131–133. ISSN: 1001-4632. DOI: 10.3969/j.issn.1001-4632.2013.01.20.

Chen, Yuanjun, Lizhong Jiang, Zhipeng Lai, and Jing Li (2023). "A Novel Evaluation of Train Running Safety on the HSR Bridges under Earthquakes Based on the Observed Track Deformation Rate." *Engineering Structures* 275, p. 115260. ISSN: 0141-0296. DOI: 10.1016/j.engstruct.2022.115260. URL: https://www.sciencedirect.com/science/article/pii/S0141029622013360.

Chopra, Anil K. (1995). *Dynamics of Structures: Theory and Applications to Earthquake Engineering*. Englewood Cliffs, USA: Prentice-Hall International. ISBN: 978-0-13-521063-5.

Claus, H. and W. Schiehlen (1998). "Modeling and Simulation of Railway Bogie Structural Vibrations." *Vehicle System Dynamics* 29 (sup1), pp. 538–552. ISSN: 0042-3114. DOI: 10.1080/00423119808969585. URL: https://doi.org/10.1080/00423119808969585.

Clough, Ray W. and Joseph Penzien (1975). *Dynamics of Structures*. Tokyo, Japan: McGraw-Hill Kogakusha. ISBN: 978-0-07-011392-3.

Comission to the European Parliament, European Council, European Economic and Social Comittee, and Committee of the Regions (2019). *The European Green Deal*. URL: https://eur-lex.europa.eu/legal-content/EN/ALL/?uri=COM%3A2019%3A640%3AFIN.

Cornell, Carl Allin (1969). "A Probabilistic Based Structural Code." *American Concrete Institute* 66.12, pp. 974–985.

Council of the European Union (2014). *Council Regulation (EU) No 642/2014 of 16 June 2014 Establishing the Shift2Rail Joint Undertaking*. URL: http://data.europa.eu/eli/reg/2014/642/oj/eng (visited on 12/16/2021).

– (2021). *Council Regulation (EU) 2021/2085 of 19 November 2021 Establishing the Joint Undertakings under Horizon Europe and Repealing Regulations (EC) No 219/2007, (EU) No 557/2014, (EU) No 558/2014, (EU) No 559/2014, (EU) No 560/2014, (EU) No 561/2014 and (EU) No 642/2014*. URL: http://data.europa.eu/eli/reg/2021/2085/oj/eng (visited on 12/16/2021).

Cremona, Christian (2013). *Structural Performance: Probability-Based Assessment*. Hoboken, USA: Wiley. xiii+429. ISBN: 978-1-118-60117-4.

Directorate-General for Mobility and Transport (European Commission) (2021). *Why Rail?* URL: https://europa.eu/year-of-rail/why-rail_en (visited on 12/15/2021).

– (2024). *EU Transport in Figures: Statistical Pocketbook 2024*. Luxembourg: Publications Office of the European Union. ISBN: 978-92-68-19812-4. URL: https://data.europa.eu/doi/10.2832/16593.

– (2025). *EU Invests Record €7 Billion in Sustainable, Safe and Smart Transport Infrastructure - European Commission*. URL: https://transport.ec.europa.eu/news-events/news/eu-invests-record-eu7-billion-sustainable-

safe-and-smart-transport-infrastructure-2024-07-17_en (visited on 02/16/2025).

ERRI D 181/RP 6 (1995). *Lateral Forces on Railway Bridges: Final Report*. Utrecht, The Netherlands: European Rail Research Institute.

ERRI D 192/RP 5 (1996). *Loading Diagram to Be Taken into Consideration for the Calculation of Rail-Carrying Structures on Lines Used by International Services*. Utrecht, The Netherlands: European Rail Research Institute.

ERRI D 202/RP 11 (1997). *Parametric Study and Sensitivity Analysis of CWERRI*. Utrecht, The Netherlands: European Rail Research Institute.

ERRI D 214/RP 6 (1999). *Rail Bridges for Speeds > 200 Km/h: Calculations for Bridges with Simply Supported Beams during the Passage of a Train*. Utrecht, The Netherlands: European Rail Research Institute.

ERRI D 214/RP 8 (1999). *Rail Bridges for Speeds > 200 Km/h: Confirmation of Values against Experimental Data*. Utrecht, The Netherlands: European Rail Research Institute.

ERRI D 214/RP 9 (1999). *Rail Bridges for Speeds > 200 Km/h, Final Report*. Utrecht, The Netherlands: European Rail Research Institute.

EU Funding & Tenders Portal (2025). *EU-RAIL JU Call Proposals 2022-02 (HORIZON-ER-JU-2022-02)*. URL: https://ec.europa.eu/info/funding-tenders/opportunities/portal/screen/opportunities/topic-details/horizon-er-ju-2022-explr-02 (visited on 02/16/2025).

European Comission (2002). *Consolidated Text: Commission Decision of 30 May 2002 Concerning the Technical Specification for Interoperability Relating to the Infrastructure Subsystem of the Trans-European High-Speed Rail System Referred to in Article 6(1) of Council Directive 96/48/EC (Notified under Document Number C(2002) 1948) (Text with EEA Relevance) (2002/732/EC)*. URL: https://eur-lex.europa.eu/eli/dec/2002/732/2002-09-12 (visited on 09/08/2021).

European Parliament and Council of the European Union (2020). *Decision (EU) 2020/2228 of the European Parliament and of the Council of 23 December 2020 on a European Year of Rail (2021)*. URL: http://data.europa.eu/eli/dec/2020/2228/oj/eng (visited on 12/15/2021).

European Railway Research Advisory Council (2024). *Railway Research and Innovation Agenda (RRIA)*. ERRAC. Brussels, Belgium. ISBN: 978-2-7461-3438-6. URL: https://errac.org/publications/rail-research-and-innovation-agenda-rria/.

European Union Agency for Railways (2020). *Fostering the Railway Sector Through the European Green Deal*. ERA1234. Valenciennes, France. URL: https://www.era.europa.eu/content/report-fostering-railway-sector-through-european-green-deal_en.

– (2022). *ERA1193-TD-01-2022 - ERA Technical Note on Work Needed for Closing TSI Open Points on Bridge Dynamics*. Valenciennes, France. URL: https://rail-research.europa.eu:443/about-europes-rail/europes-rail-reference-documents/additional-technical-material/ (visited on 01/22/2024).

– (2024a). *Rail Environmental Report*. Luxembourg: Publications Office of the European Union. ISBN: 978-92-9477-455-2. URL: https://www.era.europa.eu/content/all-aboard-european-railways-focus-era-launched-brussels-2024-report-railway-safety-and#oe-content-paragraph-3867.

European Union Agency for Railways (2024b). *Report on Railway Safety and Interoperability in the EU*. Luxembourg: Publications Office of the European Union. ISBN: 978-92-9477-458-3. URL: https://www.era.europa.eu/content/all-aboard-european-railways-focus-era-launched-brussels-2024-report-railway-safety-and#oe-content-paragraph-3867.

Falomi, Stefano, Monica Malvezzi, and Enrico Meli (2011). "Multibody Modeling of Railway Vehicles: Innovative Algorithms for the Detection of Wheel–Rail Contact Points." *Wear*. Proceedings of the 8th International Conference on Contact Mechanics and Wear of Rail / Wheel Systems, Florence, 2009 271.1, pp. 453–461. ISSN: 0043-1648. DOI: 10.1016/j.wear.2010.10.039. URL: https://www.sciencedirect.com/science/article/pii/S004316481000373X.

FEMIX (2009). *4.0 - Finite Element Analysis*. Porto, Portugal: Álvaro Azevedo.

Ferreira, G., P. Montenegro, A. Andersson, A. A. Henriques, R. Karoumi, and R. Calçada (2024a). "Critical analysis of the current Eurocode deck acceleration limit for evaluating running safety in ballastless railway bridges." *Engineering Structures* 312, p. 118127. ISSN: 0141-0296. DOI: 10.1016/j.engstruct.2024.118127.

Ferreira, G., P. Montenegro, J. R. Pinto, A. A. Henriques, and R. Calçada (2024b). "A discussion about the limitations of the Eurocode's high-speed load model for railway bridges." *Railway Engineering Science* 32.2, pp. 211–228. ISSN: 2662-4745. DOI: 10.1007/s40534-023-00321-5.

Ferreira, G., Montenegro P., C. Adam, A. A. Henriques, and R. Calçada (2025). "Evaluation of the Eurocode's Safety Factor for Deck Acceleration Limit on Ballasted Track Railway Bridges." Submitted for publication.

García-Macías, Enrique and A. E. Martínez-Castro (2020). "Hilbert Transform-Based Semi-Analytic Meta-Model for Maximum Response Envelopes in Dynamics of Railway Bridges." *Journal of Sound and Vibration* 487, p. 115618. ISSN: 0022-460X. DOI: 10.1016/j.jsv.2020.115618. URL: https://www.sciencedirect.com/science/article/pii/S0022460X20304491.

Glatz, Bernhard and Josef Fink (2021). "A Redesigned Approach to the Additional Damping Method in the Dynamic Analysis of Simply Supported Railway Bridges." *Engineering Structures* 241, p. 112415. ISSN: 0141-0296. DOI: 10.1016/j.engstruct.2021.112415. URL: https://www.sciencedirect.com/science/article/pii/S0141029621005654.

Goicolea, José M. (2014). *Simplified Mechanical Description of AVE S-103 - ICE3 Velaro E High Speed Train*. School of Civil Engineering, Technical University of Madrid-UPM. URL: https://oa.upm.es/43946/.

Gong, Wei, Zhihui Zhu, Yu Liu, Ruitao Liu, Yongjiu Tang, and Lizhong Jiang (2020). "Running Safety Assessment of a Train Traversing a Three-Tower Cable-Stayed Bridge under Spatially Varying Ground Motion." *Railway Engineering Science* 28.2, pp. 184–198. ISSN: 2662-4753. DOI: 10.1007/s40534-020-00209-8. URL: https://doi.org/10.1007/s40534-020-00209-8.

Grigoriou, Vasileios and Eugen Brühwiler (2016). "Monitoring-Based Safety Verification at the Ultimate Limit State of Fracture of the RC Slab of a Short Span Railway Underpass." *Structural Safety* 60, pp. 16–27. ISSN: 0167-4730. DOI: 10.1016/j.strusafe.2016.01.002. URL: https://www.sciencedirect.com/science/article/pii/S0167473016000138.

Hasofer, Abraham M. and Niels C. Lind (1974). "Exact and Invariant Second-Moment Code Format." *Journal of the Engineering Mechanics Division* 100.1, pp. 111–121. DOI: 10.1061/JMCEA3.0001848. URL: https://ascelibrary.org/doi/abs/10.1061/JMCEA3.0001848.

He, C., Z. Chen, and W. Zhai (2018). "Mapping relationship between uneven settlement of subgrade and rail deformation in subgrade-bridge transition section and its dynamic application." *Zhongguo Kexue Jishu Kexue/Scientia Sinica Technologica* 48.8, pp. 881–890. ISSN: 1674-7259. DOI: 10.1360/N092017-00257.

Heiland, Till, Marius Hägle, Theodoros Triantafyllidis, Lothar Stempniewski, and Alexander Stark (2022). "Stiffness Contributions of Ballast in the Context of Dynamic Analysis of Short Span Railway Bridges." *Construction and Building Materials* 360, p. 129536. ISSN: 0950-0618. DOI: 10.1016/j.conbuildmat.2022.129536. URL: https://www.sciencedirect.com/science/article/pii/S0950061822031920.

Henriques, António Abel (1998). "Aplicação de Novos Conceitos de Segurança No Dimensionamento Do Betão Estrutural." Doctoral Thesis. Porto, Portugal: Faculdade de Engenharia da Universidade do Porto. URL: https://repositorio-aberto_up_pt_ipv6.scftvc.com/handle/10216/11700.

Hertz, Heinrich (1882). "Ueber die Berührung fester elastischer Körper." *Journal für die reine und angewandte Mathematik* 92, pp. 156–171. ISSN: 1435-5345. DOI: 10.1515/crll.1882.92.156. URL: https://www.degruyter.com/document/doi/10.1515/crll.1882.92.156/html.

Hirzinger, Benjamin, Christoph Adam, Michael Oberguggenberger, and Patrick Salcher (2020). "Approaches for Predicting the Probability of Failure of Bridges Subjected to High-Speed Trains." *Probabilistic Engineering Mechanics* 59, p. 103021. ISSN: 0266-8920. DOI: 10.1016/j.probengmech.2020.103021. URL: https://www.sciencedirect.com/science/article/pii/S0266892020300060.

Hirzinger, Benjamin, Christoph Adam, Patrick Salcher, and Michael Oberguggenberger (2019). "On the Optimal Strategy of Stochastic-Based Reliability Assessment of Railway Bridges for High-Speed Trains." *Meccanica* 54.9, pp. 1385–1402. ISSN: 1572-9648. DOI: 10.1007/s11012-019-00999-0. URL: https://doi.org/10.1007/s11012-019-00999-0.

Horas, Cláudio Carlos da Silva (2011). "Comportamento Dinâmico de Pontes Com Tabuleiro Pré-Fabricado Em Vias de Alta Velocidade." Master's Thesis. Porto, Portugal: Faculdade de Engenharia da Universidade do Porto. URL: https://repositorio-aberto.up.pt/handle/10216/66380.

Hou, Bowen, Di Wang, Bingbing Wang, Xingyu Chen, and João Pombo (2022). "Vibration Reduction in Ballasted Track Using Ballast Mat: Numerical and Experimental Evaluation by Wheelset Drop Test." *Applied Sciences* 12.4 (4), p. 1844. ISSN: 2076-3417. DOI: 10.3390/app12041844. URL: https://www.mdpi.com/2076-3417/12/4/1844.

Hu, Nan, Gong-Lian Dai, Bin Yan, and Ke Liu (2014). "Recent Development of Design and Construction of Medium and Long Span High-Speed Railway Bridges in China." *Engineering Structures* 74, pp. 233–241. ISSN: 0141-0296.

DOI: 10.1016/j.engstruct.2014.05.052. URL: https://www.sciencedirect.com/science/article/pii/S0141029614003502.

IN2TRACK2 (2018). *IN2TRACK2*. URL: https://projects.shift2rail.org/s2r_ip3_n.aspx?p=IN2TRACK2 (visited on 12/16/2021).

IN2TRACK3 (2021). *IN2TRACK3*. URL: https://projects.shift2rail.org/s2r_ip3_n.aspx?p=IN2TRACK3 (visited on 12/16/2021).

InBridge4EU (2023). *InBridge4EU - Enhancing European Railway Bridge Standards*. URL: https://inbridge4eu.eu/ (visited on 01/22/2024).

JCSS (2001). *Probabilistic Model Code*. JCSS-OSTL/DIA/VROU -10-11-2000. Joint Commitee on Structural Safety (JCSS). URL: https://www.jcss-lc.org/jcss-probabilistic-model-code/.

Kalker, J. J. (1967). "On the Rolling Contact of Two Elastic Bodies in the Presence of Dry Friction." Doctoral Thesis. Delft, The Netherlands: Dept. Mech. Eng., Technische Hogeschool, Delft.

– (1979). "The Computation of Three-Dimensional Rolling Contact with Dry Friction." *International Journal for Numerical Methods in Engineering* 14.9, pp. 1293–1307. ISSN: 1097-0207. DOI: 10.1002/nme.1620140904. URL: https://onlinelibrary.wiley.com/doi/abs/10.1002/nme.1620140904.

– (1982). "A Fast Algorithm for the Simplified Theory of Rolling Contact." *Vehicle System Dynamics* 11.1, pp. 1–13. ISSN: 0042-3114. DOI: 10.1080/00423118208968684. URL: https://doi.org/10.1080/00423118208968684.

– (1996). "Book of Tables for the Hertzian Creep-Force Law." 2nd Mini Conference on Contact Mechanics and Wear of Wheel/Rail Systems. Budapest, Hungary.

Lai, Zhipeng, Lizhong Jiang, Wangbao Zhou, Jian Yu, Yuntai Zhang, Xiang Liu, and Wen Zhou (2022). "Lateral Girder Displacement Effect on the Safety and Comfortability of the High-Speed Rail Train Operation." *Vehicle System Dynamics* 60.9, pp. 3215–3239. ISSN: 0042-3114. DOI: 10.1080/00423114.2021.1942507. URL: https://doi.org/10.1080/00423114.2021.1942507.

Lee, Yong-Seon and Sang-Hyo Kim (2010). "Structural Analysis of 3D High-Speed Train-Bridge Interactions for Simple Train Load Models." *Vehicle System Dynamics* 48.2, pp. 263–281. ISSN: 0042-3114. DOI: 10.1080/00423110902751912. URL: https://doi.org/10.1080/00423110902751912.

Ling, Liang, Manicka Dhanasekar, Kaiyun Wang, Wanming Zhai, and Bill Weston (2019). "Collision Derailments on Bridges Containing Ballastless Slab Tracks." *Engineering Failure Analysis* 105, pp. 869–882. ISSN: 1350-6307. DOI: 10.1016/j.engfailanal.2019.07.042. URL: https://www.sciencedirect.com/science/article/pii/S1350630719303930.

Liu, Xiang, Li-zhong Jiang, Ping Xiang, Zhi-peng Lai, Yu-lin Feng, and Shan-shan Cao (2021). "Dynamic Response Limit of High-Speed Railway Bridge under Earthquake Considering Running Safety Performance of Train." *Journal of Central South University* 28.3, pp. 968–980. ISSN: 2227-5223. DOI: 10.1007/s11771-021-4657-2. URL: https://doi.org/10.1007/s11771-021-4657-2.

Lu, Chunfang and Chaoxun Cai (2020). "Overview on Safety Management and Maintenance of High-Speed Railway in China." *Transportation Geotechnics* 25, p. 100397. ISSN: 2214-3912. DOI: 10.1016/j.trgeo.2020.100397. URL: https://www.sciencedirect.com/science/article/pii/S2214391220302853.

Luo, Xiu (2005). "Study on Methodology for Running Safety Assessment of Trains in Seismic Design of Railway Structures." *Soil Dynamics and Earthquake Engineering* 25.2, pp. 79–91. ISSN: 0267-7261. DOI: 10.1016/j.soildyn.2004.10.005. URL: https://www.sciencedirect.com/science/article/pii/S026772610400171X.

Manterola, Javier (2006). *Puentes: apuntes para su diseño, cálculo y construcción*. Colegio de Ingenieros de Caminos, Canales y Puertos. ISBN: 978-84-380-0321-3.

Mao, Jianfeng, Zhiwu Yu, Yuanjie Xiao, Cheng Jin, and Yu Bai (2016). "Random Dynamic Analysis of a Train-Bridge Coupled System Involving Random System Parameters Based on Probability Density Evolution Method." *Probabilistic Engineering Mechanics* 46, pp. 48–61. ISSN: 0266-8920. DOI: 10.1016/j.probengmech.2016.08.003. URL: https://www.sciencedirect.com/science/article/pii/S0266892016300972.

Marques, Filipe, Hugo Magalhães, João Pombo, Jorge Ambrósio, and Paulo Flores (2020). "A Three-Dimensional Approach for Contact Detection between Realistic Wheel and Rail Surfaces for Improved Railway Dynamic Analysis." *Mechanism and Machine Theory* 149, p. 103825. ISSN: 0094-114X. DOI: 10.1016/j.mechmachtheory.2020.103825. URL: https://www.sciencedirect.com/science/article/pii/S0094114X2030046X.

Marvillet, Dominique and Jean-Pierre Tartary (2003). "Bridges, High Speed and Dynamic Calculation – Short Version." *Structures for High-Speed Railway Transportation*, pp. 80–81. DOI: 10.2749/222137803796329132. URL: https://structurae.net/en/literature/conference-paper/bridges-high-speed-and-dynamic-calculation-short-version.

MATLAB® (2018). *Academic Research*. Version Release R2018a. Natick, Massachusetts, USA.

Matsuoka, Kodai, Andrea Collina, Claudio Somaschini, and Masamichi Sogabe (Dec. 1, 2019). "Influence of Local Deck Vibrations on the Evaluation of the Maximum Acceleration of a Steel-Concrete Composite Bridge for a High-Speed Railway." *Engineering Structures* 200, p. 109736. ISSN: 0141-0296. DOI: 10.1016/j.engstruct.2019.109736. URL: https://www.sciencedirect.com/science/article/pii/S0141029618342627.

Matsuoka, Kodai, Mizuki Tsunemoto, and Munemasa Tokunaga (2022). "Dynamic Behaviour of Railway Poles Built on Bridges under Train Passage in High-Speed Railways and a Simple Evaluation Method." *Engineering Structures* 257, p. 114099. ISSN: 0141-0296. DOI: 10.1016/j.engstruct.2022.114099. URL: https://www.sciencedirect.com/science/article/pii/S0141029622002383.

Mazzino, N. et al. (2017). *Rail 2050 Vision. Rail - The Backbone of Europe's Mobility*. Brussels, Belgium. URL: https://errac.org/publications/rail-2050-vision-document/.

McKay, M. D., R. J. Beckman, and W. J. Conover (1979). "A Comparison of Three Methods for Selecting Values of Input Variables in the Analysis of Output from a Computer Code." *Technometrics* 21.2, pp. 239–245. ISSN: 0040-1706. DOI: 10.2307/1268522. JSTOR: 1268522. URL: https://www.jstor.org/stable/1268522.

Melchers, Robert (1999). *Structural Reliability Analysis and Prediction*. 2nd ed. Chichester, UK: John Wiley & Sons. xviii+437. ISBN: 978-0-471-98771-0.

Menezes, José Maria Correia de Oliveira Brandão de (2024). "Modelling of the Dynamic Behaviour of Ballast on Railway Bridges." Master's Thesis. Faculdade de Engenharia da Universidade do Porto. URL: https://repositorio-aberto.up.pt/handle/10216/162090.

Meymand, Sajjad Z., Alexander Keylin, and Mehdi Ahmadian (2016). "A Survey of Wheel–Rail Contact Models for Rail Vehicles." *Vehicle System Dynamics* 54.3, pp. 386–428. ISSN: 0042-3114. DOI: 10.1080/00423114.2015.1137956. URL: https://doi.org/10.1080/00423114.2015.1137956.

Moliner, E., M. D. Martínez-Rodrigo, and P. Museros (2017). "Dynamic Performance of Existing Double Track Railway Bridges at Resonance with the Increase of the Operational Line Speed." *Engineering Structures* 132, pp. 98–109. ISSN: 0141-0296. DOI: 10.1016/j.engstruct.2016.11.031. URL: https://www.sciencedirect.com/science/article/pii/S0141029616312639.

Montenegro, P. A., D. Barbosa, H. Carvalho, and R. Calçada (2020). "Dynamic Effects on a Train-Bridge System Caused by Stochastically Generated Turbulent Wind Fields." *Engineering Structures* 211, p. 110430. ISSN: 01410296. DOI: 10.1016/j.engstruct.2020.110430. URL: https://linkinghub.elsevier.com/retrieve/pii/S0141029619338040.

Montenegro, P. A., H. Carvalho, M. Ortega, F. Millanes, J.M. Goicolea, W. Zhai, and R. Calçada (2022). "Impact of the Train-Track-Bridge System Characteristics in the Runnability of High-Speed Trains against Crosswinds - Part I: Running Safety." *Journal of Wind Engineering and Industrial Aerodynamics* 224, p. 104974. ISSN: 01676105. DOI: 10.1016/j.jweia.2022.104974. URL: https://linkinghub.elsevier.com/retrieve/pii/S0167610522000794.

Montenegro, P. A., H. Carvalho, D. Ribeiro, R. Calçada, M. Tokunaga, M. Tanabe, and W.M. Zhai (2021). "Assessment of Train Running Safety on Bridges: A Literature Review." *Engineering Structures* 241, p. 112425. ISSN: 0141-0296. DOI: 10.1016/j.engstruct.2021.112425. URL: https://www.sciencedirect.com/science/article/pii/S0141029621005757.

Montenegro, P. A., S.G.M Neves, R. Calçada, M. Tanabe, and M. Sogabe (2015). "Wheel-Rail Contact Formulation for Analyzing the Lateral Train-Structure Dynamic Interaction." *Computers & Structures* 152, pp. 200–214. URL: https://www.sciencedirect.com/science/article/pii/S0045794915000139.

Museros, P., A. Andersson, V. Martí, and R. Karoumi (2021). "Dynamic Behaviour of Bridges under Critical Articulated Trains: Signature and Bogie Factor Applied to the Review of Some Regulations Included in EN 1991-2." *Proceedings of the Institution of Mechanical Engineers, Part F: Journal of Rail and Rapid Transit* 235.5, pp. 655–675. ISSN: 0954-4097. DOI: 10.1177/0954409720956476.

Museros, P., E. Moliner, and M. D. Martínez-Rodrigo (2013). "Free Vibrations of Simply-Supported Beam Bridges under Moving Loads: Maximum Resonance, Cancellation and Resonant Vertical Acceleration." *Journal of Sound and Vibration* 332.2, pp. 326–345. ISSN: 0022-460X. DOI: 10.1016/j.jsv.2012.08.008. URL: https://www.sciencedirect.com/science/article/pii/S0022460X12006293.

Nadal, M. J. (1908). *Locomotives à Vapeur*. Vol. 186. Collection E. Paris, France: Encyclopédie Scientifique.

Naess, A., B. J. Leira, and O. Batsevych (2009). "System Reliability Analysis by Enhanced Monte Carlo Simulation." *Structural Safety* 31.5, pp. 349–355. ISSN: 0167-4730. DOI: 10.1016/j.strusafe.2009.02.004. URL: https://www.sciencedirect.com/science/article/pii/S0167473009000186.

National Railway Administration of the People's Republic of China (2014). *Code for Design of High Speed Railway*. TB 10621-2014. Beijing, China.

– (2017). *Code for Design on Railway Bridge and Culvert*. TB 10002-2017. Beijing, China.

Neto, J., P. A. Montenegro, C. Vale, and R. Calçada (2021). "Evaluation of the Train Running Safety under Crosswinds - a Numerical Study on the Influence of the Wind Speed and Orientation Considering the Normative Chinese Hat Model." *International Journal of Rail Transportation* 9.3, pp. 204–231. ISSN: 2324-8378, 2324-8386. DOI: 10.1080/23248378.2020.1780965. URL: https://www.tandfonline.com/doi/full/10.1080/23248378.2020.1780965.

Neves, S. G. M., A. F. M. Azevedo, and R. Calçada (2012). "A Direct Method for Analyzing the Vertical Vehicle–Structure Interaction." *Engineering Structures* 34, pp. 414–420. ISSN: 0141-0296. DOI: 10.1016/j.engstruct.2011.10.010. URL: https://www.sciencedirect.com/science/article/pii/S014102961100407X.

Neves, S. G. M., P. A. Montenegro, A. F. M. Azevedo, and R. Calçada (2014). "A Direct Method for Analyzing the Nonlinear Vehicle-Structure Interaction." *Engineering Structures* 69, pp. 83–89. ISSN: 0141-0296. DOI: 10.1016/j.engstruct.2014.02.027. URL: https://www.sciencedirect.com/science/article/pii/S0141029614001205.

Newmark, Nathan M. (1959). "A Method of Computation for Structural Dynamics." *Journal of the Engineering Mechanics Division* 85.3, pp. 67–94. DOI: 10.1061/JMCEA3.0000098. URL: https://ascelibrary.org/doi/abs/10.1061/JMCEA3.0000098.

Norris, Paul, Tony Wilkins, and Ian Bucknall (2003). "Permissible Deck Accelerations for Rail Bridge Dynamic Assessments." *IABSE Symposium Antwerp 2003*. IABSE Symposium: *Structures for High-Speed Railway Transportation*, Antwerp, Belgium, 27-29 August 2003, pp. 82–83. DOI: 10.2749/222137803796329123. URL: https://structurae.net/en/literature/conference-paper/permissible-deck-accelerations-for-rail-bridge-dynamic-assessments.

Olmos, José M. and Miguel Á. Astiz (2018). "Non-Linear Vehicle-Bridge-Wind Interaction Model for Running Safety Assessment of High-Speed Trains over a High-Pier Viaduct." *Journal of Sound and Vibration* 419, pp. 63–89. ISSN: 0022-460X. DOI: 10.1016/j.jsv.2017.12.038. URL: https://www.sciencedirect.com/science/article/pii/S0022460X17308970.

Park, Joonam and Peeranan Towashiraporn (2014). "Rapid Seismic Damage Assessment of Railway Bridges Using the Response-Surface Statistical Model." *Structural Safety* 47, pp. 1–12. ISSN: 0167-4730. DOI: 10.1016/j.strusafe.2013.10.001. URL: https://www.sciencedirect.com/science/article/pii/S0167473013000787.

Pascal, J.-P. (1993). "About Multi-Hertzian-Contact Hypothesis and Equivalent Conicity in the Case of S1002 and UIC60 Analytical Wheel/Rail Profiles." *Vehicle System Dynamics* 22.2, pp. 57–78. ISSN: 0042-3114. DOI: 10.1080/00423119308969021. URL: https://doi.org/10.1080/00423119308969021.

Paulsson, Björn, Jan Olofsson, Hans Hedlund, Brian Bell, Björn Täljsten, and Lennart Elfgren (2010). "Sustainable Bridges – Results from a European Integrated Research Project." *Large Structures and Infrastructures for Environmentally Constrained and Urbanised Areas*, pp. 314–315. DOI: 10.2749/222137810796024727. URL: https://structurae.net/en/literature/conference-paper/sustainable-bridges-results-from-a-european-integrated-research-project.

Pimentel, R., C. Barbosa, N. Costa, D. Ribeiro, L. A. Ferreira, F. M. Araújo, and R. Calçada (2007). "Characterization of Railway Traffic and Its Effects on a Short Span Bridge by Using a Hybrid Fibre Optic/Electrical Measurement System." *Third European Workshop on Optical Fibre Sensors*. Vol. 6619. International Society for Optics and Photonics, 66193Y. DOI: 10.1117/12.738786. URL: https://www.spiedigitallibrary.org/conference-proceedings-of-spie/6619/66193Y/Characterization-of-railway-traffic-and-its-effects-on-a-short/10.1117/12.738786.short.

Pombo, João, Jorge Ambrósio, and Miguel Silva (2007). "A New Wheel–Rail Contact Model for Railway Dynamics." *Vehicle System Dynamics* 45.2, pp. 165–189. ISSN: 0042-3114. DOI: 10.1080/00423110600996017. URL: https://doi.org/10.1080/00423110600996017.

Prud'homme, A. (1967). "La Résistance de La Voie Aux Efforts Transversaux Éxercés Par Le Material Roulant." *Revue générale des chemins de fer*, pp. 1–3.

Quost, Xavier, Sebes Michel, Eddhahak Anissa, Ayasse Jean-Bernard, Chollet Hugues, Gautier Pierre-Etienne, and Fabrice Thouverez (2006). "Assessment of a Semi-Hertzian Method for Determination of Wheel–Rail Contact Patch." *Vehicle System Dynamics* 44.10, pp. 789–814. ISSN: 0042-3114. DOI: 10.1080/00423110600677948. URL: https://doi.org/10.1080/00423110600677948.

Rackwitz, Rüdiger and Bernd Fiessler (1978). "Structural Reliability under Combined Random Load Sequences." *Computers & Structures* 9.5, pp. 489–494. ISSN: 0045-7949. DOI: 10.1016/0045-7949(78)90046-9. URL: https://www.sciencedirect.com/science/article/pii/0045794978900469.

Railway Technical Research Institute (2006). *Outline of Design Standards for Railway Structures and Commentary (Displacement Limits)*. Tokyo, Japan: Maruzen Co., Ltd.

Ramu, Palaniappan, Nam H. Kim, and Raphael T. Haftka (2010). "Multiple Tail Median Approach for High Reliability Estimation." *Structural Safety* 32.2, pp. 124–137. ISSN: 0167-4730. DOI: 10.1016/j.strusafe.2009.09.002. URL: https://www.sciencedirect.com/science/article/pii/S0167473009000721.

Rebelo, C., L. Simões da Silva, C. Rigueiro, and M. Pircher (2008). "Dynamic Behaviour of Twin Single-Span Ballasted Railway Viaducts — Field Measurements and Modal Identification." *Engineering Structures* 30.9, pp. 2460–2469. ISSN: 0141-0296. DOI: 10.1016/j.engstruct.2008.01.023. URL: https://www.sciencedirect.com/science/article/pii/S0141029608000291.

Reiterer, Michael, Andrei Firus, Alois Vorwagner, Geert Lombaert, Jens Schneider, and Kohl (2021). "Railway Bridge Dynamics: Development of a New High-Speed Train Load Model for Dynamic Analyses of Train Crossing." *Structural Engineering for Future Societal Needs*, pp. 1633–1642. DOI: 10.2749/ghent.2021.1633. URL: https://structurae.net/en/literature/conference-paper/railway-bridge-dynamics-development-of-a-new-high-speed-train-load-model-for-dynamic-analyses-of-train-crossing.

Reiterer, Michael, Antonia M. Kohl, Alois Vorwagner, Maciej Kwapisz, Andrei Firus, and Geert Lombaert (2022). "Development of a New High-Speed Load Model and Validation on Existing Railway Bridges." *The Fifth International Conference on Railway Technology: Research, Development and Maintenance*. Montpellier, France. DOI: 10.4203/ccc.1.6.11. URL: http://www.ctresources.info/ccc/paper.html?id=9518.

Reiterer, Michael, Maciej Kwapisz, Andrei Firus, Maximilian Rupp, and Geert Lombaert (2023). "Development of a New High-Speed Train Load Model for Dynamic Calculation of Railway Bridges." *ce/papers* 6.5, pp. 422–429. ISSN: 2509-7075. DOI: 10.1002/cepa.2210. URL: https://onlinelibrary.wiley.com/doi/abs/10.1002/cepa.2210.

Rocha, João M. (2015). "Probabilistic Methodologies for the Safety Assessment of Short Span Railway Bridges for High-Speed Traffic." Doctoral Thesis. Porto, Portugal: Faculdade de Engenharia da Universidade do Porto. URL: https://repositorio-aberto.up.pt/handle/10216/83809.

Rocha, João M., António Abel Henriques, and Rui Calçada (2016). "Probabilistic Assessment of the Train Running Safety on a Short-Span High-Speed Railway Bridge." *Structure and Infrastructure Engineering* 12.1, pp. 78–92. ISSN: 1573-2479. DOI: 10.1080/15732479.2014.995106. URL: https://doi.org/10.1080/15732479.2014.995106.

RSSB (2024). *Guidance on Evaluating Excessive Dynamic Effects in Underline Bridges*. GEG N8616. London, UK: Rail Safety and Standards Board.

Salcher, Patrick and Christoph Adam (2020). "Estimating Exceedance Probabilities of Railway Bridge Vibrations in the Presence of Random Rail Irregularities." *International Journal of Structural Stability and Dynamics* 20.13, p. 2041005. ISSN: 0219-4554. DOI: 10.1142/S0219455420410059. URL: https://www.worldscientific.com/doi/abs/10.1142/S0219455420410059.

Salcher, Patrick, Helmuth Pradlwarter, and Christoph Adam (2014). "Reliability of High-Speed Railway Bridges with Respect to Uncertain Characteristics." *9th European Conference on Structural Dynamics*. Porto, Portugal.

Shabana, Ahmed A., Mahmoud Tobaa, Hiroyuki Sugiyama, and Khaled E. Zaazaa (2005). "On the Computer Formulations of the Wheel/Rail Contact Problem." *Nonlinear Dynamics* 40.2, pp. 169–193. ISSN: 1573-269X. DOI: 10.1007/s11071-005-5200-y. URL: https://doi.org/10.1007/s11071-005-5200-y.

Shi, H., Z. Yu, and H. Shi (2016). "An Improved Method for Dynamic Modelling of a Slab Track on a High-Speed Railway." *Computers in Railways XV*. Madrid, Spain, pp. 225–237. DOI: 10.2495/CR160211. URL: http://library.witpress.com/viewpaper.asp?pcode=CR16-021-1.

Silva, A., D. Ribeiro, P. Montenegro, G. Ferreira, A. Andersson, A. Zangeneh, R. Karoumi, and R. Calçada (2023). "New Contributions for Damping Assessment on Filler-Beam Railway Bridges Framed on In2Track EU Projects." *Applied Sciences (Switzerland)* 13.4. ISSN: 2076-3417. DOI: 10.3390/app13042636.

SNCF (1998). *Règles de Conception et de Calcul Des Ouvrages En Béton, En Métal Ou Mixtes. Tome IV - Ouvrages d'art - Fascicule 2.01*. Paris, France: Société Nationale des Chemins de Fer.

State Administration for Market Regulation and Standardization Administration of PRC (2019). *Specification for Dynamic Performance Assessment and Testing Verification of Rolling Stock*. GB/T 5599–2019. Beijing, China.

Stollwitzer, A., L. Bettinelli, and J. Fink (2024). "Vertical Track-Bridge Interaction in Railway Bridges with Ballast Superstructure: Experimental Analysis of Dynamic Stiffness and Damping Behavior." *International Journal of Structural Stability and Dynamics*. DOI: 10.1142/S0219455425400085.

Sugiyama, Hiroyuki and Yoshihiro Suda (2009). "On the Contact Search Algorithms for Wheel/Rail Contact Problems." *Journal of Computational and Nonlinear Dynamics* 4.041001. ISSN: 1555-1415. DOI: 10.1115/1.3187211. URL: https://doi.org/10.1115/1.3187211.

Unterweger, Harald, DI Andreas Schörghofer, and Andreas Taras (2017). "06.01: Critical Bridges in High-Speed Railway Lines: Systematic Identification for Specific Trains." *Proceedings of Eurosteel 2017* 1.2-3, pp. 1427–1436. ISSN: 2509-7075. DOI: 10.1002/cepa.185. URL: https://onlinelibrary.wiley.com/doi/abs/10.1002/cepa.185.

Uribe, Felipe (2016). *Monte Carlo and Subset Simulation Example*. URL: https://www.mathworks.com/matlabcentral/fileexchange/57947-monte-carlo-and-subset-simulation-example (visited on 02/15/2025).

Vestroni, F. and S. Vidoli (2007). "Closed-Form Solutions for the Structural Response to Train Loads." *Journal of Sound and Vibration* 303.3, pp. 691–706. ISSN: 0022-460X. DOI: 10.1016/j.jsv.2007.01.040. URL: https://www.sciencedirect.com/science/article/pii/S0022460X07001125.

Vorwagner, Alois, Maciej Kwapisz, Rainer Flesch, Antonia M. Kohl, Andrei Firus, Michael Vospernig, and Tomás Arana Villafán (2021). "FEM Based Approach for Development of a New High-Speed Load Model for Railway Bridges." *Structural Engineering for Future Societal Needs*, pp. 1614–1622. DOI: 10.2749/ghent.2021.1614. URL: https://structurae.net/de/fachliteratur/tagungsbeitrag/fem-based-approach-for-development-of-a-new-high-speed-load-model-for-railway-bridges.

Weinstock, Herbert (1984). "Wheel Climb Derailment Criteria for Evaluation of Rail Vehicle Safety." *ASME Winter Annual Meeting*. ASME Winter Annual Meeting. New Orleans, USA: American Society of Mechanical Engineers. URL: https://rosap.ntl.bts.gov/view/dot/12061 (visited on 02/25/2025).

Xin, Lifeng, Xiaozhen Li, Yan Zhu, and Ming Liu (2020). "Uncertainty and Sensitivity Analysis for Train-Ballasted Track–Bridge System." *Vehicle System Dynamics* 58.3, pp. 453–471. ISSN: 0042-3114. DOI: 10.1080/00423114.2019.1584678. URL: https://doi.org/10.1080/00423114.2019.1584678.

Xu, Zhiwei, Gonglian Dai, Y. Frank Chen, Huiming Rao, and Zhibin Huang (2023). "Extreme Response Analysis of Train-Track-Bridge-Wind Interac-

tion System Based on in-Situ Monitoring Wind Data." *Structural Safety* 100, p. 102288. ISSN: 0167-4730. DOI: 10.1016/j.strusafe.2022.102288. URL: https://www.sciencedirect.com/science/article/pii/S0167473022000959.

Yang, Y. B. and J. D. Yau (2017). "Resonance of High-Speed Trains Moving over a Series of Simple or Continuous Beams with Non-Ballasted Tracks." *Engineering Structures* 143, pp. 295–305. ISSN: 0141-0296. DOI: 10.1016/j.engstruct.2017.04.022. URL: https://www.sciencedirect.com/science/article/pii/S0141029616308173.

Yotsui, H., K. Matsuoka, and K. Kaito (2024). "Acceleration Evaluation of a High-Speed Railway PC Box Girder Bridge with Slab Track." *Conference Proceedings of the Society for Experimental Mechanics Series*, pp. 25–32. ISBN: 978-3-031-36662-8. DOI: 10.1007/978-3-031-36663-5_4.

Zacher, Manfred and Matthias Baeßler (2008). "Dynamic Behaviour of Ballast on Railway Bridges." *Dynamics of High–Speed Railway Bridges. Selected and Revised Papers from the Advanced Course on 'Dynamics of High–Speed Railway Bridges', Porto, Portugal, 20–23 September 2005*. CRC Press, pp. 125–142.

Zhai, W. M., K. Y. Wang, and J. H. Lin (2004). "Modelling and Experiment of Railway Ballast Vibrations." *Journal of Sound and Vibration* 270.4, pp. 673–683. ISSN: 0022-460X. DOI: 10.1016/S0022-460X(03)00186-X. URL: https://www.sciencedirect.com/science/article/pii/S0022460X0300186X.

Zhai, Wanming, Pengfei Liu, Jianhui Lin, and Kaiyun Wang (2015). "Experimental Investigation on Vibration Behaviour of a CRH Train at Speed of 350 Km/h." *International Journal of Rail Transportation* 3.1, pp. 1–16. ISSN: 2324-8378. DOI: 10.1080/23248378.2014.992819. URL: https://doi.org/10.1080/23248378.2014.992819.

Zhang, Nan, Ziji Zhou, and Zhaozhi Wu (2022). "Safety Evaluation of a Vehicle–Bridge Interaction System Using the Pseudo-Excitation Method." *Railway Engineering Science* 30.1, pp. 41–56. ISSN: 2662-4753. DOI: 10.1007/s40534-021-00259-6. URL: https://doi.org/10.1007/s40534-021-00259-6.

Zuev, Konstantin M. (2013). "Subset Simulation Method for Rare Event Estimation: An Introduction." *Encyclopedia of Earthquake Engineering*. Ed. by Michael Beer, Ioannis A. Kougioumtzoglou, Edoardo Patelli, and Ivan Siu-Kui Au. Heidelberg, Germany: Springer, pp. 1–25. ISBN: 978-3-642-36197-5. DOI: 10.1007/978-3-642-36197-5_165-1. URL: https://doi.org/10.1007/978-3-642-36197-5_165-1.

COLOPHON

This document was typeset in LaTeX using `classicthesis` developed by André Miede and Ivo Pletikosić.